

THE UNIVERSITY
of EDINBURGH

This thesis has been submitted in fulfilment of the requirements for a postgraduate degree (e.g. PhD, MPhil, DClinPsychol) at the University of Edinburgh. Please note the following terms and conditions of use:

This work is protected by copyright and other intellectual property rights, which are retained by the thesis author, unless otherwise stated.
A copy can be downloaded for personal non-commercial research or study, without prior permission or charge.
This thesis cannot be reproduced or quoted extensively from without first obtaining permission in writing from the author.
The content must not be changed in any way or sold commercially in any format or medium without the formal permission of the author.
When referring to this work, full bibliographic details including the author, title, awarding institution and date of the thesis must be given.

The origins and heterogeneity of adipose tissue: investigating the role of the Wilms' tumour 1 (*Wt1*) gene

Louise K. Cleal

Thesis submitted for the degree of
Doctor of Philosophy

The University of Edinburgh
2017

INSTITUTE OF GENETICS
& MOLECULAR MEDICINE

Declaration

This thesis has been entirely composed by me. Apart from where stated the experiments were carried out solely by me. The work has not been submitted for any other degree or professional qualification.

Louise K. Cleal, December 2017

Abstract

Largely as a consequence of the ongoing obesity epidemic, research into adipose tissue biology has increased substantially in recent years. Worldwide, the number of people classed as overweight or obese is growing, and this represents a major public health concern. Adipose tissue is broadly divided into two types; white and brown. Whilst white adipose tissue (WAT) functions to store and mobilise triglycerides, brown adipose tissue burns chemical energy to generate heat. WAT is further divided into visceral "bad" fat and subcutaneous "good" fat depots, and it is an increase in the former that is linked to obesity-associated diseases. As well as adipocytes, several other cell types including haematopoietic and endothelial are found within adipose tissue, and comprise the stromal vascular fraction (SVF). Adipocyte precursor cells (APCs) also reside within the SVF and are essential for the maintenance and expansion of adipose tissue.

The protein encoded by the Wilms' tumour 1 (*Wt1*) gene is predominantly known to function as a transcription factor, but also has a role in post-transcriptional processing. Deletion of *Wt1* in adult mice results in a considerable loss of fat tissue. Moreover, recent work has revealed that a proportion of the APCs from all visceral WAT depots express *Wt1*, therefore revealing heterogeneity within the APC population. Additionally, visceral WAT depots are encapsulated by a WT1 expressing mesothelial layer, which has its origins in the lateral plate mesoderm (LPM), and can give rise to mature adipocytes. Lineage tracing has demonstrated that a significant proportion of the mature adipocytes in all adult visceral WAT depots (but not subcutaneous) are derived from cells that express *Wt1* in late gestation. These findings uncovered key ontogenetic differences between visceral and subcutaneous WAT and led us to ask whether *Wt1* functions in visceral adipose tissue biology.

Preliminary work has shown that adipocytes derived from *Wt1* expressing ($Wt1^+$) precursor cells have fewer, larger lipid droplets than those derived from non-*Wt1* expressing ($Wt1^-$) precursors. In this thesis, this heterogeneity is explored further using a $Wt1^{GFP/+}$ knock-in mouse. When $Wt1^+$ and $Wt1^-$ APCs are cultured separately, the

$Wt1^+$ population differentiate into adipocytes more readily. Moreover, the $Wt1^+$ APCs are more proliferative than the $Wt1^-$. Preliminary results also suggest that the $Wt1^+$ APCs may secrete a factor(s) that causes the $Wt1^-$ APCs to exhibit improved adipogenic differentiation, a result that is supported by data from comparative transcriptomic analysis. Finally, the percentage of APCs decreases when mice are fed a high fat diet. Interestingly, this decrease is more pronounced for the $Wt1^+$ population. Therefore, it appears that as well as exhibiting differing behaviours *in vitro*, the $Wt1^+$ and $Wt1^-$ populations respond differently to physiologically relevant conditions *in vivo*.

Whilst the LPM is a major source of visceral WAT, the origin of subcutaneous WAT is currently unknown. Here, the *Prx1-Cre* and *Prx1-Cre*^{ERT2} mouse lines are used to investigate this. It is shown that the majority of subcutaneous WAT adipocytes and APCs are labelled by Prx1-Cre, however this is not the case for most of the visceral WAT depots. The exception to this is the pericardial (heart fat) depot, in which approximately 70% of the adipocytes and 40% of the APCs are labelled. Moreover, a proportion of the Prx1-Cre labelled pericardial APCs also express *Wt1*, therefore suggesting additional heterogeneity. Preliminary results show that this heterogeneity may have functional consequences, at least *in vitro*. Additionally, lineage tracing studies suggest that the somatic LPM may be one source of subcutaneous WAT and pericardial visceral WAT

Finally, it is shown that the conditional deletion of *Wt1* in the Prx1-Cre lineage results in abnormal diaphragm development. Congenital diaphragmatic hernia (CDH) is severe birth defect, the etiology of which is not well understood. Here, a new model of CDH has been developed, and the cellular and molecular mechanisms responsible for the defect in this model are investigated.

Lay summary

Worldwide, the number of clinically obese people has doubled since 1980. According to the World Health Organisation, in 2014 39% of adults were clinically overweight and 13% were obese. Obesity is associated with several diseases including heart disease, type II diabetes and cancer, therefore this global epidemic represents a significant public health concern. In line with this increasing problem, there has been heightened interest in researching adipose tissue (fat) biology.

Mammals have two types of adipose tissue: brown (BAT) and white (WAT). BAT primarily burns energy in the form of heat, whilst WAT stores it in the form of lipid. WAT exists as two types; "good fat" or subcutaneous WAT, and "bad fat" or visceral WAT. The stereotypical female "pear shaped" figure is indicative of subcutaneous WAT accumulation, whilst the typically male "apple shape" is associated with the expansion of visceral WAT. Visceral WAT is distributed within the body cavity, close to major organs, and is divided into distinct locations, for example surrounding the heart and the stomach.

Recent work has shown that a gene, Wilms' tumour 1 (*Wt1*), is switched on in a proportion of the precursor cells that will go on to form visceral WAT. However, this is not the case for the precursor cells of the subcutaneous WAT or BAT. *Wt1* functions in the development and maintenance of various organs including the heart, and now it is thought it may also have a role in the biology of visceral WAT. The aim of this project was to gain a greater understanding of what this role is.

To do so, several approaches were taken. Firstly, mouse adipose tissue precursor cells in which *Wt1* is switched on, were compared to precursor cells in which *Wt1* is switched off. By understanding differences between these two populations of cells, it was hoped that we would learn more about the function of the gene. The behaviour of the cells, when grown in a dish, was compared, and this showed that the "Wt1 on" cells could replicate themselves and become mature fat cells more easily than "Wt1 off" cells. Additionally, when we compared other genes that were switched on and off

in the two populations, many differences were identified. Finally, when the mice were fed a high fat diet which caused them to gain weight quickly, the percentage of cells in which *Wt1* was switched on decreased, suggesting that external influences, such as diet, could affect the behaviour of these cells.

We were also interested to know more about where adipose tissue comes from during embryonic development and growth. Because fat is distributed into discrete and specific locations around the body, the different compartments are often thought of as separate "mini-organs", which may all function slightly differently. Therefore, understanding how the different areas of fat arise and expand during development, may lead to therapeutic interventions that alter body fat distribution. To learn more about the developmental origin of subcutaneous WAT or "good fat", a technique known as lineage tracing was performed. This allows specific cells to be fluorescently labelled. This labelling is passed on to their daughter cells and all future generations, so the offspring of one population of cells can be followed through development and into adulthood. This has given us some insight into the possible origin of good fat.

Finally, it is known *Wt1* has a role in the development of the diaphragm, and whilst attempting to delete the gene in the adipose tissue precursor cells, we disrupted diaphragm formation and generated a new mouse model of congenital diaphragmatic hernia (CDH). CDH is a severe birth defect that affects approximately 1/2000 pregnancies, however the causative mechanisms underlying this malformation are not particularly well understood. Hence, another aspect of this project has been to investigate these mechanisms using this newly developed mouse model of CDH.

Acknowledgements

I would first like to thank my supervisors for all the encouragement and guidance they have given me over the last three years. Thank you to You-Ying for your continued support and for all the knowledge you have imparted to me, not to mention the cake supplies on long lab days. Thank you to Nick for giving me the opportunity to work in the lab and for all the interesting discussions, many scientific but several about the latest BBC drama!

A special thanks to Sophie, without whom I would not have made it this far, we had a lot of fun (perhaps too much?!), and this Christmas wasn't the same without the glove tree, definitely one of the greatest achievements of my PhD. Also thanks to all members of the W3 lab, past and present, for making it such an enjoyable and happy place to work. Especially to Victor for answering all my silly questions and letting me pinch several antibodies. And to Luke and David for the hilarious chat, despite the constant food-related mocking...

I am so appreciative of everyone who has helped me throughout my PhD, particularly Lizzie for her FACS wizardry, I dread to think how many tubes of cells I've brought through those doors. And of course, Allyson, the Queen of histology! Thank you to all the imaging staff for your patience and assistance and to the technical staff who keep the place running. A special mention must go to Anna and the rest of the mouse team who are all superstars! Finally, thank you to my thesis committee (Bob, Ian and Julia), for all your help and advice.

Thank you to the other PhD girls, Flora, Ailsa, Fiona and Katy, for the film nights, the cake, the theatre trips and for ALL the PhD stress related conversations – we made it! Also to my non-sciencey friends who have done an excellent job of pretending to understand what I do!

A massive thank you to all my family for your constant encouragement and belief in me, especially my parents who are now very familiar with the M6! And particularly to

my wonderful mum who is always there to listen to my rantings. Also to Will's family who have looked out for me from day one in Edinburgh - Richard, I've finally finished.

Lastly, an enormous thank you to my fiancé Will. I certainly would not be in this position without your constant support, and well done for putting up with my late-night presentation practices!



Table of Contents

Declaration ii
Abstract iii
Lay summary v
Acknowledgements vii
Table of contents ix
List of figures xiv
List of tables xviii
List of abbreviations xx

Chapter 1: Introduction

1.1 Adipose tissue overview 2
1.1.1 Adipose tissue types and depots 2
1.1.2 Adipocyte precursor cells (APCs) 7
1.1.3 Adipose tissue development 13
1.1.4 Adipose tissue homeostasis 19
1.1.5 Adipose tissue expansion 25
1.1.6 Inter and intra-depot heterogeneity 27

1.2 Overview of *WT1* 31
1.2.1 WT1 in development 36
1.2.2 WT1 in adult homeostasis 40

1.3 Overview of the *Prx1-Cre* mouse line 42
1.3.1 Prx1-Cre and adipose tissue 44

1.4 Congenital diaphragmatic hernia (CDH) 45
1.4.1 Development of the diaphragm 47
1.4.2 WT1 and the diaphragm 49
1.4.3 Prx1-Cre and the diaphragm 51

1.5 Summary 52
1.5.1 Hypothesis 54
1.5.2 Aims 54

Chapter 2: Materials and methods

2.1 General reagents 56

2.2 Transgenic animal models 56
2.2.1 Animal husbandry 56
2.2.2 Genotyping of mice 57
2.2.3 *Wt1*$^{GFP/+}$ knock-in mouse line 57
2.2.4 WER mouse line 57
2.2.4.1 Cre control mouse line 57

2.2.5 *Wt1-Cre^{ERT2};R26R-mTmG* mouse line 58
2.2.5.1 *In vivo* lineage tracing 58
2.2.6 *Prx1-Cre;R26R-mTmG* and *Prx1-Cre^{ERT2};R26R-mTmG* mouse lines 58
2.2.6.1 *In vivo* lineage tracing 59
2.2.7 *Prx1-Cre;tdRFP;Wt1$^{GFP/+}$* mouse line 59
2.2.8 *Prx1-Cre;Wt1$^{loxP/loxP}$* and *Prx1-Cre;Wt1$^{loxP/GFP}$* mouse lines .. 60
2.2.9 High fat diet feeding 60

2.3 Immunohistochemistry/Immunocytochemistry 61
2.3.1 Sample preparation for immunohistochemistry 61
2.3.2 Immunofluorescence staining paraffin sections 61
2.3.2.1 Solutions for immunofluorescence staining 61
2.3.2.2 Immunofluorescence staining 64
2.3.3 Haematoxylin and Eosin staining 65
2.3.4 Immunocytochemistry 65
2.3.5 Imaging 66
2.3.5.1 Analysis using Definiens® software 67

2.4 Flow cytometry & fluorescence activated cell sorting (FACS) 67
2.4.1 Isolation of murine stromal vascular fraction (SVF) cells from adipose tissue 67
2.4.2 Isolation of APCs from the SVF 68

2.5 Tissue culture 70
2.5.1 Isolation and expansion of murine SVF cells 70
2.5.2 Adipogenic differentiation 71
2.5.3 Conditioned media 71

2.6 Gene expression analysis 72
2.6.1 RNA extraction using TRIzol® reagent 72
2.6.2 RNA quality and quantity 73
2.6.3 cDNA synthesis 73
2.6.4 Quantitative realtime polymerase chain reaction (qRT-PCR).. 73
2.6.5 Custom qRT-PCR plates 74

2.7 Gene expression microarrays 75
2.7.1 Microarray sample preparation – cRNA amplification 75
2.7.2 Gene expression 76
2.7.3 Gene expression analysis 76

2.8 Statistical analysis 77

Chapter 3: Comparing Wt1^{+} and Wt1^{-} adipocyte precursor cells (APCs)

3.1 Introduction 79

3.2 Comparing Wt1^{+} and Wt1^{-} SVF cells *in vitro* 80

3.2.1 Adipogenic differentiation of $Wt1^+$ and $Wt1^-$ APCs cultured separately 80
3.2.2 Comparing proliferation and apoptosis of $Wt1^+$ and $Wt1^-$ APCs 85

3.3 *Wt1* deletion *in vitro* 90
3.3.1 The effect of *in vitro Wt1* deletion on proliferation 90
3.3.2 Cre control cultures 94

3.4 Culturing $Wt1^-$ APCs in media condition by $Wt1^+$ APCs 96

3.5 Microarray analysis of freshly isolated $Wt1^+$ and $Wt1^-$ APCs 97
3.5.1 GO terms identified for genes with higher expression in $Wt1^+$ APCs 98
3.5.2 Gene expression validation 102
3.5.3 GO terms identified for genes with lower expression in $Wt1^+$ APCs 104

3.6 Assessing the effects of a high fat diet on different adipose tissue depots 106
3.6.1 The effect of a high fat diet on the proportion of $Wt1^+$ cells in the SVF 106
3.6.2 Gene expression microarray analysis 112
3.6.2.1 GO terms identified for genes upregulated in APCs from HFD mice 113
3.6.2.2 GO terms identified for genes downregulated in APCs from HFD mice 115
3.6.2.3 Analysis of genes differentially expressed specifically in $Wt1^+$ or $Wt1^-$ APC populations 116
3.6.2.4 Gene expression validation 117

3.7 The effect of a high fat diet on the proportion of Wt1 lineage traced cells using *Wt1-Cre^{ERT2};R26R-mTmG* mice 127
3.7.1 The effect of a high fat diet on the proportion of Wt1 lineage traced cells in the SVF 128
3.7.2 The effect of a high fat diet on the proportion of Wt1 lineage traced mature adipocytes 131

3.8 Discussion 133

Chapter 4: Prx-Cre labelling of adipose tissue

4.1 Introduction 145

4.2 Prx1-Cre labelling of subcutaneous white adipose tissue 146
4.2.1 Prx1-Cre labelling of adult mature subcutaneous adipocytes 146
4.2.2 Prx1-Cre labelling of cells from the adult

subcutaneous SVF 148
4.2.3 Prx1-Cre labelling of embryonic subcutaneous adipose tissue (E18.5) 154

4.3 Prx1-Cre labelling of visceral white adipose tissue 155
4.3.1 Prx1-Cre labelling of adult mature visceral adipocytes 155
4.3.2 Prx1-Cre labelling of cells from the adult visceral SVF 157

4.4 Lineage tracing using *Prx1-Cre^{ERT2};R26R-mTmG* mice 159
4.4.1 Induction embryonically and analysis at E18.5 159
4.4.2 Induction embryonically/postnatally and analysis at 6 weeks 161
4.4.3 Induction *in vitro* 166

4.5 *Wt1* expressing and Prx1-Cre lineage positive pericardial pre-adipocyte populations overlap 168
4.5.1 *Wt1* expressing and Prx1-Cre lineage positive pericardial pre-adipocytes 168
4.5.2 Comparing behaviour of pericardial pre-adipocyte populations *in vitro* 171
4.5.3 Developmental origins of Prx1-Cre lineage positive cells ... 174

4.6 Discussion 177

Chapter 5: *Wt1* deletion in the Prx1-Cre lineage

5.1 Introduction 184

5.2 *Prx1$^{Cre/+}$;Wt1$^{loxP/loxP}$* mice have diaphragmatic hernias 184

5.3 PPF development is disrupted in *Prx1$^{Cre/+}$;Wt1$^{loxP/loxP}$* embryos ... 191

5.4 Prx1-Cre labelling of the developing diaphragm 194

5.5 PPF development is disrupted in *Prx1$^{Cre/+}$;Wt1$^{GFP/loxP}$* embryos ... 196

5.6 Muscle fibre orientation is altered in *Prx1$^{Cre/+}$;Wt1$^{loxP/loxP}$* embryos 197

5.7 Investigating the molecular mechanisms responsible for disrupted diaphragm development 199

5.8 Discussion 207

Chapter 6: Discussion

6.1 Introduction 215

6.2 Assessing the functional consequences of APC heterogeneity ….. 215
6.2.1 $Wt1^+$ and $Wt1^-$ APC behaviour *in vitro* ……... 215
6.2.2 Transcriptomic analysis of $Wt1^+$ and $Wt1^-$ APC populations 217
6.2.3 The effect of a HFD $Wt1^+$ and $Wt1^-$ APCs …….. 219
6.2.3.1 Transcriptomic analysis of $Wt1^+$ and $Wt1^-$ APCs from HFD fed mice …… 221

6.3 Prx1-Cre labelling of white adipose tissue …….. 223
6.3.1 Investigating the origin of subcutaneous white adipose tissue …… 224
6.3.2 Prx1-Cre labelling of pericardial visceral white adipose tissue …… 226

6.4 *Prx1*$^{Cre/+}$;*Wt1*$^{loxP/loxP}$ mice have diaphragmatic hernias ……. 228
6.4.1 WT1 and the diaphragm …….. 228
6.4.2 *Wt1* deletion in the PPFs ……. 229
6.4.3 Investigating causative mechanisms for disrupted diaphragm development ……... 230

6.5 Conclusion ……. 232

References …….. 233

Appendix

Appendix 1: Flow cytometry plots for gating strategies ……..... 260

Appendix 2: Flow cytometry plots for gating strategies using antibody stained cells …….. 261

Appendix 3: Flow cytometry plots for single-stained controls …… 262

Appendix 4: Genes downregulated in $Wt1^+$ Lin^-;$CD31^-$;$CD29^+$;$CD34^+$ cells from HFD-fed mice ……. 263

Appendix 5: Genes downregulated in $Wt1^-$ Lin^-;$CD31^-$;$CD29^+$;$CD34^+$ cells from HFD-fed mice ……. 264

Appendix 6: Genes upregulated in $Wt1^+$ Lin^-;$CD31^-$;$CD29^+$;$CD34^+$ cells from HFD-fed mice ……. 267

Appendix 7: Genes upregulated in $Wt1^-$ Lin^-;$CD31^-$;$CD29^+$;$CD34^+$ cells from HFD-fed mice ……. 268

Appendix 8: Flow cytometry plots for lineage panel stained cells …. 270

Appendix 9: GFP expression in limb buds of *Prx1-Cre*^{ERT2}; *R26R-mTmG* E14.5 embryos, tamoxifen dosed at E11.5 ……. 271

List of Figures

Chapter 1

Figure 1.1.	Overview of the human and murine adipose tissue depots	4
Figure 1.2.	The pericardial membrane and visceral heart fat	6
Figure 1.3.	A schematic representation depicting how adipocyte progenitor cells and pre-adipocytes can be isolated from the SVF	11
Figure 1.4.	An illustration of the cascade leading to the terminal differentiation of adipocytes	13
Figure 1.5.	The *WT1* locus which encodes at least 36 isoforms is found on chromosome 11 (band p13)	31
Figure 1.6.	The cyclical behaviour of EMT and MET	33
Figure 1.7.	The origins of murine adipose tissue types	40
Figure 1.8.	WT1 is necessary for the maintenance of homeostasis in adult tissues	42
Figure 1.9.	The adult diaphragm	49

Chapter 2

Figure 2.1.	Representative images of cells analysed using Definiens® software	67
Figure 2.2.	The 96 genes were replicated 4 times on each RealTime ready Custom Plate	75

Chapter 3

Figure 3.1.	*In vivo Wt1* mRNA expression	81
Figure 3.2.	GFP^+ ($Wt1^+$) cells differentiate into adipocytes more readily than GFP^- ($Wt1^-$) cells, when cultured separately	81
Figure 3.3.	GFP^+ ($Wt1^+$) APCs differentiate into adipocytes more readily than GFP^- ($Wt1^-$) APCs, when cultured separately	83
Figure 3.4.	GFP^+ ($Wt1^+$) pre-adipocytes differentiate into adipocytes more readily than GFP^- ($Wt1^-$) pre-adipocytes, when cultured separately	84
Figure 3.5.	GFP^+ ($Wt1^+$) APC and GFP^- ($Wt1^-$) APC populations are not apoptotic *in vitro*	87
Figure 3.6.	GFP^+ ($Wt1^+$) APCs are more proliferative than GFP ($Wt1^-$) APCs when cultured separately	88
Figure 3.7.	GFP^+ ($Wt1^+$) APCs are more proliferative than GFP ($Wt1^-$) APCs when cultured together	89

Figure 3.8.	The percentage of WT1 expressing APCs from *CAGG*$^{CreER/+}$;*Wt1*$^{loxP/loxP}$ mice is significantly reduced when cultured in the presence of 4-OH tamoxifen	92
Figure 3.9.	The percentage of KI67 expressing APCs from *CAGG*$^{CreER/+}$;*Wt1*$^{loxP/loxP}$ mice is unchanged when *Wt1* is deleted	93
Figure 3.10.	The percentage of KI67 expressing APCs from *CAGG*$^{CreER/+}$ (Cre control) mice is not significantly different when cultured in the presence of 4-OH tamoxifen	95
Figure 3.11.	GFP$^-$ (Wt1$^-$) APCs are more adipogenic when cultured in media conditioned by GFP$^+$ (Wt1$^+$) APCs	97
Figure 3.12.	qRT-PCR validation of genes with upregulated expression in Wt1$^+$ cells, as identified by microarray analysis	103
Figure 3.13.	Mice fed a HFD over 17 weeks become significantly heavier than mice fed a CD	107
Figure 3.14.	The percentage of GFP$^+$ (Wt1$^+$) cells in the SVF of *Wt1*$^{GFP/+}$ knock-in mice is lower for the HFD fed mice than for the CD fed mice	107
Figure 3.15.	A HFD changes the percentages of cells in the different populations that make up the SVF and the percentages of GFP$^+$ (Wt1$^+$) cells in these different populations	109
Figure 3.16.	The breakdown of 451 differential gene expression changes comparing mice fed a HFD and mice fed a CD	113
Figure 3.17.	qRT-PCR validation of *Wt1* mRNA expression in GFP$^+$ (Wt1$^+$) and GFP$^-$ (Wt1$^-$) Lin$^-$;CD31$^-$;CD29$^+$;CD34$^+$ perigonadal SVF cells from HFD and CD mice	118
Figure 3.18.	qRT-PCR validation of genes downregulated in Lin$^-$;CD31$^-$;CD29$^+$;CD34$^+$ perigonadal GFP$^+$ (Wt1$^+$) cells in the HFD state, as identified by microarray analysis	119
Figure 3.19.	qRT-PCR validation of genes downregulated in Lin$^-$;CD31$^-$;CD29$^+$;CD34$^+$ perigonadal GFP$^-$ (Wt1$^-$) cells in the HFD state, as identified by microarray analysis	122
Figure 3.20.	qRT-PCR validation of genes upregulated in Lin$^-$;CD31$^-$;CD29$^+$;CD34$^+$ perigonadal GFP$^+$ (Wt1$^+$) cells in the HFD state, as identified by microarray analysis	125
Figure 3.21.	qRT-PCR validation of genes upregulated in Lin$^-$;CD31$^-$;CD29$^+$;CD34$^+$ perigonadal GFP$^-$ (Wt1$^-$) cells in the HFD state, as identified by microarray analysis	126
Figure 3.22.	The percentage of GFP$^+$ cells in the SVF of male *Wt1*^{CreERT2};*R26R-mTmG* mice is lower for the HFD fed mice than for the CD fed mice	129
Figure 3.23.	A HFD affects the percentage of GFP$^+$ cells in the different populations that make up the SVF of visceral adipose tissue depots from male *Wt1*^{CreERT2};*R26R-mTmG* mice	130

Figure 3.24. *Wt1* expressing cells in male *Wt1^{CreERT2};R26R-mTmG* pups contribute to mature adipocytes in the visceral adipose depots of adult mice, fed either normal or high fat chow 132

Chapter 4

Figure 4.1. Prx1-Cre labels mature adipocytes in the subcutaneous white adipose tissue of 6 week old *Prx1-Cre;R26R-mTmG* male and female mice 147

Figure 4.2. Prx1-Cre labels adipocyte precursor cells in the subcutaneous white adipose tissue of 6 week old *Prx1-Cre;R26R-mTmG* male and female mice 149

Figure 4.3. GFP positive Lin$^+$CD31$^+$ cells from the subcutaneous SVF of *Prx1-Cre;R26R-mTmG* mice are predominantly macrophages and endothelial cells 153

Figure 4.4. Prx1-Cre labels subcutaneous adipose tissue of E18.5 *Prx1-Cre;R26R-mTmG* mouse embryos 154

Figure 4.5. Prx1-Cre labels mature adipocytes in pericardial white adipose tissue of 6 week old *Prx1-Cre;R26R-mTmG* male and female mice 156

Figure 4.6. Prx1-Cre labels adipocyte precursor cells in the pericardial white adipose tissue of 6-week old *Prx1-Cre;R26R-mTmG* male and female mice 158

Figure 4.7. Subcutaneous adipose tissue of E18.5 *Prx1-Cre^{ERT2};R26R-mTmG* mouse embryos induced *in vivo* at E9.5 has more eGFP labelled cells than that from those induced at E11.5 160

Figure 4.8. Subcutaneous adipose tissue from 6 week old *Prx1-Cre^{ERT2};R26R-mTmG* mice tamoxifen dosed at either E11.5, E13.5 or postnatally (P0-P21) has low numbers of eGFP labelled cells 162

Figure 4.9. Visceral adipose tissue from 6 week old *Prx1-Cre^{ERT2};R26R-mTmG* mice induced *in vivo* at either E11.5, E13.5 or postnatally has no eGFP labelled cells 164

Figure 4.10. SVF cells from subcutaneous and pericardial white adipose tissue of adult *Prx1Cre^{ERT2};R26R-mTmG* mice do not become eGFP positive when induced *in vitro* 167

Figure 4.11. A proportion of *Wt1* expressing pericardial pre-adipocytes are labelled with Prx1-Cre 170

Figure 4.12. Prx1-Cre lineage positive and Prx1-Cre lineage negative *Wt1* expressing pericardial pre-adipocytes behave differently *in vitro* 173

Figure 4.13. Cells of the somatic lateral plate mesoderm (LPM) are Prx1-Cre lineage positive 176

Figure 4.14. The parietal pericardium of the heart is Prx1-Cre lineage positive 176

Chapter 5

Figure 5.1.	E19.5 *Prx1*$^{Cre/+}$;*Wt1*$^{loxP/loxP}$ embryos and P0 *Prx1*$^{Cre/+}$;*Wt1*$^{loxP/loxP}$ pups have diaphragmatic hernias	187
Figure 5.2.	E14.5 *Prx1*$^{Cre/+}$;*Wt1*$^{loxP/loxP}$ embryos have diaphragmatic hernias	188
Figure 5.3.	E16.5 *Prx1*$^{Cre/+}$;*Wt1*$^{loxP/loxP}$ embryos have diaphragmatic hernias	188
Figure 5.4.	The percentage of diaphragmatic hernias in different locations in *Prx1*$^{Cre/+}$;*Wt1*$^{loxP/loxP}$ embryos/pups aged E14.5 and older	191
Figure 5.5.	E11.5 *Prx1*$^{Cre/+}$;*Wt1*$^{GFP/loxP}$ embryos have disrupted PPF formation	192
Figure 5.6.	E12.5 *Prx1*$^{Cre/+}$;*Wt1*$^{loxP/loxP}$ embryos have disrupted PPF formation	193
Figure 5.7.	The PPFs, but not the PHMP, are Prx1-Cre lineage positive	195
Figure 5.8.	*Wt1* deletion in the PPFs causes disrupted PPF development in *Prx1*$^{Cre/+}$;*Wt1*$^{GFP/loxP}$ embryos	197
Figure 5.9.	E16.5 *Prx1*$^{Cre/+}$;*Wt1*$^{GFP/loxP}$ embryos have thickened diaphragms and disrupted muscle fibre orientation	199
Figure 5.10.	Wt1 deletion in the PPFs does not affect VIM or CDH1 expression in *Prx1*$^{Cre/+}$;*Wt1*$^{GFP/loxP}$ embryos	202
Figure 5.11.	Wt1 deletion in the PPFs does not affect proliferation in *Prx1*$^{Cre/+}$;*Wt1*$^{GFP/loxP}$ embryos	203
Figure 5.12.	The PPFs of *Prx1*$^{Cre/+}$;*Wt1*$^{GFP/loxP}$ embryos exhibit increased RALDH2 expression compared to *Prx1*$^{+/+}$;*Wt1*$^{GFP/loxP}$ littermate controls	205
Figure 5.13.	The PPFs of *Prx1*$^{Cre/+}$;*Wt1*$^{GFP/loxP}$ embryos exhibit decreased b-catenin expression at cell membranes compared to *Prx1*$^{+/+}$;*Wt1*$^{GFP/loxP}$ littermate controls	206

List of Tables

Chapter 1

Table 1.1.	Overview of the mouse models that have been used to investigate WAT origin, development, homeostasis and expansion	18

Chapter 2

Table 2.1.	Processing conditions and timings for embedding adipose tissue and mouse embryos using a Tissue-Tek VIP® Jr. Vacuum Infiltration Processor	63
Table 2.2.	Antibody information	64
Table 2.3.	Flow cytometry antibody information	69
Table 2.4.	Primer and probe information for each gene used in qRT- PCR	74
Table 2.5.	Cycling conditions for qRT-PCR	74

Chapter 3

Table 3.1.	Enriched DAVID GO terms for genes upregulated in $Wt1^+$ cells (q-value <0.05)	100
Table 3.2.	Enriched DAVID GO terms for genes upregulated in $Wt1^+$ cells (q-value <0.05, LogFC >1.5)	100
Table 3.3.	All genes upregulated in $Wt1^+$ cells with q-value <0.05 and LogFC >1.5	101
Table 3.4.	Enriched DAVID GO terms for genes downregulated in $Wt1^+$ cells (q-value <0.05)	105
Table 3.5.	Enriched DAVID GO terms for genes downregulated in $Wt1^+$ cells (q-value <0.05, LogFC <-1.5)	105
Table 3.6.	Enriched GOrilla GO terms of genes upregulated in $Lin^-;CD31^-;CD29^+;CD34^+$ perigonadal SVF cells from mice fed a HFD (q-value <0.05)	114
Table 3.7.	Enriched DAVID GO terms of genes upregulated in $Lin^-;CD31^-;CD29^+;CD34^+$ perigonadal SVF cells from mice fed a HFD (q-value <0.05, LogFC >1.5)	114
Table 3.8.	Enriched GOrilla GO terms of genes downregulated in $Lin^-;CD31^-;CD29^+;CD34^+$ perigonadal SVF cells from mice fed a HFD (q-value <0.05)	115
Table 3.9.	Enriched DAVID GO terms of genes downregulated in $Lin^-;CD31^-;CD29^+;CD34^+$ perigonadal SVF cells from mice fed a HFD (q-value <0.05, LogFC <-1.5)	115
Table 3.10.	Enriched DAVID GO terms of genes downregulated in	116

	$Wt1^{+}$ Lin^{-};$CD31^{-}$;$CD29^{+}$;$CD34^{+}$ perigonadal SVF cells from mice fed a HFD (q-value <0.05, LogFC <-1.5)	
Table 3.11.	Enriched DAVID GO terms of genes downregulated in $Wt1^{-}$ Lin^{-};$CD31^{-}$;$CD29^{+}$;$CD34^{+}$ perigonadal SVF cells from mice fed a HFD (q-value <0.05, LogFC <-1.5)	117
Table 3.12.	Enriched DAVID GO terms of genes upregulated in $Wt1^{-}$ Lin^{-};$CD31^{-}$;$CD29^{+}$;$CD34^{+}$ perigonadal SVF cells from mice fed a HFD (q-value <0.05, LogFC >1.5)	117

Chapter 5

Table 5.1.	The number of $Prx1^{Cre/+};Wt1^{loxP/loxP}$ embryos obtained at each developmental stage, compared to the expected number	185
Table 5.2.	Phenotype and image information for the $Prx1^{Cre/+};Wt1^{loxP/loxP}$ embryos/pups at all developmental stages	190

Abbreviations

APC	adipocyte precursor cell
ASC	adipose stem cell
ATP	adenosine triphosphate
BAT	brown adipose tissue
bp	base pair
BrdU	bromodeoxyuridine
BSA	bovine serum albumin
CD	control diet
CDH	congenital diaphragmatic hernia
cDNA	complementary deoxyribonucleic acid
cRNA	complementary ribonucleic acid
DAPI	4',6-diamidino-2-phenylindole
dH_2O	deionised water
DMEM	Dulbecco's modified Eagle medium
DNA	deoxyribonucleic acid
dNTP	deoxynucleotide triphosphate
DXM	dexamethasone
E	embryonic stage
EDTA	ethylene diamine tetraacetic acid
EMT	epithelial-to-mesenchymal transition
EPDCs	epicardial derived cells
ER	oestrogen receptor
ERT	oestrogen receptor tamoxifen inducible
EtOH	ethanol
FACS	fluorescence activated cell sorting
FCS	foetal calf serum
FDR	false discovery rate
g	gram
(e)GFP	(enhanced) green fluorescence protein
GO	gene ontology
HFD	high fat diet
HGU	human genetics unit
H&E	haematoxylin and eosin
IBMX	3-isobutyl 1-methylxanthine
LPM	lateral plate mesoderm

Lin	lineage
LogFC	log fold change
M	molar
MET	mesenchymal-to-epithelial transition
mg	milligram
ml	millilitre
mm	millimetre
mRNA	messenger ribonucleic acid
MSC	mesenchymal stem cell
µg	microgram
µl	microlitre
µM	micromolar
µm	micrometre
PBS	phosphate buffered saline
PFA	paraformaldehyde
PHMP	post hepatic mesenchymal plate
PPF	pleuroperitoneal fold
qRT-PCR	quantitative realtime polymerase chain reaction
(td)RFP	(tandem dimer) red fluorescent protein
RNA	ribonucleic acid
SEM	standard error of the mean
ST	septum transversum
SVF	stromal vascular fraction
SWAT	subcutaneous white adipose tissue
VWAT	visceral white adipose tissue
WAT	white adipose tissue
YFP	yellow fluorescent protein

Gene/mRNA symbols are italicised. Lowercase for mouse (i.e. *Wt1*) and uppercase for human (i.e. *WT1*).

Protein symbols are capitalised but not italicised, for both human and mouse (i.e. WT1).

Chapter 1

Introduction

1.1 Adipose tissue overview

1.1.1 Adipose tissue types and depots

Over the last few decades, research into the biology of adipose tissue has increased considerably, largely due to the ongoing global obesity epidemic. According to the World Health Organisation, 39% of adults were overweight and 13% were obese in 2014, meaning that worldwide obesity has doubled since 1980. Obesity is a major risk factor for numerous diseases, including cardiovascular disease, type II diabetes and certain cancers. Therefore, this global increase in obesity is a major public health concern (Berry, Jeffery and Rodeheffer, 2014; WHO, 2015). However, it is only in the last 70 years that adipose tissue has been appreciated as a complex endocrine organ, with an extensive role in nutrient homeostasis, rather than as a form of connective tissue (Rosen and Spiegelman, 2014). A major focus of the advancing research has been on uncovering the mechanisms responsible for controlling adipose tissue development, distribution, homeostasis and expansion (Sanchez-Gurmaches and Guertin, 2014a).

Mammalian adipose tissue is traditionally divided into two distinct types: white adipose tissue (WAT) and brown adipose tissue (BAT). Both forms have a role in the maintenance of energy balance, however they assume contrasting functions (Billon and Dani, 2012). The bulk of WAT comprises large unilocular adipocytes, and it primarily acts to store and mobilise triglycerides (Billon and Dani, 2012; Rosen and Spiegelman, 2014). The predominant function of BAT, on the other hand, is to burn chemical energy (such as fatty acids and glucose) to produce heat, a process known as adaptive (non-shivering) thermogenesis (Wang and Seale, 2016). Brown adipocytes are multilocular and are packed with mitochondria, it is the iron within the mitochondria that gives the tissue its characteristic colour (Wu, Jun and McDermott, 2015). They express high levels of uncoupling protein-1 (UCP-1), which is localised to the inner mitochondrial membrane and required for the uncoupling of ATP synthesis and respiration, via catalysis of a proton leak across the membrane, thus permitting energy expenditure in the form of heat (Fedorenko, Lishko and Kirichok, 2012; Wang and Seale, 2016). BAT is highly vascularised, giving the depots a rich nutrient and

oxygen supply, and permitting distribution of the generated heat (Billon and Dani, 2012; Rosen and Spiegelman, 2014).

Unlike BAT, WAT is highly capable of significant expansion, which can occur through both an increase in adipocyte size (hypertrophy) and number (hyperplasia or adipogenesis) (Hausman *et al.*, 2001; Joe *et al.*, 2009; Billon and Dani, 2012; Wang *et al.*, 2013). It is this expansion, which can lead to excess WAT, that is linked to obesity and associated metabolic diseases (Billon and Dani, 2012). Genetics and obesogenic stimuli do influence the extent to which WAT expands by hypertrophy and/or hyperplasia, however the intrinsic mechanisms responsible for the regulation of adipocyte number and size *in vivo* remain largely unknown (Berry, Jeffery and Rodeheffer, 2014). Moreover, as an endocrine organ WAT secretes multiple adipokines with numerous modes of action. For example, leptin (perhaps the most famous adipokine), functions in the control of eating behaviour, whilst adiponectin acts to increase insulin sensitivity. Much ongoing work is focused on understanding the autocrine, paracrine and endocrine functions of adipose tissue (Giralt, Cereijo and Villarroya, 2016).

WAT is further divided into two distinct types: subcutaneous WAT (SWAT), which is found under the skin, and visceral WAT (VWAT), which is located within the body cavity, surrounding the major organs (Cinti, 2005). Whilst SWAT or “good fat” is harmless, and even protective, excess VWAT or “bad fat” is principally associated with metabolic syndrome and is a large risk factor for the various obesity-associated pathologies (Bergman *et al.*, 2006; Wajchenburg, 2014). Understanding exactly how the expansion of WAT is regulated at the different locations is critical if we are to resolve how this expansion causes and influences metabolic disease (Berry, Jeffery and Rodeheffer, 2014).

SWAT and VWAT are subdivided into multiple distinct depots, or fat pads. Mice have six identifiable VWAT depots, these include the perigonadal depot, which is located around the gonads and known as epididymal in males and periovarian in females; the mesenteric depot, surrounding the intestines; the omental depot, next to the stomach;

the perirenal depot, around the kidneys; the retroperitoneal depot, behind the kidneys at the back of the peritoneal cavity and the pericardial depot, adjacent to the heart (Cinti, 2005). SWAT is also divided into anterior and posterior depots, with the latter being the most commonly dissected, and also known as inguinal SWAT (Cinti, 2005). In humans the depots are similarly named and located, however they differ in size considerably. By far the largest and most commonly studied human VWAT depots are the omental and mesenteric, (which are often considered as one entity), whilst in mice the omental depot is amongst the smallest. However, the perigonadal depot, which is one of the largest murine VWAT depots, has not been described in humans. Additionally, human and murine SWAT depots differ in location. Whilst mice have anterior and posterior SWAT depots, the two major human SWAT depots are located in the abdominal and gluteofemoral regions (Chusyd *et al.*, 2016). An overview of the different human and murine depots is presented in Figure 1.1.

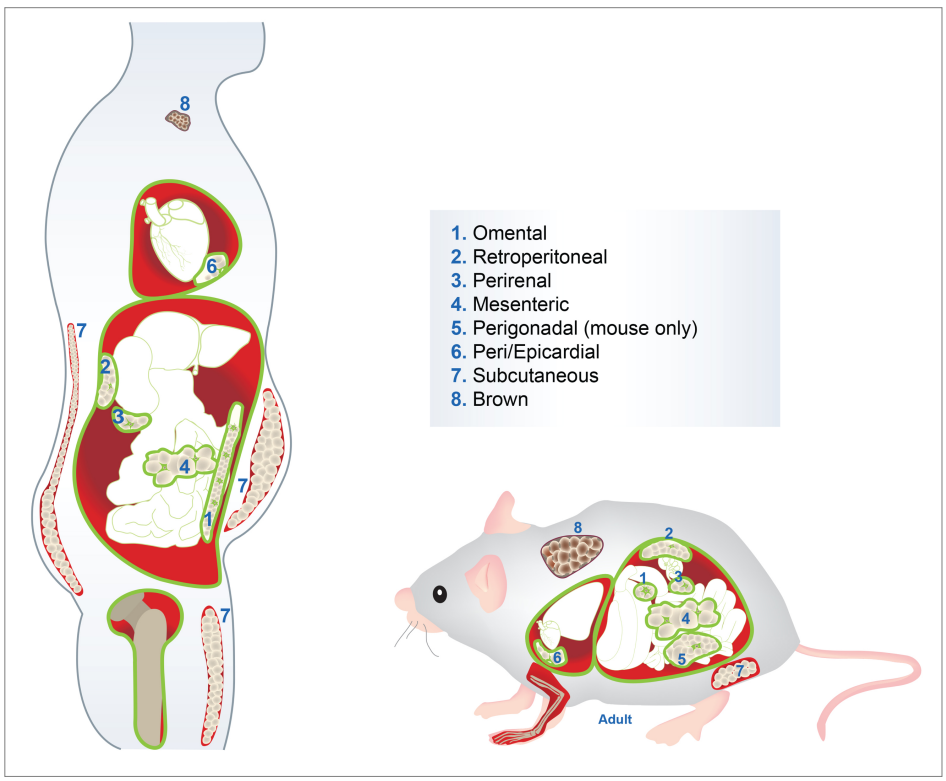


Figure 1.1. Overview of the human and murine adipose tissue depots. *Depots 1-6 depict the visceral white adipose tissue (VWAT), there is no perigonadal depot in humans (5). The subcutaneous white adipose tissue (SWAT) is illustrated by depot 7; abdominal, gluteal and femoral in human and inguinal in mouse. The brown adipose tissue (BAT) is shown in depot 8. (Cleal, Aldea and Chau, 2017).*

Regarding the VWAT located in and around the heart, the description above is simplified, because in fact there are two distinct depots: the pericardial and the epicardial (Iacobellis, 2009). Surrounding the heart is the pericardial membrane, which consists of three layers: an outer fibrous layer (the fibrous pericardium), and two inner layers (the serous pericardium). The innermost serous layer, or the epicardium (also known as the visceral pericardium), is attached to the heart, whilst the outermost serous layer, or the parietal pericardium, is attached to the outer fibrous pericardium. Serous fluid, which protects the heart, is located within the pericardial cavity between the epicardium and parietal pericardium (Rene Rodriguez and Tan, 2017). Importantly, the epicardial fat resides between the outer wall of the heart muscle (the myocardium) and the epicardium, so directly abuts the heart myocardium. However, the pericardial fat is found outside the epicardium, on the external surface of the parietal pericardium, so not in direct contact with the heart (Iacobellis, 2009). Figure 1.2 illustrates the described composition and structure of the pericardial membrane and the location of the epicardial and pericardial fat depots. Until recently it was generally accepted that mice do not have epicardial fat, only pericardial (Yamaguchi *et al.*, 2015). Moreover, it is not uncommon that the terms epicardial and pericardial are used interchangeably to mean the same depot. However, recent studies have shown that mice do have epicardial adipose tissue, which is located in the atrial-ventricular groove (Liu *et al.*, 2014; Yamaguchi *et al.*, 2015). Furthermore, during development, a proportion of the epicardial adipocytes differentiate from cells of the epicardium. Interestingly, lineage tracing studies have also revealed that following myocardial infarction, epicardial adipocytes that form in the injured heart are derived from the epicardial cells. However, during normal adult heart homeostasis, this is not that case, and no new epicardial adipocytes arise from the epicardium (Liu *et al.*, 2014). However, this murine depot is very small, and therefore the pericardial depot is still the most commonly utilised and studied.

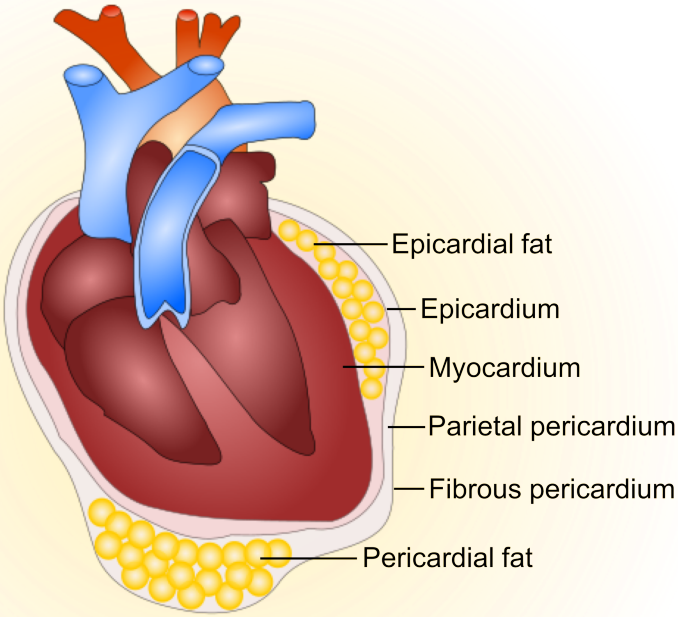


Figure 1.2. The pericardial membrane and visceral heart fat. *The heart is encased in the pericardial membrane, which is composed of the fibrous pericardium, the parietal pericardium and the epicardium. Epicardial adipose tissue is located between the myocardium of the heart and the epicardium, the pericardial fat lies outside the epicardium, on the external surface of the parietal pericardium. (Adapted from Iacobellis, 2015)*

Within the last ten years a third form of adipose tissue has been characterised in rodents. Beige or brite (brown in white) adipocytes are located within WAT depots, however, as the name suggests, they are morphologically and functionally comparable to brown adipocytes (Petrovic *et al.*, 2010; Wang and Yang, 2017). For example, they express a number of key BAT specific genes, such as the master regulator of thermogenesis; *Ucp-1*, and consequently are thermogenic (Wu, Jun and McDermott, 2015; Wang and Yang, 2017). Both visceral and subcutaneous WAT depots have been shown to harbour thermogenic adipocytes, and originally in SWAT they were called beige, whilst in VWAT they were termed brite, although the two terms are often used interchangeably (Wang and Yang, 2017). However, SWAT is more susceptible to browning. The process of browning and the recruitment of beige adipocytes typically occurs in response to certain stimuli, particularly exposure to the cold (Rosenwald *et al.*, 2013; Wang and Seale, 2016; Wang and Yang, 2017). Conversely, the opposite

process has been demonstrated using lineage tracing in mouse models, whereby following warm adaptation for five weeks, cold-induced beige adipocytes were converted into cells which appeared morphologically and molecularly akin to white adipocytes (Rosenwald *et al.*, 2013). Moreover, whilst it is commonly accepted that cold-induced beige adipocytes are generated through the de-novo differentiation of precursor cells, increasing evidence from murine studies indicates that they can also arise through the transdifferentiation of mature white adipocytes (Y. H. Lee *et al.*, 2012; Lee and Cowan, 2013; Rosenwald *et al.*, 2013; Wang *et al.*, 2013; Lee *et al.*, 2015; Wang and Yang, 2017).

Multiple factors are thought to influence the development and activation of beige adipocytes, with signals arising from numerous organs and tissues. The central and sympathetic nervous systems, skeletal muscle, the heart and the gastrointestinal tract have all been suggested to play a role (Wang and Yang, 2017). Notably, one study that used genetic manipulation to significantly increase the number of beige adipocytes in mice, demonstrated that such an increase can protect against obesity, making this a compelling area of research (Seale *et al.*, 2011). Whilst beige adipocytes are similar to brown, they do have a distinct gene expression signature, thus permitting the identification of true brown adipocytes versus beige. Consequently, using murine markers of beige adipocytes, it has been shown that in humans, depots which have traditionally been classified as BAT, do in fact resemble murine beige adipose tissue more closely than traditional brown fat, therefore suggesting that beige adipocytes do exist in humans (Sharp *et al.*, 2012; Wu *et al.*, 2012). The focus of my PhD project has been on WAT, therefore BAT and beige fat will not be discussed in detail going forward.

1.1.2 Adipocyte precursor cells (APCs)

WAT is composed of a variety of cell types, and whilst the majority of its volume and mass can be attributed to the large, lipid-filled mature adipocytes, in terms of cell number these adipocytes account for less than half (Church, Berry and Rodeheffer, 2014). The rest of the cells comprise the stromal vascular fraction (SVF), which includes haematopoietic, endothelial, mesenchymal and other un-defined stromal

cells. Crucially, adipocyte precursor cells (APCs) also reside within the SVF. This was first discovered when culturing the heterogeneous SVF led to the generation of lipid-filled adipocytes *in vitro* (Ng *et al.*, 1971; Church, Berry and Rodeheffer, 2014). The presence of these APCs is essential for the development, homeostasis and expansion of WAT. Mature adipocytes are terminally differentiated and post-mitotic, therefore the formation of new adipocytes from the WAT-resident precursor cells is fundamental both for the replacement of dying adipocytes during adulthood, as well as for the expansion of adipose tissue depots in obesity (Herberg *et al.*, 1974; Spalding *et al.*, 2008; Arner *et al.*, 2010; Church, Berry and Rodeheffer, 2014). Despite the on-going turnover of adipocytes in adult WAT, their number is carefully regulated and maintained. Any disruption to this must be a consequence of an imbalance between adipogenesis and adipocyte death. Henceforth, a thorough understanding of the adipocyte lineage is essential if we are to fully appreciate the mechanisms implicated in the homeostasis and expansion of WAT (Berry and Rodeheffer, 2013).

In 1964 Rodbell developed a method by which rodent WAT could be digested to permit the isolation and culture of mature adipocytes *in vitro* (Rodbell, 1964). Following this, as detailed above, Ng *et al*. (1971) cultured human SVF cells and showed that this heterogeneous population of cells was capable of differentiating into lipid-filled adipocytes (Ng *et al.*, 1971). These initial studies paved the way for what is now commonly practiced in hundreds of labs worldwide. The APCs, which are often referred to as adipose stem cells (ASCs), are a major focus for much research, both due to their potential applications in regenerative medicine, but also because understanding the properties of these cells is essential if we are to better understand obesity, how it develops, and potentially what interventions may be suitable.

Traditionally, ASCs have been isolated simply by culturing the entire SVF. The adherent cells from this population are classed as the ASCs, and can be expanded for further studies. Adipose stem/precursor cells are in fact mesenchymal stem cells (MSCs) that are resident in adipose tissue and are capable of *in vitro* differentiation into the major mesenchymal lineages: osteoblasts, chondrocytes, adipocytes and skeletal myocytes (Zuk *et al.*, 2002; Gimble, Katz and Bunnell, 2007). Interestingly,

adipose tissue is an abundant source of MSCs, with ASCs accounting for ~3% of the SVF, compared to the frequency of MSCs in bone-marrow which is ~0.002% (Baer, 2014). Given that one of the major criteria for identifying MSCs is that they should adhere to plastic (Dominici *et al.*, 2006), the isolation of ASCs from human (and rodent) adipose tissue using this method has long been considered sufficient. However, much work has shown that even after multiple rounds of passage, this adherent ASC population is highly heterogeneous (Zuk *et al.*, 2002; Mitchell *et al.*, 2006; Berry, Jeffery and Rodeheffer, 2014). Additionally, it has been demonstrated that the majority of the differentiation that occurs towards a particular lineage *in vitro,* is the result of a few sub-populations of cells, rather than the entire adherent population (Mitchell *et al.*, 2006). Moreover, when transplanted into mice, the adherent ASC populations are apparently no longer capable of multi-lineage differentiation, and are unable to form adipocytes (Zheng *et al.*, 2006). Therefore, given these findings, it would seem that selection by adherence is not the optimal method for isolating ASCs and understanding the *in vivo* adipocyte cell lineage (Berry, Jeffery and Rodeheffer, 2014).

Recent studies have utilised multicolour flow cytometry and fluorescence activated cell sorting (FACS) to identify and enrich for adipogenic populations from different tissues (Joe *et al.*, 2010; Uezumi *et al.*, 2010; Festa *et al.*, 2011; Berry and Rodeheffer, 2013). Two particularly influential studies from Rodeheffer *et al*. (2008) and Berry & Rodeheffer (2013) identified populations of adipocyte progenitor cells and pre-adipocytes in the adult murine WAT SVF (Rodeheffer, Birsoy and Friedman, 2008; Berry and Rodeheffer, 2013). Currently there is no single marker that permits the characterisation and separation of these cells from the non-adipogenic fraction of the SVF, therefore a panel of cell-surface markers has been utilised (Berry, Jeffery and Rodeheffer, 2014). Two subpopulations of cells within the SVF, which both lacked expression of CD45, CD31 and Ter119 (all blood and endothelial markers), but were both positive for the expression of CD29, CD34 and Sca-1 (mesenchymal and stem cell markers) were identified (Rodeheffer, Birsoy and Friedman, 2008). Crucially, both populations were demonstrated to be highly adipogenic *in vitro* and express platelet-derived growth factor receptor alpha (*Pdgfrα)*; a known marker of the

adipocyte precursor cell lineage (although not exclusively an adipocyte precursor cell marker) (Berry and Rodeheffer, 2013).

The two populations differed in their expression of CD24. In addition to being adipogenic *in vitro,* the $CD45^{-};CD31^{-};Ter119^{-};CD29^{+};CD34^{+};Sca\text{-}1^{+};CD24^{+}$ cells (known as adipocyte progenitor cells), were also capable of developing into completely functional WAT depots when transplanted into lipodystrophic mice. Conversely, the $CD45^{-};CD31^{-};Ter119^{-};CD29^{+};CD34^{+};Sca\text{-}1^{+};CD24^{-}$ cells (or pre-adipocytes), whilst being adipogenic *in vitro*, were not able to form WAT depots *in vivo* (Rodeheffer, Birsoy and Friedman, 2008). Furthermore, it was also ascertained, using flow cytometry, that the $CD24^{-}$ pre-adipocytes were in fact derived from the $CD24^{+}$ progenitor cell population *in vivo*. In support of this it was shown that, prenatally, no $CD24^{-}$ cells were detectable, but a large population of $CD24^{+}$ cells was present and adipogenic *in vitro*. However, postnatally, these ratios shifted, revealing a substantial increase in the amount of $CD24^{-}$ cells, coupled with a reciprocal decrease in the numbers of $CD24^{+}$ cells (Berry and Rodeheffer, 2013). Collectively these findings suggest that the $CD24^{-}$ cells are more committed to the adipocyte lineage. In agreement with this, gene expression analysis of the two populations showed that markers of adipogenesis, such as peroxisome proliferator-activated receptor gamma (*Pparγ2)*, were enriched in the $CD24^{-}$ cells compared to the $CD24^{+}$ cells (Berry and Rodeheffer, 2013). Figure 1.3 is a schematic representation of how the SVF cells can be sorted to obtain adipocyte progenitor cells and pre-adipocytes. Whilst the described cell surface marker profiles allow enrichment of adipocyte progenitor and pre-adipocyte populations from the SVF of mice, such profiles do not currently exist for humans. CD34 has been used for the enrichment of APC populations from human WAT SVF. However, there is no obvious human homolog for Sca-1, therefore suggesting that human APC profiles are not the same as murine (Sengenès *et al.*, 2005; Berry, Jeffery and Rodeheffer, 2014).

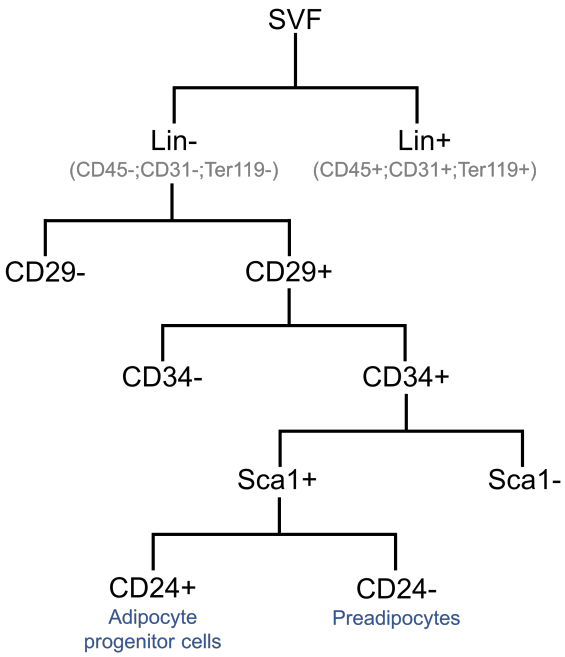


Figure 1.3. A schematic representation depicting how adipocyte progenitor cells and pre-adipocytes can be isolated from the SVF. *(Adapted from Rodeheffer, Birsoy and Friedman, 2008)*

Adipogenesis, the formation of a fat cell from a precursor cell, is a complex and well studied process. A significant amount of research *in vitro* has uncovered the transcriptional regulatory programme required for adipogenesis to occur. However, adipogenesis *in vivo* is less well studied, and thus it is unknown as to whether the processes exactly reflect those that occur *in vitro* (Berry, Jiang and Graff, 2016). Adipogenesis involves two key phases: commitment of the cell to the adipocyte lineage, and differentiation of the cell into the mature adipocyte (Cristancho and Lazar, 2011). Commitment has been defined as the process whereby a multipotent cell type undergoes a cell fate decision to convert to the adipocyte lineage (Cristancho and Lazar, 2011). Following commitment, the expression of adipocyte-associated metabolic genes and adipokines is triggered in response to a transcriptional cascade.

The key components of the cascade are PPARγ2, CCAAT/enhancer-binding protein-α (C/EBPα), C/EBPβ and C/EBPδ. Upon the addition of adipogenic stimuli, including cyclic AMP agonists and glucocorticoids, C/EBPβ and C/EBPδ expression is induced.

Committed pre-adipocytes express low levels of C/EBPβ prior to the addition of such stimuli. In these committed pre-adipocytes, C/EBPβ is bound to enhancer regions of *Pparγ2*, and following the addition of adipogenic stimuli, the transcription activation complex (including glucocorticoid receptor (GR), signal transducer and activator of transcription 5A (STAT5A) and retinoid X receptor (RXR)), and a co-activator complex, are recruited to these regions, leading to the expression of PPARγ2. Additionally, cAMP agonists activate the production of an endogenous PPARγ2 ligand (the nature of which is currently unknown) (Cristancho and Lazar, 2011). Several other factors also regulate PPARγ2 expression and activity, these include GATA2 and 3 which inhibit PPARγ2 activation, and transducin-like enhancer protein 3 (TLE3) which is a co-activator of PPARγ2. The target genes of PPARγ2 and C/EBP include fatty acid binding protein 4 (*Fabp4*) and adiponectin (*AdipoQ*); both markers of mature adipocytes. Figure 1.4 illustrates the cascade leading to PPARγ2 activation that occurs during the commitment and terminal differentiation of precursor cells into adipocytes. Many other signalling molecules and factors are also thought to play a role and influence the adipogenic cascade, such as transforming growth factor beta (TGFβ) superfamily members (for example bone morphogenetic protein 2 and 4 (BMP2 and 4)). Conversely, multiple signalling pathways and factors, such as WNT signalling and retinoic acid signalling, are known to block adipogenesis (Cristancho and Lazar, 2011; Berry, Jiang and Graff, 2016). Adipogenesis is therefore a highly complex process, influenced by many elements, with several essential master regulators.

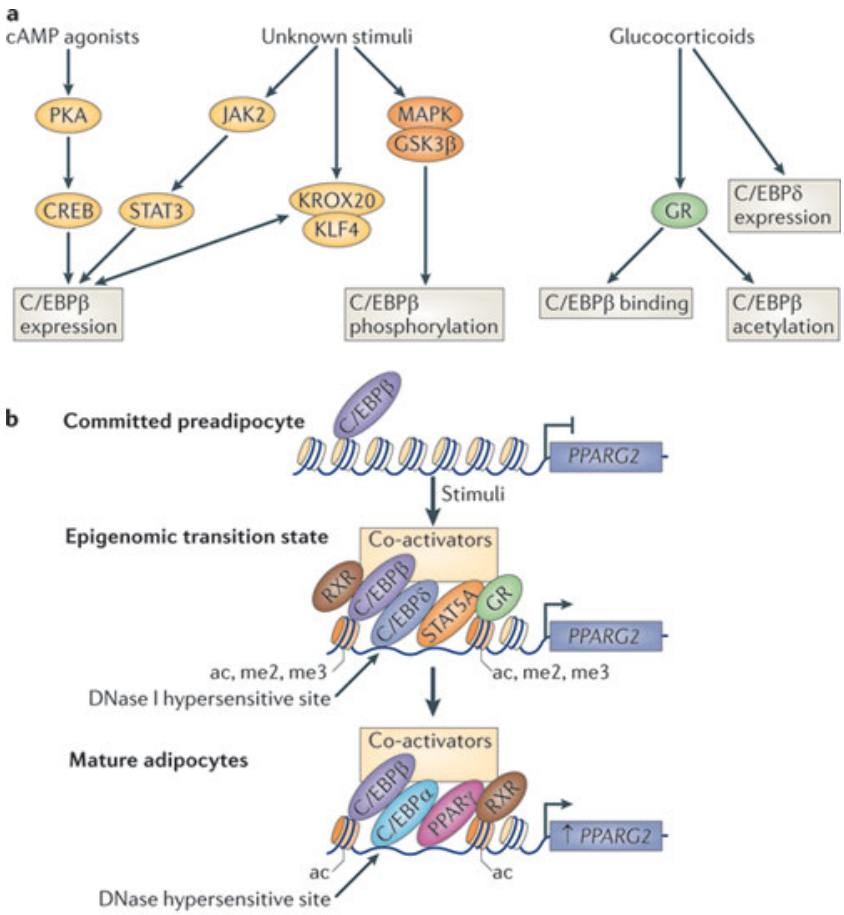


Figure 1.4. An illustration of the cascade leading to the terminal differentiation of adipocytes. *The C/EBPs are activated by various adipogenic stimuli (a). In committed pre-adipocytes C/EBPβ occupies the enhancer regions of Pparγ. When adipogenic stimuli are added, C/EBPβ and C/EBPδ levels increase, resulting in the recruitment of the transcription activation complex and a co-activator complex to the enhancer regions of Pparγ, leading to the expression of PPARγ (b) (Cristancho and Lazar, 2011).*

1.1.3 Adipose tissue development

APCs are necessary for three fundamental aspects of WAT biology. The first is the initial development or organogenesis of WAT, the second is adipose tissue homeostasis, and the third is adipose tissue expansion as a result of external stimuli, such as diet (Berry, Jiang and Graff, 2016). In both mice and humans, WAT is established early in life, however the timing of this establishment varies between the depots (Berry, Jeffery and Rodeheffer, 2014). By postnatal day 1 (P1), mice already possess small lipid-filled adipocytes in the BAT and subcutaneous WAT depots (Birsoy *et al.*, 2011; Han *et al.*, 2011). Leptin-luciferase mice have been used to show that at E16.0, adipocytes begin to form in these depots (Birsoy *et al.*, 2011). However,

in the perigonadal VWAT depot, adipocytes do not start to appear until P4, with organogenesis occurring between approximately P4 and P14 (Han *et al.*, 2011). Mesenteric VWAT is established slightly later, between the second and third weeks of life, whilst retroperitoneal VWAT is intermediate and is formed during pre and postnatal development (Jiang *et al.*, 2014; Berry, Jiang and Graff, 2016). In human SWAT, precursor cells begin to fill with lipid throughout the second trimester. The size and number of adipocytes increases steadily until the twenty-third week of gestation, at which point the number stops increasing and further growth occurs predominantly through hypertrophy. The timing and development of human VWAT is not well understood (Berry, Jeffery and Rodeheffer, 2014; Berry, Jiang and Graff, 2016).

Murine epididymal (male perigonadal) adipocytes develop from and eventually replace a membrane-like epididymal appendage (attached to the epididymis and testis), clustering around blood vessels. When this appendage was excised at P4, mice were unable to develop mature epididymal adipose tissue, even by 1 month of age, therefore indicating that it is essential for the correct development of epididymal VWAT (Han *et al.*, 2011). Moreover, when the SVF cells of the appendage/ epididymal VWAT were cultured, only those isolated from mice older than P7 were capable of forming large numbers of adipocytes *in vitro*. Additionally, various assays have indicated that SVF cells isolated from the epididymal appendage of P4 mice possess many characteristics of MSCs that have not yet committed to the adipose lineage (Han *et al.*, 2011). It has long been known that angiogenesis and adipogenesis have a close temporal and spatial relationship in both murine and human development. The term "primitive fat organ" is often used to describe the vasculature around which mature visceral adipose tissue develops (Crandall, Hausman and Kral, 1997; Berry, Jeffery and Rodeheffer, 2014). As discussed, the epididymal appendage, being fairly separate from surrounding tissues (unlike for the other visceral depots), offers an ideal system in which to study the development and origin of adipose tissue *in vivo* (Han *et al.*, 2011). Work previously performed in our group, which is described in detail in section 1.2.1, took advantage of this system to understand whether *Wt1* expressing cells give rise to visceral adipocytes (Chau *et al.*, 2014). It is evident that WAT organogenesis is

a carefully controlled and timed process. Moreover, the distinct developmental timing of the various depots may imply differing requirements and functions (Berry, Jiang and Graff, 2016).

Regarding the physical growth of WAT during development, the extent to which hypertrophy and hyperplasia contribute to this is not well understood. Nevertheless, several studies in rats have shown that, for perigonadal and retroperitoneal VWAT, both hypertrophy and hyperplasia occur early in postnatal life. However, at about three months of age, the number of adipocytes stops increasing, therefore continued expansion is a consequence of hypertrophy (Hirsch and Han, 1969; Johnson *et al.*, 1971; Greenwood and Hirsch, 1974). A similar result was noted for SWAT, however the initial period of growth by hypertrophy and hyperplasia persisted for longer (approximately 6 months) (Johnson *et al.*, 1971). More recently, the "AdipoChaser" mouse model, which uses the adiponectin promoter and a doxycycline-inducible system to label and trace mature adipocytes, has been used to investigate this further. This has shown that whilst most of the adipocytes in SWAT are formed prenatally, perigonadal VWAT adipocytes form postnatally, but by early adulthood the contribution of hyperplasia to growth is negligible (Wang *et al.*, 2013). Therefore, there are significant temporal differences between SWAT and VWAT in terms of how the depots expand, but for both, hyperplasia and hypertrophy initially contribute to growth, with the former ceasing prior to adulthood. Similar patterns of growth and development have been revealed for other organisms such as birds and fish (Berry, Jeffery and Rodeheffer, 2014). Under normal, non-obese circumstances, the number of adipocytes in adults remains fairly constant, through tight control over the rates of adipogenesis and adipocyte death (Berry, Jeffery and Rodeheffer, 2014). Various lines of evidence support the hypothesis that this critical number is set prior to adulthood. For example, when SWAT was removed from rats before the onset of adulthood, it re-grew to harbour the same number of adipocytes as control animals. However, when a similar experiment was performed in adult animals, there was no re-growth (Kral, 1976; Faust, Johnson and Hirsch, 1977a, 1977b).

Several studies have utilised various transgenic mouse lines and lineage tracing tools to try and understand the developmental origins of the different adipose depots, however this remains one of the least-understood areas of fat biology (Sanchez-Gurmaches, Hung and Guertin, 2016). Knowing the developmental lineages from which adipocytes are derived is essential for a complete understanding of adipose tissue formation. Given the described differences between various adipose depots in the timing of organogenesis, it seems plausible that they may have different embryonic origins (Berry, Jiang and Graff, 2016). The *Myf5-Cre* mouse model has been used to show that a population of Myf5-Cre expressing cells in the paraxial mesoderm give rise to interscapular BAT, but not periaortic BAT (Seale *et al.*, 2008; Sanchez-Gurmaches *et al.*, 2012; Sanchez-Gurmaches and Guertin, 2014b). Interestingly, Myf5-Cre also traces a proportion of retroperitoneal VWAT adipocytes and precursor cells, as well as anterior SWAT, but does not trace perigonadal VWAT, mesenteric VWAT or posterior SWAT. *Pax3-Cre* is another mouse line that labels interscapular BAT, and generally it highlights similar populations as the *Myf5-Cre* line, regarding the WAT depots. However, in contrast to Myf5-Cre, Pax3-Cre also labels approximately 60% of the male perigonadal VWAT adipocytes and precursor cells, but does not trace any female perigonadal VWAT, thus indicating that there are gender-linked differences regarding adipose lineages (Sanchez-Gurmaches and Guertin, 2014b).

Recently, it has emerged that SWAT, but not VWAT can be traced using the *Prx1-Cre* mouse model, raising the possibility that this Cre marks a pool of progenitor cells during development that give rise to SWAT (Sanchez-Gurmaches, Hsiao and Guertin, 2015). Additionally, work from our group has shown that a proportion of the adipocytes in all VWAT depots, but not SWAT or BAT depots, arise from *Wt1* expressing precursor cells, and highlights the mesothelium and thus the lateral plate mesoderm as a source of VWAT. Importantly, *Wt1* is only expressed in the precursor cells and not in mature adipocytes (Chau *et al.*, 2014). These latter two studies shall be discussed in further detail later in the introduction and in chapters 3-4. Therefore, it seems to be the case that the different adipose tissue types do differ in their developmental origin and lineage. However, the picture is far from simple. Evidently,

Myf5-Cre and Pax3-Cre are capable of tracing both white and brown depots, but only distinct subsets of these (Sanchez-Gurmaches *et al.*, 2012; Sanchez-Gurmaches and Guertin, 2014b). Similarly, in addition to SWAT, periaortic BAT can be lineage traced using the *Prx1-Cre* model, and as described, *Wt1* expressing precursor cells give rise to a subset of VWAT adipocytes (the proportion of which varies between the different depots) (Chau *et al.*, 2014; Sanchez-Gurmaches, Hsiao and Guertin, 2015). Therefore, none of these models are capable of exclusively tracing all adipocytes of an individual depot/adipose type.

Pdgfrα-Cre labels all mature adipocytes in both visceral and subcutaneous depots, and given that *Pdgfrα* is not expressed in mature adipocytes, the labelling must be a consequence of lineage tracing (Y. H. Lee *et al.*, 2012; Church, Berry and Rodeheffer, 2014; Berry, Jiang and Graff, 2016). Moreover, $CD45^{-}$;$CD31^{-}$;$Ter119^{-}$;$CD29^{+}$;$CD34^{+}$;$Sca\text{-}1^{+}$;$CD24^{+}$ and $CD24^{-}$ populations (adipocyte progenitor cells and pre-adipocytes, respectively), are both traced by Pdgfrα-Cre, whilst other cell populations within the SVF are not. *Pdgfrα* has a broad expression pattern during early-mid embryogenesis, therefore whilst it can be used for the specific genetic manipulation of APCs it is not a suitable tool for informing on developmental origin (Church, Berry and Rodeheffer, 2014; Berry, Jiang and Graff, 2016). Several other Cre drivers have been used to study various aspects of WAT development and origin, as well as homeostasis, and these are summarised in Table 1.1. The emerging picture seems to suggest that VWAT adipocytes may in fact arise from several origins, and this may also be the case for BAT and SWAT (Sanchez-Gurmaches, Hung and Guertin, 2016).

LINEAGE MARKER	WAT LABELLED	PHASE (DEVELOPMENT, HOMEOSTASIS, EXPANSION)	REFERENCES
aP2-Cre	All SWAT and VWAT	Development and homeostasis	(Abel *et al.*, 2001; Tang *et al.*, 2008)
Adiponectin-rTA; "AdipoChaser"	All SWAT and VWAT	All phases	(Wang *et al.*, 2013)
Cdh5-Cre	All SWAT and VWAT	Development and homeostasis	(Tran *et al.*, 2012)
Myf5-Cre	Anterior SWAT, interscapular BAT, retroperitoneal VWAT	Not determined	(Sanchez-Gurmaches and Guertin, 2014b)
Pax3-Cre	Anterior SWAT, interscapular BAT, retroperitoneal VWAT, epididymal VWAT	Not determined	(Sanchez-Gurmaches and Guertin, 2014b)
PDGFRα-Cre	All SWAT and VWAT	Not determined	(Berry and Rodeheffer, 2013)
PDGFRα-Cre^{ERT2}	VWAT	Expansion	(Y. H. Lee *et al.*, 2012)
PDGFRβ-Cre	Inguinal SWAT, retroperitoneal VWAT	Not determined	(Tang *et al.*, 2008)
PDGFRβ-rtTA; "MuralChaser"	Inguinal SWAT, perigonadal VWAT	Expansion	(Vishvanath *et al.*, 2016)
PPARγ-tTA; "AdipoTrak"	All SWAT and VWAT	All phases	(Tang *et al.*, 2008; Jiang *et al.*, 2014)
Pref-1-rtTA	All SWAT and VWAT	Development and homeostasis	(Hudak *et al.*, 2014)
Prx1-Cre	Inguinal and anterior SWAT	Not determined	(Sanchez-Gurmaches, Hsiao and Guertin, 2015)
SMA-Cre^{ERT2}	All SWAT and VWAT	Homeostasis	(Jiang *et al.*, 2014)
Tbx18-Cre^{ERT2}	No labelling	N/A	(Guimarães-Camboa *et al.*, 2017)
Tie2-Cre	No labelling	N/A	(Berry and Rodeheffer, 2013)
Vav1-Cre	No labelling	N/A	(Berry and Rodeheffer, 2013)
Wt1-Cre^{ERT2}	VWAT	Development and homeostasis	(Chau *et al.*, 2014)

Table 1.1. Overview of the mouse models that have been used to investigate WAT origin, development, homeostasis and expansion

1.1.4 Adipose tissue homeostasis

As mentioned previously, terminally differentiated adipocytes are post-mitotic, therefore APCs are required to continually replace dying adipocytes. Thus, the presence of resident precursor cells is essential to maintain homeostasis (Herberg *et al.*, 1974; Spalding *et al.*, 2008; Arner *et al.*, 2010; Church, Berry and Rodeheffer, 2014). The studies by Rodeheffer and colleagues discussed above (1.1.2) revealed that populations of progenitors ($CD24^+$) and pre-adipocytes ($CD24^-$) are resident within adult WAT, and it is now commonly accepted that these cells reside within the SVF (Rodeheffer, Birsoy and Friedman, 2008; Berry and Rodeheffer, 2013). The precise origin/location of the WAT resident precursor cells is a contentious topic. Results from multiple studies suggest that at least a proportion of them are located within the perivascular niche as mural cells (pericytes and vascular smooth muscle cells) (Berry, Jiang and Graff, 2016). In fact, such thinking is not new; early adipose tissue studies noted that adipocytes are located close to blood vessels (Wassermann, 2011). Moreover, as described for the epididymal depot, adipogenesis and angiogenesis have a close relationship (Crandall, Hausman and Kral, 1997; Berry, Jeffery and Rodeheffer, 2014).

Importantly, perivascular cells isolated from several human tissues, including WAT, are able to differentiate into adipocytes, chondrocytes, osteocytes and skeletal myocytes *in vitro*, and therefore behave as MSCs (Crisan, Yap, *et al.*, 2008). Furthermore, these freshly isolated perivascular cells express several surface markers commonly used to identify MSCs, including CD44, CD73, CD90 and CD105 (Crisan, Yap, *et al.*, 2008). Pericytes typically surround capillaries and microvessels and can be defined by a lack of CD31, CD45 and CD34 expression, but the presence of CD146 expression. However, adventitial stromal cells; another perivascular cell type, exist in association with larger vessels, and can give rise to the distinct cell lineages associated with MSCs, as well as expressing MSC markers. The adventitial stromal cells differ from pericytes and are defined by the expression of CD34, but lack expression of CD31, CD45 and CD146 (Corselli *et al.*, 2012). Indeed, $CD34^+$ adipocyte stem cells isolated from the SVF of human SWAT express common mesenchymal markers and are associated with blood vessels *in vivo*, therefore providing additional support for

the perivascular nature of adipose resident precursor cells (Traktuev *et al.*, 2008). Given what we know from work performed by Rodeheffer and colleagues regarding the expression profiles of pre-adipocytes and progenitor cells in WAT (albeit in mice), the $CD31^{-};CD45^{-};CD146^{-};CD34^{+}$ adventitial stromal cells could represent these populations (Rodeheffer, Birsoy and Friedman, 2008; Berry and Rodeheffer, 2013). Interestingly, a population of $CD34^{+}$ cells isolated from human skeletal muscle can differentiate into brown adipocytes *in vitro* when cultured in adipogenic medium, as demonstrated by their expression of UCP1 (Crisan, Casteilla, *et al.*, 2008). Thus, it appears that a population of perivascular cells outwith the adipose tissue possess the ability to form brown adipocytes, and could be of therapeutic importance in tackling obesity (Crisan, Casteilla, *et al.*, 2008).

Two key studies generated several important findings regarding the nature and location of adipocyte precursor cells, namely that there appears to be (at least) two different niches; one for precursor cells required during development, and one for cells required during adult homeostasis (Tang *et al.*, 2008; Jiang *et al.*, 2014). Importantly, they showed that at least some of those required in the adult, reside in the perivascular niche. PPARγ is a master regulator of adipogenesis, therefore Tang *et al*. (2008) utilised PPARγ expressing cells to understand more about *in vivo* adipogenesis and lineage specification. Having generated a PPARγ reporter model, named "AdipoTrak", they showed that the AdipoTrak labelled cells possessed stem-like properties, including the capacity to self-renew and proliferate as well as differentiate into adipocytes. Both during development and in adults, the AdipoTrak labelled cells formed adipocytes (Tang *et al.*, 2008). To understand whether these cells were necessary for the development and maintenance of adipose tissue, the researchers modified the AdipoTrak system to permit conditional deletion of *Pparγ* specifically in the AdipoTrak+ cells. Given that PPARγ is essential for adipogenesis, its deletion in cells that are necessary for fat formation and maintenance should be detrimental. When deletion was induced at P10, mice at P60 exhibited decreased adiposity and reduced adipose depot size (of the subcutaneous depot), as well as hyperglycemia and reduced expression of *Pparγ*. The same was true when deletion was induced at P30. Additionally, when the SVF cells from the mice were isolated and cultured under

adipogenic conditions, they failed to differentiate. These results indicated that the AdipoTrak labelled cells were necessary for the development and homeostasis of adipose tissue (Tang *et al.*, 2008; Jiang *et al.*, 2014).

The researchers further investigated the location of the AdipoTrak labelled cells, and showed that it differed between mice according to age. Whilst at P10, the cells were not observed to be surrounding the vessels, by P30 they were. Moreover, when a mural cell fate-mapping model was used (*SMA-Cre*^{ERT2}), it was shown that SMA expressing precursor cells could give rise to adipocytes in adults, but not during organogenesis, therefore implying that vascular smooth muscle cells residing in the perivascular niche (SMA+) can provide the adipocytes required for homeostasis, but not those required for development (Tang *et al.*, 2008; Jiang *et al.*, 2014). Additionally, when the SMA-Cre^{ERT2} driven reporter was induced at P30, labelled adipocytes in both subcutaneous and visceral depots were also AdipoTrak+ at P60, but this was not the case when induced at P10. Thus, the "adipose lineage" and the "mural lineage" overlap, but only in adult mice. Furthermore, when the *SMA-Cre*^{ERT2} model was used to drive the conditional deletion of *Pparγ* in adults, the phenotype was similar to that described for the mice in which *Pparγ* had been deleted using the AdipoTrak mice (Tang *et al.*, 2008; Jiang *et al.*, 2014). Using the AdipoTrak mice, it was estimated that, under normal homeostatic conditions, 10-20% of the adipocytes were newly formed each month, depending on depot (Tang *et al.*, 2008; Jiang *et al.*, 2014; Berry, Jiang and Graff, 2016). A similar figure has been reported for adipocyte turnover in humans, when assessed using radioactive isotopic decay (Spalding *et al.*, 2008). Not only does the described study reveal that at least a proportion of the adipocytes formed in adults are derived from cells located in the perivascular niche, but also that if these cells are unable to form new adipocytes, metabolic dysfunction occurs (Berry, Jiang and Graff, 2016).

Additional evidence for the presence and importance of mural cells comes from Gupta *et al*. (2012). They showed that perivascular cells in WAT were labelled with GFP when a *Zfp423*^{GFP} reporter model was used (they had previously shown that ZFP423 is essential for pre-adipocyte commitment to the adipocyte lineage), and that these

cells expressed *Pparγ* and *Pdgfrβ* (another mural cell marker). The cells could be fate-mapped to mature adipocytes, however they only did so when the mice were fed a high fat diet (Gupta *et al.*, 2010, 2012; Vishvanath *et al.*, 2016). ZFP423 acts upstream of PPARγ, therefore they mark precursor cells at earlier and later stages of adipogenesis, respectively. However, ZFP423 is also expressed in endothelial cells, and therefore is not exclusively a marker of perivascular-resident precursor cells (Berry, Jeffery and Rodeheffer, 2014).

Interestingly, further work indicates that WAT resident adult APCs have embryonic origins. Moreover, evidence suggests that these cells are specified before the precursor cells that give rise to adipocytes during development (Jiang *et al.*, 2014). A small population of cells located in the anterior region of the embryo near the developing nervous system and neural crest at E10.5, can give rise to adult VWAT and SWAT, but not developing WAT (Jiang *et al.*, 2014). Labelled precursor cells from this embryonic region are not present within WAT prior to, or during development, and thus infiltrate the depots once development has finished, to reside in the perivascular niche. These cells express key markers of adipocyte precursor cells: PPARγ and PREF-1 (Jiang *et al.*, 2014). Whilst this study utilised the AdipoTrak model described previously, another similar study utilised a reporter model for PREF-1, which also highlighted a population of cells in the dorsal mesenteric region of the E10.5 embryo. However, using this reporter it was shown that these cells were important for both the development and expansion of WAT in adults, thus differing from what was reported in the AdipoTrak study (Hudak *et al.*, 2014).

Recently, results from one group challenged the idea that mural cells represent an endogenous population of tissue-resident progenitor cells. Using a *Tbx18-Cre*^{ERT2} model to selectively label and track the fate of mural cells in adult mice, they concluded that pericytes are not APCs. Despite allowing the mice to age to one and a half years old they did not observe any labelled adipocytes, and the same was seen when the mice were fed a high fat diet. Moreover, they disputed the suitability of the commonly used *Pdgfrβ-Cre* model for tracking the fate of mural cells. They showed that the constitutive *Pdgfrβ-Cre* allele is expressed in multiple lineages during

embryogenesis and thus labelled adipocytes in the adult may not necessarily arise from the mural cell lineage (Guimarães-Camboa *et al.*, 2017). However, the conclusions from this study have been disputed by Vishvanath *et al*. (2017), who highlighted that the high fat diet regime used by the group is not that typically used to model adipogenesis. Therefore, the adipose tissue expansion they observed may have been the result of hypertrophy and not hyperplasia, meaning that no new adipocytes will have been formed, explaining why they did not observe any adipocyte labelling using the *Tbx18-Cre*^{ERT2} model (Vishvanath *et al.*, 2017). The authors responded to this challenge, suggesting that adipocyte progenitor cells are not mural cells, but instead are adventitial fibroblasts. The two cell types are very closely situated and have similar morphologies (both have cytoplasmic projections), thus explaining why the two may be confused. Moreover, they stated that whilst many of the models that have been used to label and fate-map mural cells also label adventitial fibroblasts, the *Tbx18-Cre*^{ERT2} model they employed labels mural cells specifically. Additionally, they suggested that results from lineage tracing studies using the *Pdgfrα-Cre*^{ERT2} model, support their findings, given that Pdgfrα-Cre^{ERT2} selectively labels adventitial fibroblasts and that these labelled cells can give rise to adipocytes (Y. H. Lee *et al.*, 2012; Berry and Rodeheffer, 2013; Guimarães-Camboa and Evans, 2017).

In addition to perivascular cells, other potential origins for adult adipocytes have been investigated. CDH5 is a marker of mature endothelial cells and *Cdh5-Cre* mice have been used to assess whether endothelial cells can give rise to adipocytes. Using *Cdh5-Cre;LacZ* mice, it was shown that adipocytes in white and brown adipose tissue can be derived from *Cdh5* expressing precursor cells (Tran *et al.*, 2012). However, subsequently another group used the *R26R-mTmG* reporter, which is more suitable for visualising and studying adipocytes, due to is membranous, rather than cytoplasmic labelling. Prior to Cre-mediated LoxP recombination, all cells express the red Tomato reporter, however following recombination, eGFP labels Cre expressing cells and their progeny (Muzumdar *et al.*, 2007). They were unable to find eGFP+ adipocytes in any of the major WAT or BAT depots from *Cdh5-Cre;R26R-mTmG* mice, therefore conflicting with the results from the previous study (Berry and Rodeheffer, 2013). Moreover, a different endothelial-driven Cre model (*Tie2-Cre*), also failed to confirm

the results obtained using the *Cdh5-Cre;LacZ* mouse (Berry and Rodeheffer, 2013). Hence, it is now generally acknowledged that adipocytes are not normally derived from endothelial cells *in vivo*.

As well as WAT resident precursor cells, additional external sources have been suggested, including haematopoietic cells from the bone marrow (Crossno *et al.*, 2006; Tomiyama *et al.*, 2008; Sera *et al.*, 2009; Majka *et al.*, 2010, 2012). There is an on-going debate as to whether this is the case. Using bone marrow cells from transgenic GFP expressing mice, one group demonstrated that when these cells were transplanted into wildtype mice they were capable of generating adipocytes. Moreover, when administered with a high fat diet or a PPARγ agonist, hyperplasia of the GFP expressing cells was induced (Crossno *et al.*, 2006). However, subsequently another group suggested that this was not the case, and that the GFP expressing "adipocytes" were in fact macrophages (Koh *et al.*, 2007). Nevertheless, additional studies by other groups have added further support to the hypothesis that adipocytes can develop from the haematopoietic lineage (Sera *et al.*, 2009; Majka *et al.*, 2010, 2012). Sera *et al.* (2009), transplanted eGFP expressing haematopoietic stem cells into irradiated mice and after approximately ten months, the omental, perirenal and retroperitoneal depots were examined, revealing many eGFP expressing adipocytes. The investigators did also note the presence of a few eGFP expressing macrophages, thus agreeing to some extent with both previous studies. Moreover, they showed that the eGFP expressing haematopoietic cells were capable of forming adipocytes *in vitro* (Sera *et al.*, 2009). Using the *Vav1-Cr*e model to label all haematopoietic lineages, Berry and Rodeheffer (2013) failed to obtain adipocyte labelling, despite all WAT resident CD45+ cells being labelled. Labelled structures were present when the mice had been fed a high fat diet, however they too concluded that these cells were macrophages (Berry and Rodeheffer, 2013). Therefore, these findings also dispute that WAT adipocytes have a haematopoietic origin. Recently, the contribution of bone marrow cells to adipose tissue has been assessed in humans. Taking advantage of the fact that donor and recipient cells are genetically different, the investigators revealed that over the lifespan of the recipient, 10% of the SWAT adipocytes were derived from progenitors from the donor bone marrow (Rydén *et al.*, 2015). Henceforth, it does appear that adipocytes

can be derived from progenitor cells in the bone marrow, but evidently there are also other sources, and the topic is still much debated. An interesting point raised by Berry *et al*. (2016) is that it will now be fascinating to compare the perivascular and haematopoietic stem cell lineages to understand how they are temporally related and how they differ, regarding homeostasis and expansion of WAT (Berry, Jiang and Graff, 2016).

Whilst it is therefore evident that a population of APCs does exist within adult WAT, and that this population is essential for homeostasis, the precise location and origin of these cells is still debated, as is their similarity and relationship to the precursors required during development. Additionally, work from our group has shown that VWAT depots are covered by a WT1 expressing mesothelial layer, which can give rise to adipocytes, thus highlighting another potential source (Chau *et al.*, 2014). This work is further explained in section 1.2.1. Moreover, several studies suggest that WAT adipocytes can also arise from haematopoietic cells in the bone marrow, although the idea is contested. There are several possible explanations for why different studies present conflicting results. Each study typically utilises a different mouse model and thus a different genetic tool to label and trace the cells; each gene will have a very specific expression pattern, likely different to that of another gene, and so it is possible that different populations of cells are being labelled and investigated. This in itself is interesting and may be exploited to tease apart different populations of precursor cells present *in vivo*. It is also highly likely that there are several sources. Moreover, the depot being studied will have a significant influence on the results obtained. Additional factors such as differences in the sex, age and background of the mouse models will likely also have an effect (Berry, Jiang and Graff, 2016). In addition to listing lineage markers used to investigate WAT development and origin, Table 1.1 also summarises the tools used to study homeostasis and expansion.

1.1.5 Adipose tissue expansion

The expansion of WAT in obesity and under HFD conditions involves both hypertrophy and hyperplasia (Berry, Jeffery and Rodeheffer, 2014; Berry, Jiang and

Graff, 2016). The extent to which each of these mechanisms contributes to expansion is debated, with different studies obtaining contradictory results. Several factors seemingly influence the expansion including age, gender and the duration of the HFD/obesogenic stimuli, which may help to explain the differing findings (Berry, Jiang and Graff, 2016). A recent study compared the contribution of hyperplasia and hypertrophy to the expansion of subcutaneous and perigonadal murine adipose tissue. When fed a chow diet, no significant expansion of the adipose tissue occurred and no new adipocytes were formed in either depot. However, after one month on a HFD, adipocytes in both depots increased in size, but not in number, thus displaying hypertrophy. Furthermore, following 8-12 weeks on a HFD, the perigonadal depot contained many newly formed adipocytes, indicating the occurrence of hyperplasia, whilst no new adipocytes were observed in the subcutaneous depot (Wang *et al.*, 2013). Therefore, the mechanisms of expansion differ between visceral and subcutaneous depots.

A subsequent study reported similar findings, and also showed that in the perigonadal depot (but not the subcutaneous), there is a burst of precursor cell proliferation within the first week of HFD feeding, which subsides by the second week. The new precursor cells then undergo adipogenesis to form mature adipocytes over several weeks (Jeffery *et al.*, 2015). The results from these two studies contrast to those obtained by another group, who used analysis of BrdU incorporation to assess hyperplasia under HFD conditions, and showed that SWAT is more hyperplastic than VWAT (Joe *et al.*, 2009). Numerous factors could be responsible for these disparate results, in particular differences in the timing of HFD feeding (Joe *et al.*, 2009; Wang *et al.*, 2013; Jeffery *et al.*, 2015). Importantly, it has also been shown that hyperplasia, rather than hypertrophy, is the major cause of omental VWAT expansion in human obesity (Arner *et al.*, 2013).

Various lines of evidence also indicate that the ability of rodent APCs to proliferate and differentiate declines with age, and thus hyperplasia is not as prevalent in older HFD fed animals (Tchkonia *et al.*, 2010; Kim *et al.*, 2014). Additionally, a recent study has shown that differences in hyperplasia between SWAT and VWAT depots are

dependent on sex. In agreement with the studies described above, in male mice, hyperplasia was increased in VWAT but not SWAT, when fed a HFD. However, hyperplasia increased in both SWAT and VWAT depots in female HFD fed mice. This difference is thought to be a consequence of the influence of sex hormones on adipocyte formation (Jeffery *et al.*, 2016). In humans, premenopausal women typically gain subcutaneous, rather than visceral fat, however, for men the opposite is true. For postmenopausal women there is shift to a more male-like fat distribution, therefore advocating the idea that sex hormones play an important role in the response to external factors, such as diet (Gesta, Tseng and Kahn, 2007; Karastergiou *et al.*, 2012; Jeffery *et al.*, 2016).

Certain lines of evidence indicate that cell-extrinsic factors present in the microenvironment control the proliferation of APCs in response to HFD feeding. Murine transplantation studies showed that, in male mice, SWAT precursor cells transplanted into the VWAT depot proliferated upon HFD feeding, whilst VWAT cells transplanted into the SWAT depot did not. Therefore the precursor cells adopted the behaviour of the depot into which they had been transplanted (Jeffery *et al.*, 2016). A crucial next step is to gain an understanding of the signals that determine the activation of the precursor cells in obesity. In summary, both hyperplasia and hypertrophy have been demonstrated to contribute to WAT expansion under obesogenic conditions, and evidently the contribution of these mechanisms is influenced by multiple factors including gender, age, depot and microenvironment.

1.1.6 Inter and intra-depot heterogeneity

As adipose tissue research has progressed, it has become increasingly evident that there are numerous differences between WAT depots. Such differences have led to the rationale that individual depots exist as separate “mini-organs” (Cartwright *et al.*, 2010). Moreover, recent work from our group has added further support to the idea that heterogeneity also exists within the APC population of a single depot, and that these differences at the precursor cell level may have consequences for the mature adipocytes derived from them (Chau *et al.*, 2014). Understanding these inter and intra-

depot differences is potentially clinically relevant, given that depots contrast in their pathogenicity.

Many studies, both human and rodent, have compared the gene expression profiles of different WAT depots, particularly focusing on SWAT versus VWAT. Often, total fat is investigated (mature adipocytes and SVF) (Cantile *et al.*, 2003; Linder *et al.*, 2004; Vohl *et al.*, 2004; Wu *et al.*, 2008), however some studies concentrate on just the APCs (Tchkonia *et al.*, 2005, 2007; Cartwright *et al.*, 2010; Macotela *et al.*, 2012; Perrini *et al.*, 2013; Kim *et al.*, 2016; Meissburger *et al.*, 2016). Several groups have reported the differential expression of genes involved in developmental processes, when comparing SWAT and VWAT (typically murine inguinal SWAT versus perigonadal VWAT and human abdominal SWAT versus omental/mesenteric VWAT) (Cantile *et al.*, 2003; Vohl *et al.*, 2004; Gesta *et al.*, 2006; Macotela *et al.*, 2012; Perrini *et al.*, 2013). Differences in gene expression between individual VWAT depots have also been described (Tchkonia *et al.*, 2007; Cartwright *et al.*, 2010; Yamamoto *et al.*, 2010). One study that focused on human WAT precursor cells, revealed that there were distinct differences in the expression profiles of mesenteric and omental VWAT, and that again there was an enrichment of developmental genes. Surprisingly, based on the developmental gene expression profile, the mesenteric precursor cells clustered with subcutaneous rather than omental (Tchkonia *et al.*, 2007). A comprehensive study performed by Yamamoto *et al*. (2010), showed that the expression of key developmental genes (*Tbx15, Shox2, En1, Hoxc9, Hoxc5* and *Hoxa5),* differed considerably between murine interscapular and inguinal SWAT and perigonadal, perirenal and mesenteric VWAT. Each depot displayed a unique pattern of expression, even for just six genes (Yamamoto *et al.*, 2010). Given what has been discussed about the developmental timing and origins of the different depots, such differences in the gene expression profiles of developmental genes is intriguing.

Differential expression analysis has also revealed other categories of genes that differ between WAT depots. Those that function in adipogenesis have been highlighted when comparing human subcutaneous, mesenteric and omental APCs (Tchkonia *et al.*, 2002, 2007). *In vitro*, upon induction of differentiation, SWAT precursor cells

expressed higher levels of PPARγ and C/EBP-α than omental and mesenteric (Tchkonia *et al.*, 2002). Additionally, gene ontology analysis of microarray data from human retroperitoneal and subcutaneous precursor cells, highlighted that genes implicated in lipid metabolism and cholesterol biosynthesis were enriched in the retroperitoneal population (Kim *et al.*, 2016). Moreover, expression of pro-inflammatory genes is higher in rat perirenal precursor cells than in perigonadal. It is known that VWAT secretes more inflammatory cytokines that SWAT, but it has also been shown that differences exist between visceral depots (Xu *et al.*, 2012; Tchkonia *et al.*, 2013). Furthermore, genes that function in replication, apoptosis and angiogenesis have all been noted as being differentially expressed between different WAT depots (Cartwright *et al.*, 2010; Kim *et al.*, 2016).

As well as comparing gene expression profiles, the *in vitro* differentiation potential of precursor cells isolated from different WAT depots has been investigated. The predominant result from both human and rodent studies is that SWAT precursor cells differentiate into adipocytes more efficiently than those isolated from VWAT (Tchkonia *et al.*, 2002, 2006; Hutley *et al.*, 2003; Baglioni *et al.*, 2009; Joe *et al.*, 2009; Toyoda *et al.*, 2009; Macotela *et al.*, 2012; Kim *et al.*, 2016; Meissburger *et al.*, 2016). Moreover, mesenteric precursor cell cultures have a higher percentage of proliferating and differentiating cells than omental precursor cell cultures (Tchkonia *et al.*, 2002, 2005). Given that, according to gene expression studies, mesenteric cells cluster with subcutaneous rather than omental, this *in vitro* result suggests that such differences and similarities at the expression level may have functional consequences. The addition of certain factors to the culture media also appears to affect SWAT and VWAT cells differently. When cultures of subcutaneous and perigonadal cells were treated with BMP4 before the addition of differentiation media, approximately 90% of the cells in the perigonadal cultures formed lipid droplets, compared to just 20% in the cultures that were not treated with BMP4. However, in the subcutaneous cultures, 90% of the cells formed lipid droplets, regardless of whether BMP4 was added. Further work revealed that standard differentiation media is unable to induce the expression of *Pparγ* in visceral precursor cells, but that treatment with BMP4 overcomes this. Comparable results were also obtained for BMP2. Moreover, microarray analysis

showed that subcutaneous precursor cells express higher levels of BMP4 and 2 than perigonadal, perhaps explaining why subcutaneous cells do not require the exogenous addition of BMP4/2 (Macotela *et al.*, 2012). Therefore, inherent differences in the precursor cells from different depots clearly influence their capacity for adipogenesis.

Heterogeneity also exists within adipose depots. Several studies indicate that individual adipocytes from the same depot respond differently to drugs and genetic perturbations (Sanchez-Gurmaches and Guertin, 2014a). For example, when the insulin receptor was deleted from all adipocytes, the response to this deletion was not uniform. Whilst the efficiency of the deletion was comparable across all adipocytes, two distinct populations prevailed. Approximately 45% of the adipocytes decreased in size whilst the rest increased in size, in comparison to wild type mice. The small adipocytes were protected from increased triglyceride load, whilst the larger cells responded normally to the excess triglyceride. The authors suggested that this disparity in size and function reflected intrinsic heterogeneity in the adipocytes, which was unmasked upon deletion of the insulin receptor, and was confirmed by gene expression analysis (Blüher *et al.*, 2002, 2004). Similarly, small and large adipocytes isolated from human SWAT have been shown to exhibit different gene expression profiles (Jernås *et al.*, 2006).

Intra-depot heterogeneity also exists at the level of the precursor cells, as recently illustrated by our group. *Wt1* is expressed in adipocyte progenitor cells and pre-adipocytes from all VWAT depots, but not SWAT or BAT. However, within each VWAT depot it is only expressed in a subset of the progenitors and pre-adipocytes, and the proportion of *Wt1* expressing cells varies across the depots. For example, in the omental depot ~40% of the pre-adipocytes express *Wt1*, whilst in the mesenteric depot, only ~12% do so (Chau *et al.*, 2014). Interestingly the two depots with the largest percentages of *Wt1* expressing cells are the omental and epi/pericardial, which are the two depots principally linked to obesity-associated disease. Moreover, preliminary data suggests that the adipocytes derived from *Wt1* expressing precursor cells have fewer, larger lipid droplets than those derived from non-*Wt1* expressing cells (Chau *et al.*, 2014). Therefore, this suggests that the heterogeneity at the precursor

cell level may influence the physical properties of the mature adipocytes into which they differentiate.

1.2 Overview of *WT1*

The Wilms' tumour gene, *WT1*, was first cloned in 1990 and is located on chromosome 11 (band p13). It has ten exons, generating approximately a 3kb mRNA, and the protein it encodes has four C-terminal zinc finger domains, typical of transcription factors (Call *et al.*, 1990). At least 36 isoforms are theoretically possible, due to alternative start codons, alternative splicing and RNA editing (Figure 1.5) (Hohenstein and Hastie, 2006). Of these, the best characterised are the KTS and exon 5 isoforms. The exon 5 variants are a consequence of the skipping, or use of the 51 nucleotide exon, whilst the KTS variants are due to the presence or absence of the three amino acids: lysine, threonine and serine (KTS) between zinc fingers 3 and 4 (Hohenstein and Hastie, 2006). The existence of a residue in exon 6 that is susceptible to RNA editing, an upstream CTG start codon and an ATG start codon at the end of exon 1, contribute to occurrence of other alternative isoforms. Interestingly, whilst the exon 5 variants and those due to the alternative start codons are conserved across mammals, the ±KTS isoforms are the only ones known to be conserved in all vertebrates (Hohenstein and Hastie, 2006). Moreover, mice that lack either the +KTS isoform or –KTS isoform die shortly after birth due to kidney defects (although the precise phenotypes are different), whereas those that lack other isoforms, such as those missing exon 5, do not exhibit an obvious phenotype (Hammes *et al.*, 2001; Natoli *et al.*, 2002).

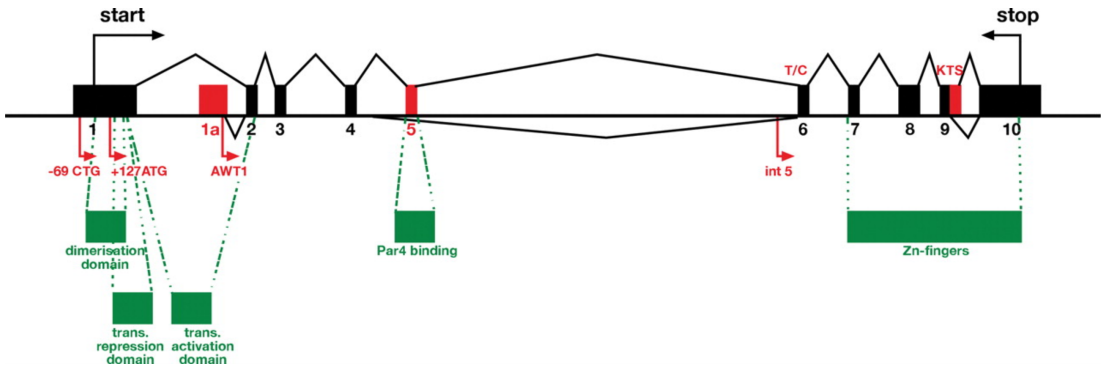


Figure 1.5. The WT1 locus which encodes at least 36 isoforms is found on chromosome 11 (band p13). *Shown in red are alternative start codons, splices, exons and RNA editing. The affected functional domains are shown in green (Hohenstein and Hastie, 2006).*

Originally discovered as a tumour suppressor gene, mutations in *WT1* can result in the eponymous paediatric kidney tumour, but also to gonadal dysgenesis, kidney glomerulosclerosis and sometimes diaphragmatic hernia and heart defects (Chau and Hastie, 2012). WT1 was first described as a transcriptional regulator, with a large array of target genes (Toska and Roberts, 2014). The number of physiologically relevant targets, with roles in development, homeostasis and disease, is growing (Motamedi *et al.*, 2014; Dong *et al.*, 2015; Kann *et al.*, 2015). Importantly, it is predominantly the –KTS isoforms, which make up approximately one third of the total WT1 protein, that function in transcriptional regulation, due to their high affinity for DNA binding (Hohenstein and Hastie, 2006; Yang *et al.*, 2007). However, the precise role of WT1 in transcriptional regulation is paradoxical, as it can act as both a transcriptional activator and repressor due to distinct protein domains that function independently (Toska and Roberts, 2014). Various factors have been shown to influence which of these roles it assumes, including the level of expression, the isoform, the cell type and the context. Moreover, cofactors including BASP1 and WTIP have been shown to act as co-suppressors (Hohenstein and Hastie, 2006; Yang *et al.*, 2007). For many years it has been suggested that WT1, in particular the +KTS isoforms, also function in the post-transcriptional processing of RNA. The finding that these isoforms associate with splicing factors and integrate into active splice complexes provided strong evidence for a post-transcriptional role (Larsson *et al.*, 1995; Davies *et al.*, 1998; Markus *et al.*, 2006). It has also been shown that WT1 shuttles between the nucleus and cytoplasm (Niksic *et al.*, 2004). However, until recently, a lack of known endogenous WT1 RNA targets has hampered research and mechanistic understanding in this area. Bharathavikru *et al*. (2017) used a combination of RNA immunoprecipitation and sequencing, as well as cross-linking techniques, to show that WT1 interacts directly with physiologically important RNAs and regulates their stability. Intriguingly, they identified a few genes that are both transcriptional and post-transcriptional targets of WT1, including *Podx1* and *Rspo1*. However, generally there is little overlap between the targets of the two functions (Bharathavikru *et al.*, 2017).

The mechanisms by which WT1 acts are evidently diverse. Correspondingly, its roles in both development and homeostasis are also varied, and often contradictory. A

classic example of this is how it functions in regulating the balance of epithelial and mesenchymal states. WT1 is required for both mesenchymal-to-epithelial transition (MET) and epithelial-to-mesenchymal transition (EMT), and cells cycle through the two processes during development (Figure 1.6) (Pérez-Pomares and Muñoz-Chápuli, 2002; Chau and Hastie, 2012). Epithelial cells form basement membranes, have apical-basal polarity, tight junctions and crucially are immobile. Conversely, mesenchymal cells do not have basement membranes, apical-basal polarity or tight junctions and are mobile. In line with their different properties, the two cell types also have characteristic protein expression profiles (Chau and Hastie, 2012). Epithelial cells express E-cadherin, which is important for initiating adhesion. Additionally, the major intermediate filaments of epithelial cells are comprised of cytokeratins, whilst in mesenchymal cells, vimentin is the predominant component. Several transcription factors function in the regulation of EMT/MET, including members of the Snail family which downregulate E-cadherin and therefore promote EMT (Chau and Hastie, 2012).

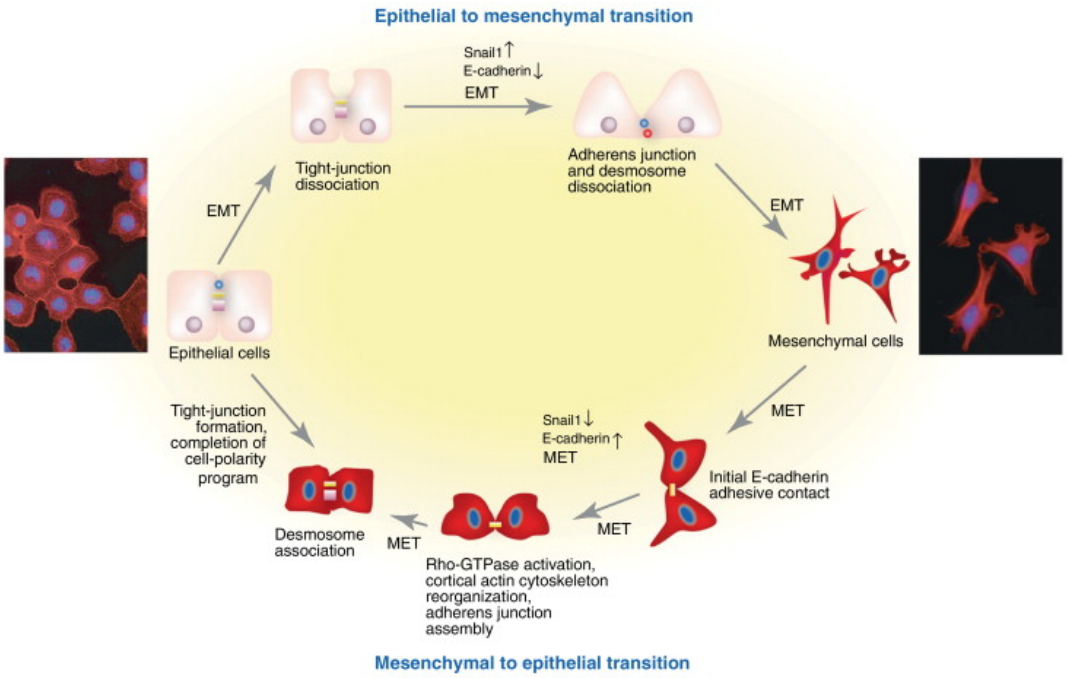


Figure 1.6. The cyclical behaviour of EMT and MET. *Epithelial, but not mesenchymal cells, have tight junctions, basement membranes and exhibit apical-basal polarity (Chau and Hastie, 2012).*

The necessity for WT1 in both MET and EMT is evidenced when studying the development of the kidneys and the heart, respectively (Martínez-Estrada *et al.*, 2010; Essafi *et al.*, 2011). Two embryonic tissues, the metanephric mesenchyme and the epithelial ureteric buds are important in nephrogenesis. Initially, the ureteric bud invades the mesenchyme, which then undergoes MET and condenses around the bud. The epithelial cells that are generated eventually form the nephron (Stark *et al.*, 1994). WNT4, which is produced by the mesenchyme, is necessary and sufficient for MET and thus is essential for nephron development (Stark *et al.*, 1994; Kispert, Vainio and McMahon, 1998). WT1 is required at several stages of kidney development; for the survival of the mesenchyme before it is induced, for MET and nephron generation, for podocyte formation and for the maintenance of kidney function into adulthood (Kreidberg *et al.*, 1993; Hammes *et al.*, 2001; Chau *et al.*, 2011; Essafi *et al.*, 2011; Chau and Hastie, 2012; Miller-Hodges and Hohenstein, 2012). Crucially, mesenchyme-specific deletion of *Wt1* using the *Nestin-Cre* line resulted in a lack of MET and consequently a failure of nephron formation. Moreover, *Wnt4* is a direct transcriptional target of WT1, and thus there is a drastic reduction of WNT4 in the mesenchyme of the $Nestin^{Cre/+};Wt1^{loxP/loxP}$ mice (Essafi *et al.*, 2011).

In the developing heart the situation is very different. Epicardial cells undergo EMT to generate mesenchymal epicardial-derived cells (EPDCs), which subsequently invade the heart and give rise to vascular smooth muscle cells, fibroblasts and some cardiomyocytes. Using the *Gata5-Cre* model to delete *Wt1* in the epicardium resulted in a dramatic reduction in the number of EPDCs, and consequently the coronary vasculature did not develop (Martínez-Estrada *et al.*, 2010). Moreover, it was shown that WT1 directly activates the transcription of *Snai1* but represses *Cdh1*, and thus the levels of SNAI1 and CDH1 were decreased and increased in the *Wt1* knockout model, respectively (Martínez-Estrada *et al.*, 2010). The contrasting roles that WT1 plays in the developing kidneys and heart have been attributed to a "chromatin flip-flop" mechanism (Essafi *et al.*, 2011). WT1 switches ("flips") the chromatin state of the CCCTC-binding factor (Ctcf)-bound *Wnt4* locus. Therefore, in the developing kidney WT1 directly activates the expression of *Wnt4*, but in the epicardium it represses it,

thus explaining how it differentially regulates MET and EMT during development (Essafi *et al.*, 2011).

Clearly WT1 also plays a role in cancer, however, here too, its function is contradictory. Wilms' tumour affects one in ten-thousand live births, making it the most common paediatric renal tumour (Menke *et al.*, 1998). In Wilms' tumour, WT1 acts as a tumour suppressor and approximately 15% of sporadic Wilms' tumour cases occur as the result of mutations in *WT1* (Little and Wells, 1997; Yang *et al.*, 2007). Around 10% of the sporadic cases exhibit gross deletions and re-arrangements of *WT1*, whilst intragenic mutations account for roughly 5%. These mutations include nonsense and missense types that are located throughout the coding sequence (Little and Wells, 1997; Rivera and Haber, 2005). However, the majority of sporadic cases do not have mutations in *WT1*, but express the wild-type version. Therefore, it appears that mutations in *WT1* only account for a limited number of Wilms' tumour cases and that mutations in downstream effectors may also be important (Rivera and Haber, 2005; Yang *et al.*, 2007).

Whilst most Wilms' tumours occur sporadically, some are associated with various congenital anomaly syndromes. These include Wilms' tumour with sporadic aniridia, genitourinary dysplasia and mental retardation (WAGR) syndrome, Denys-Drash Syndrome (DDS) and Frasier Syndrome (Rivera and Haber, 2005; Yang *et al.*, 2007). WT1 is also implicated in several adult cancers, including both haematological and non-haematological types, however, here it is thought to act as an oncogene. These include primary breast tumours (Loeb *et al.*, 2001), colorectal cancers (Oji *et al.*, 2003), *de novo* lung cancers (Oji *et al.*, 2002) and many more (Yang *et al.*, 2007). Given that WT1 is not normally expressed in these tissue types, its high expression in the tumours suggests its oncogenic action. Moreover, no mutations have been found in the gene in these cancers (Hohenstein and Hastie, 2006). The exception to this is in acute myeloid leukaemia, for which mutations in *WT1* are found in approximately 14% of cases (King-Underwood, Renshaw and Pritchard-Jones, 1996; King-Underwood and Pritchard-Jones, 1998). Further evidence to support its oncogenic role comes from *in vitro* studies in which the use of *WT1* antisense oligonucleotides inhibit the growth

of several glioblastoma cell lines (Oji *et al.*, 2004). Similarly, expression of WT1 was found to be increased in several breast cancer cell lines, and these cells exhibited reduced cell cycle arrest and apoptosis. However, upon the addition of WT1 antisense oligomers, cell cycle arrest and apoptosis were induced and proliferation decreased (Tuna, Chavez-Reyes and Tari, 2005). These contrasting actions of WT1 in different cancers may be, at least partially, due to its paradoxical roles in EMT/MET as discussed earlier. For example, most of the adult tumours in which WT1 is implicated are derived from epithelial cells and undergo EMT during their development. Thus, the activation of *WT1* may be important in the tumourigenic mesenchymal cell establishment/preservation. Conversely, Wilms' tumours develop from mesenchymal cells. During normal kidney development WT1 functions to shift the cells into an epithelial state, however a loss of WT1 could lead to the cells being maintained in the tumour-associated mesenchymal state (Hohenstein and Hastie, 2006).

1.2.1 WT1 in development

WT1 plays an essential role in the development of multiple tissues and as a result, *Wt1* null mice die at mid-gestation due to defective formation of the coronary vasculature (Kreidberg *et al.*, 1993; Moore *et al.*, 1999; Martínez-Estrada *et al.*, 2010). They also fail to develop kidneys, a spleen, gonads and adrenal glands, and have diaphragmatic hernias (Kreidberg *et al.*, 1993; Herzer *et al.*, 1999; Moore *et al.*, 1999). Latterly it has also been discovered that they do not form retinal ganglia or olfactory epithelia and exhibit reduced proliferation of the neuronal progenitor cells (Wagner *et al.*, 2002, 2005). Moreover, WT1 has recently been demonstrated to be involved in the development of taste buds (Gao *et al.*, 2014).

In mice, WT1 is first expressed at approximately E8.5-E9, in the intermediate and lateral plate mesoderms (Armstrong *et al.*, 1993; Chau and Hastie, 2012). The WT1 expressing cells of the intermediate mesoderm will ultimately contribute to the gonads and kidneys, whilst the lateral plate mesoderm will give rise to the coelomic epithelium. The genital ridge, gonads and adrenal gland are all contributed to by progenitors that have their origin in the coelomic epithelium. Additionally, the

mesothelial layer, which lines the body cavity and all visceral organs, is derived from the coelomic epithelium and thus the lateral plate mesoderm. At E9.5 the septum transversum mesenchyme also expresses WT1 and will contribute to several tissues/organs including the hepatic sinusoids and diaphragm (Chau and Hastie, 2012). By E11-E11.5 there is enhanced expression of WT1 in the condensing metanephric mesenchyme, and additionally there is weak expression in the spinal cord (Armstrong *et al.*, 1993). Throughout development, expression persists in the developing kidney and in the mesothelial linings of the body cavity and organs. Moreover, expression is present, for the first time, in the differentiating body-wall musculature at E13.5 and in the fourth ventricle of the brain at E15.5. By E19, the expression domain of WT1 is largely reduced, and is restricted mainly to the kidney, gonads and mesothelia (Armstrong *et al.*, 1993). Human embryos were observed to exhibit a very similar expression pattern as that described for mouse, between 28 and 70 days of gestation (E10-E15 in mouse) (Armstrong *et al.*, 1993).

As described previously, WT1 is required at several stages of kidney development. Consequently, *Wt1* null mice fail to form kidneys; the ureteric bud does not develop and there is increased apoptosis in the metanephric mesenchyme, meaning that by E12, no mesenchymal cells are present (Kreidberg *et al.*, 1993). Additionally, gonad development is disrupted in *Wt1* null mice. Thickening of the epithelium over the surface of the urogenital ridge at E11 initiates gonad development, however in mutant mice this thickening is reduced and subsequent gonadal development is halted (Kreidberg *et al.*, 1993). The adrenal gland also does not form in the mutant mice, which is probably due to the gonads and adrenal gland deriving from a common primordium (Moore *et al.*, 1999). Moreover, *Wt1* null mice fail to develop a spleen due to increased apoptosis of the primordial splenic cells (Herzer *et al.*, 1999). Mutant mice also present with diaphragmatic hernias, which is discussed in further detail in section 1.4. However, mid-gestational death in *Wt1* null mice is caused by disrupted heart development. The mutant mice present with significant oedema from around E12, with an obvious accumulation of blood in the systemic veins and haemorrhage into the pericardial cavity. As already discussed, WT1 is necessary for the generation

of proliferating progenitor cells from the epicardium to form the coronary vasculature (Kreidberg *et al.*, 1993; Martínez-Estrada *et al.*, 2010).

Lineage tracing has been used to show that WT1 expressing mesothelial cells also contribute to the development of other organs including the intestines, lungs and liver. In the developing gut, mesothelial cells do not appear until E11.5 and the mesothelium is not fully established until E13.5. Crucially, lineage tracing has revealed that WT1 expressing gut mesothelial cells undergo EMT and give rise to the vascular smooth muscle cells of the gut (Wilm *et al.*, 2005). Moreover, at least a proportion of the interstitial cells of Cajal are also thought to be derived from the WT1 expressing mesothelium (Carmona *et al.*, 2013). Similarly, in the developing lung, WT1 is only expressed in the mesothelial cells, and these cells are a source of vascular smooth muscle (Que *et al.*, 2008). Additionally, the WT1 expressing mesothelial cells contribute to the bronchial musculature, fibroblast-like interstitial cells, bronchial and tracheal cartilage and pulmonary endothelial cells (Cano, Carmona and Muñoz-Chápuli, 2013). In the developing liver, WT1 expressing mesothelial cells give rise to hepatic stellate cells, and are thus implicated in hepatic injury and fibrosis (Ijpenberg *et al.*, 2007; Friedman, 2008; Asahina *et al.*, 2011).

Most recent, and highly relevant to this thesis, is the discovery that WT1 expressing cells also contribute to visceral adipose tissue (Chau *et al.*, 2014). Using the tamoxifen inducible *Wt1-Cre*^{ERT2} transgenic mouse line, crossed with the *R26R-mTmG* reporter line, Chau *et al*. (2014) showed that one year old mice that had been tamoxifen treated at E14.5, possessed a high percentage of eGFP expressing, and thus Wt1-lineage positive, mature adipocytes in the visceral depots. Therefore, WT1 expressing cells present in the embryo at E14.5 gave rise to mature visceral adipocytes in the adult animal. The specific percentages varied between the depots; 77% of the adipocytes in the epididymal fat were positive, 66% in the heart fat, 47% in the omental and 28% in the mesenteric. Crucially, no adipocytes in the subcutaneous or brown adipose depots were lineage-traced using this model (Chau *et al.*, 2014).

As discussed previously, the visceral adipose depots do not develop until after birth, therefore it is not possible to investigate whether, as with the organs described above, the mesothelium is important for their development embryonically. However, it was shown that in the adult mouse, the visceral adipose depots are also covered by a layer of WT1 expressing mesothelium. Moreover, in the one year old Wt1-lineage tracing mice, this mesothelial layer was Wt1-lineage positive, indicating that it was derived from WT1 expressing cells that were present in the embryo at E14.5 (Chau *et al.*, 2014). Additionally, when tamoxifen was administered at E14.5, and the embryos analysed at E16.5, mesothelial cells present at the locations where the fat pads subsequently develop were the only cells labelled, thus providing further evidence for a mesothelial adipocyte origin. Moreover, these mesothelial cells expressed the characteristic cell surface markers of adipose progenitors ($Lin^-;CD31^-;CD29^+;CD34^+;Sca\text{-}1^+;CD24^+$) and pre-adipocytes ($Lin^-;CD31^-;CD29^+;CD34^+;Sca\text{-}1^+;CD24^-$), with the relative proportions shifting postnatally and into adulthood, in line with what has been demonstrated for subcutaneous WAT (Berry and Rodeheffer, 2013; Chau *et al.*, 2014).

The epididymal appendage that gives rise to epididymal adipocytes, is remarkably mesothelial in appearance, and expresses GFP in E18.5 $Wt1^{GFP/+}$ knock-in embryos (Han *et al.*, 2011; Chau *et al.*, 2014). Removing this appendage from *Wt1-*Cre^{ERT2}*;R26R-mTmG* pups, and culturing it *ex vivo* with 4-OH tamoxifen, showed that, after 5-10 hours in culture, some of the cells expressed eGFP, and migrated away, before producing lipid droplets. Therefore, this epididymal mesothelial structure can give rise to Wt1-lineage positive adipocytes (Chau *et al.*, 2014). Henceforth, as is the case for several organs, various lines of evidence indicate that at least a proportion of mature visceral adipocytes in adult mice have a mesothelial origin, and are derived from WT1 expressing precursor cells present embryonically. Given that the mesothelium is derived from the lateral plate mesoderm, it is likely that this is a source of visceral WAT progenitor cells (depicted in Figure 1.7) (Chau *et al.*, 2014).

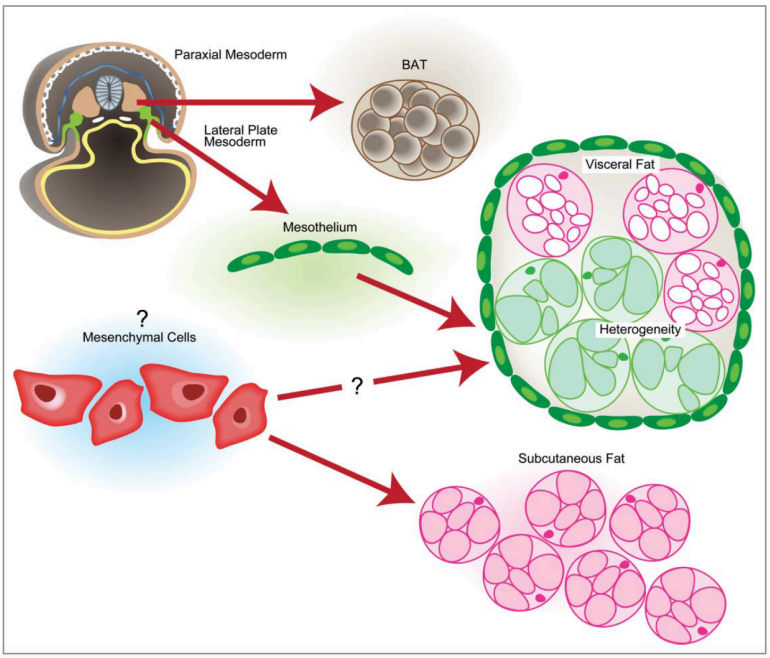


Figure 1.7. The origins of murine adipose tissue types. *WT1 expressing mesothelial cells, which cover the VWAT depots and are derived from the lateral plate mesoderm, can give rise to VWAT adipocytes. MYF5 expressing cells in the paraxial mesoderm of the E8.5 embryo give rise to BAT. The origin of SWAT is currently not known (Chau and Hastie, 2015).*

1.2.2 WT1 in adult homeostasis

Unlike in development, WT1 is only expressed in a limited number of cells and tissues in the adult. Expression has been noted in specific cells of the adult kidney and gonads, as well as in the mesothelium that surrounds the visceral organs, and in 1.2% of the $CD34^{+}$ haematopoietic progenitor cell population in the bone marrow (Walker *et al.*, 1994; Hosen *et al.*, 2007). Within the adult kidney, WT1 is expressed in the glomerular podocyte cells, and within the gonads expression is seen in the Sertoli/granulosa cells of the testis/ovaries (Pelletier *et al.*, 1991; Armstrong *et al.*, 1993; Rao *et al.*, 2006). In the Sertoli cells, WT1 is important for spermatogenesis, as it functions in the communication between the Sertoli and germ cells (Rao *et al.*, 2006).

Despite its limited expression in the adult, a study performed by Chau *et al.* (2011) showed that WT1 is essential for the homeostatic maintenance of multiple organs and tissues (summarised in Figure 1.8). *CAGG-CreER™* and $Wt1^{loxP/loxP}$ mice were crossed, to permit tamoxifen inducible ubiquitous *Wt1* deletion. Mice administered

with tamoxifen at either 3, 10 or 13 weeks of age all rapidly became very sick, presenting with multiple organ failure, meaning they had to be culled within 10 days of tamoxifen administration (Chau *et al.*, 2011). Before being culled, the mice became less active and oedemic, which was confirmed by the presence of fluid subcutaneously and in the abdominal cavity when dissected post-mortem. The weights of both the spleen and heart were reduced, although the heart itself did not exhibit any clear pathology, additionally the testes and ovaries were smaller. The kidneys were pale and there was severe splenic and pancreatic atrophy. However, not all organs were obviously affected by the deletion; the lungs, intestine and liver all appeared normal (Chau *et al.*, 2011).

Upon further investigation, it was shown that there was a complete loss of WT1 expression in the podocytes of the kidney. The foot processes of the podocytes, which are required for the filtration of urine, were absent in the mutant mice and ultimately they exhibited acute glomerulosclerosis. Additionally, in the spleen, the number of proliferating cells was reduced and haematopoiesis was disrupted. The mutant mice displayed a near-complete absence of erythrocytes, and when their bone marrow cells were cultured under conditions to induce haematopoietic differentiation, no red blood cells were formed due to a reduction in the numbers of erythrocyte progenitor cells (Chau *et al.*, 2011). The exocrine, but not endocrine, pancreas displayed significant cell loss, with an increase in the number of apoptotic cells. Furthermore, there was a rapid loss of bone and fat in the mutant mice. The maintenance of bone mass relies on a balance of bone synthesis by osteoblasts and resorption by osteoclasts. Chau *et al*. (2011) showed that there was an in increase in osteoclasts in the mutant mice, coupled with data showing that mesenchymal stem cells had a reduced capacity for osteoblast differentiation *in vitro*.

Regarding the fat, the mutant mice displayed a reduction in size of the SWAT and interscapular BAT depots. In both, the size of the lipid vacuoles of the mature adipocytes was reduced, coupled with a reduction in the expression of *Fabp4* (a lipid transport protein expressed in mature adipocytes), although this result was more variable in the mice given tamoxifen at 13 weeks. However, the numbers of

proliferating and apoptotic cells were comparable to those of control mice. For the first time, in this study, *Wt1* was shown to be expressed in adipose tissue, although intriguingly only in the VWAT depots and not in the SWAT or BAT. Additionally, adipocytes reside in the bone marrow, and the mutant mice also showed a reduction in the number of these marrow-resident adipocytes. The mice also exhibited a dramatic reduction in the levels of circulating IGF-1 and FGF21, which may, at least partially, account for the reduction in bone and fat mass (Chau *et al.*, 2011).

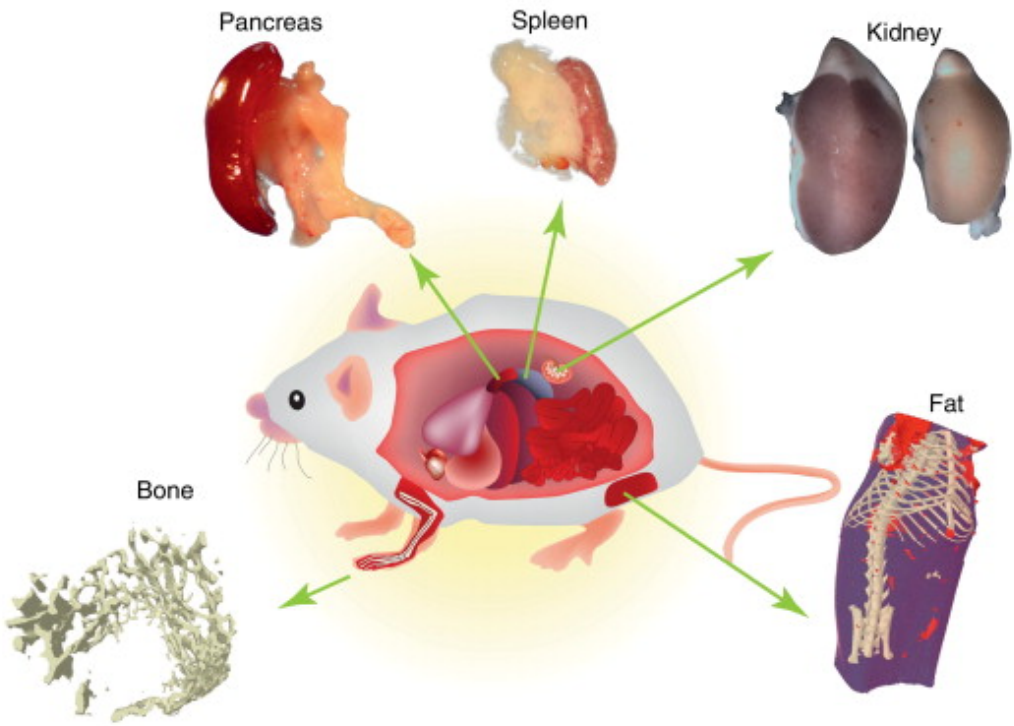


Figure 1.8. WT1 is necessary for the maintenance of homeostasis in adult tissues. *Wt1 deletion in adult mice causes atrophy of the exocrine pancreas, glomerulosclerosis, disruption to erythropoiesis and significant bone and adipose tissue loss. (Adapted from Chau and Hastie, 2012).*

1.3 Overview of the *Prx1-Cre* mouse line

A significant proportion of the work in this PhD has utilised the *Prx1-Cre* mouse line, therefore it shall be introduced here, in the context of adipose tissue. *Prx1* (Paired-related homeobox gene-1, formally called *MHox1*) is expressed in several cell types of mesodermal origin during embryonic development, and plays an important role in the regulation of mesenchymal cell fate (Cserjesi *et al.*, 1992; Du *et al.*, 2013). Its

expression is first detectable at approximately E9 in the lateral plate mesoderm and the visceral arches (pieces of cartilage/bone important in craniofacial development). As the limb buds begin to form at E9.5 they exhibit strong *Prx1* expression. Additionally, the dorsal dermomyotome of the somites (which will give rise to skin and muscle) also expresses *Prx1* at this early developmental stage, as does the dorsal aorta. As development progresses, high levels of expression are maintained in the facial and limb structures, and at E15.5 expression is also seen in the diaphragm and intercostal muscles (Cserjesi *et al.*, 1992). Throughout development, the expression remains restricted to the mesodermal structures, with none observed in the central nervous system. Additionally, no expression is seen in the internal organs including the heart, liver and gut. The pattern of developmental expression is compatible with the gene functioning as a regulator of muscle creatine kinase expression (Cserjesi *et al.*, 1992). In the adult mouse, it is expressed in the skeletal muscle, heart and uterus, and low levels are detected in the lung, but not in the brain, intestine, kidney, liver, pancreas, spleen or stomach (Cserjesi *et al.*, 1992). Studies in which *Prx1* (and the closely related *Prx2*) were mutated, demonstrated the importance of these genes in the regulation of limb skeletal development (Martin, Bradley and Olson, 1995; Lu *et al.*, 1999).

The transgenic *Prx1-Cre* line was first developed by Logan *et al.* (2002). Prior to its generation, an enhancer element that drives *Prx1* expression in the limb bud mesenchyme and a proportion of the craniofacial mesenchyme, was identified in a 2.4kb genomic flanking region (Martin and Olson, 2000). Although at early developmental stages (~E9.5), this 2.4kb region did not drive the expression of a LacZ reporter gene in the craniofacial region or dermomyotome, thus not reflecting endogenous *Prx1* expression, at later stages (E12.5) its expression was activated in the relevant structures. However, throughout development, expression of the reporter gene in the limb bud mesenchyme faithfully recapitulated that of the endogenous gene. It was thus concluded that this 2.4kb region housed the majority of the *Prx1* limb enhancer (Martin and Olson, 2000). Logan *et al*. (2002) situated the *Cre-recombinase* gene under the regulation of this 2.4kb element, and additionally included an insulator element at the 5' end to limit position effects upon transgenic integration. Following microinjection of the transgene into the pronuclei of fertilized zygotes and breeding,

the location of Cre expression was assessed by crossing the mice to the *Z/AP* reporter line. The authors concluded that the pattern of alkaline phosphatase expression, and thus transgene expression, recapitulated that of endogenous *Prx1* in the limb (Logan *et al.*, 2002).

1.3.1 Prx1-Cre and adipose tissue

Traditionally, the *Prx1-Cre* line has largely been used to investigate the skeletal development of the limb, for obvious reasons. However, given the early expression of *Prx1* in the lateral plate mesoderm, and in the mesenchymal progenitor cells of various tissues, we hypothesised that it might also be useful for investigating aspects of adipose tissue development (Martin and Olson, 2000; Logan *et al.*, 2002; Calo *et al.*, 2010). Specifically, we hoped that we might use it to drive the conditional deletion of *Wt1* in visceral adipose tissue precursor cells, without affecting the vital organs. Thus, allowing the mice to survive and permitting us to assess the effects of *Wt1* deletion on visceral adipose tissue development. For reasons that will become apparent, this proved not to be possible, however we still obtained some interesting findings. Additionally, in a study that used the *Prx1-Cre* mouse to understand the role of pRb in establishing lineage commitment of mesenchymal stem cells, *Prx1-Cre* mice were crossed with *lox-stop-lox-LacZ* reporter mice and LacZ staining was observed in the WAT of 4-6 week old animals. Thus showing that Prx1-Cre expressing cells do contribute to WAT (Calo *et al.*, 2010). However, it was not obvious from this study which WAT depot was analysed and whether it was SWAT or VWAT.

Interestingly, *Prx1* has been demonstrated to function in adipogenesis (Du *et al.*, 2013). *Prx1* expression is decreased during adipogenesis both *in vivo* and *in vitro*, and knockdown of *Prx1* leads to increased adipogenesis. Moreover, its expression is increased in obesity. It is thought to function through controlling the expression of the TGFβ ligands: *Tgfb2* and *Tgfb3*, as when *Prx1* is knocked-down, the expression of *Tgfb2* and *Tgfb3* also decreases. Additionally, if TGFβ signalling is blocked during adipogenesis, the effects of *Prx1* knockdown are mimicked (Du *et al.*, 2013).

As described in chapter 4, we initially began by characterising which adipose tissue depots exhibited Prx1-Cre activity, to understand if Prx1-Cre expressing cells contribute to all adipose depots, or to a subset. Whilst we were doing so, it was shown that the majority of the inguinal SWAT precursor cells and mature adipocytes can be labelled with Prx1-Cre, however labelling in perigonadal, mesenteric and retroperitoneal VWAT was very limited (restricted mainly to a small percentage of cells in the female perigonadal VWAT) (Krueger *et al.*, 2014; Sanchez-Gurmaches, Hsiao and Guertin, 2015). Importantly, *Cre* expression was not detected in any of the adipose depots from the six week old mice, indicating that it was expressed earlier in development/life, and that, at least some of the labelling at this age was likely due to lineage tracing. However, high levels of *Prx1* expression were detected in the SWAT, with much lower levels detected in the VWAT depots, therefore showing that, in the six week old mice, *Cre* expression did not reflect endogenous *Prx1* expression (Sanchez-Gurmaches, Hsiao and Guertin, 2015). The authors did highlight the possibility that Prx1-Cre labels a progenitor population during development that gives rise to SWAT (but not VWAT). However, they noted several caveats, the main one being that it could not easily be determined when Prx1-Cre was first expressed, and thus when the initial recombination event occured. Additionally, it was not known if there was a single recombination event that leads to all observed labelling, or multiple (Sanchez-Gurmaches, Hsiao and Guertin, 2015). Given we know that *Cre* expression in these mice does not completely recapitulate endogenous *Prx1* expression, we cannot rely on knowing when and where *Prx1* is expressed to understand when Cre-mediated recombination occurs. As illustrated in chapter 4, we have attempted to address some of these caveats in our work, to gain a better understanding of the developmental origin of SWAT.

1.4 Congenital diaphragmatic hernia (CDH)

As described above, one aim of my PhD was to use the *Prx1-Cre* mouse line to drive the conditional deletion of *Wt1* in VWAT precursor cells, in order to understand more about the role of *Wt1* in adipose tissue development. However, as described in chapter 5, we discovered that the $Prx1^{Cre/+};Wt1^{loxP/loxP}$ genotype was lethal, with the pups dying immediately after birth. It subsequently became apparent that these pups had

diaphragmatic hernias, and were therefore unable to breathe, thus explaining the lethality. Consequently, one focus of my work has been on trying to understand the mechanisms responsible for causing this phenotype in the $Prx1^{Cre/+};Wt1^{loxP/loxP}$ mice.

CDH is a severe developmental defect with a prevalence of approximately 1/2000 pregnancies and 1/3000 live births (Greer, 2013; Paris, Coles and Ackerman, 2015). Aberrant diaphragm development permits herniation of the peritoneal organs into the thoracic cavity, often resulting in pulmonary hypoplasia (Greer, 2013). 80-90% of cases are Bochdalek-type CDH, characterised by hernias in the posterolateral region of the diaphragm. In >85% of the cases, Bochdalek hernias are left sided, whilst 10% occur on the right, and 5% are bilateral (Pober, Russell and Ackerman, 2010). Less common are hernias in the anterior region of the diaphragm, or Morgagni CDH, which account for approximately 2% of all cases. Additionally, central hernias have been described, although these are rare (Pober, Russell and Ackerman, 2010). Moreover, incomplete muscularisation, or diaphragmatic eventration, occurs in certain cases, meaning a thin membranous sheet is present, but due to the lack of muscle, peritoneal organs can push on the diaphragm, into the thoracic cavity. In some cases, diaphragmatic eventration is diagnosed in combination with Bochdalek CDH (Pober, Russell and Ackerman, 2010).

Around 50-60% of hernias occur as an isolated incident, however 40-50% are associated with additional defects, or arise as a result of a chromosome abnormality or single-gene disorder. For example, children with Denys-Drash, Meacham and WAGR syndromes, all of which can be caused by deletion of/mutations in *WT1*, sometimes present with CDH, although this is not always the case (Scott *et al.*, 2005; Suri *et al.*, 2007; Antonius *et al.*, 2008; Carmona *et al.*, 2016). Through a combination of molecular cytogenetic analysis of CDH patients and mouse studies, more than 50 candidate genes have been identified as being potentially causative of CDH, one of which is *WT1* (Holder *et al.*, 2007; Russell *et al.*, 2012; Merrell *et al.*, 2015). However, in most cases, the mechanisms by which these candidate genes cause CDH is not well known.

1.4.1 Development of the diaphragm

Whilst clinically CDH is well studied, the causative mechanisms are still largely unknown. Hence, animal models, such as the one generated in this study are valuable for learning more about the etiology of the defect (Carmona *et al.*, 2016). Evidently, understanding normal diaphragm development is important if we are to fully apprehend what is going wrong in CDH, and the cellular and molecular mechanisms responsible. Traditionally, the nitrofen rat model of CDH has been used to study how diaphragm development deviates from the norm. Nitrofen (2,4-dicholoro-phenyl-p-nitrophenylether) is given to pregnant females, leading to several developmental defects, one of which is CDH associated with pulmonary hypoplasia, thought to be comparable to the human disorder (Mayer, Metzger and Kluth, 2011). Additionally, several mouse models have been utilised to understand better the genetic and cellular basis of CDH.

Normal diaphragm development involves several embryonic structures; the pleuroperitoneal folds (PPFs), the septum transversum (ST), the post hepatic mesenchymal plate (PHMP) and the somites (Merrell and Kardon, 2014; Carmona *et al.*, 2016). The PPFs are mesodermal outgrowths of the body wall that form between the thoracic and peritoneal cavities, at around E10.5-E11.5 in mice (Merrell *et al.*, 2015; Carmona *et al.*, 2016). Along the length of the dorsal body wall, a pair of crests is present at either side. It has been suggested that anteriorly these crests form the PPFs, whilst posteriorly they form the renal ridges (Carmona *et al.*, 2016). As well as contributing to the non-muscle mesenchyme of the diaphragm, the PPFs are thought to be required for guiding the expansion and movement of the myogenic cells that originate in the somites (Merrell *et al.*, 2015). Therefore, if PPF formation/development is disrupted, the muscular component of the diaphragm will also fail to form correctly.

The ST, which traditionally was postulated to be the major origin of the diaphragm, gives rise to the central tendon (Iritani, 1984). In the fully formed diaphragm, the muscular component, which is responsible for movement during breathing, is

positioned at the edge of the central tendon. Two distinct domains of muscle are present; the costal diaphragm, which is comprised of myofibers that extend from the ribs to the central tendon, and the crural diaphragm, which is thicker and located posteriorly to the central tendon, surrounding the oesophagus and aorta and attaching to the vertebrae (Merrell and Kardon, 2014). Movement of the central tendon, driven by the surrounding muscle, permits the thorax volume to be altered (Iritani, 1984).

The PHMP, which is thought to be derived from the mesenchymal population of the lateral ST, overlays the liver, first appearing at ~E10.5 in mice (Iritani, 1984; Carmona *et al.*, 2016). The fusion of the PPFs with the PHMP is an essential step in diaphragm development, and failure to do so can result in the occurrence of lateral hernias. Therefore, during development, the PPFs and PHMP form a membranous continuum, separating the thoracic and peritoneal cavities, and this membrane is subsequently muscularised as myoblasts migrate from the somite (Carmona *et al.*, 2016). Hence, there are several opportunities for development to go awry, both during the fusion of the PPFs and PHMP and in diaphragm muscularisation. A simplified illustration of the fully formed diaphragm is presented in Figure 1.9, including information on the developmental origin of the major components. The mature diaphragm is composed of several tissue types, including muscle, connective tissue, tendon, nerves, blood vessels, mesothelium and lymphatics. In addition to deficiencies in the PPFs/PHMP and muscle, defects in a number of the other components have been described. For example, mouse models of CDH caused by failure of the central tendon to form correctly (Yuan *et al.*, 2003; Coles and Ackerman, 2013; Domyan *et al.*, 2013), as well as those resulting from a disruption to angiogenesis (Zhang *et al.*, 2014) have been developed.

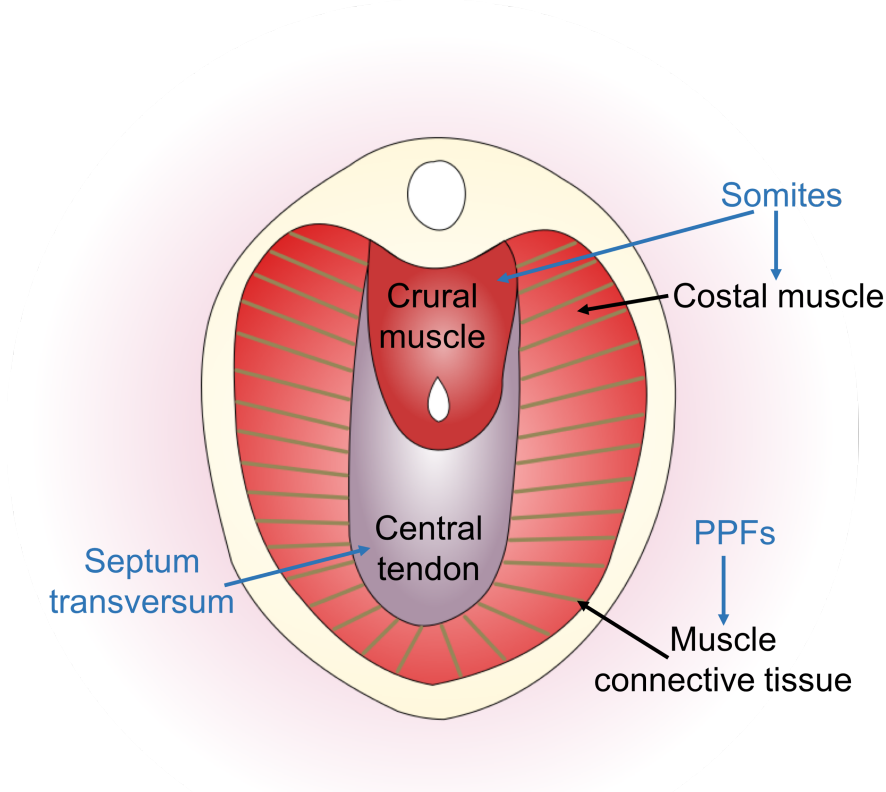


Figure 1.9. The adult diaphragm. *The major components of the adult diaphragm are shown. The myocytes of the crural and costal muscle are derived from the somites. The pleuroperitoneal folds (PPFs) give rise to the muscle connective tissue of the diaphragm, and the central tendon arises from the septum transversum. Note that the nerves, blood vessels, lymphatics and mesothelium are not shown.*

1.4.2 WT1 and the diaphragm

As mentioned previously, mutations in *WT1*, and deletion of chromosome 11p13 (the location of *WT1*) have been described in patients with CDH (Scott *et al.*, 2005; Holder *et al.*, 2007; Suri *et al.*, 2007; Antonius *et al.*, 2008). Additionally, homozygous *Wt1* null mouse embryos develop diaphragmatic hernias (Kreidberg *et al.*, 1993). Interestingly, a phenotypic comparison has been performed between the *Wt1* null model, the nitrofen rat model described above, and a third CDH model: the vitamin A-deficient rat model. The authors concluded that all three had defects in the formation of the PPFs, leading to classic Bochdalek CDH, and thus shared a common pathogenic origin (Clugston *et al.*, 2006).

Indeed, it has also been shown that WT1 is expressed in the PPFs of the developing diaphragm (Paris, Coles and Ackerman, 2015). Mesothelial cells can be found on the surface of both the mature and developing diaphragm (initially just at the thoracic side,

although following total separation of the diaphragm from the liver, also at the abdominal side) (Shinohara, 1997). Paris *et al*. (2015) illustrated that both the mesothelial cells, and the mesenchymal cells of the developing and mature diaphragm express WT1, although this expression is strongest in the mesothelial cells (Paris, Coles and Ackerman, 2015). Moreover, using lineage tracing they showed that when tamoxifen induced recombination occurs at E10.5, the labelled cells contribute to the posterior diaphragm to a greater extent than when recombination is induced at E8.5-E9.5 (Paris, Coles and Ackerman, 2015). Therefore, this has implications for the timing of *Wt1* deletion and the phenotype that prevails. Additionally, this study revealed that conditional deletion of *Ctnnb1* in WT1 expressing cells of the developing diaphragm, leads to diaphragmatic hernia, and that *Ctnnb1* lies downstream of *Wt1*. The deletion of *Wt1* or *Ctnnb1* resulted in both an increase in apoptosis and a decrease in proliferation of the mesothelial cells. Moreover, the deletion of these genes caused a failure of mesenchymal differentiation in the non-muscle mesenchymal cells, due to a lack of TWIST1 expression. The authors concluded that mesothelial signalling, regulated by WT1, is essential for the proper differentiation and formation of the diaphragm (Paris, Coles and Ackerman, 2015).

Another recent paper used the G2 enhancer of the *Gata4* gene to drive the conditional deletion of *Wt1* in the murine lateral plate mesoderm, to further investigate the role of WT1 in diaphragm development (Carmona *et al.*, 2016). 80% of the *G2-Gata4*^{Cre}*;Wt1*$^{loxP/loxP}$ embryos presented with Bochdalek-type CDH. They used lineage tracing to show that both the mesenchymal PPF and PHMP cells are derived from a Wt1-Cre expressing lineage, and express WT1 themselves. Notably, they observed that *G2-Gata4*^{Cre}*;R26R*^{YFP} reporter embryos exhibited YFP expression in the cells of the PHMP and PPFs. Additionally, they showed that whilst the lateral mesenchymal cell population of the ST did express YFP, the central area did not. This is significant, given that the PHMP is thought to be derived from the lateral ST (Carmona *et al.*, 2016). Therefore, the *G2-Gata4*^{Cre} line could be used to drive deletion in this specific region of the ST, and the structures that arise from it.

In the *G2-Gata4^{Cre};Wt1$^{loxP/loxP}$* embryos, defects in the PHMP were evident from E10.5. Fewer mesenchymal cells were noted between the mesothelium of the PHMP and the liver, and it was observed that the mesenchymal cells that were present did not migrate towards the PPFs, and therefore the thoracic and peritoneal cavities were not separated (Carmona *et al.*, 2016). Moreover, given the role that WT1 plays in EMT, CDH1 expression was checked in control and mutant E11.5 embryos, revealing increased expression in the mesothelial and mesenchymal cells of the PHMP in the mutants (Carmona *et al.*, 2016). This suggests that WT1 may be important for EMT in the developing diaphragm. Additionally, it was noted that retinaldehyde dehydrogenase 2 (RALDH2) expression decreased in the PHMP of the mutant embryos, and that treatment with retinoic acid (which is synthesised endogenously from retinaldehyde via catalysis by RALDH2), could partially rescue the phenotype (Carmona *et al.*, 2016). The retinoic acid signalling pathway has been well described as being involved in diaphragm development, and nitrofen acts by inhibiting retinoic acid synthesis (Greer, Babiuk and Thebaud, 2003; Mey *et al.*, 2003). Moreover, it is known that, in the epicardium, retinoic acid signalling is important for EMT, and that WT1 activates the transcription of *Raldh2* (Guadix *et al.*, 2011; von Gise *et al.*, 2011). Therefore, the finding that RALDH2 expression and retinoic acid signalling was disrupted during diaphragm development in this model was not unsurprising. It was therefore concluded that the loss of function of *Wt1* in this model resulted in the defective formation of the PHMP mesenchyme, possibly as a consequence of disrupted retinoic acid signalling and EMT (Carmona *et al.*, 2016). Moreover, it was proposed that the predominance of left sided hernias was a consequence of fewer mesenchymal cells in the left PHMP compared to the right, therefore making the left more vulnerable to deformities when defects occurred in the PHMP cells (Carmona *et al.*, 2016).

1.4.3 Prx1-Cre and the diaphragm

Evidently, WT1 is known to function in the development of the diaphragm, and possible mechanisms of action are beginning to be described. Additionally, it has recently been shown that *Prx1-Cre;Rosa26^{LacZ}* mice exhibit labelling of the PPFs, therefore indicating that the cells of the PPFs are derived from a Prx1-Cre expressing

lineage (Merrell *et al.*, 2015). Moreover, these Prx1-Cre lineage positive PPF cells expressed the muscle connective tissue marker TCF4, as did the lineage positive cells in the mature diaphragm. This demonstrates that the PPFs are not only important during development but also give rise to tissue within the fully formed diaphragm (Merrell *et al.*, 2015). Importantly, no labelling of the ST was reported in these mice, although it was subsequently suggested by Carmona *et al*. (2016), that perhaps this only applied to the central ST (Merrell *et al.*, 2015; Carmona *et al.*, 2016). Additionally, time-lapse videos show the collective cell migration of the Prx1-Cre lineage positive PPF cells across the surface of the liver in an *ex vivo* culture system, which the authors conclude to be essential for the expansion and morphogenesis of the muscle progenitor cells (Merrell *et al.*, 2015). Thus, it is clear that the mesenchymal cells of the PPFs are derived from both Prx1-Cre and Wt1-Cre expressing lineages, and these cells give rise to the connective tissue fibroblasts of the diaphragm. Hence, it is perhaps not unsurprising that the $Prx1^{Cre/+};Wt1^{loxP/loxP}$ mice generated by us present with diaphragmatic hernias. As described in chapter 5, the focus of this aspect of my PhD was on elucidating the mechanisms by which *Wt1* deletion in the Prx1-Cre lineage resulted in defective diaphragm development.

1.5 Summary

Considerable efforts have focused on gaining a greater understanding of adipocyte ontogeny, in the hope that doing so will inform on how and why distinct adipose depots differ in their contribution to obesity and its associated pathologies. Recent work has shown that the tumour suppressor gene, *Wt1*, is expressed in a subset of APCs from VWAT, but not those from SWAT or BAT (Chau *et al.*, 2014). Moreover, lineage tracing demonstrates that *Wt1* expressing cells present embryonically at E14.5, give rise to mature adipocytes in the visceral adipose depots of adult mice. Additionally, cells of the epididymal appendage, which is necessary for the formation of the epididymal visceral depot, express *Wt1* and can form adipocytes in an *ex vivo* culture system. Hence, *Wt1* expressing cells contribute to VWAT depots (Chau *et al.*, 2014). However, the adipocyte precursor cell populations are heterogeneous, with not all expressing *Wt1*, which begs the question as to whether this heterogeneity has a

functional consequence. Moreover, how do the precursor cells from the Wt1 lineage contribute to visceral adipose organogenesis and function?

Additionally, it is known that BAT has its developmental origins in the paraxial mesoderm, and that the lateral plate mesoderm gives rise to at least a proportion of visceral adipocytes, but the embryonic origin of SWAT is not well understood (Chau *et al.*, 2014; Sanchez-Gurmaches and Guertin, 2014b). Given that subcutaneous adipose tissue is known as "good fat" and thus is not associated with metabolic disease and other obesity related disorders, not knowing from where it is derived represents a major gap in adipose tissue knowledge and understanding.

1.5.1 Hypothesis

The original goal of my thesis was to test the hypothesis that WT1 is required for the development of visceral white adipose tissue.

1.5.2 Aims

The initial aim of this project was to determine the role of *Wt1* in the development of visceral white adipose tissue. I also hoped to further investigate the heterogeneity that exists within the visceral adipocyte precursor cell population, regarding *Wt1* expression.

As will become evident, due to several findings, the aims of my project changed somewhat over the course of my PhD. Therefore, the main aims have been as follows:

- To define if/what differences exist between *Wt1* expressing and non-expressing visceral adipocyte precursor cells, at the behavioural and transcriptomic level.
- To determine how high fat diet conditions influence the *Wt1* expressing precursor cell population.
- To investigate the Prx1-Cre lineage in adipose tissue.
- To elucidate the cellular and molecular mechanisms responsible for the development of congenital diaphragmatic hernia in $Prx1^{Cre/+};Wt1^{loxP/loxP}$ mice.

Chapter 2

Materials & Methods

2.1 General reagents

The reagents listed below were prepared by the Core Scientific Services of the MRC IGMM Human Genetics Unit (HGU):

PBS

Phosphate Buffered Saline (pH 7.3): 8 g Sodium Chloride NaCL, 0.2 g Potassium Chloride KCl, 1.15 g Disodium Hydrogen Phosphate Na_2HPO_4, 0.2 g Potassium Dihydrogen Phosphate KH_2PO_4, made up in 1 litre distilled water. This was made by dissolving 10 Dulbecco's tablets in 1 litre of distilled water (Cat# BR0014, Oxoid Limited, Hampshire, RG24 8PW, UK).

Trypsin

2 g Trypsin (1:250), 5 ml Phenol Red, 0.06 g Penicillin, 0.13 g Streptomycin, made up to 1 litre in PBS. pH altered to 7.8 using $NaHCO_3$.

Versene

0.4 g Sodium EDTA and 5 ml 0.2% Phenol Red made up to 1 litre in PBS.

Penicillin/Streptomycin (P/S)

7 g ($10x10^8$ units) Penicillin and 13 g Streptomycin, made up to 1 litre with distilled water.

2.2 Transgenic animal models

2.2.1 Animal husbandry

All mice used were housed in one of two facilities: The Transgenic Unit (TGU); a barrier facility for animals generated using transgenic methods, and the Biomedical Research Facility (BRF); a semi-barrier facility for other mice. Where required, all procedures were performed under a Personal and Project Home Office Licence.

2.2.2 Genotyping of mice

Genomic DNA extracted from mouse ear clips was used for PCR genotyping. Anna Thornburn, from the MRC Human Genetics Unit (HGU) performed all ear clipping and genotyping.

2.2.3 *Wt1*$^{GFP/+}$ knock-in mouse line

The knock-in reporter GFP mouse line (*Wt1*$^{GFP/+}$) used in this study was made by Hosen *et al*. (2007). In these mice, GFP replaces exon 1 of *Wt1* and is expressed under the endogenous transcriptional regulatory elements of the *Wt1* gene. Therefore, any *Wt1* expressing cells fluoresce green. The loss of one *Wt1* allele does not affect viability (Hosen *et al.*, 2007).

2.2.4 WER mouse line

A *Wt1* conditional line was developed in our group, whereby loxP sites flank the first exon of *Wt1* resulting in *Wt1*$^{loxP/loxP}$ mice (Martínez-Estrada *et al*., 2010). To drive the conditional deletion of *Wt1*, these mice were crossed with *CAGG-CreER*^{TM} mice, in which the expression of Cre is driven by the CAGG promoter. The administration of tamoxifen to the *CAGG-CreER*^{TM}*;Wt1*$^{loxP/loxP}$ (WER) mice, or cells isolated from them, results in ubiquitous deletion of *Wt1* (Chau *et al.*, 2011). *In vitro*, 1 μM 4-OH tamoxifen ((z)-4-hydrotamoxifen) (Cat# H7904, Sigma-Aldrich Company Ltd., Dorset, England) was added to the culture media to induce Cre mediated *loxP* recombination.

2.2.4.1 Cre control mouse line

To evaluate the toxicity of the dissociated Cre, pure *C57BL/6J* mice (The Jackson Laboratory, Maine, 04609, USA) were crossed with *CAGG-CreER*^{TM} mice to generate *CAGG*$^{Cre/+}$ (Cre+) and *CAGG*$^{+/+}$ (Cre-) offspring.

2.2.5 *Wt1-Cre^{ERT2};R26R-mTmG* mouse line

To label and trace *Wt1* expressing cells, a tamoxifen inducible *Wt1-Cre^{ERT2};R26R-mTmG* mouse line was used (Chau *et al.*, 2014). This line was generated by crossing a knock-in mouse with a tamoxifen inducible Cre recombinase at the *Wt1* promoter (*Wt1-Cre^{ERT2}*) (Zhou *et al.*, 2008) with the *R26R-mTmG* double-fluorescent Cre reporter mouse (Muzumdar *et al.*, 2007). In these mice, prior to Cre mediated recombination, Tomato is ubiquitously expressed under a pCA promoter, labelling all cells red. However, following tamoxifen administration and thus Cre mediated loxP recombination, driven by the *Wt1* promoter, Tomato is excised. Therefore, all Cre expressing cells and their progeny express eGFP.

2.2.5.1 *In vivo* lineage tracing

To induce Cre mediated loxP recombination *in vivo* in *Wt1-Cre^{ERT2};R26R-mTmG* mice, tamoxifen (Cat# T5648, Sigma-Aldrich Company Ltd., Dorset, England) was dissolved in Glyceryl Trioctanoate (Cat# T9126, Sigma-Aldrich Company Ltd., Dorset, England) at a concentration of 20 mg/ml. Tamoxifen was gavaged into the mice at a dose of 8 mg/40 g body weight. 4 doses of tamoxifen (2 per week) were given to mothers beginning at P0 (thus after giving birth), so the pups could receive the tamoxifen postnatally via the mother's milk, and the offspring were analysed at either 7.5 months or 1 year old, as described in chapter 3.

2.2.6 *Prx1-Cre;R26R-mTmG* and *Prx1-Cre^{ERT2};R26R-mTmG* mouse lines

In order to label and trace Prx1-Cre expressing cells, transgenic male *Prx1-Cre* mice (Logan *et al.*, 2002) were crossed with female *R26R-mTmG* double-fluorescent Cre reporter mice (Muzumdar *et al.*, 2007) to generate the *Prx1-Cre;R26R-mTmG* mouse line. As described in 2.2.5 all cells are labelled red prior to Cre mediated loxP recombination. However, following Cre expression, driven a *Prx1* derived enhancer element, all Cre expressing cells express eGFP. Therefore, all Prx1-Cre expressing cells, and their progeny are labelled with eGFP, and fluoresce green.

Additionally, tamoxifen-inducible *Prx1-Cre^{ERT2};R26R-mTmG* mice were used (Hasson, Del Buono and Logan, 2007; Muzumdar *et al.*, 2007). In these mice, Cre mediated loxP recombination does not occur until tamoxifen is administered, therefore allowing the timing of recombination to be controlled. Again, male *Prx1-Cre^{ERT2}* mice were crossed with female *R26R-mTmG* mice to generate the *Prx1-Cre^{ERT2};R26R-mTmG* line. At the time of tamoxifen administration, all Prx1-Cre^{ERT2} expressing cells are labelled with eGFP, as are their progeny.

2.2.6.1 *In vivo* lineage tracing

Induction of Cre mediated loxP recombination *in vivo* in *Prx1-Cre^{ERT2};R26R-mTmG* mice was performed as described in 2.2.5.1. One dose of tamoxifen was administered to pregnant mice at either E9.5, E11.5 or E13.5 and the offspring were analysed at E18.5, or fostered by CD1 mothers and analysed at 6 weeks (tamoxifen administration prevents the mice from being able to give birth, therefore the pups have to be fostered onto a CD1 mouse, this was performed by Anna Thornburn). Alternatively, 4 doses of tamoxifen (2 per week) were given to mothers beginning at P0 (thus after giving birth), so the pups could receive the tamoxifen postnatally via the mother's milk, and the offspring were analysed at 6 weeks.

2.2.7 *Prx1-Cre;tdRFP;Wt1$^{GFP/+}$* mouse line

To label and trace Prx1-Cre expressing cells, whilst at the same time labelling *Wt1* expressing cells, a new mouse line was generated. This was designed to allow us to assess whether any, and if so what percentage of cells were Prx1-Cre lineage positive and *Wt1* expressing. Mice that have GFP knocked-in at the *Wt1* locus (Hosen *et al.*, 2007) (see 2.2.3 for description), were crossed with tandem-dimer red-fluorescent-protein (ROSA26-tdRFP) Cre reporter mice (Luche *et al.*, 2007). Female *tdRFP;Wt1$^{GFP/+}$* mice were then crossed with male *Prx1-Cre* mice to generate the *Prx1-Cre;tdRFP;Wt1$^{GFP/+}$* mouse line. In these mice, all *Wt1* expressing cells are labelled with GFP and thus fluoresce green, and in addition to this, all Prx1-Cre expressing cells, and their progeny are labelled with tdRFP, and thus fluoresce red.

2.2.8 *Prx1-Cre;Wt1*$^{loxP/loxP}$ and *Prx1-Cre;Wt1*$^{loxP/GFP}$ mouse lines

To understand the effects of conditionally deleting *Wt1* in Prx1-Cre expressing cells, the *Prx1-Cre;Wt1*$^{loxP/loxP}$ mouse line was generated. A *Wt1* conditional line was generated in our group, whereby loxP sites flank the first exon of *Wt1* resulting in *Wt1*$^{loxP/loxP}$ mice (Martínez-Estrada *et al.*, 2010). Male *Prx1-Cre* mice were crossed with female *Wt1*$^{loxP/loxP}$ mice to generate this line, which, as described in chapter 5, is lethal at birth.

Additionally, a *Prx1-Cre;Wt1*$^{loxP/GFP}$ mouse line was generated, whereby one copy of *Wt1* is flanked by *loxP* sites, and the other copy has GFP knocked in, replacing exon 1 and disrupting function (as described in 2.2.3). Therefore, all *Wt1* expressing cells fluoresce green, and have one functional copy of *Wt1*, however, upon Cre expression the second copy of *Wt1* is deleted. Hence, any cells that express *Wt1* or would normally express *Wt1*, fluoresce green. This is a useful tool, as it allows us to identify in which cells *Wt1* has been deleted.

2.2.9 High fat diet feeding

To study the effects of a high fat diet (HFD) on the percentage and properties of *Wt1* expressing adipocyte precursor cells (APCs), and the percentage of adipocytes derived from *Wt1* expressing cells, we put *Wt1*$^{GFP/+}$ knock-in mice and *Wt1-Cre*^{ERT2}*;R26R-mTmG* mice on a HFD regime. ~3 month old male *Wt1*$^{GFP/+}$ knock-in mice were fed either a HFD (58% of kcal from fat) (Cat# D12331, Research Diets Inc., New Brunswick, NJ 08901 USA) or a control diet (CD) (11% of kcal from fat) (Cat# D12329, Research Diets Inc., New Brunswick, NJ 08901 USA) for ~4 months. The mice were weighed once per week for the duration of the study. ~1 month old male *Wt1-Cre*^{ERT2}*;R26R-mTmG* mice were fed a HFD (58% of kcal from fat) (Cat# D12331, Research Diets Inc., New Brunswick, NJ 08901 USA) for ~7.5 months.

2.3 Immunohistochemistry/ Immunocytochemistry

2.3.1 Sample preparation for immunohistochemistry

Samples were washed in PBS and fixed in 4% Paraformaldehyde (Cat# P6148, Sigma-Aldrich Company Ltd., Dorset, England) dissolved in PBS. Typically, samples were fixed at 4°C overnight, unless otherwise stated. Samples were then washed twice in PBS for 10 minutes and stored in 70% Ethanol at 4°C before processing. Samples were processed and embedded in paraffin wax using a Tissue-Tek VIP® Jr. Vacuum Infiltration Processor (Sakura Finetek UK Ltd., Thatcham, RG19 4LW, UK). E9.5 mouse embryos were embedded by hand. Processing conditions and timings are shown in Table 2.1.

Paraffin sections were cut ~5-6 μm thick using a Leica RM2235 Rotary Microtome (Leica Biosystems Ltd., Newcastle Upon Tyne, NE12 8EW, UK), mounted on SuperFrost® Plus Microscope Slides (Cat# 631-0108, VWR International, Leicestershire, LE17 4XN) and dried at 50°C overnight.

2.3.2 Immunofluorescence staining paraffin sections

2.3.2.1 Solutions for immunofluorescence staining

<u>TEG Buffer pH 9.0</u>

2.422 g TRIS – (hydroxymethyl) aminomethane (Cat# 103156X, VWR International, Leicestershire, LE17 4XN), 0.38 g EGTA (Ethylene glycol-bis (2-aminoethylether)-N,N,N',N'- tetraacetic acid), (Cat# E3889, Sigma-Aldrich Company Ltd., Dorset, England), made up to 2 litres in distilled water.

<u>50 mM NH_4Cl in PBS</u>

2.675 g NH_4Cl dissolved in 1 litre 0.01M PBS, pH 7.4.

Wash 1 (0.01 M PBS, 1% BSA, 0.2% Gelatine, 0.05% Saponin, pH 7.4)

2 g Gelatine (Cat# G1890, Sigma-Aldrich Company Ltd., Dorset, England) and 200 ml 0.01 M PBS (pH7.4) microwave heated until Gelatine is dissolved. This is added to 10 g BSA (Cat# A3294, Sigma-Aldrich Company Ltd., Dorset, England), 0.5 g Saponin (Cat# S4521, Sigma-Aldrich Company Ltd., Dorset, England), dissolved in 800 ml 0.01 M PBS pH 7.4, to make 1 litre.

Wash 2 (0.01 M PBS, 0.1% BSA, 0.2% Gelatine, 0.05% Saponin, pH 7.4)

2 g Gelatine (Cat# G1890, Sigma-Aldrich Company Ltd., Dorset, England) and 200 ml 0.01 M PBS (pH7.4) microwave heated until Gelatine is dissolved. This is added to 1 g BSA (Cat# A3294, Sigma-Aldrich Company Ltd., Dorset, England), 0.5 g Saponin (Cat# S4521, Sigma-Aldrich Company Ltd., Dorset, England), dissolved in 800 ml 0.01 M PBS pH 7.4, to make 1 litre.

Antibody Solution (0.01 M PBS, 0.1% BSA, 0.3% Triton™ X-100)

0.05 g BSA dissolved in 50 ml 0.01 M PBS. Add 150 µl Triton™ X-100 (Cat# T8787, Sigma-Aldrich Company Ltd., Dorset, England) and mix.

Table 2.1. Processing conditions and timings for embedding adipose tissue and mouse embryos using a Tissue-Tek VIP® Jr. Vacuum Infiltration Processor

STAGE	SOLUTION	TIME FOR: ADULT ADIPOSE TISSUE (MINUTES)	E18.5 EMBRYO	E16.5 EMBRYO	E14.5 EMBRYO	E12.5 EMBRYO	E11.5 EMBRYO	E10.5 EMBRYO	E9.5 EMBRYO
P/V	Alternating pressure & vacuum during processing	Off	On after stage 5	On after stage 5	On after stage 5	Off	Off	Off	N/A Hand embedded
1	70% EtOH	12	120	100		30	15	12	
2	70% EtOH	12	120	100		30	15	12	
3	85% EtOH	12	120	100		30	15	12	
4	95% EtOH	12	120	100		30	15	12	
5	100% EtOH	12	120	100		30	15	12	
6	100% EtOH	12	120	100		30	15	12	
7	100% EtOH	12	120	100		30	15	12	
8	Xylene	12	120	100		30	15	12	
9	Xylene	12	120	100		30	15	12	
10	Xylene	12	120	100		30	15	12	
11	Wax	12	120	100		30	15	12	
12	Wax	12	120	100		30	15	12	
13	Wax	12	120	100		30	15	12	
14	Wax	12	120	100		30	15	12	

2.3.2.2 Immunofluorescence staining

Slides were dewaxed in xylene for a minimum of 2 hours and then the sections were rehydrated using a series of ethanol washes (3x 10 minutes in 100% EtOH, 2x 10 minutes in 96% EtOH, 1x 10 minutes in 70% EtOH), before finally washing in dH_2O. To perform antigen retrieval, slides were placed in 1 litre of TEG Buffer in a pressure cooker, and boiled for 5 minutes. Slides were then allowed to cool (in the TEG Buffer) and washed for 30 minutes in 50 mM NH_4Cl. Blocking was performed by washing the slides for 3x 10 minutes in Wash 1. Sections were incubated with primary antibodies overnight at 4°C. All primary antibody details and concentrations can be found in Table 2.2.

The following day, slides were washed 3x 10 minutes with Wash 2, and incubated for 1 hour in the dark at room temperature with the relevant secondary antibodies (outlined in Table 2.2). Finally, slides were washed in PBS and distilled water and mounted using VectaShield Mounting Medium with DAPI (H-1200, Vector Laboratories, Inc., Peterborough, PE2 6XS, United Kingdom) and stored in the dark before imaging.

Table 2.2. Antibody information

ANTIBODY	DESCRIPTION	DILUTION	MANUFACTURER CAT #
Wt1	Rabbit Polyclonal	1:1000	Abcam ab89901
Ki67	Rabbit Polyclonal	1:1000	Abcam ab15580
GFP	Goat Polyclonal	1:1000	Abcam ab5450
Perilipin	Rabbit Polyclonal	1:10,000	Sigma P1998
CD31	Rabbit Polyclonal	1:200	Santa Cruz sc-1506
Pax2	Rabbit Polyclonal	1:100	Biolegend 901001
MF20	Mouse Monoclonal	1:20	DSHB AB_2147781
Vimentin	Goat Polyclonal	1:100	Santa Cruz sc-7557
E-cadherin	Mouse Monoclonal	1:100	BD 610181
Raldh2	Goat Polyclonal	1:200	Santa Cruz sc-22591
β-catenin	Rabbit Polyclonal	1:1000	Sigma C2206
AlexaFluor® 488	Donkey Anti-Goat IgG	1:1000	Invitrogen A11055
AlexaFluor® 594	Donkey Anti-Rabbit IgG	1:1000	Invitrogen A21207
AlexaFluor® 488	Donkey Anti-Mouse IgG	1:1000	Invitrogen A21202

2.3.3 Haematoxylin and Eosin staining

Slides were dewaxed in xylene (3x 5 minute washes), before being rehydrated in a series of ethanol washes (3x 5 minutes in 100% EtOH, followed by 2 minutes each in 90%, 70%, 50% and 30% EtOH). Slides were washed in tap water and stained for 5 minutes with Mayer's Haematoxylin (S3309, Dako UK Ltd., Cambridgeshire, CB7 4EX). After another wash with tap water, sections were differentiated in 1% HCl in 70% EtOH for a few seconds and washed with tap water. Slides were then placed in Saturated Lithium Carbonate solution for a few seconds and washed in running tap water for 5 minutes. After staining with Eosin for 2-5 minutes, slides were rinsed in tap water again before placing into 100% EtOH. Following 3 more washes in 100% EtOH (1-2 minutes each), the slides were cleared in xylene (3x 5 minute washes) and mounted using DPX mounting medium (Cat# SEA-0302-00A, CellPath Ltd., Powys, SY16 4LE). Eosin stain: 3 parts 1% aqueous Eosin and 1 part 1% EtOH, with Acetic Acid 0.05% final concentration.

2.3.4 Immunocytochemistry

Cells that were grown in chamber slides (Cat# 94.6170.802, Sarstedt Ltd., Leicester, LE4 1AW), as described in 3.2.2, were stained as follows. Media was removed and cells were washed with PBS before being fixed using 4% paraformaldehyde (Cat# P6148, Sigma-Aldrich Company Ltd., Dorset, England) dissolved in PBS, for 20 minutes at room temperature. Paraformaldehyde was removed and cells were washed 2x with PBS. 3x 5 minute washes with 0.01 M PBS, 1% BSA (Cat# A3294, Sigma-Aldrich Company Ltd., Dorset, England) were performed and cells were blocked in 0.01M PBS, 1% BSA (Cat# A3294, Sigma-Aldrich Company Ltd., Dorset, England), 0.3% Triton™ X-100 (Cat# T8787, Sigma-Aldrich Company Ltd., Dorset, England) for 45 minutes at room temperature. Cells were stained using primary antibodies outlined in Table 2.2 (diluted in 0.01 M PBS, 1% BSA (Cat# A3294, Sigma-Aldrich Company Ltd., Dorset, England)) overnight at 4°C.

The following day, the primary antibodies were removed and cells washed 3x 5 minutes with 0.01 M PBS, 1% BSA (Cat# A3294, Sigma-Aldrich Company Ltd., Dorset, England). Secondary antibodies, as described in Table 2.2 (diluted in 0.01 M PBS, 1% BSA (Cat# A3294, Sigma-Aldrich Company Ltd., Dorset, England)), were applied for 1 hour at room temperature. The secondary antibodies were removed and cells were washed 3x with PBS before being mounted using VectaShield Mounting Medium with DAPI (H-1200, Vector Laboratories, Inc., Peterborough, PE2 6XS, United Kingdom) and stored in the dark before imaging.

2.3.5 Imaging

Matthew Pearson, Harris Morrison, Laura Murphy and Ann Wheeler from the MRC HGU gave guidance and assistance with the imaging work carried out for this thesis. A Zeiss Axioplan II microscope (Carl Zeiss Ltd., Cambridge, CB1 3JS, UK) was used to view immunofluorescence and H&E stained sections and cells. The immunofluorescence imaging system used consisted of a Photometrics Coolsnap HQ2 CCD camera (Photometrics Ltd, Tucson, AZ), Zeiss Axioplan II fluorescence microscope with Plan-neofluar or Plan-Apochromat objectives, a 100W Hg source (Carl Zeiss, Welwyn Garden City, UK) and Chroma #89014ET three colour filter set (Chroma Technology Corp., Rockingham, VT). The single excitation and emission filters were installed in motorised filter wheels (Prior Scientific Instruments, Cambridge, UK). Image capture was performed using the open source microscopy software: µManager (version 1.4) (Edelstein *et al.*, 2014). For brightfield colour imaging the imaging system comprised a Qimaging Micropublisher 3.3MP cooled colour CCD camera (Qimaging, Burnaby, BC), Zeiss Axioplan II fluorescence microscope with Plan-neofluar or Plan Apochromat objectives (Carl Zeiss, Welwyn Garden City, UK). Image capture was performed using the open source microscopy software: µManager (version 1.4) (Edelstein *et al.*, 2014).

When quantifying the percentage of eGFP expressing adipocytes in chapters 3 and 4, more than 100 adipocytes were counted per sample.

In sections 3.2.2 and 3.3, cells cultured in chamber slides before being fixed and stained with anti-Ki67 and anti-GFP antibodies were imaged. An average of 60 images were taken per well and these were quantified using Definiens® software, as described below.

2.3.5.1 Analysis using Definiens® software

Definiens® tissue phenomics software was used to quantify the percentage of KI67 expressing cells in the chamber slide cultures. As shown in Figure 2.1, the software detected all DAPI positive nuclei (coloured grey in B) and also detected the KI67 expressing cells (coloured yellow in B). A table of raw results showing the total number of nuclei and the number of KI67 expressing nuclei, based on these images, was produced by the software.

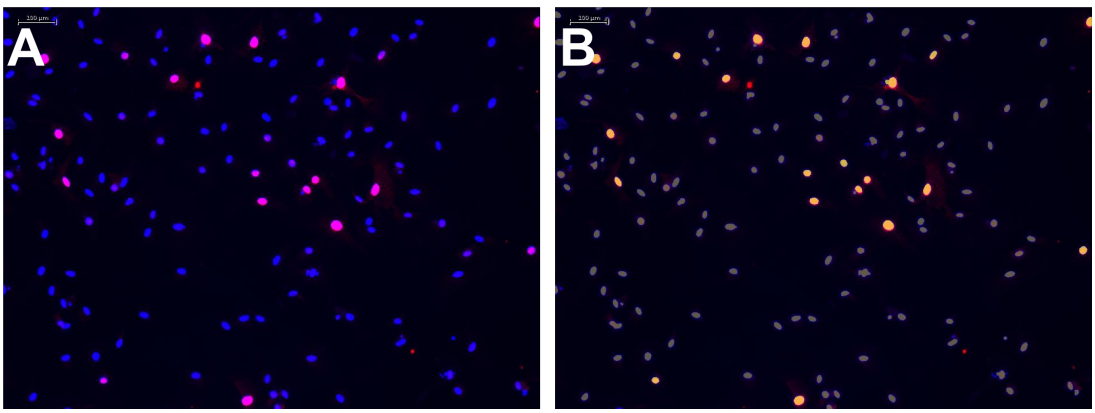


Figure 2.1. Representative images of cells analysed using Definiens® software. (A) *shows the image that was input to the software for the analysis,* ***(B)*** *shows a processing step performed by Definiens® to detect all KI67 expressing nuclei.*

2.4 Flow cytometry & fluorescence activated cell sorting (FACS)

2.4.1 Isolation of murine stromal vascular fraction (SVF) cells from adipose tissue

APCs reside within the SVF of individual adipose tissue depots. The SVF is comprised of various cell types. For this PhD project, it was necessary to isolate the SVF from the adipose tissue, and subsequently isolate the APCs from the other SVF cell types.

The required adipose tissue depots were dissected out of the mice and washed in 0.1 M PBS. The tissue was transferred to a 10 cm culture dish and using carbon steel surgical blades, was chopped into 1-2 mm pieces. This chopped tissue was combined with ~10 ml Collagenase B (Cat# 11088815001, Roche Diagnostics Ltd, Burgess Hill, RH15 9RY) (1 mg/ml) in 0.1 M PBS with 4 mg/ml Bovine Serum Albumin (BSA) (Cat# A3294, Sigma-Aldrich Company Ltd., Dorset, England) and 1% penicillin/streptomycin. This was transferred to a 15 ml Falcon tube and incubated at 37°C for 1 hour in a rocking chamber. The tubes were shaken vigorously by hand to obtain a single cell suspension, and the contents filtered through a 70 μm nylon cell strainer into a 50 ml Falcon tube. The filtered cell suspensions were spun down at 300 RCF for 5 minutes at 4°C using an Allegra X-22R Centrifuge (Beckman Coulter (UK) Ltd., High Wycombe, HP11 1JU). Using vacuum aspiration, the supernatant, containing the enzyme and floating mature adipocytes, was removed. The cell pellet that remained in the tube was the SVF, and was re-suspended in 1 ml of FACS buffer. FACS buffer: 0.01M PBS, 5% Fetal Calf Serum (FCS) and 1% penicillin/streptomycin.

2.4.2 Isolation of APCs from the SVF

To remove non-adipogenic SVF cells and obtain primarily the APCs, the SVF cells were stained with various antibodies against cell surface markers and sorted using FACS. The list of antibodies and their dilutions can be found in Table 2.3. Not all antibodies were used for all isolations, and this is outlined in the appropriate sections within the results chapters. Furthermore, additional antibodies that were used for labelling cells of other lineages where required are listed.

For all antibodies used, the protocol was the same. The cell suspension from 2.4.1 was filtered into a Falcon® 5 ml polystyrene round-bottom tube with cell strainer cap (35 μM) (Corning Inc, Flintshire, CH5 3XD) and spun down at 300 RCF for 5 minutes at 4°C using an Allegra X-22R Centrifuge (Beckman Coulter (UK) Ltd., High Wycombe, HP11 1JU). Pelleted SVF cells were re-suspended in 100 μl of the diluted antibody(s), and incubated at room temperature for 15 minutes in the dark. Antibodies were diluted

in FACS buffer (See 2.4.1). To wash, 3 ml of FACS buffer was added to the samples and they were spun down at 300 RCF for 5 minutes at 4°C using an Allegra X-22R Centrifuge (Beckman Coulter (UK) Ltd., High Wycombe, HP11 1JU). The supernatant was removed and the pelleted cells either stained with additional antibodies or re-suspended in ~400 µl FACS buffer ready for sorting. With the exception of the antibodies in the Biotin Lineage Panel, all antibodies used are fluorescently conjugated, so only required one staining step. However, the 5 antibodies within the Biotin Lineage Panel are not fluorescently conjugated, but are biotinylated, therefore required a secondary antibody staining step with a fluorescently conjugated Streptavidin antibody. Between each staining step, 3 ml of FACS buffer was added to the samples and they were spun down at 300 RCF for 5 minutes at 4°C using an Allegra X-22R Centrifuge (Beckman Coulter (UK) Ltd., High Wycombe, HP11 1JU), and the supernatant removed. Appropriate compensation controls were performed every time (when multiple antibodies were used, individual samples of cells were stained with one antibody only, allowing correct gating to be applied). Appendices 1, 2 and 3 show representative flow cytometry plots for gating strategies, dead cell removal and singlet selection.

Table 2.3. Flow cytometry antibody information

ANTIBODY	DILUTION	COMPANY
Biotin Lineage Panel (CD3e, CD11b, CD45R, Ly-6G and Ly-6C, TER-119)	1:50 (each antibody)	#559971, BD Pharmingen™
Streptavidin PerCP-Cy5.5	1:340	#45-4317-82, eBioscience, Ltd.
CD31 PerCP-eFluor®710	1:100	#46-0311-82, eBioscience, Ltd.
CD29 APC	1:100	#17-0291-82, eBioscience, Ltd.
CD34 PE-Cy5	1:50	#119312, BioLegend
Sca-1 Pacific Blue	1:160	#122520, BioLegend
CD24 eFluor®780	1:200	#47-0242-82, eBioscience, Ltd.
CD31 APC	1:100	#17-0311-82, eBioscience, Ltd.
F4/80 APC	1:100	#17-4801-82 Invitrogen Ltd.

Flow cytometry and FACS was carried out by Elisabeth Freyer and Christopher McRandle at MRC HGU using a BD FACSAria^{TM} II System (BD Biosciences, Oxford, OX4 4DQ, UK) equipped with 5 lasers and fluorescence detectors. Flow cytometry analysis was performed using FlowJo Software Version 7.6.5

(http://www.flowjo.com, Tree Star, Inc., Ashland, 97520, USA). Cells were either sorted into 1 ml media for cell culture (See 2.5.1 for media composition), or into 500 µl TRIzol® Reagent or PBS for RNA extraction (See 2.6.1). Alternatively, cells were used for analysis only and not sorted.

2.5 Tissue culture

2.5.1 Isolation and expansion of murine SVF cells

As described in section 2.4.1, adipose tissue depots were dissected out of the mice and chopped up, before being made into a single cell suspension using Collagenase B (Cat# 11088815001, Roche Diagnostics Ltd, Burgess Hill, RH15 9RY). The SVF was then isolated by centrifugation (see 2.4.1 for full protocol). The isolated SVF cells were either sorted using FACS before being plated out for culture (see 2.4), or cultured directly without sorting. For both methods, the cell pellets were re-suspended in culture media and plated. The culture media used was Dulbecco's Modified Eagle Medium 1x (DMEM) (Cat# 41965-039, Life Technologies Ltd, Paisley, PA4 9RF), with 10% Fetal Calf Serum (FCS), 2% penicillin/streptomycin (P/S) and 1% sodium pyruvate (Cat# 11360070, Thermo Fisher Scientific, Renfrew, PA4 9RF). The size of dish used for culture was dependent on how many cells were being plated. Typically, following FACS ~10,000 cells would be plated per well of a 96 well plate, or ~40,000-80,000 cells would be plated per well of a 24 well plate. Importantly, when comparing two cell populations, for example $Wt1^+$ cells and $Wt1^-$ cells, the same number of cells was plated for each sample. Cells were incubated under normoxic conditions (20% O_2) in a Heracell^{TM} 150i Incubator (Thermo Fisher Scientific, Renfrew, PA4 9RF).

Media was aspirated and cells were fed with fresh DMEM +10% FCS +2% P/S +1% sodium pyruvate every 2-3 days (exact time depending on how well cells had attached to the dish). Typically, cells were cultured for 7 days before they were differentiated into adipocytes (section 2.5.2).

When appropriate, and as described in the relevant results chapters, cells were cultured in the presence of 1 μM 4-OH tamoxifen ((z)-4-hydrotamoxifen) (Cat# H7904, Sigma-Aldrich Company Ltd., Dorset, England). Tamoxifen was supplied for the duration of the culture. To control for the potential effects of the ethanol in which the tamoxifen was dissolved, ethanol-only controls were always performed. One well of cells was cultured in the presence of 100% EtOH (administered at the same volume as the tamoxifen).

As outlined in 3.2.2, 1 μg/ml Staurosporine (Cat# S6942, Sigma-Aldrich Company Ltd., Dorset, England) was added to some of the cultures to induce apoptosis. Cells were treated with staurosporine (added to culture media) for 5 hours prior to fixing the cells.

2.5.2 Adipogenic differentiation

As described above, cells were cultured in DMEM +10% FCS +2% P/S +1% sodium pyruvate for ~7 days before adipogenic differentiation media was supplied. 50 ml of adipogenic differentiation media contained: 45 ml DMEM, 5 ml FCS, 1 ml P/S, 0.5 ml sodium pyruvate, 0.05 ml Insulin (10 μg/ml) (Cat# I0516, Sigma-Aldrich Company Ltd., Dorset, England), 0.05 ml Dexamethasone (DXM 1 μM) (Cat# D4902, Sigma-Aldrich Company Ltd., Dorset, England), 0.05 ml 3-isobutyl 1-methylxanthine (IBMX 0.5 mM), (Cat# I5879, Sigma-Aldrich Company Ltd., Dorset, England) and 0.0025 ml Recombinant Mouse Bone Morphogenetic Protein 4 (BMP4 100 μg/ml) (Cat# 5020-BP, R&D Systems Inc., Abingdon, OX14 3NB). Typically, cells were cultured for an additional 7 days in the presence of the differentiation media and then imaged as outlined in 2.3.5, before being trypsinised for 5 minutes (10 ml trypsin in 50 ml versene) and pelleted.

2.5.3 Conditioned media

In section 3.4, $Wt1^-$ APCs were cultured in media that had previously been conditioned by $Wt1^+$ APCs. As described in 2.4, APCs were isolated from the SVF of the

perigonadal adipose depot from *Wt1*$^{GFP/+}$ knock-in mice, and sorted into GFP+ (Wt1^{+}) and GFP- (Wt1^{-}) populations using FACS. The Wt1^{+} cells were cultured for 7 days, and at each feed the aspirated media was saved and frozen for subsequent use. This media was used to feed GFP- (Wt1^{-}) APCs, from the start of the culture. After 7 days, the conditioned media was supplemented with factors to induce adipogenic differentiation (as outlined in 2.5.2), and the cells cultured for an additional 7 days. When initially plating the GFP- (Wt1^{-}) APCs, the population was divided into two, meaning that half could be cultured in normal (unconditioned) media, to act as a control, and the other half in the conditioned media.

2.6 Gene expression analysis

2.6.1 RNA extraction using TRIzol® reagent

TRIzol® Reagent was used for all RNA isolation. When RNA was extracted directly from FACS sorted cells, cells were either sorted straight into 500 µl of TRIzol® Reagent, or sorted into 500 µl of ice cold 0.01 M PBS, and subsequently spun down at 300 RCF using an Allegra X-22R Centrifuge (Beckman Coulter (UK) Ltd., High Wycombe, HP11 1JU) for 5 minutes, before removing the supernatant and re-suspending in 500 µl of TRIzol® Reagent. The TRIzol® Reagent protocol from the manufacturer's manual was followed (Cat# 15596-026, Life Technologies Ltd, Paisley, PA4 9RF).

When RNA was extracted from cultured cells, cells were trypsinised for 5 minutes (10 ml trypsin in 50 ml versene) at 37°C, transferred to a 15 ml Falcon® tube, and spun down at 300 RCF for 5 minutes. The cell pellet was re-suspended in 500 µl of TRIzol® Reagent. The TRIzol® Reagent protocol from the manufacturer's manual was followed (Cat# 15596-026, Life Technologies Ltd, Paisley, PA4 9RF).

2.6.2 RNA quality and quantity

RNA quantities were measured using a NanoDrop ND-1000 Spectrophotometer (NanoDrop, Wilmington, DE 19810, USA). The RNA quality was measured by Agnes Gallacher from the MRC HGU, who carried out Total RNA Analysis using an Agilent RNA 6000 Nano Chip and Agilent 2100 Bioanalyzer (both from Agilent Technologies UK Limited, Shropshire, SY7 8NR, UK).

2.6.3 cDNA synthesis

cDNA was synthesised from RNA using a 40 µl reaction mix: 8 µl First Strand Buffer, 0.4 µl 0.1 M DTT, 1 µl SuperScript III Reverse Transcriptase (all: Cat# 18080-044, Invitrogen Ltd, Paisley, PA4 9RF), 1 µl dNTPs (Cat# 201900, QIAGEN Ltd., West Sussex, RH10 9NQ, UK), 1 µl rRNasin Inhibitor (Cat# N251B, Promega, Madison, WI, USA) and 1.3 µl Random Primers (Cat# C118A, Promega, Madison, WI, USA). The remaining volume was made up of the RNA sample and RNase-free H_2O. The reaction mix was heated using a Peltier Thermal Cycler (PTC-225, MJ Research Inc., Canada, J3V 4PI) at 52°C for 2.5 hours.

2.6.4 Quantitative realtime polymerase chain reaction (qRT-PCR)

A 10 µl reaction mix was made for each sample of cDNA: 5 µl LightCycler 480 Probes Master (Cat# 04707494001, Roche Diagnostics Ltd., West Sussex, RH15 9RY), 0.1 µl Forward Primer, 0.1 µl Reverse Primer, 0.1 µl Probe, 2 µl cDNA and 2.7 µl distilled H_2O. Primers were Custom Oligos from Sigma-Aldrich Company Ltd., Dorset, England, and all probes were from the Universal Probe Library (Roche Diagnostics Ltd., West Sussex, RH15 9RY) and details can be found in Table 2.4. The 10 µl reaction mix for each sample was run on a clear LightCycler® 384 well plate (Roche Diagnostics Corporation, Indianapolis, USA) in a LightCycler 480 II machine (Roche Diagnostics Ltd., West Sussex, RH15 9RY) under the cycling conditions shown in Table 2.5. All samples were run in technical triplicate.

Table 2.4. Primer and probe information for each gene used in qRT-PCR

GENE	PRIMER DIRECTION	PRIMER SEQUENCE (5'-3')	PROBE NUMBER (UPL)
Wt1	Forward	CAGGATGTTCCCCAATGC	33
Wt1	Reverse	TTGGTTGCGGATGGTAGG	33
Plin	Forward	AACGTGGTAGACACTGTGGTACA	64
Plin	Reverse	TCTCGGAATTCGCTCTCG	64
Fabp4	Forward	GAAAACGAGATGGTGACAAGC	31
Fabp4	Reverse	GCCCTTTCATAAACTCTTGTGG	31
AdipoQ	Forward	GGAGAGAAAGGAGATGCAGGT	17
AdipoQ	Reverse	CTTTCCTGCCAGGGGTTC	17
18S	Forward	CGATTGGATGGTTTAGTGAGG	81
18S	Reverse	AGTTCGACCGTCTTCTCAGC	81

Table 2.5. Cycling conditions for qRT-PCR

STEP	TEMPERATURE	TIME
1. Pre Incubation	95°C	10 minutes
2. Amplification*	95°C	10 seconds
	60°C	30 seconds
	72°C	1 second
3. Cooling	40°C	30 seconds

*Step 2 is repeated 50 times

2.6.5 Custom qRT-PCR plates

To validate gene hits from microarray analysis (section 2.7), RealTime ready Custom Panel 384 qRT-PCR plates (Figure 2.2) were designed and ordered using the RealTime ready Configurator (https://configurator.realtimeready.roche.com) (Roche Diagnostics Ltd., West Sussex, RH15 9RY). Custom plates arrived containing lyophilized primers and probes. A 10 µl reaction mix was made for each sample of cDNA: 5 µl LightCycler 480 Probes Master (Cat# 04707494001, Roche Diagnostics Ltd., West Sussex, RH15 9RY), made up to 10 µl with cDNA sample and distilled H_2O. Each Custom plate was run in a LightCycler 480 II machine (Roche Diagnostics Ltd., West Sussex, RH15 9RY) under the cycling conditions shown in Table 2.5. All samples were run in technical triplicate.

	1	2	3	4	5	6
A	*Wt1*	*Enpp6*	*Cthrc1*	*Fgf7*	*Plin2*	*Pak1*
B	*Ngef*	*Mmp13*	*Cxcl14*	*Sox11*	*Hgf*	*Il6*
C	*Areg*	*Serpinb2*	*Il11*	*Krt19*	*Upk3b*	*Msln*
D	*Clic3*	*Cldn3*	*Serpina3c*	*Rspo1*	*Gdpd5*	*Ptgs1*
E	*Wnt10b*	*Clic5*	*Smo*	*Kcnc4*	*Sulf2*	*Dlg2*
F	*Stmn4*	*Calr*	*Pp2r1a*	*Disp1*	*Prg4*	*Csprs*
G	*Itih2*	*Adcy2*	*Tmem176b*	*Hsd11b2*	*Adam12*	*Snai2*
H	*Saa3*	*C4b*	*Mpeg1*	*Wisp1*	*F2rl1*	*Ccl9*
I	*H2-DMb1*	*Cd276*	*Retnla*	*Ramp1*	*Slc17a7*	*Nmb*
J	*Sult1e1*	*Fbxo2*	*Prokr1*	*Bmp7*	*Adm*	*Dpp4*
K	*Bmp4*	*Lpar3*	*Arl4d*	*Ces3*	*Rcan2*	*Vegfc*
L	*Inhbb*	*Cfd*	*Aox3*	*Thsd7a*	*Anxa3*	*Anxa9*
M	*Gpr1*	*Col4a3*	*Lamc3*	*Tubb4*	*Scin*	*Amph*
N	*Sbsn*	*Tcf21*	*Cdh13*	*Pkp2*	*Ccrl1*	*Rn18s*
O	*Plvap*	*Kcne1*	*Kcnv2*	*Fndc5*	*Timp1*	*Actb*
P	*Clic6*	*Slpi*	*Lcn2*	*Rn18s*	*Rpl13a*	*Gapdh*

Figure 2.2. The 96 genes were replicated 4 times on each RealTime ready Custom Plate.

2.7 Gene expression microarrays

2.7.1 Microarray sample preparation – cRNA amplification

The SVF was isolated from the perigonadal adipose tissue depot (as described in 2.4.1), taken from *Wt1*$^{GFP/+}$ mice. To assess the effects of a high fat diet (HFD) on gene expression in *Wt*1 expressing and non-expressing APCs, the SVF cells isolated from mice on either a HFD or control diet were sorted using FACS to obtain only the

$Lin^-;CD31^-;CD29^+;CD34^+$ fraction, which was subsequently sorted into GFP+ and GFP- populations. RNA was extracted from the GFP+ and GFP- cells using TRIzol® Reagent (Cat# 15596-026, Life Technologies Ltd, Paisley, PA4 9RF) (as outlined in section 2.6.1). RNA quality was checked (section 2.6.2), and samples with a RIN value >7 were used for cRNA amplification. This amplification was carried out using the Epicentre® Biotechnologies TargetAmp™ Nano-g™ Biotin-aRNA Labelling Kit for the Illumina System, according to the protocol from the manufacturer's manual (Cat# TAN07924, Cambio Ltd, Cambridge, CB23 8AR). Amplification using this kit requires additional reagents including SuperScript III Reverse Transcriptase (Cat# 18080-044, Invitrogen Ltd, Paisley, PA4 9RF), and the Qiagen RNeasy® MinElute® Cleanup Kit (#74204, Qiagen Ltd, Manchester, M15 6SH) for purification of the cRNA following amplification.

2.7.2 Gene expression

cRNA yield and quality were assessed by Louise Evenden and Tamara Gilchrist at the Edinburgh Wellcome Trust Clinical Research Facility. Gene Expression was performed using the Illumina Mouse WG-6 v2 Expression BeadChip and Illumina Whole-Genome Gene Expression Direct Hybridisation Assay (WGGX) (Illumina UK, Essex, CB10 1XL, UK). This involves an initial hybridisation step and subsequent washing and staining of the beadchip prior to imaging. For each sample, 5 µl of 150 ng/µl cRNA (quantified using the Agilent 2100 Bioanalyser) was used. The Illumina HiScanSQ platform was used to image the arrays (Illumina UK, Essex, CB10 1XL, UK) and genotypes were called automatically using GenomeStudio Analysis Software Version 2011.1 (Illumina UK, Essex, CB10 1XL, UK).

2.7.3 Gene expression analysis

Illumina Gene Expression data was analysed by Graeme Grimes from MRC HGU. Pearson correlation coefficients were calculated to determine correlations in the expression data, and R was used to carry out hierarchical clustering of each subset. R beadarray (Dunning *et al.*, 2007) and LIMMA Version 3.10.2 software (Ritchie *et al.*, 2015; Phipson *et al.*, 2016) were used to perform the analysis. Quantile normalisation

was applied to allow data from multiple arrays to be compared, in addition to a linear model for the expression data of each gene. A Bayes moderated t test was applied to the results from the linear model to determine statistically differentially expressed genes. To control for the false discovery rate as a consequence of multiple testing, the Benjamini and Hochberg method was used and any genes with an adjusted p value (q-value) <0.05 were selected as differentially expressed.

Two tools were used to identify enriched gene ontology (GO) terms from a ranked list of differentially expressed genes. The first of these was the Gene Ontology Enrichment Analysis and Visualization tool (http://cbl-gorilla.cs.technion.ac.il) and the second was The Database for Annotation, Visualization and Integrated Discovery (DAVID) Version 6.8 (https://david.ncifcrf.gov).

2.8 Statistical analysis

Data is expressed as a mean value (± Standard Error), and p values were calculated using a Two-Tailed t test. Where p values were deemed to be statistically significant ($p<0.05$), the actual p values are shown on the graph.

Chapter 3

Comparing $Wt1^+$ and $Wt1^-$ adipocyte precursor cells (APCs)

3.1 Introduction

As described in the introduction (1.1.3), a proportion of the pre-adipocytes and adipocyte progenitor cells (collectively: adipocyte precursor cells (APCs)), in the six murine VWAT depots express *Wt1* (Chau *et al.*, 2014). Moreover, preliminary work suggests that *Wt1* expressing ($Wt1^+$) cells give rise to mature adipocytes that have fewer, larger lipid droplets than those derived from non-*Wt1* expressing ($Wt1^-$) cells (Chau *et al.*, 2014). Therefore, it is evident that even within the APC population from a single depot, there is heterogeneity, and this heterogeneity may have consequences for the properties of the mature adipocytes. Hence, the first aim of this project was to further define to what extent the $Wt1^+$ and $Wt1^-$ APCs differ, in terms of their behaviour and transcriptomic profiles. Whilst much of the initial work was performed *in vitro,* various *in vivo* studies were implemented to look at the effects of a high fat diet (HFD) on the percentages and transcriptomic profiles of the $Wt1^+$ APCs, as well as their propensity for adipogenesis, thus allowing us to gain an understanding of more physiologically relevant consequences of the heterogeneity. In addition to informing on the relevance of heterogeneity in APC populations, it was hoped that this work would lead to a greater understanding of the function of *Wt1* in APCs.

The majority of the work described in this chapter has been performed using the perigonadal adipose depot, as this is one of the largest murine visceral depots and therefore the most suitable for isolating sufficient numbers of cells. However, where possible, the omental and pericardial depots were also used for some aspects of the study. As shown by Chau *et al*. (2014), these two depots have the highest percentages of $Wt1^+$ APCs and are especially associated with obesity-related diseases in humans. Most of the experiments were performed using both male and female mice (unless stated otherwise), and in all cases the same results were obtained for both sexes, therefore the results have been combined.

In summary, this chapter shows that $Wt1^+$ APCs are more proliferative and adipogenic than $Wt1^-$ APCs, *in vitro*. Moreover, the two populations have differing transcriptomic

profiles. Additionally, when the mice are fed a HFD, the percentages of APCs in the SVF decrease, and this is particularly true for the $Wt1^+$ population.

3.2 Comparing $Wt1^+$ and $Wt1^-$ SVF cells *in vitro*

3.2.1 Adipogenic differentiation of $Wt1^+$ and $Wt1^-$ APCs cultured separately

To understand whether $Wt1^+$ and $Wt1^-$ cells from the SVF of visceral adipose tissue behave differently *in vitro,* fluorescence activated cell sorting (FACS) was used to isolate these two populations of cells. $Wt1^{GFP/+}$ knock-in mice, which have a GFP reporter knocked-in at the *Wt1* locus, were used (Hosen *et al.*, 2007). Therefore, $Wt1^+$ (GFP^+) cells could be separated from $Wt1^-$ (GFP^-). The perigonadal and omental fat depots were dissected out and the SVF was prepared for FACS. Cells from wild-type littermates ($Wt1^{+/+}$) were used to establish flow cytometry gates (Representative plots are shown in Appendix 1). Following sorting into GFP^+ ($Wt1^+$) and GFP^- ($Wt1^-$) fractions, qRT-PCR was used to verify that *Wt1* was expressed in the GFP^+ but not the GFP^- population (Figure 3.1). Equal numbers of cells from each population were then plated out separately for culture under standard conditions (5% CO_2 and 95% air (20% oxygen)). Medium supplemented with factors to induce adipogenic differentiation was added after one week. As illustrated in Figure 3.2, the GFP^+ ($Wt1^+$) cells differentiated into adipocytes more readily than the GFP^- ($Wt1^-$) cells, when the two populations were cultured separately. However, we were concerned that this difference in adipogenesis may have been a consequence of the $Wt1^+$ population being largely composed of pre-adipocytes (90% in the perigonadal, 70% in the omental) (Chau *et al.*, 2014), whilst the $Wt1^-$ population also consists of non-adipogenic endothelial and haematopoietic cells (Church, Berry and Rodeheffer, 2014).

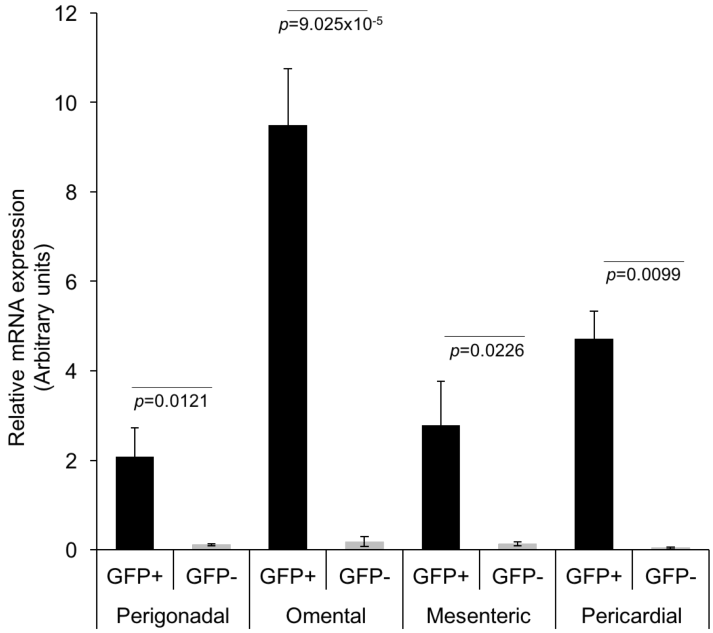


Figure 3.1. In vivo Wt1 mRNA expression. *Perigonadal, omental, mesenteric and pericardial SVF cells from $Wt1^{GFP/+}$ knock-in adult mice were sorted into GFP^+ and GFP^- populations using FACS. Wt1 mRNA expression was significantly higher in GFP^+ cells compared to GFP^- for all depots (normalised to 18S ribosomal RNA). (perigonadal & mesenteric n=5, omental & pericardial n=3; data represent the mean ± s.e.m. and two-tailed Student's t-tests were used to assess statistical significance).*

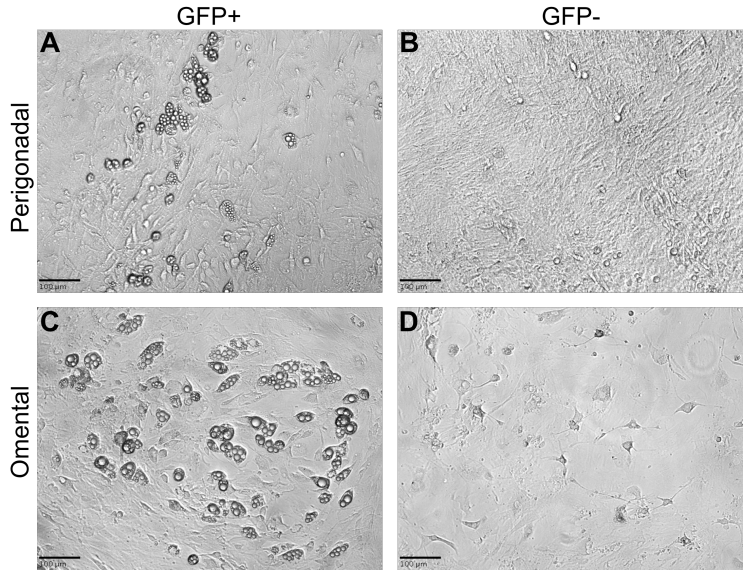


Figure 3.2. GFP^+ ($Wt1^+$) cells differentiate into adipocytes more readily than GFP^- ($Wt1^-$) cells, when cultured separately. *Perigonadal and omental SVF cells from $Wt1^{GFP/+}$ knock-in adult mice were sorted into GFP^+ ($Wt1^+$) and GFP^- ($Wt1^-$) populations using FACS. Equal numbers of the cells were plated separately and allowed to grow. Adipogenic differentiation factors were added after one week and the cultures were left for an additional week before imaging (brightfield). Adipocytes were visible in GFP^+ ($Wt1^+$) cultures **(A,C)** but not in GFP^- ($Wt1^-$) cultures (**B,D**). (Scale bar = 100μm). (n=3).*

To overcome the difference in composition of the isolated GFP^+ ($Wt1^+$) and GFP^- ($Wt1^-$) SVF cell populations, the SVF cells were stained with a panel of antibodies to detect cell-surface proteins, thus allowing predominantly APCs to be isolated. As described in the introduction (1.1.2), two cell surface marker profiles that can be used to isolate adipocyte progenitor cells ($Lin^-;CD29^+;CD34^+;Sca1^+;CD24^+$) and pre-adipocytes ($Lin^-;CD29^+;CD34^+;Sca1^+;CD24^-$) have been identified (Rodeheffer, Birsoy and Friedman, 2008; Berry and Rodeheffer, 2013). Subsequently it has been shown that the $Lin^-;CD34^+$ population is ~95% APCs (Church, Berry and Rodeheffer, 2014). Therefore, to maximise the number of cells acquired by FACS, whilst obtaining a population composed primarily of APCs, it was decided that the $Lin^-;CD34^+$ cells would be isolated. In this study, the "Lineage" (Lin) component of the marker panel comprised a panel of antibodies (CD3e, CD11b, CD45R, Ly-6G and Ly-6C, TER-119), to label the haematopoietic fraction of the SVF. Additionally, a CD31 antibody was used to label endothelial cells. The SVF cells were stained with the relevant antibodies and the $Lin^-;CD31^-;CD34^+$ cells were isolated using FACS (representative plots are shown in Appendix 2). This population was then separated into GFP^+ ($Wt1^+$) and GFP^- ($Wt1^-$) fractions. As previously, equal numbers of cells from the two populations were plated and cultured. As shown in Figure 3.3, the $Lin^-;CD31^-;CD34^+;GFP^+$ ($Wt1^+$) cells still differentiated into adipocytes more readily than the $Lin^-;CD31^-;CD34^+;GFP^-$ ($Wt1^-$) population. Thus, despite the additional sorting step to purify the populations, the same difference in adipogenesis was observed.

Despite published work reporting that the $Lin^-;CD34^+$ population is ~95% APCs (Church, Berry and Rodeheffer, 2014), we wanted to rule out the possibility that the observed differences in adipogenesis could still be due to differences in composition of the two populations. To do so, the SVF cells were stained with the complete antibody panel described by Rodeheffer *et al*. (2008) and only the pre-adipocytes ($Lin^-;CD31^-;CD29^+;CD34^+;Sca1^+;CD24^-$) were isolated (representative plots are shown in Appendix 2). These pre-adipocytes were separated into GFP^+ ($Wt1^+$) and GFP^- ($Wt1^-$) populations as before, and cultured. Again, many more adipocytes were observed in the GFP^+ ($Wt1^+$) cultures than in the GFP^- ($Wt1^-$) (Figure 3.4 A-F). This result was validated using qRT-PCR, showing that key markers of adipocyte differentiation

(adiponectin (*AdipoQ*) and fatty acid binding protein-4 (*Fabp4*)) were expressed at significantly higher levels in the GFP^+ ($Wt1^+$) cultures compared with the GFP^- ($Wt1^-$) cultures (Figure 3.4 G-L). Therefore, even when a pure pre-adipocyte population was isolated, differences in adipogenic capability still existed between $Wt1^+$ and $Wt1^-$ cells. Considering this result, we were satisfied that the differences could not be explained by the $Wt1^+$ population harbouring more pre-adipocytes than the $Wt1^-$. Consequently, all further work was performed using the $Lin^-;CD31^-;CD34^+$ profile for isolation of APCs, rather than the full $Lin^-;CD31^-;CD29^+;CD34^+;Sca1^+;CD24^-$ panel, in order to minimise cell loss.

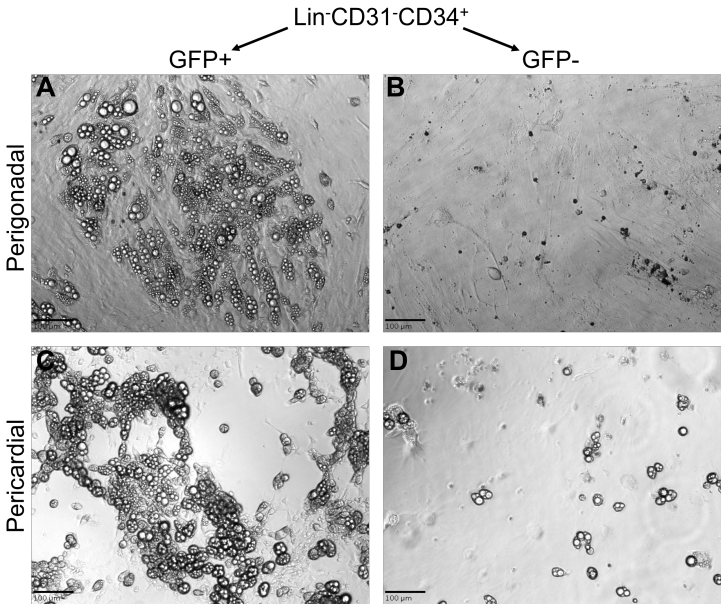


Figure 3.3. GFP^+ ($Wt1^+$) APCs differentiate into adipocytes more readily than GFP^- ($Wt1^-$) APCs, when cultured separately. *Perigonadal and pericardial SVF cells from $Wt1^{GFP/+}$ knock-in adult mice were sorted using a panel of markers to eliminate haematopoietic and other non-adipogenic cells ($Lin^-;CD31^-;CD34^+$) before sorting into GFP^+ ($Wt1^+$) and GFP^- ($Wt1^-$) populations. Equal numbers of the cells were plated separately and allowed to grow. Adipogenic differentiation factors were added after one week and the cultures were left for an additional week before imaging (brightfield). GFP^+ ($Wt1^+$) APCs **(A,C)** differentiated into adipocytes more readily than GFP^- ($Wt1^-$) **(B,D)**. (Scale bar = 100μm). (perigonadal n=8, pericardial n=5).*

Figure 3.4. (continued on next page)

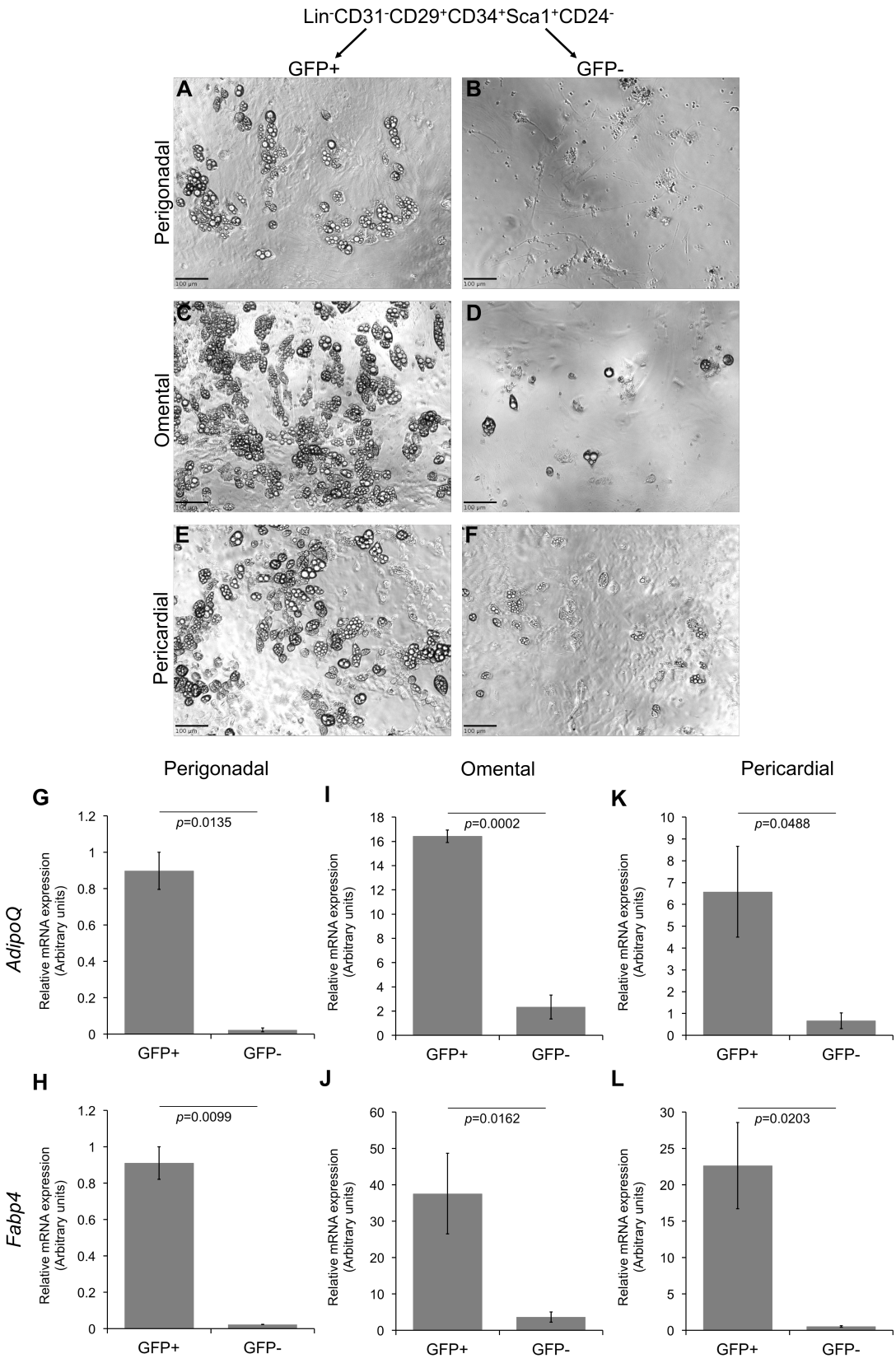


Figure 3.4. GFP$^+$ (Wt1$^+$) pre-adipocytes differentiate into adipocytes more readily than GFP$^-$ (Wt1$^-$) pre-adipocytes, when cultured separately. *Perigonadal, omental and pericardial SVF cells from Wt1$^{GFP/+}$ knock-in adult mice were sorted using a panel of markers to isolate only the pre-adipocytes (Lin$^-$;CD31$^-$;CD29$^+$;CD34$^+$;Sca1$^+$;CD24$^-$) before sorting into GFP$^+$ (Wt1$^+$) and GFP$^-$ (Wt1$^-$) populations. Equal numbers of the cells were plated separately and allowed to grow. Adipogenic differentiation factors were added after one week and the cultures were left for an additional week before imaging (brightfield). Images of cultured cells show that Wt1$^+$ pre-adipocytes **(A,C,E)** differentiated into adipocytes more readily than Wt1$^-$ pre-adipocytes **(B,D,F)**. **(G-L)** AdipoQ and Fabp4 mRNA expression was significantly higher in the cultured GFP$^+$ (Wt1$^+$) cells compared to the GFP$^-$ (Wt1$^-$) cells (normalised to 18S ribosomal RNA). (Scale bar = 100μm). (perigonadal n=2, omental & pericardial n=3 minimum; data represent the mean ± s.e.m. and two-tailed Student's t-tests were used to assess statistical significance).*

3.2.2 Comparing proliferation and apoptosis of Wt1$^+$ and Wt1$^-$ APCs

For murine APCs to efficiently differentiate into adipocytes *in vitro* they should be confluent (Ailhaud *et al.*, 1989; Church, Berry and Rodeheffer, 2014). Therefore, we considered the possibility that the Wt1$^-$ cells, when separated from the Wt1$^+$ cells, were not becoming confluent, helping to explain why they failed to differentiate. This idea was supported by the observation that there consistently appeared to be fewer cells in the Wt1$^-$ cultures compared to the Wt1$^+$, despite always plating the same numbers of both. For this reason, we wanted to investigate whether the percentage of proliferating and/or dying cells differed between the two populations of cells.

SVF cells isolated from the perigonadal depot of male *Wt1$^{GFP/+}$* mice, were stained with the panel of antibodies described previously, to permit the isolation of the Lin$^-$;CD31$^-$;CD34$^+$ APC population using FACS. These APC cells were sorted into GFP$^+$ (Wt1$^+$) and GFP$^-$ (Wt1$^-$) populations, which were plated in equal numbers, in separate wells of an eight well chamber slide. SVF cells isolated from the subcutaneous WAT depot were also plated to be used as staining controls. The cells were cultured for three days, before being fixed and stained with either an anti-Ki67 antibody to assess proliferation or an anti-caspase 3 antibody to assess apoptosis. As a positive control for the anti-caspase 3 antibody, one well of subcutaneous SVF cells was treated with staurosporine for five hours prior to fixing, to induce apoptosis. Additionally, another well of subcutaneous SVF cells was used as a positive control for the anti-Ki67 antibody, because it is known that these cells are highly proliferative *in vitro*. Three days was chosen as the time-point at which to fix the cultures because we wanted to

give the cells time to adhere and settle after being sorted, but did not want them to become confluent, as this would potentially confound the results of the proliferation study.

As shown in Figure 3.5, no cells in either the GFP^+ ($Wt1^+$) or GFP^- ($Wt1^-$) cultures were positive for caspase 3 (CASP3) expression. The presence of CASP3 expressing cells in the staurosporine treated subcutaneous population, indicated that the antibody worked well (Figure 3.5 C). Therefore, the difference in adipogenesis between the two populations was not a consequence of differing percentages of cells undergoing apoptosis. In contrast to this, as shown in Figure 3.6, a higher percentage of KI67 expressing cells was observed in the GFP^+ ($Wt1^+$) population, compared to the GFP^- ($Wt1^-$) population. To quantify this difference, multiple images were taken of each well (average of 60 images/well), and Definiens® software was used to count the total number of nuclei in each well (DAPI positive), as well as the number of KI67 expressing nuclei (DAPI positive and KI67 positive). This revealed that 12.3% of the GFP^+ ($Wt1^+$) cells were positive for KI67, compared to 5.4% of the GFP^- ($Wt1^-$) cells (Figure 3.6 E). Therefore, the GFP^+ ($Wt1^+$) cells were more proliferative than the GFP^- ($Wt1^-$) cells when the two populations were cultured separately. Given that murine APCs need to be confluent before they can efficiently differentiate into adipocytes, this finding could contribute to the contrasting abilities of the two populations to undergo adipogenesis *in vitro*.

As well as plating the GFP^+ ($Wt1^+$) and GFP^- ($Wt1^-$) cells separately, one well was plated containing a mixture of the two populations, to understand whether differences in proliferation existed between the GFP^+ ($Wt1^+$) and GFP^- ($Wt1^-$) cells when they were cultured together. Thus, for each mouse, the perigonadal SVF was sorted to obtain the $Lin^-;CD31^-;CD34^+$ population, which was then split into three: GFP^+ ($Wt1^+$), GFP^- ($Wt1^-$) and a mixed GFP^+ and GFP^- population. After culturing for three days, the mixed population was stained with anti-Ki67 and anti-GFP antibodies. The cells were imaged and, using Definiens® software, the numbers of GFP^+ and GFP^- cells present in the mixed population were counted (Figure 3.7). The percentages of GFP^+ and GFP^- cells that expressed KI67, within the mixed population was then

calculated. As shown in Figure 3.7 D, a difference in the percentage of KI67 positive cells was observed between the two populations, despite them being cultured together. 12.9% of the GFP^+ cells were positive for KI67 staining, whilst just 4.4% of the GFP^- cells were KI67 positive. These percentages are comparable to those obtained for the two populations when they were cultured separately, as described above. Therefore, the perigonadal GFP^+ ($Wt1^+$) APC cells were more proliferative than the GFP^- ($Wt1^-$) APC cells. This was the case when the cells were cultured both together and separately, thus suggesting that this difference in proliferation is a due to intrinsic differences between the cells.

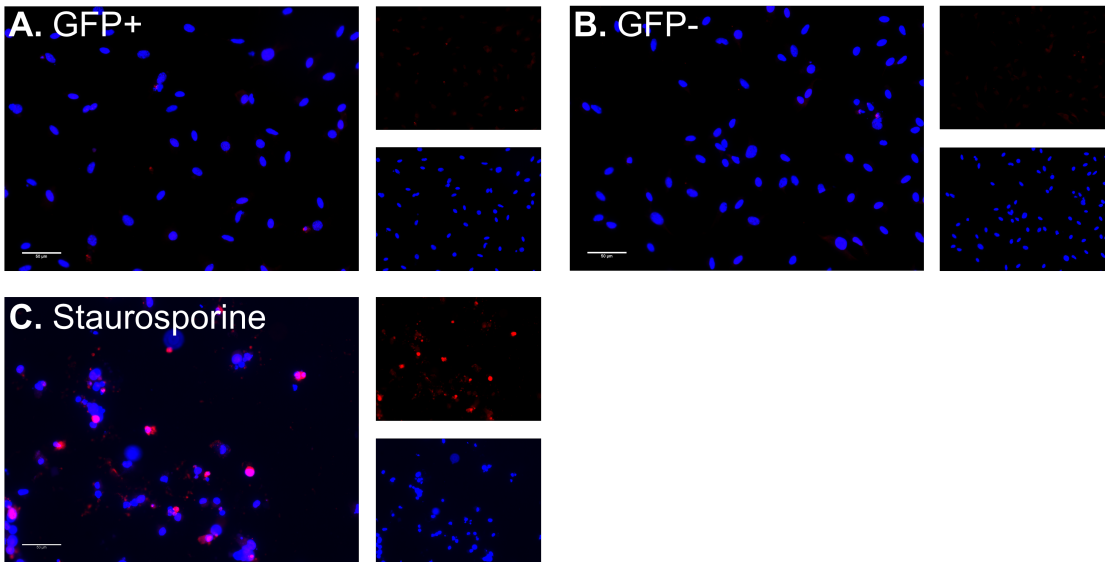


Figure 3.5. GFP^+ ($Wt1^+$) APC and GFP^- ($Wt1^-$) APC populations are not apoptotic in vitro. *Perigonadal SVF cells from $Wt1^{GFP/+}$ knock-in adult male mice were sorted using a panel of markers to eliminate haematopoietic and other non-adipogenic cells ($Lin^-;CD31^-;CD34^+$) before sorting into GFP^+ ($Wt1^+$) and GFP^- ($Wt1^-$) populations. Cells were cultured for 3 days and subsequently stained with an anti-caspase3 antibody. Cells isolated from subcutaneous adipose tissue and treated with staurosporine for 5 hours were used as a positive control **(C)**. No CASP3 expressing cells were observed in either the GFP^+ ($Wt1^+$) **(A)** or GFP^- ($Wt1^-$) **(B)** populations. Thumbnails show CASP3 (red) and DAPI (blue) channels separately. (Scale bar = 50μm). (n=3).*

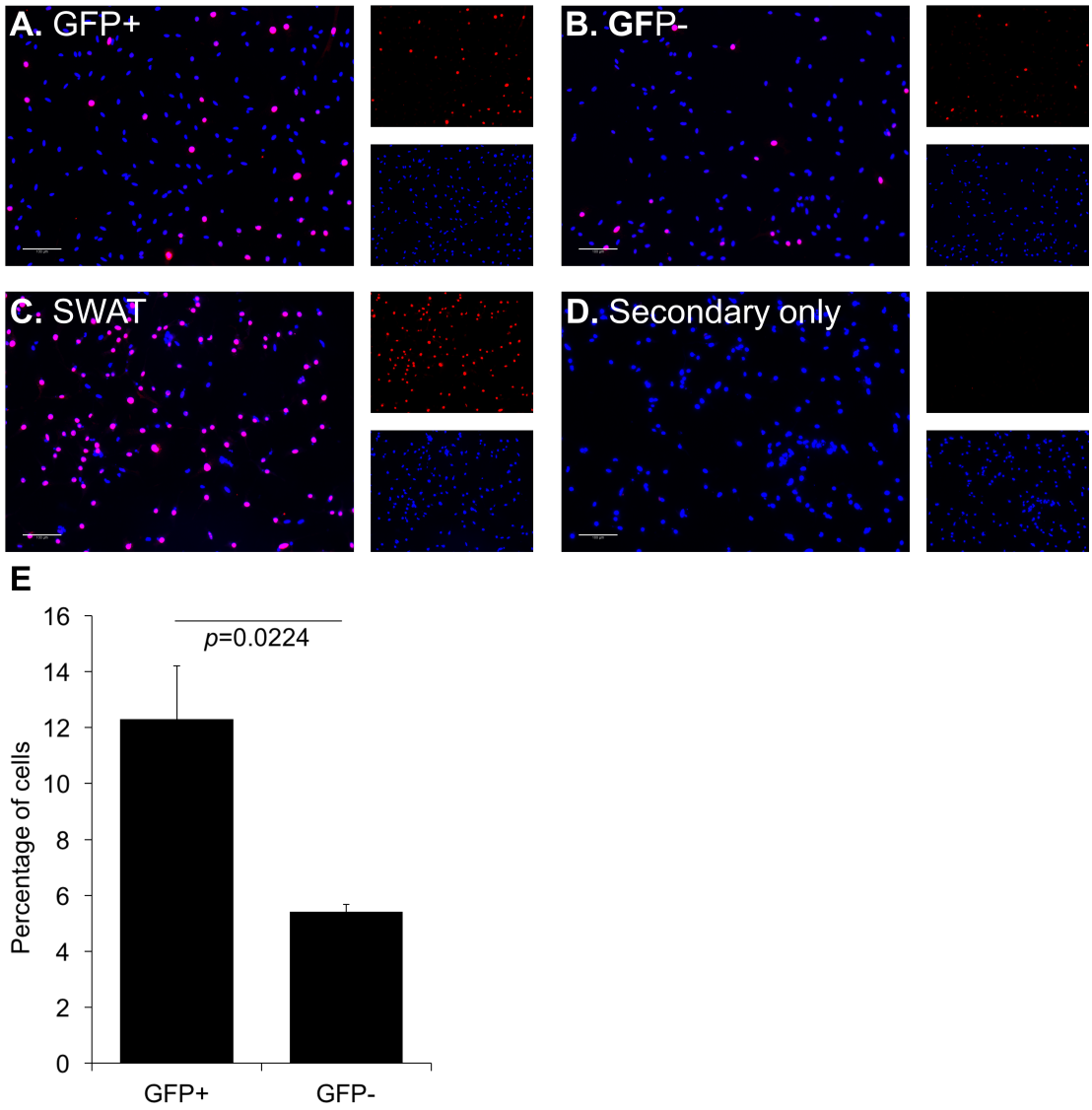


Figure 3.6. GFP$^+$ (Wt1$^+$) APCs are more proliferative than GFP$^-$ (Wt1$^-$) APCs when cultured separately. *Perigonadal SVF cells from Wt1$^{GFP/+}$ knock-in adult male mice were sorted using a panel of markers to eliminate haematopoietic and other non-adipogenic cells (Lin$^-$;CD31$^-$;CD34$^+$) before sorting into GFP$^+$ (Wt1$^+$) and GFP$^-$ (Wt1$^-$) populations. Cells were cultured for 3 days and subsequently stained with an anti-Ki67 antibody. The percentage of KI67 expressing cells was significantly higher in the GFP$^+$ (Wt1$^+$) population (12.3%)* ***(A,E)*** *than in the GFP$^-$ (Wt1$^-$) population (5.4%)* ***(B,E)****. Cells isolated from subcutaneous adipose tissue were included as a positive control for the anti-Ki67 antibody* ***(C)****, and a secondary antibody only control was performed* ***(D)****. Thumbnails show KI67 (red) and DAPI (blue) channels separately. (Scale bar = 100μm). (Approximately 60 images of each well were taken for quantification; n=3; data represent the mean ± s.e.m. and two-tailed Student's t-tests were used to assess statistical significance).*

Figure 3.7. (continued on next page)

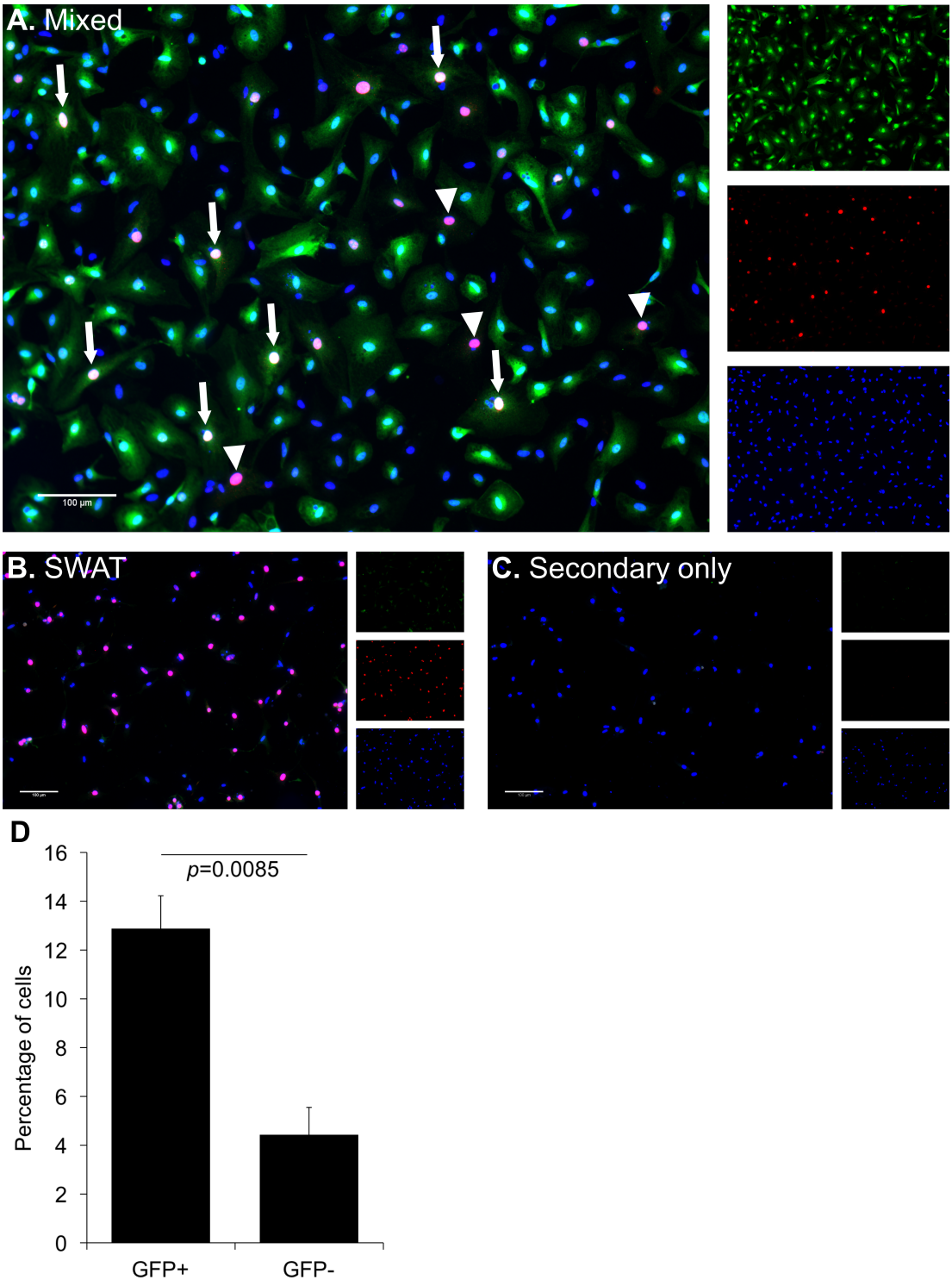


Figure 3.7. GFP$^+$ (Wt1$^+$) APCs are more proliferative than GFP$^-$ (Wt1$^-$) APCs when cultured together. *Perigonadal SVF cells from Wt1$^{GFP/+}$ knock-in adult male mice were sorted using a panel of markers to eliminate haematopoietic and other non-adipogenic cells (Lin$^-$;CD31$^-$;CD34$^+$) and GFP$^+$ (Wt1$^+$) and GFP$^-$ (Wt1$^-$) cells were kept together. Cells were cultured for 3 days and subsequently stained with anti-Ki67 and anti-GFP antibodies. The percentage of KI67 expressing cells in the GFP$^+$ (Wt1$^+$) population (12.9%) (arrows in **A**) was significantly higher than the percentage of KI67 expressing cells in the GFP$^-$ (Wt1$^-$) population (4.4%) (arrow heads in **A**) **(A,D)**. Cells isolated from subcutaneous adipose tissue were included as a positive control for the anti-Ki67 antibody and as a negative control for the anti-GFP antibody **(B)**, and a secondary antibody only control was performed **(C)**. Thumbnails show GFP (green), KI67 (red) and DAPI (blue) channels separately. (Scale bar = 100μm). (Approximately 60 images of each well were taken for quantification; n=3; data represent the mean ± s.e.m. and two-tailed Student's t-tests were used to assess statistical significance).*

3.3 *Wt1* deletion *in vitro*

3.3.1 The effect of *in vitro Wt1* deletion on proliferation

The results described thus far suggest that Wt1$^+$ APCs are more proliferative than Wt1$^-$ and that this is a consequence of intrinsic differences between the two cell populations. Therefore, we next wanted to know if the presence/absence of *Wt1* expression was the reason for this proliferative difference. To investigate this, the *CAGG-CreER™;Wt1$^{loxP/loxP}$* (WER) mouse line was used. In these mice, CreER is ubiquitously expressed, as it is under the regulation of the CAGG promoter. CreER recombinases are generated by fusing Cre to the oestrogen receptor. This fusion results in the CreER recombinase being inactive (Feil, Valtcheva and Feil, 2009). However, 4-OH tamoxifen is a synthetic ligand for the oestrogen receptor, and therefore can activate the CreER recombinase (Feil, Valtcheva and Feil, 2009). Therefore, upon 4-OH tamoxifen administration, CreER recombinase is activated and recombines the loxP sites that flank exon one of *Wt1*, leading to ubiquitous *Wt1* deletion. Lin$^-$;CD31$^-$;CD34$^+$ perigonadal APCs were isolated from male WER mice using FACS, as previously described. The cells were plated and cultured in the presence of either 1 μM 4-OH tamoxifen, to induce *Wt1* deletion, or ethanol. The 4-OH tamoxifen was reconstituted in 100% ethanol, therefore to ensure that any effects observed were not a consequence of ethanol being added to the culture, an ethanol-only control was included. In addition to culturing APCs from *CAGG$^{CreER/+}$;Wt1$^{loxP/loxP}$* (Cre+) mice, cells from *CAGG$^{+/+}$;Wt1$^{loxP/loxP}$* (Cre-) littermates were also plated. Therefore, four cultures were set up; two using cells from the Cre+ mice (one with 1 μM 4-OH

tamoxifen and one with ethanol) and two using cells from the Cre- mice (one with 1 μM 4-OH tamoxifen and one with ethanol). The cells were cultured for three days before being fixed and stained. For each of the four cultures, one well of cells was stained with an anti-Wt1 antibody, to check for the presence/absence of WT1 protein, and another well was stained with an anti-Ki67 antibody to assess proliferation. Due to both the anti-Wt1 and anti-Ki67 antibodies being raised in the same species it was not possible to co-stain one well of cells with both antibodies. Each well was imaged, and Definiens® software was used to quantify the results.

As shown in Figure 3.8, significantly fewer WT1 expressing APCs were observed in the Cre+ cultures (with 4-OH tamoxifen) (3.6%), compared to any of the other cultures (Cre+ (with ethanol) (50.9%), Cre- (with 4-OH tamoxifen) (71.6%), Cre- (with ethanol) (63.5%)). Therefore, 4-OH tamoxifen induced *Wt1* deletion was efficient in the Cre+ cultures. However, no significant difference in the percentage of KI67 expressing APCs was observed between the cultures (Figure 3.9). 10.1% of the APCs in the Cre+ cultures (with 4-OH tamoxifen) expressed KI67, compared to 7.4% in the Cre+ cultures (with ethanol), 7.5% in the Cre- cultures (with 4-OH tamoxifen) and 6.2% in the Cre- cultures (with ethanol). Therefore, *Wt1* deletion did not lead to a reduction in the percentage of proliferating APCs.

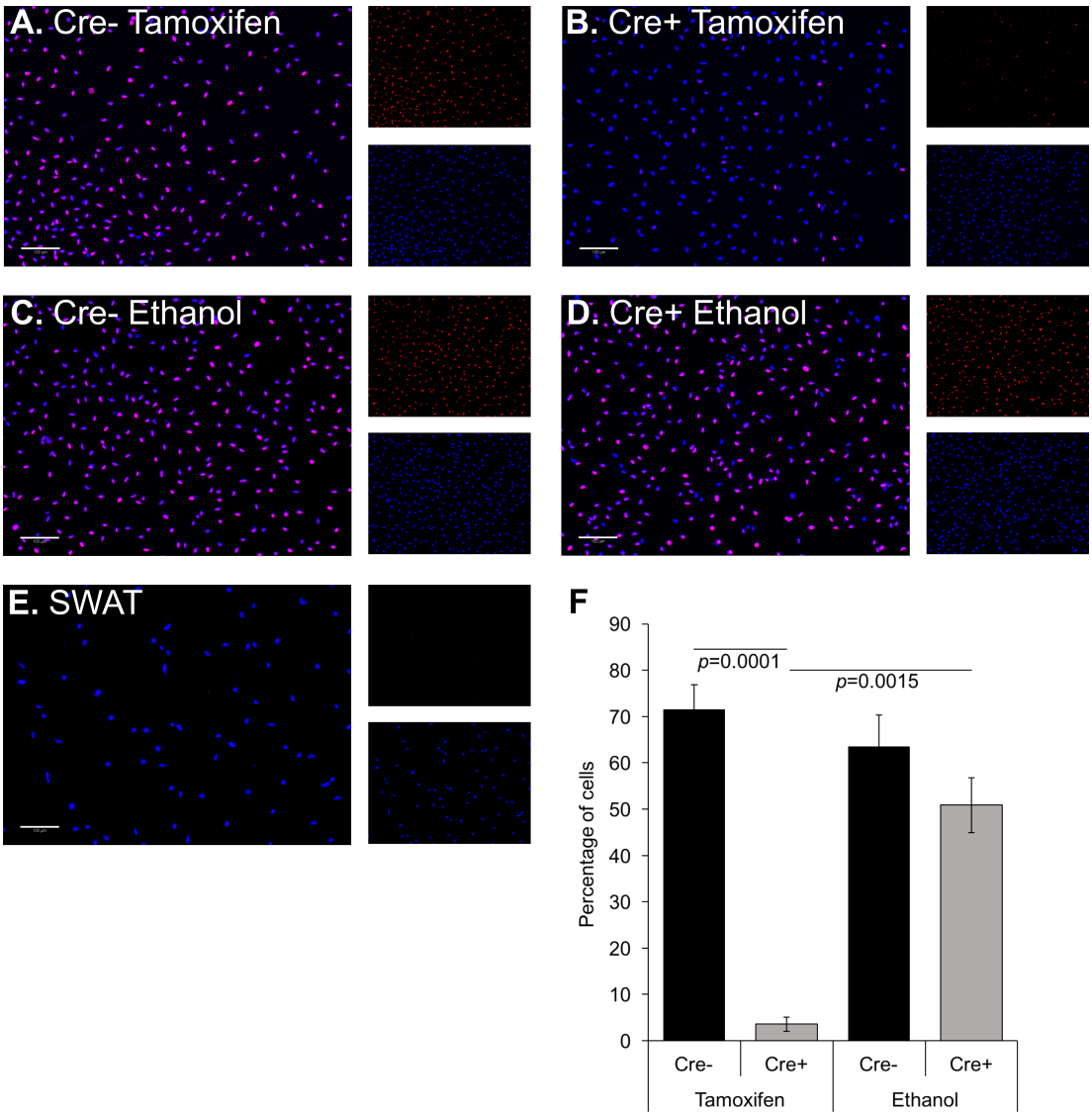


Figure 3.8. The percentage of WT1 expressing APCs from CAGG$^{CreER/+}$;Wt1$^{loxP/loxP}$ mice is significantly reduced when cultured in the presence of 4-OH tamoxifen*. Perigonadal SVF cells from CAGG$^{CreER/+}$;Wt1$^{loxP/loxP}$ (Cre+) adult male mice were sorted using a panel of markers to eliminate haematopoietic and other non-adipogenic cells (Lin$^-$;CD31$^-$;CD34$^+$). The cells were cultured in the presence of either 1 μM 4-OH tamoxifen **(B)** or 100% ethanol (vehicle control) **(D)**. APCs from CAGG$^{+/+}$;Wt1$^{loxP/loxP}$ (Cre-) littermates were also cultured with either 1 μM 4-OH tamoxifen **(A)** or 100% ethanol **(C)** to act as a control. After 3 days in culture the cells were fixed and stained with an anti-Wt1 antibody. Subcutaneous WAT cells acted as a negative control for the anti-Wt1 antibody **(E)**. The 4-OH tamoxifen administered Cre+ cultures exhibited a significant reduction in the percentage of WT1 expressing cells compared to the 4-OH tamoxifen administered Cre- cultures and the ethanol administered Cre+ cultures **(F)**. Thumbnails show WT1 (red) and DAPI (blue) channels separately. (Scale bar = 100μm). (n=3; data represent the mean ± s.e.m. and two-tailed Student's t-tests were used to assess statistical significance).*

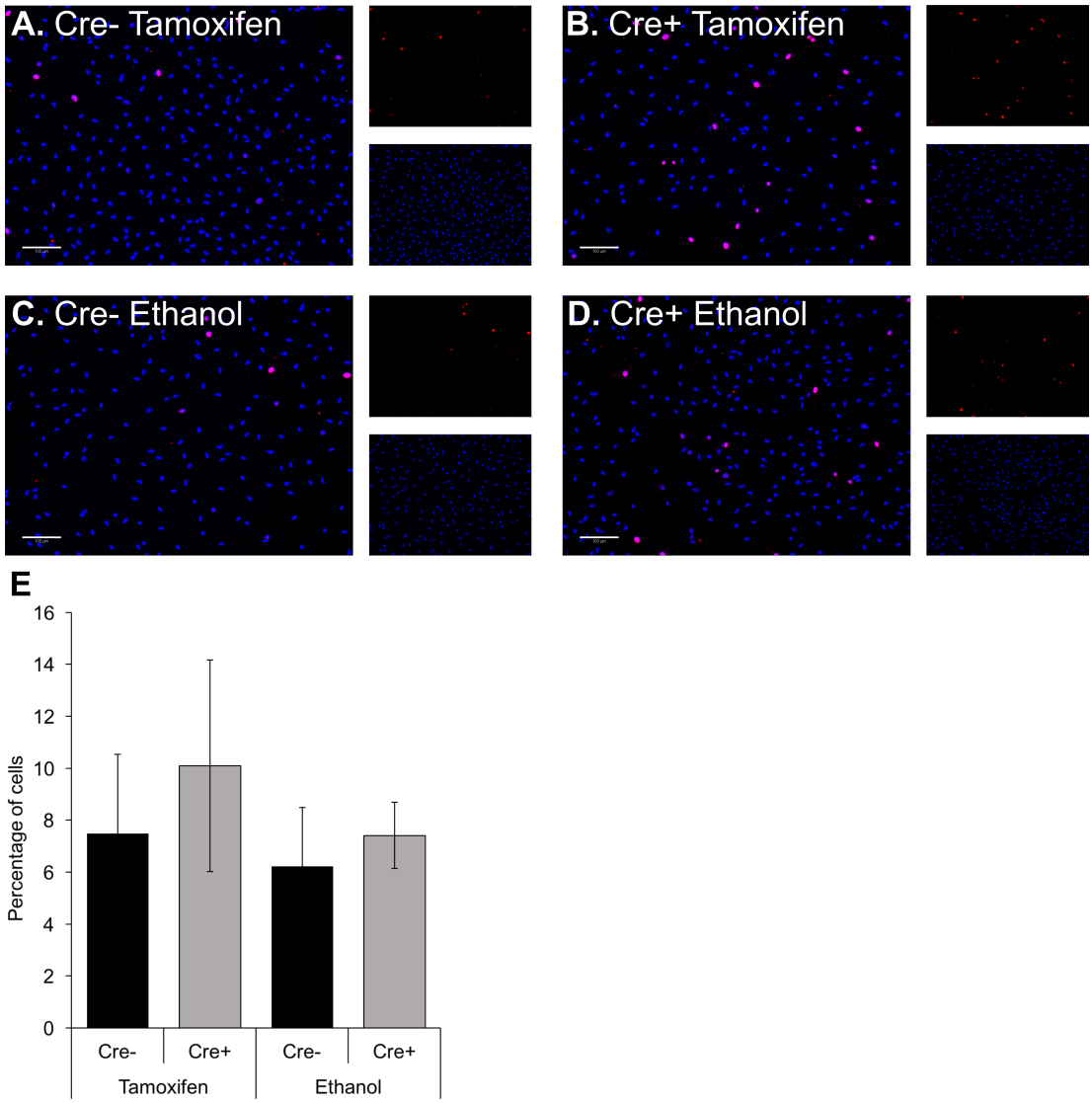


Figure 3.9. The percentage of KI67 expressing APCs from CAGG$^{CreER/+}$;Wt1$^{loxP/loxP}$ mice is unchanged when Wt1 is deleted. *Perigonadal SVF cells from CAGG$^{CreER/+}$;Wt1$^{loxP/loxP}$ (Cre+) adult male mice were sorted using a panel of markers to eliminate haematopoietic and other non-adipogenic cells (Lin^{-};CD31^{-};CD34^{+}). The cells were cultured in the presence of either 1 μM 4-OH tamoxifen (to induce Wt1 deletion)* ***(B)*** *or 100% ethanol (vehicle control)* ***(D)***. *APCs from CAGG$^{+/+}$;Wt1$^{loxP/loxP}$ (Cre-) littermates were also cultured with either 1 μM 4-OH tamoxifen* ***(A)*** *or 100% ethanol* ***(C)*** *to act as a control. After 3 days in culture the cells were fixed and stained with an anti-Ki67 antibody. There was no significant difference between the percentages of KI67 expressing APCs in the different cultures* ***(E)***. *Thumbnails show KI67 (red) and DAPI (blue) channels separately. (Scale bar = 100μm). (n=3; data represent the mean ± s.e.m. and two-tailed Student's t-tests were used to assess statistical significance).*

3.3.2 Cre control cultures

As described in section 3.3.1, CreER recombinase is not activated until the addition of tamoxifen. Work from our group has shown that the activation of CreER can have toxic effects on cultured cells, particularly when performing colony forming unit-fibroblast assays to determine the number of mesenchymal progenitor cells in bone marrow (McHaffie, Hastie and Chau, 2016). Importantly, these effects occurred in cultures from *CAGG-CreER™* mice (with no gene floxed), therefore were solely due to the activation of CreER and not the result of gene deletion (McHaffie, Hastie and Chau, 2016). Despite not observing any significant difference in the percentage of proliferating cells in section 3.3.1, Cre control cultures were still performed alongside the WER cultures to determine if CreER activation alone was having any effect. Lin^-;$CD31^-$;$CD34^+$ perigonadal APCs were isolated from male $CAGG^{CreER/+}$ (Cre+) and $CAGG^{+/+}$ (Cre-) mice using FACS. The cells were plated and cultured in the presence of either 1 μM 4-OH tamoxifen (to activate the CreER recombinase), or ethanol (vehicle control). Again, after three days the cultures were fixed and stained with an anti-Ki67 antibody and Definiens® software was used to quantify the number of KI67 positive cells.

As shown in Figure 3.10, fewer KI67 expressing cells were observed in the cultures obtained from the Cre+ mice, compared with those from the Cre- mice. This result was true both for the cells cultured with 1 μM 4-OH tamoxifen and those cultured with ethanol, however, in both cases the difference was not significant, and was only approximately 1-2%. Therefore, it is possible that the presence of the CreER construct (both activated and inactivated), did affect the percentage of proliferating cells, however as this experiment was performed using the cells from just two mice for each condition, further repeats are required to understand whether the difference is significant.

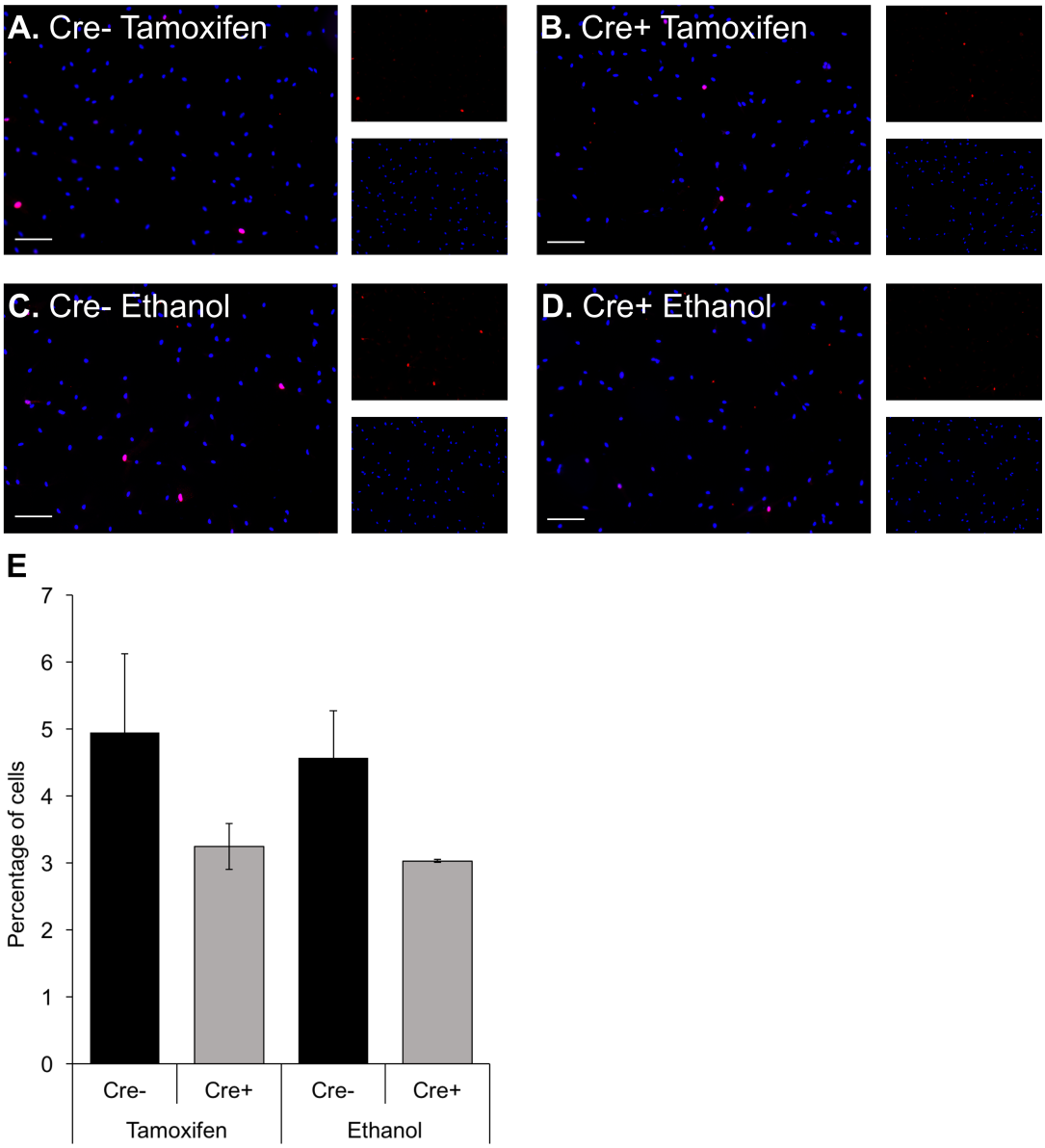


Figure 3.10. The percentage of KI67 expressing APCs from CAGG$^{CreER/+}$ (Cre control) mice is not significantly different when cultured in the presence of 4-OH tamoxifen. *Perigonadal SVF cells from CAGG$^{CreER/+}$ (Cre+) adult male mice were sorted using a panel of markers to eliminate haematopoietic and other non-adipogenic cells (Lin$^-$;CD31$^-$;CD34$^+$). The cells were cultured in the presence of either 1 μM 4-OH tamoxifen **(B)** or 100% ethanol (vehicle control) **(D)**. APCs from CAGG$^{+/+}$ (Cre-) littermates were also cultured with either 1 μM 4-OH tamoxifen **(A)** or 100% ethanol **(C)** to act as a control. After 3 days in culture the cells were fixed and stained with an anti-Ki67 antibody. There was no significant difference between the percentages of KI67 expressing APCs in the different cultures, although the percentages in the Cre+ cultures were approximately 1-2% lower than in the Cre- cultures **(E)**. Thumbnails show KI67 (red) and DAPI (blue) channels separately. (Scale bar = 100μm). (n=2; data represent the mean ± s.e.m. and two-tailed Student's t-tests were used to assess statistical significance).*

3.4 Culturing Wt1$^-$ APCs in media conditioned by Wt1$^+$ APCs

The results described in 3.2 suggest that intrinsic differences between Wt1$^+$ and Wt1$^-$ APC populations can at least partially explain the observed difference in proliferation between the two populations, and therefore may also help to explain why the Wt1$^+$ APCs are better at differentiating into adipocytes than the Wt1$^-$ APCs. It is also possible that the Wt1$^+$ cells secrete a factor/factors which is/are required by the Wt1$^-$ cells, and therefore, when the two populations are cultured separately, the Wt1$^-$ cells fail to efficiently undergo adipogenesis. It is feasible that the observed differences in behaviour could be explained by both endogenous differences and exogenous factors. To investigate this further, a conditioned media experiment was performed. Lin$^-$;CD31$^-$;CD34$^+$ GFP$^+$ (Wt1$^+$) cells were isolated from the perigonadal SVF of *Wt1*$^{GFP/+}$ mice and cultured for 7 days. At each feed, the aspirated media was retained and frozen for future use. Subsequently, Lin$^-$;CD31$^-$;CD34$^+$ cells were isolated from the perigonadal SVF of different *Wt1*$^{GFP/+}$ mice, and sorted into GFP$^+$ (Wt1$^+$) and GFP$^-$ (Wt1$^-$) populations. The GFP$^-$ (Wt1$^-$) population was split into two, and half were fed with normal (unconditioned) media, whilst the other half were fed with the previously obtained conditioned media from the GFP$^+$ (Wt1$^+$) cultures. Additionally, an equal number of GFP$^+$ (Wt1$^+$) cells was plated separately in normal media, for comparison. The cells were cultured for 7 days using either conditioned or unconditioned media as appropriate, and then the medias (conditioned/unconditioned) were supplemented with factors to induce adipogenic differentiation, for a further 7 days.

Representative images of the different cultures are shown in Figure 3.11. Additionally, the cultures were harvested for RNA extraction and qRT-PCR was performed to assess the mRNA levels of adipogenesis markers; *AdipoQ* and *Fabp4* (Figure 3.11 D,E). The results suggest that the GFP$^-$ (Wt1$^-$) cells that were cultured in media conditioned by GFP$^+$ (Wt1$^+$) cells, were more adipogenic than those cultured in unconditioned media. However, they still did not differentiate as well as the GFP$^+$ (Wt1$^+$) cells. Nevertheless, these preliminary results indicate that the Wt1$^+$ cells secrete a factor(s) that is required by the Wt1$^-$ cells in order for them to undergo adipogenesis. Due to time constraints,

it has not yet been possible to further follow this work up, however future experiments that should be considered are discussed in 3.8.

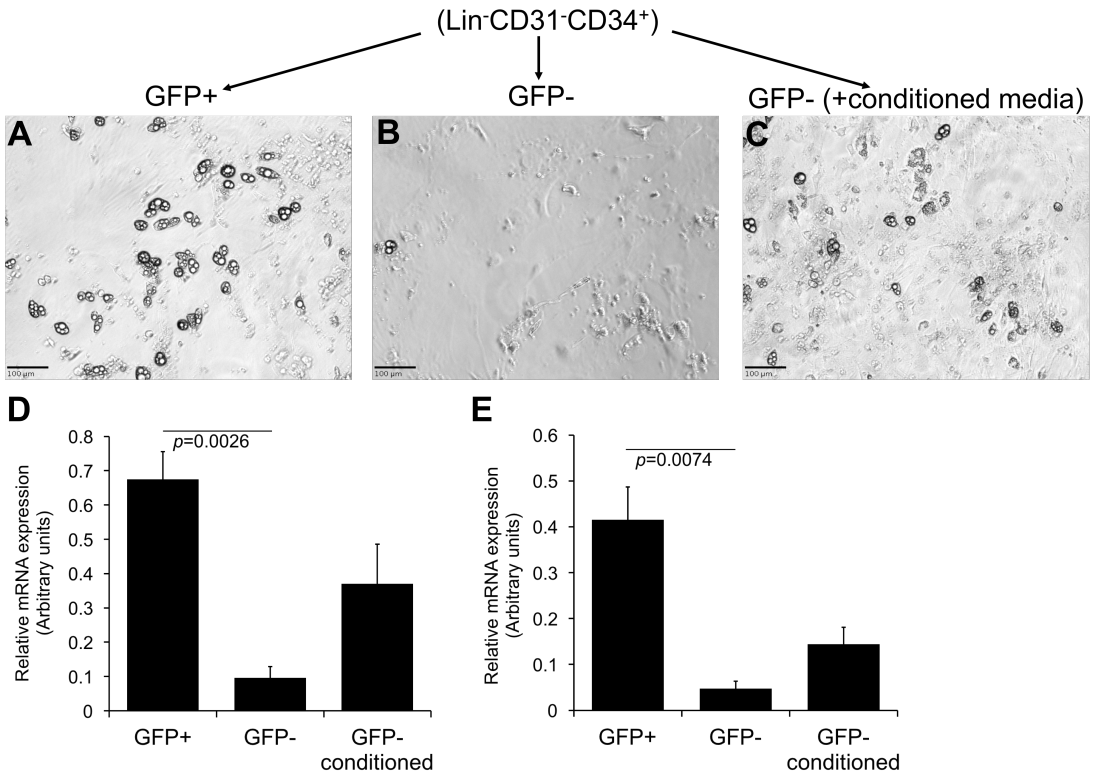


Figure 3.11. GFP$^-$ (Wt1$^-$) APCs are more adipogenic when cultured in media conditioned by GFP$^+$ (Wt1$^+$) APCs. *Perigonadal SVF cells from adult Wt1$^{GFP/+}$ knock-in mice were sorted using a panel of markers to eliminate haematopoietic and other non-adipogenic cells (Lin$^-$;CD31$^-$;CD34$^+$) before sorting into GFP$^+$ (Wt1$^+$) and GFP$^-$ (Wt1$^-$) populations. Half of the GFP$^-$ (Wt1$^-$) APCs were fed with media previously conditioned by GFP$^+$ (Wt1$^+$) APCs and half were fed with unconditioned media. The conditioned media fed GFP$^-$ (Wt1$^-$) APCs **(C)** differentiated into adipocytes more readily than those not fed with conditioned media **(B)**, but not as well as the GFP$^+$ (Wt1$^+$) APCs **(A)**. AdipoQ **(D)** and Fabp4 **(E)** mRNA expression in the cultured cells was measured by qRT-PCR (normalised to 18S ribosomal RNA). (Scale bar = 100μm). (n=3 minimum; data represent the mean ± s.e.m. and two-tailed Student's t-tests were used to assess statistical significance).*

3.5 Microarray analysis of freshly isolated Wt1$^+$ and Wt1$^-$ APCs

Evidently Wt1$^+$ and Wt1$^-$ APCs exhibited different behaviours *in vitro*. We next wanted to understand more about the properties and function of freshly isolated Wt1$^+$ and Wt1$^-$ APCs, and how they differ. To do so, gene expression microarrays were performed to assess the transcriptomic profiles of the two APC populations. As described for the differentiation, apoptosis and proliferation experiments (3.2.1-3.2.3),

the SVF was isolated from the perigonadal depot of *Wt1*$^{GFP/+}$ mice and sorted using FACS to obtain only the Lin$^-$;CD31$^-$;CD34$^+$ APC cells, these were then further sorted to separate GFP$^+$ (Wt1$^+$) and GFP$^-$ (Wt1$^-$) populations. The RNA was extracted from both cell populations, and prepared for microarray analysis.

The gene expression data was analysed by Graeme Grimes from the MRC HGU. Wt1$^+$ and Wt1$^-$ APCs differed significantly ($q<0.05$ calculated by the R Bioconductor package LIMMA) in the expression of 261 genes, with 121 genes exhibiting higher expression, and 140 genes exhibiting lower expression in the Wt1$^+$ population, compared to the Wt1$^-$. Two gene ontology tools: GOrilla (http://cbl-gorilla.cs.technion.ac.il) and DAVID (The Database for Annotation, Visualization and Integrated Discovery Version 6.8: https://david.ncifcrf.gov) were used to analyse the differentially expressed genes in order to identify enriched biological themes, functionally-related gene groups and pathways. 261 is a relatively small number of genes in which to observe expression differences, and consequently GOrilla was not able to identify any gene ontology (GO) terms. However, when the genes with higher expression in the Wt1$^+$ APCs were ordered by log fold change and analysed using DAVID, several GO terms were identified. Similarly, the genes displaying lower expression were analysed in the same way.

3.5.1 GO terms identified for genes with higher expression in Wt1$^+$ APCs

Genes with significantly higher expression in the Wt1$^+$ APCs were enriched for 40 GO terms, with an FDR (False Discovery Rate) q-value <0.05 (adjusted p-value using the Benjamini and Hochberg (1995) method), according to DAVID version 6.8. The majority of these GO terms were associated with extracellular attributes, such as "extracellular region" and "extracellular organelles". Table 3.1 shows the predominant GO terms identified in this analysis, including information on the percentage of genes implicated in the GO term, as well as a list of said genes, and the FDR q-value for the GO term. Additionally, when inputting only the genes with a LogFC >1.5 (15 of the 121 genes), the "extracellular region" and "extracellular organelle" GO terms were still present in the analysis, both with an FDR q-value <0.05. Table 3.2 outlines these

GO terms and the genes associated with them. According to QuickGO (http://www.ebi.ac.uk/QuickGO), which is a browser for Gene Ontology terms and annotations, the GO term; "extracellular region" is defined as being "the space external to the outermost structure of a cell". It also notes that "this term is intended to annotate gene products that are not attached to the cell surface". The "extracellular organelle" is defined as being an "organised structure of distinctive morphology and function, occurring outside the cell", whilst the "extracellular matrix" is "a structure lying external to one or more cells, which provides structural support for cells or tissues". Finally, the "extracellular space" is defined as "the part of a multicellular organism outside the cells proper, usually taken to be outside the plasma membranes, and occupied by fluid". Given the results described in section 3.4, regarding the improved growth and differentiation of $Wt1^-$ APCs when cultured in media conditioned by $Wt1^+$ APCs, the identification of GO terms related to extracellular activity is particularly interesting. It provides further support for the hypothesis that the $Wt1^+$ cells may be secreting a factor(s) that improves the adipogenic differentiation of the $Wt1^-$ cells. As the number of differentially expressed genes was fairly low, a table of the top enriched genes ($q < 0.05$, LogFC > 1.5) was generated, which includes additional information about each one (Table 3.3).

Table 3.1. Enriched DAVID GO terms for genes upregulated in Wt1^{+} cells. All genes with q-value <0.05 were included in the analysis.

DESCRIPTION	NUMBER OF GENES	PERCENTAGE (INVOLVED GENES/TOTAL GENES)	FDR Q-VALUE	GENES
Extracellular region	49	52.1	$5.1x10^{-9}$	*Atp1b1, Cd248, Cd55, Efhd1, Iqgap2, Ndufa4, St3gal6, Xpnpep2, Adamts16, Adamts19, Anpep, Angptl1, Angptl7, Apom, Bmp7, Crym, Dmkn, Dpp4, Efna5, Fbn1, Fgf18, Fndc5, Gldn, Hp, Hspb1, Hebp2, Islr, Igsf1, Il18, Krtdap, Lgi2, Lcn2, Matn4, Papln, Pi16, Prdx5, Pla1a, Ptgis, Scin, Sct, Slpi, Sema3e, Sdk1, Slc9a3r1, Sbsn, Tnfrsf11b, Uchl1, Upk1b, Upk3b*
Extracellular organelle	32	34	$4.3x10^{-6}$	*Atp1b1, Cd248, Cd55, Efhd1, Iqgap2, Ndufa4, St3gal6, Xpnpep2, Anpep, Angptl1, Apom, Crym, Dmkn, Dpp4, Fbn1, Hp, Hspb1, Hebp2, Islr, Il18, Lcn2, Pi16, Prdx5, Pla1a, Scin, Slpi, Sdk1, Slc9a3r1, Sbsn, Uchl1, Upk1b, Upk3b*
Extracellular matrix	11	11.7	$7x10^{-4}$	*Adamts16, Adamts19, Bmp7, Efna5, Fbn1, Gldn, Hspb1, Papln, Slpi, Sbsn, Tnfrsf11b*
Extracellular space	18	19.1	$7.9x10^{-3}$	*Anpep, Angptl1, Apom, Bmp7, Dmkn, Fbn1, Gldn, Hp, Hspb1, Il18, Lcn2, Pi16, Prdx5, Ptgis, Sct, Slpi, Sema3e*

Table 3.2. Enriched DAVID GO terms for genes upregulated in Wt1^{+} cells. Only genes with q-value <0.05 and LogFC >1.5 were included in the analysis.

DESCRIPTION	NUMBER OF GENES	PERCENTAGE (INVOLVED GENES/TOTAL GENES)	FDR Q-VALUE	GENES
Extracellular region	11	78.6	$1.6x10^{-4}$	*Adamts16, Dmkn, Dpp4, Fndc5, Lcn2, Pi16, Slpi, Sbsn, Tnfrsf11b, Upk1b, Upk3b*
Extracellular organelle	8	57.1	$3.5x10^{-3}$	*Dmkn, Dpp4, Lcn2, Pi16, Slpi, Sbsn, Upk1b, Upk3b*

Table 3.3. All genes upregulated in Wt1^{+} cells with q-value <0.05 and LogFC >1.5. Genes in black were selected for validation by qRT-PCR.

GENE	LOG FOLD CHANGE	Q-VALUE	NAME/BRIEF DESCRIPTION (UNIPROT HTTP://WWW.UNIPROT.ORG AND ENTREZ GENE HTTPS://WWW.NCBI.NLM.NIH.GOV/GENE)	GO TERMS PRESENT IN
Slpi	2.97	3.91×10^{-2}	Secretory Leukocyte Protease Inhibitor. Secreted inhibitor that protects epithelial tissues from serine proteases. Anti-inflammatory. Promotes cell proliferation and migration.	Extracellular space Extracellular organelle Extracellular region Extracellular matrix
eGFP	2.76	1.15×10^{-4}		N/A
Upk3b	2.56	1.89×10^{-2}	Uroplakin-3b. Mesothelial cell marker. Component of apical plaques of mammalian urothelium.	Extracellular organelle Extracellular region
Dmkn	2.30	1.15×10^{-4}	Dermokine. Upregulated in inflammatory diseases.	Extracellular space Extracellular organelle Extracellular region
Upk1b	2.07	4.47×10^{-2}	Uroplakin 1B. Component of urothelial cell membrane.	Extracellular organelle Extracellular region
Tnfrsf11b	2.05	1.05×10^{-2}	Tumor Necrosis Factor Receptor Superfamily Member 11b. Negative regulator of bone resorption.	Extracellular region Extracellular matrix
Cyp2s1	1.83	5.44×10^{-3}	Cytochrome P450 Family 2 Subfamily S Member 1. Catalyzes multiple reactions including synthesis of cholesterol, steroids and other lipids.	
Adamts16	1.82	2.47×10^{-3}	ADAM Metallopeptidase With Thrombospondin Type 1 Motif 19.	Extracellular region Extracellular matrix
Dpp4	1.71	3.80×10^{-2}	Dipeptidyl Peptidase 4. An intrinsic membrane glycoprotein and a serine exopeptidase that cleaves X-proline dipeptides from the N-terminus of polypeptides.	Extracellular organelle Extracellular region
Lcn2	1.69	5.44×10^{-3}	Lipocalin 2. Transports small hydrophobic molecules e.g. lipids, steroid hormones and retinoids.	Extracellular space Extracellular organelle Extracellular region
Sbsn	1.61	2.06×10^{-3}	Suprabasin.	Extracellular organelle Extracellular region Extracellular matrix
Limch1	1.60	5.01×10^{-3}	LIM And Calponin Homology Domains 1.	
Pi16	1.57	3.02×10^{-3}	Peptidase Inhibitor 16. Serine protease inhibitor.	Extracellular organelle Extracellular region Extracellular space
Chst1	1.53	8.23×10^{-3}	Carbohydrate Sulfotransferase 1.	
Fndc5	1.5	2.77×10^{-3}	Fibronectin Type III Domain Containing 5. Secreted protein released from muscle cells during exercise. Role in brown fat development.	Extracellular region

3.5.2 Gene expression validation

Several potentially interesting genes identified in the microarray were validated by qRT-PCR. As described later in this chapter (3.6.2.4), custom qRT-PCR plates were designed for the validation of 91 genes identified in the high fat diet study. A number of the interesting gene hits detected in this study were also included on these plates. These were predominantly the top enriched genes in the $Wt1^+$ cells, all of which were present in the GO terms associated with extracellular activity, including *Slpi, Upk3b, Dpp4, Lcn2* and *Sbsn*. *Wt1* was also included to confirm that the GFP^+ cells were indeed $Wt1^+$ (Figure 3.12 A). qRT-PCR was performed in technical and biological triplicate. The five genes assessed by qRT-PCR were expressed at a higher level in the GFP^+ ($Wt1^+$) APCs compared to the GFP^- ($Wt1^-$), therefore successfully validating the microarray results, however the difference in expression levels was only significant for *Dpp4* and *Upk3b* (Figure 3.12 B,C). For *Slpi, Lcn2* and *Sbsn*, the error bars were fairly large, meaning substantial variation between the biological replicates, therefore possibly helping to explain why the difference did not reach significance (Figure 3.12 D-F).

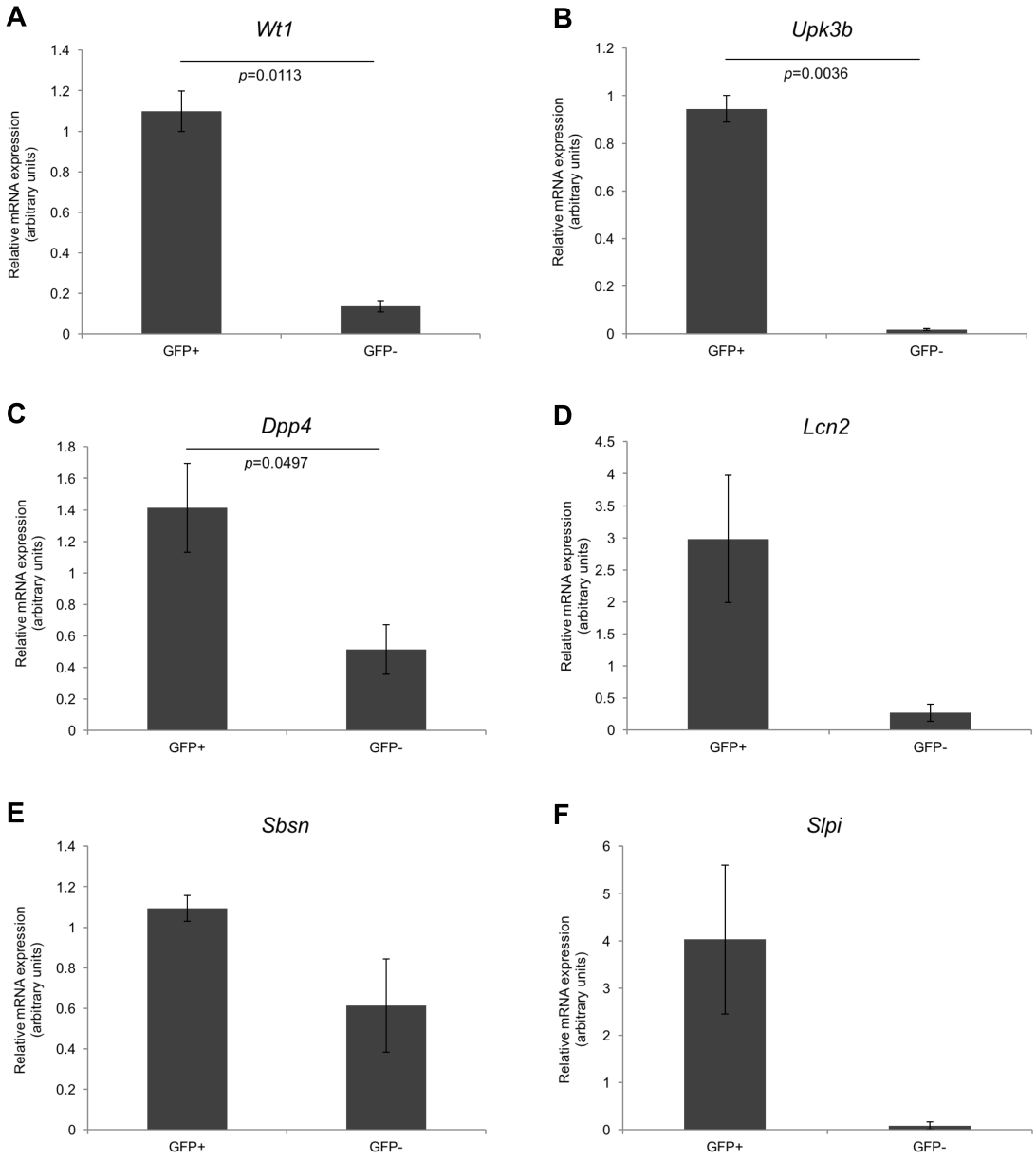


Figure 3.12. qRT-PCR validation of genes with upregulated expression in Wt1$^+$ cells, as identified by microarray analysis. *All genes selected for validation were associated with the "extracellular organelle" and "extracellular region" GO terms identified by DAVID for genes upregulated in Wt1$^+$ cells.* ***(A)*** *Wt1 expression analysis confirmed that the GFP$^+$ cells expressed significantly higher levels of Wt1 than the GFP$^-$ cells. Upk3b* ***(B)*** *and Dpp4* ***(C)*** *were expressed at significantly higher levels in the GFP$^+$ cells compared to the GFP$^-$ cells. Lcn2* ***(D)****, Sbsn* ***(E)*** *and Slpi* ***(F)*** *were expressed at higher levels in the GFP$^+$ cells compared to the GFP$^-$ but this difference was not significant. (n=2 minimum; data represent the mean ± s.e.m. and two-tailed Student's t-tests were used to assess statistical significance).*

3.5.3 GO terms present for genes with lower expression in $Wt1^+$ APCs

Genes that had significantly lower expression in the $Wt1^+$ APCs were enriched for several interesting GO terms, with an FDR q-value <0.05 according to DAVID version 6.8. These included “angiogenesis”, “cell adhesion”, “cell migration”, “cell surface receptor signalling pathway”, “cell proliferation” and “regulation of cell death”. Table 3.4 lists these GO terms and includes information on the percentage of genes implicated in each term, as well as a list of said genes, and the FDR q-value for the GO term. Furthermore, when the analysis was performed using only the genes with a LogFC <-1.5 (47 of the 140 genes), “angiogenesis”, “cell proliferation” and “cell adhesion” GO terms were still present and had an FDR q-value <0.05 (Table 3.5), these are discussed further in 3.8. The number of genes with an FDR q-value <0.05 and a LogFC <-1.5 was too high for this category, and so a table of the individual genes has not been generated. However, many of them can be seen in Tables 3.4 and 3.5, where they are associated with GO terms. Table 3.5, in particular, shows many of the top genes.

Table 3.4. Enriched DAVID GO terms for genes downregulated in Wt1^{+} cells. All genes with q-value <0.05 were included in the analysis.

DESCRIPTION	NUMBER OF GENES	PERCENTAGE (INVOLVED GENES/TOTAL GENES)	FDR Q-VALUE	GENES
Angiogenesis	23	19.3	$4.0x10^{-11}$	*Adrb2, Angpt2, Aqp1, Bmp4, C6, Cav1, Cma1, Col4a3, Ctgf, Ednra, Egfl7, Flt1, Hhip, Il1b, Lrg1, Meox2, Mmrn2, Notch3, Nrp1, Ptn, Ptprb, Robo4, Vegfc*
Cell adhesion	37	31.1	$3.1x10^{-10}$	*Adrb2, Amigo2, Angpt2, Bmp4, Cav1, Cd74, Cd83, Cldn11, Col28a1, Col4a3, Coro1a, Ctgf, Egfl7, Epha3, Gadd45g, Gas6, Gcnt2, H2-Aa, H2-Ab1, Icam1, Icosl, Il1b, Irf1, Itga7, Kit, Lamc3, Nfkbid, Plek, Ptn, Rhod, Selp, Slc11a1, Tnfaip3, Vegfc, Vtn, Vwf, Wisp2*
Cell migration	31	26.1	$5.1x10^{-9}$	*Angpt2, Aqp1, Arc, Arhgef5, Bmp4, Ccl4, Cd74, Coro1a, Ctgf, Cxcl14, Ednra, Ednrb, Egfl7, Epha3, Flt1, Gas6, Gcnt2, Icam1, Il1b, Itga7, Kit, Meox2, Mmrn2, Nrp1, Pik3cd, Ptn, Rhod, Robo4, Selp, Vegfc, Vtn*
Cell surface receptor signaling pathway	39	32.8	$5.0x10^{-7}$	*Adrb2, Angpt2, Arc, Bmp4, Cav1, Ccl4, Ccnd1, Cd74, Col4a3, Coro1a, Cpe, Ctgf, Dner, Egfl7, Epha3, Fcer1a, Flt1, Gas6, Gcnt2, Hhip, Icam1, Irf1, Itga7*
Cell proliferation	29	24.4	$4.6x10^{-5}$	*Adrb2, Aqp1, Bmp4, Cav1, Ccnd1, Cd74, Col4a3, Coro1a, Ctgf, Ednra, Ednrb, Egfl7, Gas6, Gcnt2, H2-Aa, H2-Ab1, Hhip, Icosl, Il1b, Irf1, Kit, Lrg1, Notch3, Ptch1, Ptn, Slc11a1, Tnfaip3, Vegfc, Wisp2*
Regulation of cell death	27	22.7	$1.0x10^{-4}$	*Adrb2, Amigo2, Aqp1, Bmp4, C6, Cav1, Cd74, Col4a3, Coro1a, Ctgf, Ednra, Ednrb, Gadd45g, Gas6, Hhip, Icam1, Il1b, Irf1, Kit, Nfkbid, Nrp1, Ptn, Robo4, Sort1, Tnfaip3, Unc13b, Wisp2*

Table 3.5. Enriched DAVID GO terms for genes downregulated in Wt1^{+} cells. Only genes with q-value <0.05 and LogFC <-1.5 were included in the analysis.

DESCRIPTION	NUMBER OF GENES	PERCENTAGE (INVOLVED GENES/TOTAL GENES)	FDR Q-VALUE	GENES
Angiogenesis	9	22	$8.4x10^{-4}$	*Adrb2, Angpt2, Aqp1, Cma1, Ednra, Lrg1, Meox2, Ptn, Ptprb,*
Cell proliferation	12	29.3	$1.6x10^{-2}$	*Aqp1, Cd74, Ednra, Ednrb, Hhip, H2-Aa, H2-Ab1, Kit, Lrg1, Ptch1, Ptn, Slc11a1*
Cell adhesion	10	24.4	$3.1x10^{-2}$	*Angpt2, Cd74, Cldn11, Col28a1, H2-Aa, H2-Ab1, Kit, Ptn, Selp, Slc11a1*

3.6 Assessing the effects of a high fat diet on different adipose tissue depots

The majority of the work described thus far was performed *in vitro*. Whilst the results clearly highlight differences between $Wt1^+$ and $Wt1^-$ APCs, thus reinforcing the idea that the heterogeneity within the APC population may have functional consequences, we were interested in investigating this heterogeneity in an *in vivo*, and thus more physiologically relevant setting. Given that obesity is a significant global health burden, and a widely researched field, we decided that performing *in vivo* studies in the context of obesity would be the best approach.

3.6.1 The effect of a high fat diet on the proportion of $Wt1^+$ cells in the SVF

Male $Wt1^{GFP/+}$ mice (on a pure C57BL/6 background) were fed a high fat diet (HFD) for 17 weeks. Age and gender matched mice were fed a control diet (CD) for the same amount of time. All mice were weighed once per week, and by week 3 the mice on the HFD were significantly heavier than those on the CD (Figure 3.13). After 17 weeks the mice were culled and the perigonadal, omental, pericardial, mesenteric and perirenal VWAT depots were dissected for analysis by flow cytometry and immunohistochemistry, to examine the SVF and mature adipocytes, respectively. The SVF was stained with the panel of antibodies described previously (Lin, CD31, CD29, CD34, Sca1, CD24) and analysed using flow cytometry. Therefore, the percentages of the different cell types in the SVF could be compared between HFD-fed and CD-fed mice. Due to the presence of the GFP reporter knocked in at the *Wt1* locus, it was also possible to assess whether the percentages of $Wt1^+$ and $Wt1^-$ cells changed when the mice were fed a HFD.

The trend across the five VWAT depots was a reduction in the percentage of GFP^+ SVF cells in the mice fed a HFD compared to those fed a CD. This reduction was significant for the omental (25.9% for the CD and 15.9% for the HFD) and perirenal (21.2% for the CD and 10.3% for the HFD) depots. There was a small reduction in the perigonadal (14.5% for the CD and 10.6% for the HFD) and mesenteric (14.1% for the CD and 9.9% for the HFD) depots, however this was not significant. The reduction in

the pericardial depot was negligible (26.9% for the CD and 25.6% for the HFD) (Figure 3.14). This suggests that one consequence of the HFD was a reduction in *Wt1* expression/*Wt1* expressing cells in at least the omental and perirenal VWAT depots.

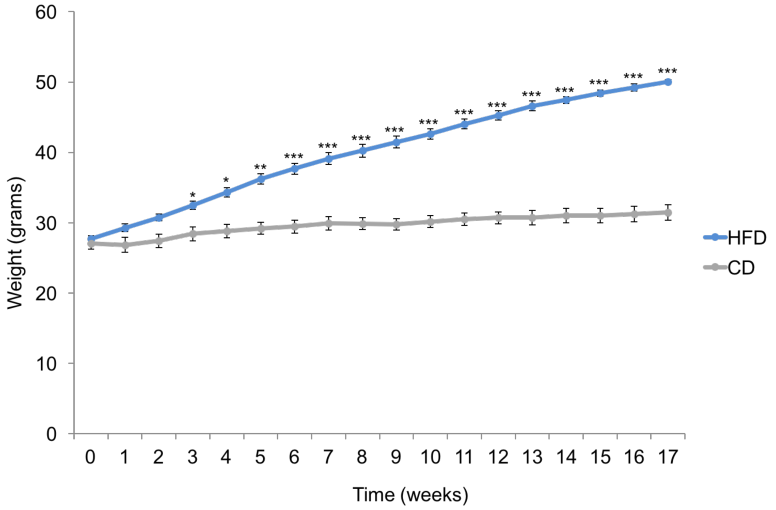


Figure 3.13. Mice fed a HFD over 17 weeks become significantly heavier than mice fed a CD. *Male $Wt1^{GFP/+}$ knock-in mice and age-matched controls were fed either a HFD or CD for 17 weeks, their weight was recorded once per week for the duration of the study. By week 3 the mice fed the HFD were significantly heavier than those fed the CD (*=p<0.005, **=p<0.001, ***=p<0.0001). (n=10; data represent the mean ± s.e.m. and two-tailed Student's t-tests were used to assess statistical significance).*

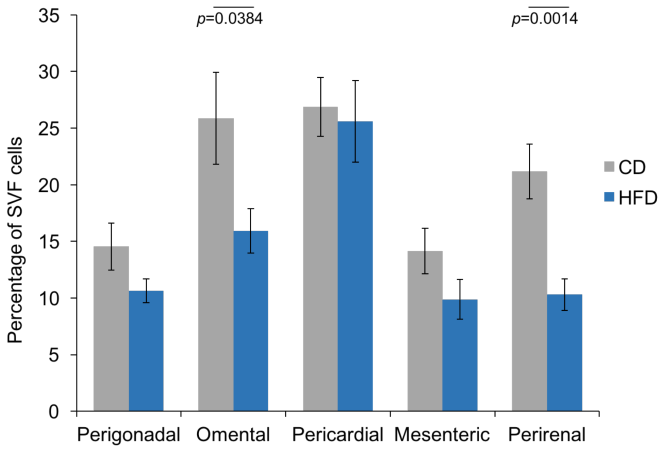


Figure 3.14. The percentage of GFP^+ ($Wt1^+$) cells in the SVF of $Wt1^{GFP/+}$ knock-in mice is lower for the HFD fed mice than for the CD fed mice. *The SVF was isolated from the visceral fat depots of $Wt1^{GFP/+}$ knock-in mice fed either a HFD or CD and analysed using flow cytometry. The percentage of GFP^+ ($Wt1^+$) cells in the SVF of the omental and perirenal depots was significantly lower in the mice fed HFD compared to those fed a CD. There was also a reduction in the perigonadal and mesenteric depots, however this was not significant. (n=5 CD minimum, 8 HFD; data represent the mean ± s.e.m. and two-tailed Student's t-tests were used to assess statistical significance).*

We next looked at how the percentages of the different cell populations that comprise the SVF differed in the mice fed a HFD compared to those fed a CD. The trend across the VWAT depots was an increase in the percentage of $Lin^+;CD31^+$ cells in the mice fed the HFD, coupled with a decrease in the percentage of $Lin^-;CD31^-$ cells, and therefore also a decrease in the percentage of $CD34^+$ APCs, $CD24^-$ pre-adipocytes and $CD24^+$ adipocyte progenitor cells. The exception to this trend was the pericardial depot, in which very little difference was observed (Figure 3.15 G). For the other four visceral depots, a number of the differences were significant (Figure 3.15 A,D,J,M).

It was important to understand whether these differences in SVF composition were due to a combined influence of the (GFP^+) $Wt1^+$ and (GFP^-) $Wt1^-$ cells, or if one population was affected more than the other. The most striking result was in the omental depot; a significant increase in the percentage of $Lin^+;CD31^+;GFP^-$ cells in the HFD-fed mice was observed, whilst there was no change in the percentage of $Lin^+;CD31^+;GFP^+$ cells. Conversely, the percentages of $Lin^-;CD31^-;GFP^+$, $Lin^-;CD31^-;CD29^+;CD34^+;GFP^+$, $Lin^-;CD31^-;CD29^+;CD34^+;Sca1^+;CD24^-;GFP^+$ and $Lin^-;CD31^-;CD29^+;CD34^+;Sca1^+;CD24^+;GFP^+$ cells were decreased in the SVF from the HFD mice but the reciprocal GFP^- populations were unchanged (Figure 3.15 E,F). Hence, it appears that the increase in $Lin^+;CD31^+$ cells caused by the HFD was the result of an increase in $Wt1^-$ cells, whilst the decrease in $Lin^-;CD31^-$ cells, $CD34^+$ APCs, $CD24^-$ pre-adipocytes and $CD24^+$ adipocyte progenitor cells was due to a decrease in $Wt1^+$ cells, at least for the omental depot. The same trend is true for the perirenal depot; the increase in Lin^+CD31^+ cells in the HFD condition was predominantly due to an increase in GFP^- cells, and whilst there was also a decrease in GFP^- $CD34^+$ and $CD24^-$ cells, this decrease was more significant for the GFP^+ population (Figure 3.15 N,O). The perigonadal and mesenteric depots are slightly different; both the GFP^+ and GFP^- populations contributed to the differences observed. The percentage of Lin^+CD31^+ cells increased for both the GFP^- and GFP^+ populations, and there was a reduction in the percentages of $CD34^+$ and $CD24^-$ cells for both populations in the HFD condition (Figure 3.15 B,C,K,L). As described previously, there was no change in the percentage of cells for either population in the pericardial depot (Figure 3.15 H,I).

Figure 3.15. (continued on next page)

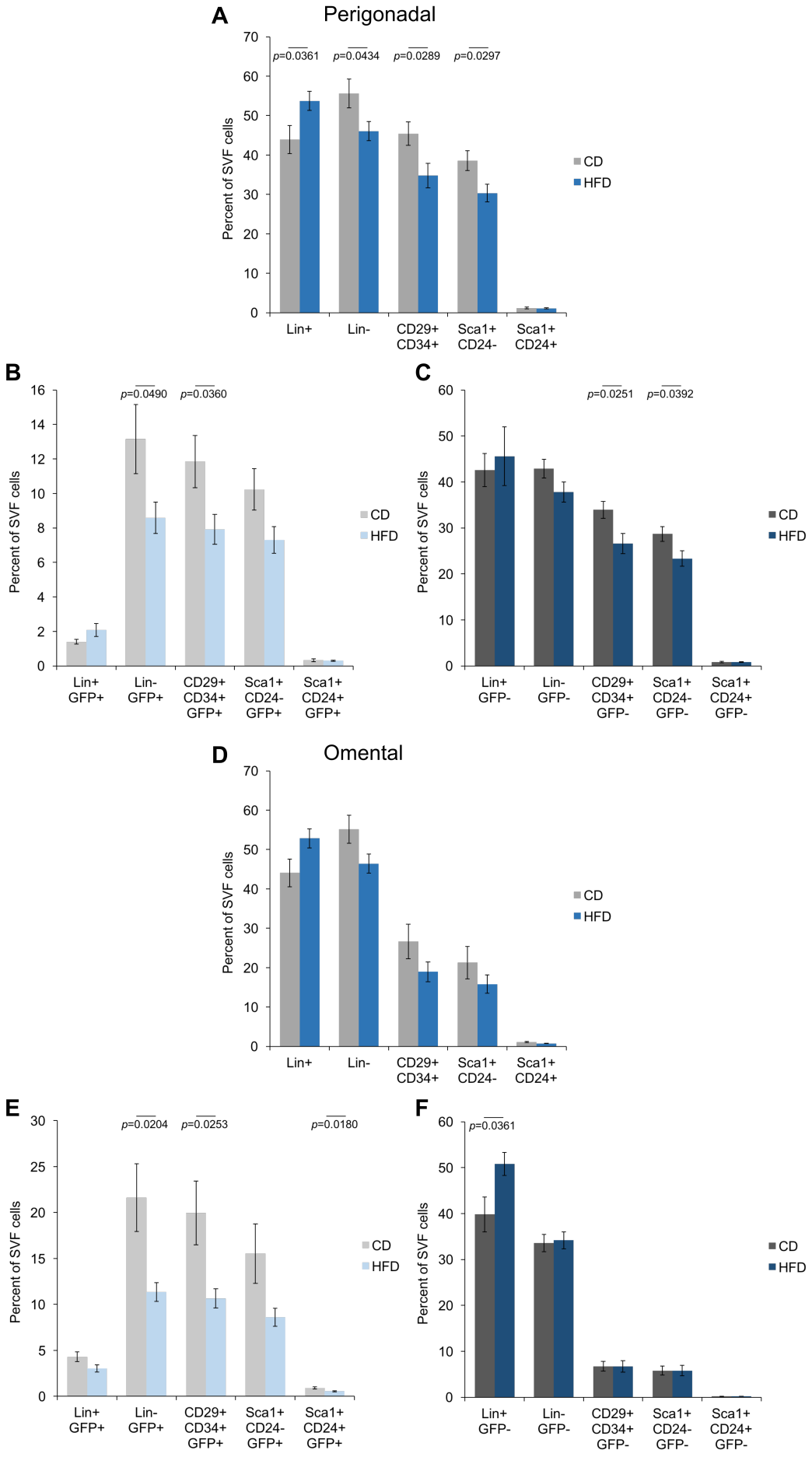
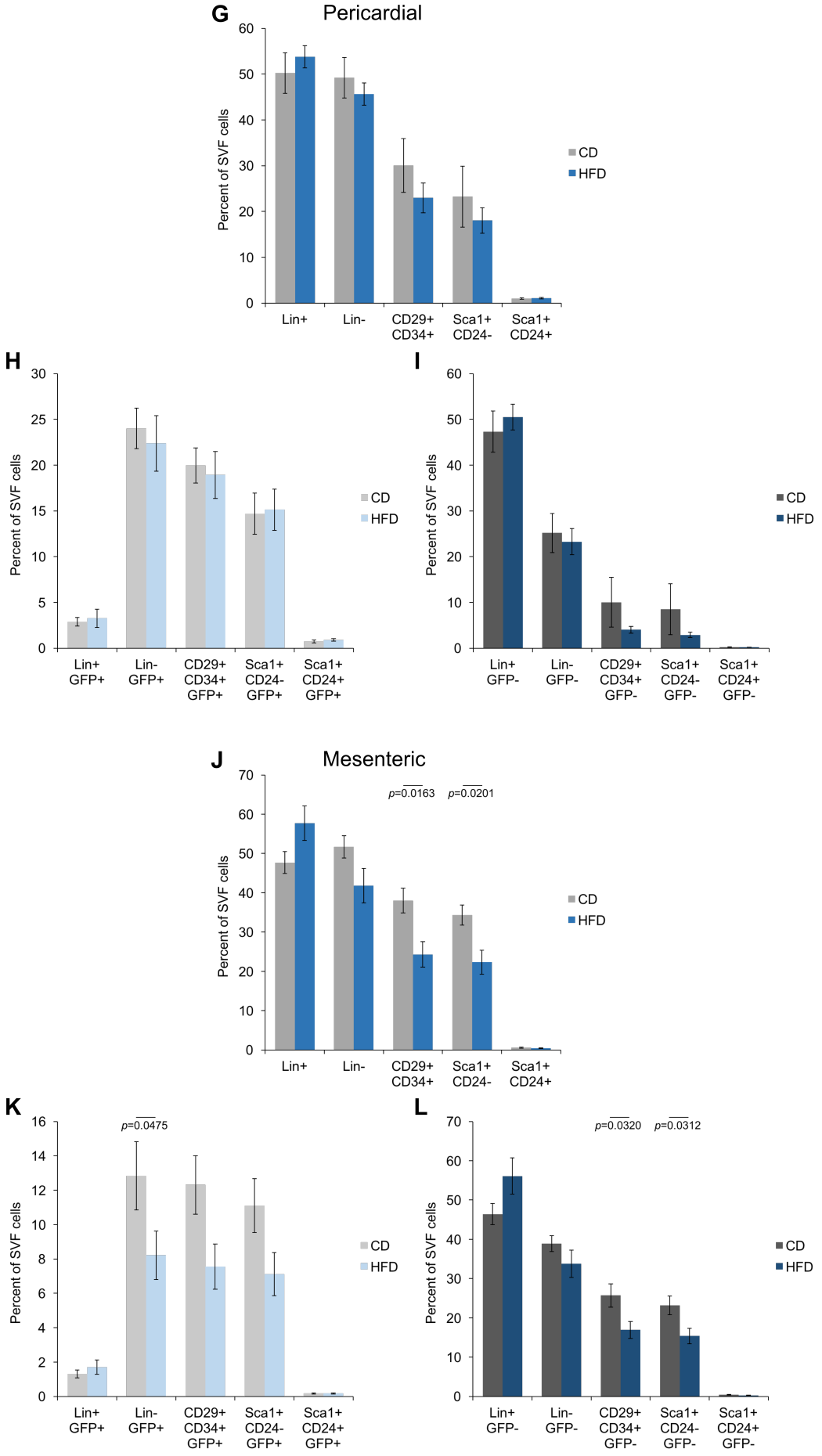


Figure 3.15. (continued on next page)



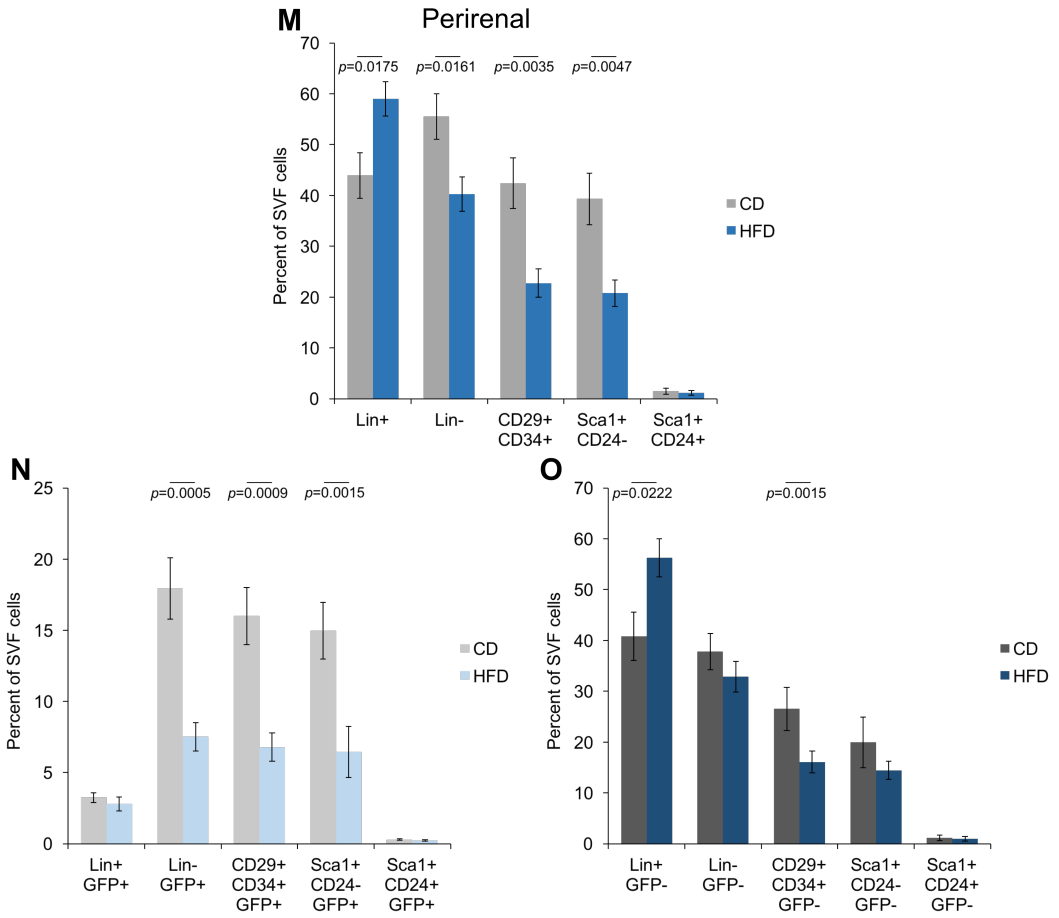


Figure 3.15. A HFD changes the percentages of cells in the different populations that make up the SVF and the percentages of GFP$^+$ (Wt1$^+$) cells in these different populations. *The SVF was isolated from the visceral fat depots of Wt1$^{GFP/+}$ knock-in mice fed either a HFD or CD and stained with a panel of antibodies (Lin, CD31, CD29, CD34, Sca1, CD24), before being analysed using flow cytometry. There was a reduction in the percentages of Lin$^-$;CD31$^-$, Lin$^-$;CD31$^-$;CD29$^+$;CD34$^+$, Lin$^-$;CD31$^-$;CD29$^+$;CD34$^+$;Sca1$^+$;CD24$^-$ and Lin$^-$;CD31$^-$;CD29$^+$;CD34$^+$;Sca1$^+$;CD24$^+$ cells in the SVF of the HFD mice compared to the CD mice for the perigonadal **(A)**, omental **(D)**, mesenteric **(J)** and perirenal **(M)** depots, but not for the pericardial depot **(G)**. Conversely there was an increase in the percentages of Lin$^+$;CD31$^+$ cells in the SVF of the HFD mice compared to the CD mice for the perigonadal **(A)**, omental **(D)**, mesenteric **(J)** and perirenal **(M)** depots, but not for the pericardial depot **(G)**. For the perigonadal **(B)**, omental **(E)**, mesenteric **(K)** and perirenal **(N)** depots the percentage of Lin$^-$;CD31$^-$GFP$^+$ (Wt1$^+$) cells was lower in the SVF from the HFD mice compared to the CD mice, but not for the pericardial depot **(H)**. The percentage Lin$^-$;CD31$^-$GFP$^-$ (Wt1$^-$) cells was also reduced in the HFD mice for some, but not all of the depots **(C,F,I,L,O)**. (Lin+ represents Lin$^+$;CD31$^+$. Lin- represents Lin$^-$;CD31$^-$. CD29$^+$;CD34+ represents Lin$^-$;CD31$^-$;CD29$^+$;CD34$^+$. Sca1$^+$;CD24$^-$ represents Lin$^-$;CD31$^-$;CD29$^+$;CD34$^+$;Sca1$^+$;CD24$^-$. Sca1$^+$;CD24$^+$ represents Lin$^-$;CD31$^-$;CD29$^+$;CD34$^+$;Sca1$^+$;CD24$^+$). (n=5 minimum CD, 8 HFD; data represent the mean ± s.e.m. and two-tailed Student's t-tests were used to assess statistical significance).*

3.6.2 Gene expression microarray analysis

In addition to understanding how a HFD influenced the composition of the SVF and the percentage of $Wt1^+$ APCs, we also wanted to assess the effect of the HFD at a transcriptional level. In order to do so, gene expression microarrays were carried out. All microarray analysis was performed using $Lin^-;CD31^-;CD29^+;CD34^+$ (GFP^+/GFP^-) APCs isolated from the perigonadal depot of $Wt1^{GFP/+}$ knock-in mice. This fat pad was chosen, because it is the largest visceral fat pad, and therefore is the best depot for isolating large numbers of SVF cells, thus permitting the extraction of large enough quantities of RNA, sufficient for microarray analysis. Moreover, most of the work performed in sections 3.2-3.5, comparing GFP^+ ($Wt1^+$) and GFP^- ($Wt1^-$) cells, utilised SVF cells from this depot.

Comparisons were made between the samples from mice fed a HFD and mice fed a CD, for both GFP^+ ($Wt1^+$) and GFP^- ($Wt1^-$) populations. Again, gene expression analysis was performed by Graeme Grimes from the MRC HGU. APCs from HFD-fed mice and CD-fed mice differed significantly in the expression of 451 genes ($q<0.05$ calculated by the R Bioconductor package LIMMA) (Figure 3.16). 234 genes showed increased expression in the HFD cells, compared to the CD, and 217 genes exhibited decreased expression. As shown in Figure 3.16, these two categories of genes were further broken down according to whether the differential expression was observed in only the GFP^+ ($Wt1^+$) cells, only the GFP^- ($Wt1^-$) cells, or in both. Again, two gene ontology tools: GOrilla (http://cbl-gorilla.cs.technion.ac.il) and DAVID (https://david.ncifcrf.gov) were used to analyse the differentially expressed genes to identify interesting pathways and genes. The 451 significantly changed genes were ordered by log fold change and analysed using GOrilla. GOrilla calculates enrichment values for each GO term, taking into account the total number of genes on the microarray, the total number of genes associated with the GO term, and the amount and ranking of the associated genes that are present in the microarray results.

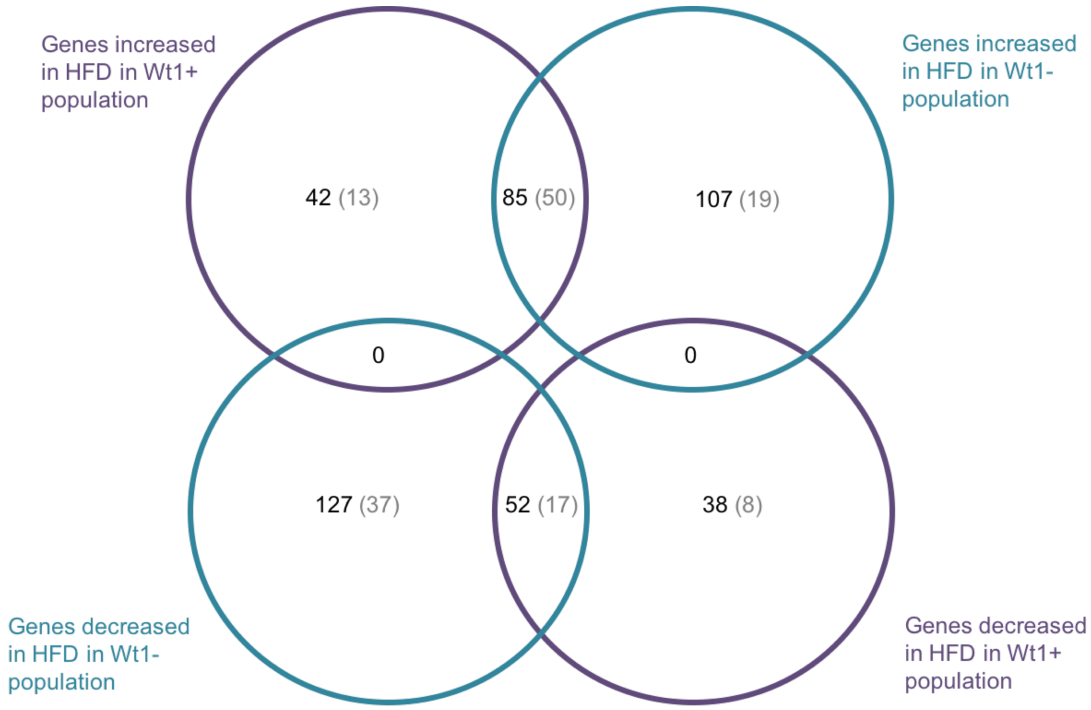


Figure 3.16. The breakdown of 451 differential gene expression changes comparing mice fed a HFD and mice fed a CD. *The data is taken from GFP^+ ($Wt1^+$) and GFP^- ($Wt1^-$) Lin^-;$CD31^-$;$CD29^+$;$CD34^+$ perigonadal SVF cells isolated from $Wt1^{GFP/+}$ knock-in mice. All genes exhibiting significantly different gene expression have been included (q<0.05). Numbers in parentheses represent the number of genes that also have a LogFC value of >1.5 (increased expression) or <-1.5 (decreased expression).*

3.6.2.1 GO terms identified for genes upregulated in APCs from HFD mice

As was the case previously, 451 genes is a relatively small number to be analysed by GOrilla. Nevertheless, a few GO terms were identified, however none of them reached a significance level of q<0.05. Table 3.6 shows the GO terms that were identified by this analysis, along with their FDR q-value. Most of the GO terms were associated with an inflammatory/immune response, for example, "leukocyte migration", "lymphocyte migration" and "regulation of defence response". The genes that exhibited a LogFC >1.5 were then analysed using DAVID, which revealed many GO terms with an FDR q-value <0.05 (adjusted p-value using the Benjamini and Hochberg (1995) method). As shown in Table 3.7, most of the significantly enriched GO terms were also associated with an immune response, thus supporting the results obtained from the GOrilla analysis.

Table 3.6. Enriched GOrilla GO terms of genes upregulated in Lin$^-$;CD31$^-$;CD29$^+$;CD34$^+$ perigonadal SVF cells from mice fed a HFD. All genes with a q-value <0.05 were included in the analysis.

GO TERM	DESCRIPTION	NUMBER OF GENES	ENRICHMENT	FDR Q-VALUE
GO:0060326	Cell chemotaxis	9	4.04	5.21×10^{-2}
GO:0050900	Leukocyte migration	8	4.04	1.11×10^{-1}
GO:0048870	Cell motility	20	2.25	1.73×10^{-1}
GO:0048247	Lymphocyte chemotaxis	4	8.31	2.52×10^{-1}
GO:0040011	Locomotion	21	2.08	2.94×10^{-1}
GO:0050727	Regulation of inflammatory response	11	2.96	3.11×10^{-1}
GO:0006928	Movement of cell or subcellular component	22	2.05	3.34×10^{-1}
GO:0031347	Regulation of defense response	10	3.46	3.59×10^{-1}

Table 3.7. Enriched DAVID GO terms for genes upregulated in Lin$^-$;CD31$^-$;CD29$^+$;CD34$^+$ perigonadal SVF cells from mice fed a HFD. Only genes with a q-value <0.05 and a LogFC >1.5 were included in the analysis.

DESCRIPTION	NUMBER OF GENES	PERCENTAGE	FDR Q-VALUE	GENES
Extracellular region	30	48.4	6.4×10^{-5}	*Lypd1, Marcksl1, Amn, Ccl9, Cxcl14, Cx3cl1, C4a, C4b, Crlf1, Enpp6, Fndc5, Fbln7, Hgf, Il1r2, Il1rl1, Kng1, Kng2, Lgmn, Mmp12, Mmp3, Mdk, Plvap, Prkar2b, Prg4, Runx1 Spp1, Sele, Saa3, Tnc, Timp1*
Extracellular space	18	29	1.2×10^{-4}	*Amn, Ccl9, Cxcl14, Cx3cl1, C4a, C4b, Crlf1, Hgf, Il1rl1, Kng1, Kng2, Mmp3, Pg4, Spp1, Sele, Saa3, Tnc, Timp1*
Cell migration	16	25.8	2.3×10^{-4}	*Arap3, Ccl9, Cxcl14, Cx3cl1, Ch25h, Cyp7b1, Hgf, Mmp13, Mdk, Plvp, Spp1, Sele, Sema7a*
Inflammatory response	12	19.4	3.5×10^{-4}	*Ccl9, Cx3cl1, C4a, C4b, Hgf, Il1r2, Il1rl1, Kng1, Spp1, Sele, Sema7a, Saa3*
Leukocyte migration	8	12.9	1.2×10^{-3}	*Ccl9, Cxcl14, Cx3cl1, Ch25h, Cyp7b1, Plvap, Spp1, Sele*
Cell chemotaxis	8	12.9	1.6×10^{-3}	*Ccl9, Cxcl14, Cx3cl1, Ch25h, Cyp7b1, Hgf, Spp1, Saa3*
Lymphocyte chemotaxis	5	8.1	3.2×10^{-3}	*Ccl9, Cxcl14, Cx3cl1, Ch25h, Cyp7b1*
Response to stimulus	38	61.3	7.3×10^{-3}	*Arap3, Gpr176, Lypd1, Bcat1, Ccl9, Cxcl14, Cx3cl1, Ch25h, C4a, C4b, Cyp7b1, Cox8b, Crlf1, Dgkz, Fndc5, Hgf, Il1r2, Kng1, Kng2, Lgmn, Mmp12, Mmp3, Mdk, Pex11a, Pde1b, Plvap, Prkar2b, Prg4, Rgs16, Runx1, Spp1, Sele, Sema7a, Saa3, Slc40a1, Tnc, Timp1*
Immune system process	16	25.8	1.1×10^{-2}	*Ccl9, Cxcl14, Cx3cl1, Ch25h, C4a, C4b, Cyp7b1, Il1rl1, Pde1b, Plap, Prg4, Runx1, Spp1, Sele, Sema7a, Slc40a1*

3.6.2.2 GO terms identified for genes downregulated in APCs from HFD mice

The 451 significantly different genes were subsequently ordered with those decreased in expression at the top of the list and again analysed using GOrilla. As in 3.6.2.1, a few GO terms were identified, however none of them reached significance (Table 3.8). Again, the significant genes with a LogFC <-1.5 were analysed using DAVID, which did generate some significant GO terms, including "extracellular region", "vesicle" and "single-organism process" (Table 3.9).

Table 3.8. Enriched GOrilla GO terms for genes downregulated in $Lin^{-};CD31^{-};CD29^{+};CD34^{+}$ perigonadal SVF cells from mice fed a HFD. All genes with a q-value <0.05 were included in the analysis.

GO TERM	DESCRIPTION	NUMBER OF GENES	ENRICHMENT	FDR Q-VALUE
GO:0097756	Negative regulation of blood vessel diameter	2	42.6	$7.56x10^{-1}$
GO:0042310	Vasoconstriction	2	42.6	$9.07x10^{-1}$
GO:0007088	Regulation of mitotic nuclear division	3	13.31	1
GO:0014824	Artery smooth muscle contraction	2	42.6	1
GO:0014820	Tonic smooth muscle contraction	2	42.6	1
GO:0014829	Vascular smooth muscle contraction	2	42.6	1

Table 3.9. Enriched DAVID GO terms for genes downregulated in $Lin^{-};CD31^{-};CD29^{+};CD34^{+}$ perigonadal SVF cells from mice fed a HFD. Only genes with a q-value <0.05 and a LogFC <-1.5 were included in the analysis.

DESCRIPTION	NUMBER OF GENES	PERCENTAGE	FDR Q-VALUE	GENES
Extracellular region	20	58.8	$4.2x10^{-6}$	*Nt5e, Cd82, Fbxo2, Adgrg2, Anxa9, Bmp7, Clic6, Col4a3, Col4a4, Edn1, Gsta3, Gnai1, Ramp1, Retnla, Scin, Slc6a13, Sbsn, Tubb4a, Upk3b, Wnt5b*
Vesicle	18	52.9	$1.4x10^{-4}$	*Nt5e, Cd82, Fbxo2, Adgrg2, Anxa9, Bmp7, Clic6, Edn1, Gsta3, Gnai1, Scin, Slc17a7, Slc47a1, Slc6a13, Sbsn, Tubb4a, Upk3b, Wnt5b*
Single-organism process	27	79.4	$2.7x10^{-2}$	*Nt5e, Bik, Cd82, Fbxo2, Adgrg2, Anxa9, Ackr1, Bmp7, Chst1, Cadm3, Clic6, Col4a3, Col4a4, Edn1, Fez1, Gsta3, Gnai1, Ramp1, Scin, Slc17a7, Slc47a1, Slc6a13, Smpd3, Tubb4a, Upk3b, Wnt5b, Zfp385a*

3.6.2.3 Analysis of genes differentially expressed specifically in $Wt1^+$ or $Wt1^-$ APC populations

As described above, when comparing differences in gene expression between all APCs from HFD-fed mice and CD-fed mice, the major pathways and genes that were enriched for appear to be implicated in immune system processes and inflammation. This is unsurprising, given it is know that a major consequence of obesity is an activation of inflammatory pathways and increased inflammation (Monteiro and Azevedo, 2010). Perhaps the more interesting data obtained from this study concerns the differences in gene expression that occur in a HFD state, specifically in either the $Wt1^+$ or $Wt1^-$ cell populations. As shown in Figure 3.16, 42 genes exhibited a significant increase in expression, specifically in $Wt1^+$ cells, in the HFD state compared to the CD state, whilst 127 genes exhibited decreased expression. Conversely, 107 genes were upregulated specifically in the $Wt1^-$ cells, in the HFD state compared to the CD state, whilst 38 genes exhibited decreased expression.

Tables in Appendices 4, 5, 6 and 7 list all genes with significantly different expression ($q<0.05$), and a LogFC >1.5 (or <-1.5 where decreased expression is applicable). These tables are broken down into the four categories described above; increased or decreased expression in either the $Wt1^+$ or $Wt1^-$ cell populations. In these tables each gene is accompanied by a short description, and if any existing information exists in the literature regarding a function in or a link to adipose tissue, this is also detailed. These gene lists were also ordered by log fold change and analysed using DAVID, however, due to the small numbers of genes, the number of significant GO terms generated was quite low. Any GO terms that had an FDR q-value <0.05 are detailed in Tables 3.10, 3.11, 3.12.

Table 3.10. Enriched DAVID GO terms for genes downregulated in $Wt1^+$ Lin^-;$CD31^-$;$CD29^+$;$CD34^+$ perigonadal SVF cells from mice fed a HFD. Only genes with a q-value <0.05 and a LogFC <-1.5 were included in the analysis.

DESCRIPTION	NUMBER OF GENES	PERCENTAGE	FDR Q-VALUE	GENES
Extracellular region	6	100	$3.4x10^{-3}$	*Clic3, Cldn3, Krt19, Msln, Serpina3c, Upk3b*

Table 3.11. Enriched DAVID GO terms for genes downregulated in Wt1$^-$ Lin$^-$;CD31$^-$;CD29$^+$;CD34$^+$ perigonadal SVF cells from mice fed a HFD. Only genes with a q-value <0.05 and a LogFC <-1.5 were included in the analysis.

DESCRIPTION	NUMBER OF GENES	PERCENTAGE	FDR Q-VALUE	GENES
Extracellular region	23	60.5	$7.5x10^{-6}$	*Cd82, Fbxo2, Sec11a, Adm, Alpl, Anxa3, Anxa9, St6gal1, Bmp4, Bmp7, Cdh13, Col4a3, Dpp4, Gnai1, Lamc3, Nmb, Ramp1, Retnla, Scin, Slc6a13, Sbsn, Tubb4a, Vit*
Blood vessel development	10	26.3	$1.3x10^{-3}$	*Arhgap22, Adm, Anxa3, Bmp4, Bmp7, Cdh13, Col4a3, Prokr1, Ramp1, Tcf21*
Biological adhesion	10	26.3	$2.8x10^{-2}$	*Anxa9, St6gal1, Bmp4, Bmp7, Cdh13, Col4a3, Dpp4, Lamc3, Pkp2, Vit*
Cell proliferation	12	31.6	$3.1x10^{-2}$	*Fbxo2, Adm, St6gal1, Bmp4, Bmp7, Cdh13, Col4a3, Dpp4, Nmb, Osr2, Pkp2, Scin*

Table 3.12. Enriched DAVID GO terms for genes upregulated in Wt1$^-$ Lin$^-$;CD31$^-$;CD29$^+$;CD34$^+$ perigonadal SVF cells from mice fed a HFD. Only genes with a q-value <0.05 and a LogFC >1.5 were included in the analysis.

DESCRIPTION	NUMBER OF GENES	PERCENTAGE	FDR Q-VALUE	GENES
Immune system process	8	40	$4.2x10^{-2}$	*Cd276, Ccl9, F2rl1, C4a, C4b, H2-Dmb1, Prg4, Tmem176b*

3.6.2.4 Gene expression validation

In order to validate the data obtained from the microarray analysis, qRT-PCR was performed using custom plates for 91 of the interesting gene hits, as well as 5 reference genes. This validation was performed in technical and biological triplicate. Genes were chosen for validation, based on whether their up/downregulation was significant, and the log fold change values were also taken into consideration (although not all of those validated had a LogFC >1.5 or <-1.5). Additionally, as outlined in the tables in Appendices 4, 5, 6 and 7, many of the genes have existing information detailed in the literature about links to and roles in adipose tissue function, therefore these genes were selected for validation. Furthermore, any genes that were highlighted as being enriched in relevant GO terms were also chosen, for example those implicated in blood vessel development, proliferation or immune system processes.

As shown in Figure 3.17, *Wt1* expression was also checked by qRT-PCR. Firstly, this confirmed that expression in GFP^+ cells was significantly higher than expression in GFP^- cells, therefore verifying that the cells had been sorted correctly. Additionally, this expression analysis revealed that, even within the GFP^+ cell population, the cells taken from mice fed a HFD expressed significantly lower levels of *Wt1* than those from the mice fed a CD. As described in section 3.6.1, a decrease in the percentage of GFP^+ cells was observed in the APC populations from the HFD mice compared to the CD. It now appears that not only were there fewer GFP^+ cells in the HFD condition, the expression level of *Wt1* was lower in these cells than in the CD condition.

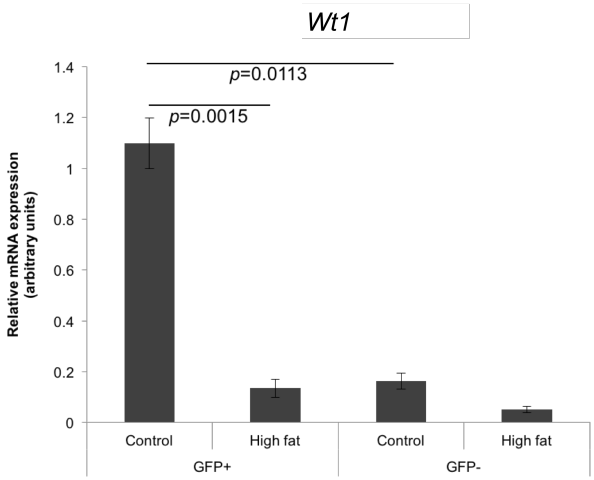
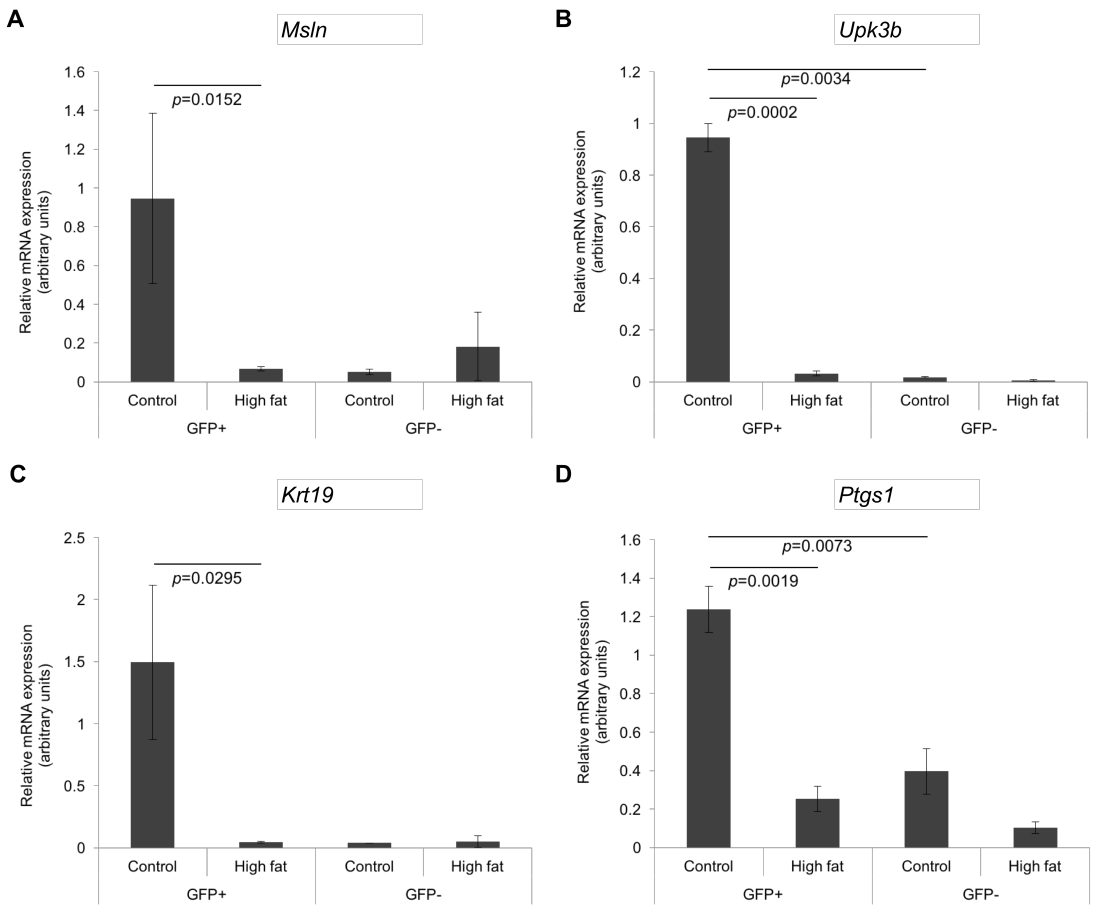


Figure 3.17. qRT-PCR validation of Wt1 mRNA expression in GFP^+ ($Wt1^+$) and GFP^- ($Wt1^-$) $Lin^-;CD31^-;CD29^+;CD34^+$ perigonadal SVF cells from HFD and CD mice. *Wt1 expression analysis confirmed that the GFP^+ cells expressed significantly higher levels of Wt1 than the GFP^- and that the GFP^+ cells from the HFD mice expressed significantly lower levels of Wt1 than those from the CD mice. (n=2 minimum; data represent the mean ± s.e.m. and two-tailed Student's t-tests were used to assess statistical significance).*

The results from the qRT-PCR validation are shown in Figures 3.18-3.21. The results are categorised according to which of the four groups the genes fell into following the microarray analysis (increased or decreased expression in HFD, in either $Wt1^+$ or $Wt1^-$ cells). Unfortunately, a large number of the genes were not well validated in this assay, and therefore the data have not been shown for these. This lack of validation was due either to the qRT-PCR itself not working well, or because no difference in gene expression was observed between the HFD and CD cells by qRT-PCR. For several genes, there was significant variation between the results from the different biological replicates, which also meant they were not well validated. Nevertheless, many

interesting genes were validated by the qRT-PCR. For example, most of the genes that displayed downregulation in the $Wt1^+$ HFD cells were verified (Figure 3.18). These included multiple genes that are typically highly expressed in the mesothelium, such as *Msln, Upk3b* and *Krt19* (Figure 3.18 A-C). All three exhibited significantly lower expression in the $Wt1^+$ HFD cells compared to the CD cells, but no difference in expression was observed in the $Wt1^-$ cells between the two conditions. Other genes that were well validated in this category included *Ptgs1, Rspo1* and *Serpina3c* (Figure 3.18 D-F). Additionally, *Clic3* was significantly downregulated in the $Wt1^+$ HFD cells compared to the CD, but also showed a significant downregulation in the $Wt1^-$ cells (Figure 3.18 G). Finally, *Wnt10b* and *Smo* appeared to be downregulated, however the difference was not significant (Figure 3.18 H,I).

Figure 3.18. (continued on next page)



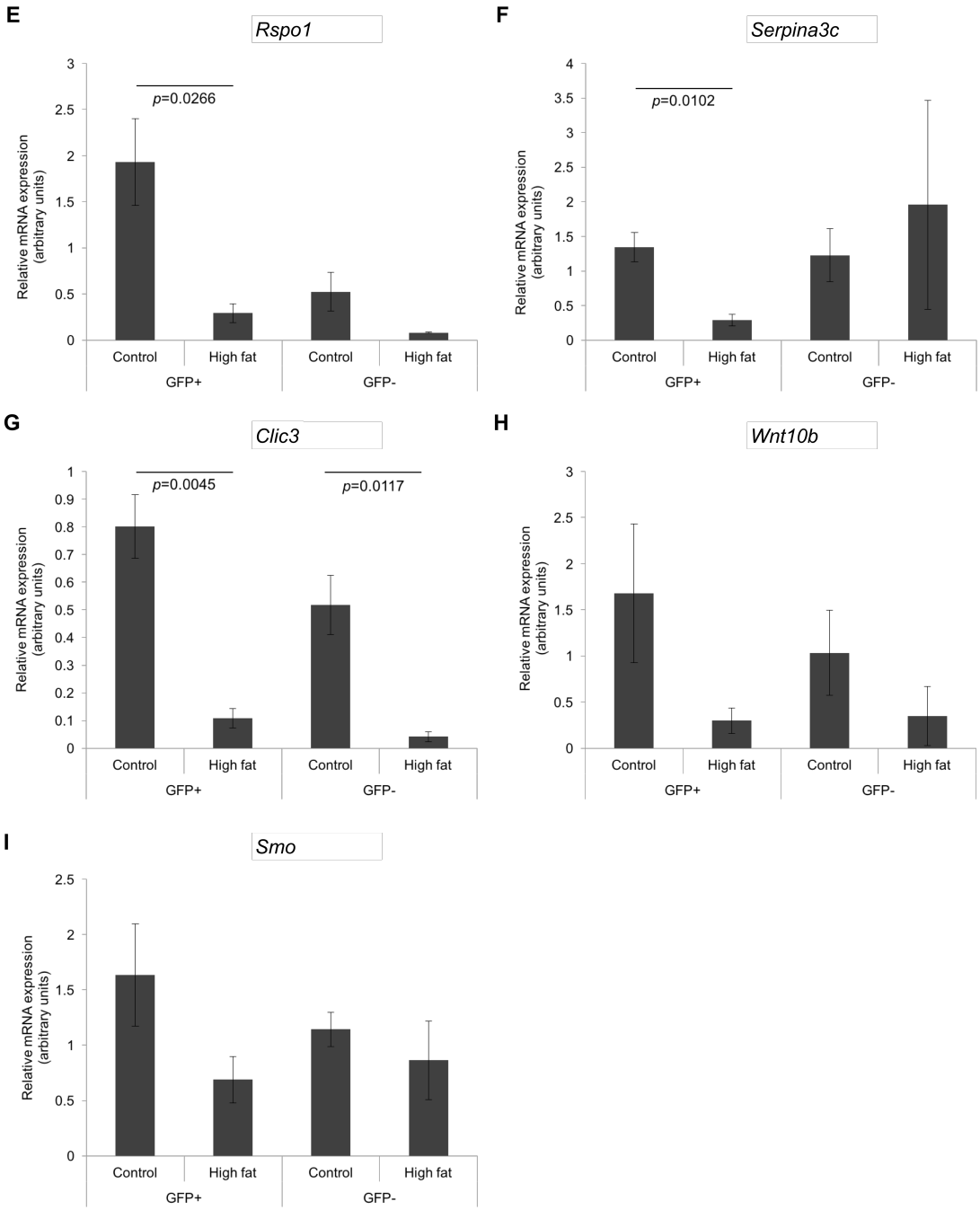


Figure 3.18. qRT-PCR validation of genes downregulated in Lin$^-$;CD31$^-$;CD29$^+$;CD34$^+$ perigonadal GFP$^+$ (Wt1$^+$) cells in the HFD state, as identified by microarray analysis. (A-F) *Expression levels of Msln, Upk3b, Krt19, Ptgs1, Rspo1 and Serpina3c confirmed the microarray result.* ***(G)*** *Expression levels of Clic3 confirmed the microarray result, but also showed reduced expression in the GFP$^-$ (Wt1-) cells in the HFD state.* ***(H,I)*** *Wnt10b and Smo also appeared to be expressed at lower levels in the HFD state, however the differences were not significant. (A-C n=2 minimum, D-I n=3; data represent the mean ± s.e.m. and two-tailed Student's t-tests were used to assess statistical significance).*

The majority of the genes that, according to the microarray, were downregulated in the $Wt1^-$ HFD cells compared to CD, were well validated by qRT-PCR (Figure 3.19). However, most of these genes also exhibited decreased expression in the $Wt1^+$ HFD cells compared to controls. Therefore, the decreased expression in the HFD state was not unique to the $Wt1^-$ cells. Despite this, many of the genes highlighted in the various GO terms including blood vessel development, proliferation, extracellular region and biological adhesion (Table 3.11), were confirmed by qRT-PCR as having lower expression in the HFD cells. Additionally, many of these genes have known links to adipose tissue biology, as do those genes which have been validated by the qRT-PCR, but did not appear in any of the GO terms (Figure 3.19). Not all the genes exhibited a significant difference in expression, however, those for which a difference was apparent, despite not being significant, have been included.

The genes that showed increased expression in the HFD state according to the microarray data, were generally not well validated by the qRT-PCR, for both the $Wt1^+$ and $Wt1^-$ populations. However, amongst those that were validated were some interesting hits (Figures 3.20-3.21), and these are discussed in section 3.8. Additionally, where existing links to adipose tissue biology were found in the literature, these are detailed in Appendices 5 and 6. Moreover, a few of the genes described in the GO term "immune system process" (Table 3.12), were validated (although not all significantly), by the qRT-PCR (Figure 3.21).

Figure 3.19. (continued on next page)

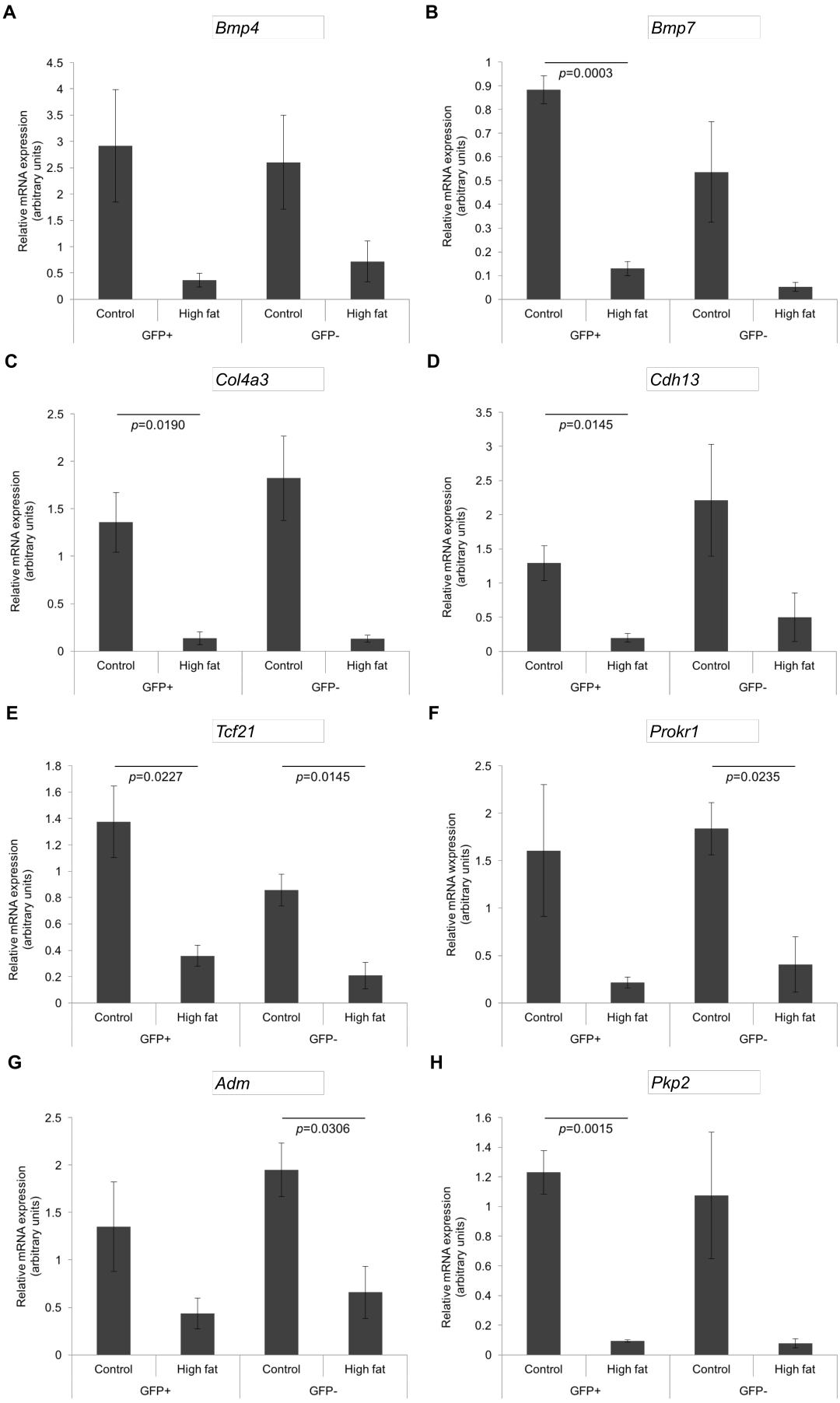
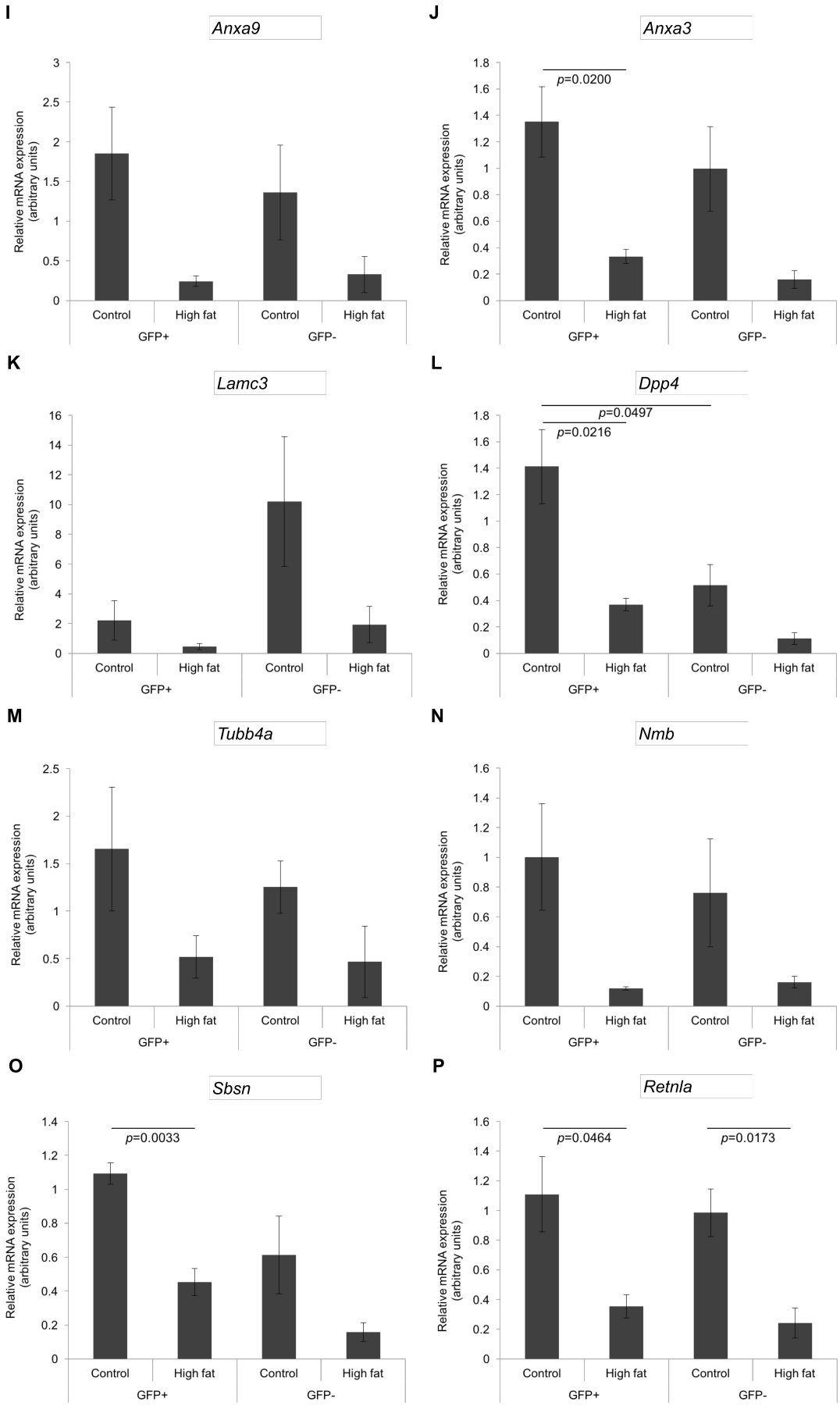


Figure 3.19. (continued on next page)



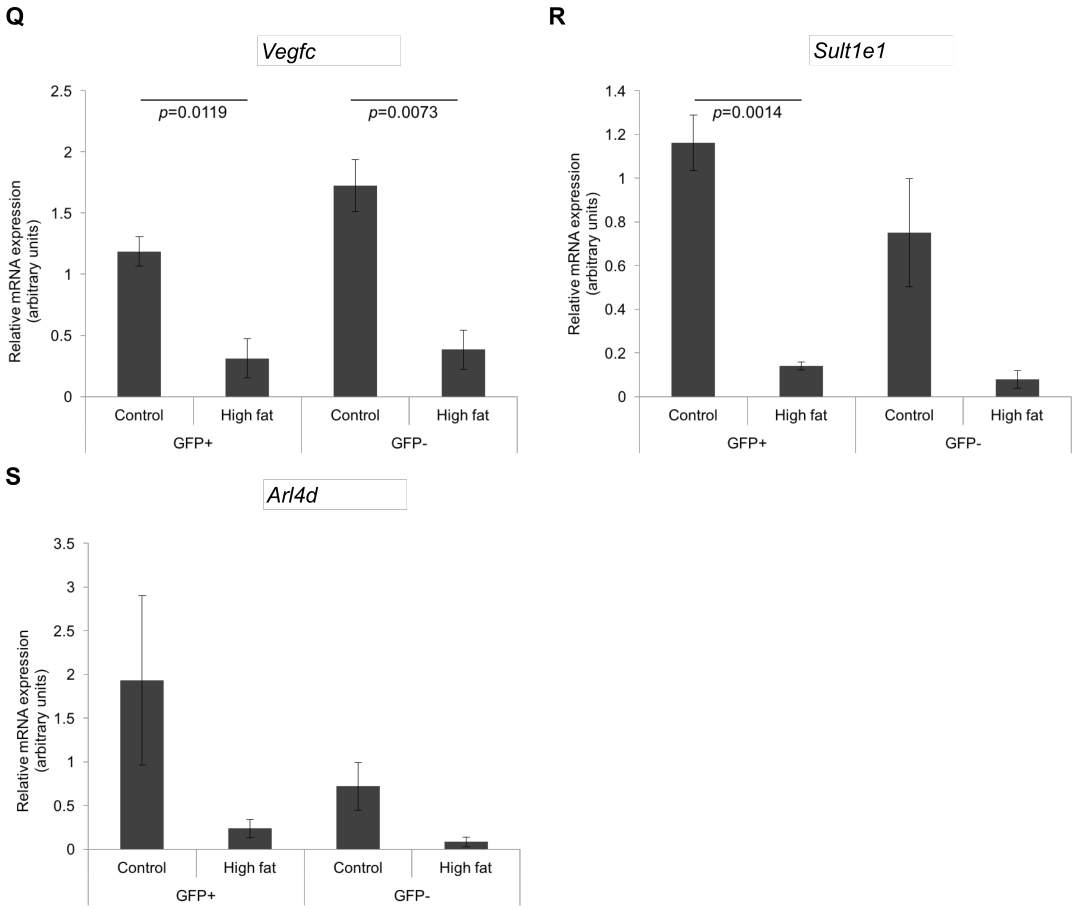


Figure 3.19. qRT-PCR validation of genes downregulated in Lin$^-$;CD31$^-$;CD29$^+$;CD34$^+$ perigonadal GFP$^-$ (Wt1$^-$) cells in the HFD state, as identified by microarray analysis. *The majority of the genes identified by the microarray analysis as being downregulated in the GFP$^-$ cells in the HFD state, were validated by qRT-PCR, although not all significantly. Most genes also showed decreased expression in the GFP$^+$ (Wt1$^+$) cells in the HFD state compared to the CD state. All genes appeared in at least one of the GO terms identified by DAVID including blood vessel development, proliferation, extracellular region and biological adhesion **(A-P)** (Table 3.11), or have known links to adipose tissue biology **(Q-S)** Appendix 5. (n=3; data represent the mean ± s.e.m. and two-tailed Student's t-tests were used to assess statistical significance).*

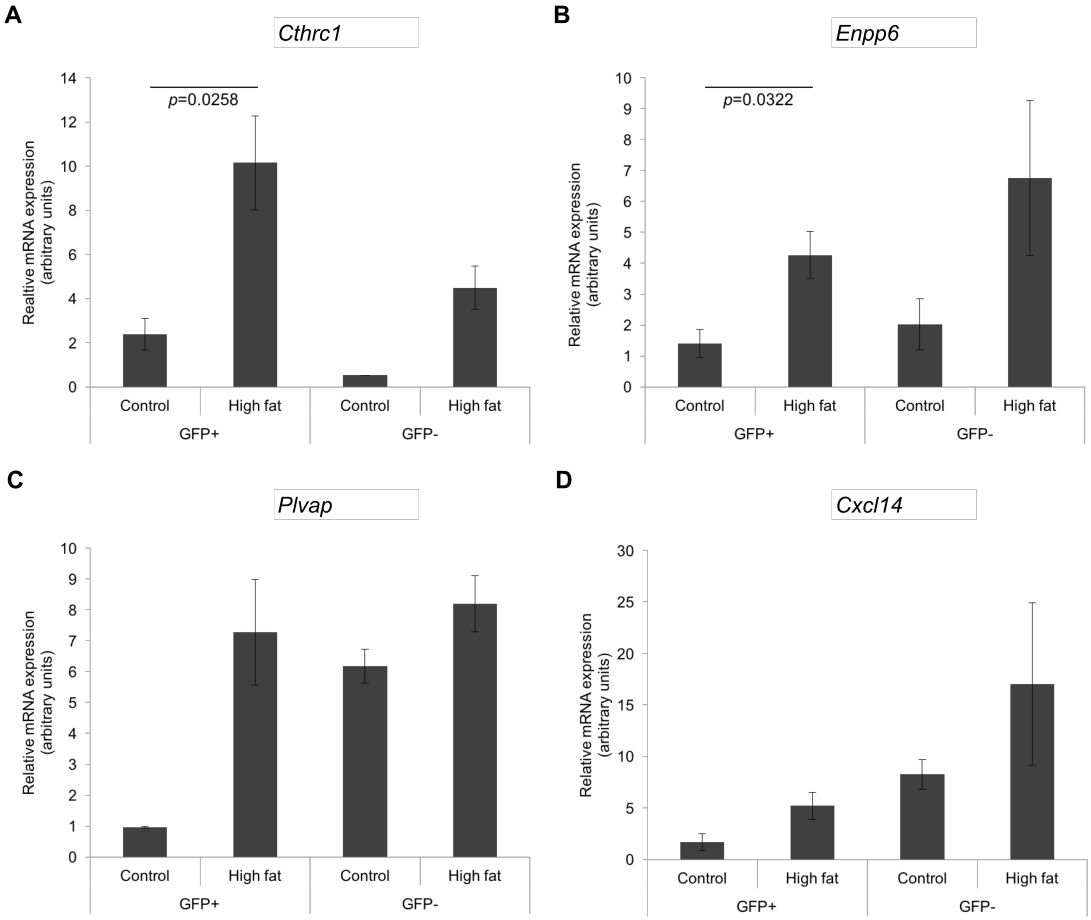


Figure 3.20. qRT-PCR validation of genes upregulated in Lin$^-$;CD31$^-$;CD29$^+$;CD34$^+$ perigonadal GFP$^+$ (Wt1$^+$) cells in the HFD state, as identified by microarray analysis. *The majority of the genes identified by the microarray analysis as being upregulated in the GFP$^+$ (Wt1$^+$) cells in the HFD state, were not validated by qRT-PCR.* ***(A-B)*** *Cthrc1 and Enpp6 did show significant upregulation of expression in the GFP$^+$ (Wt1$^+$) cells in the HFD state compared to the CD state.* ***(C-D)*** *Plvap and Cxcl14 also appeared to be upregulated in the GFP$^+$ (Wt1$^+$) cells in the HFD state compared to the CD state, although not significantly. (n=3; data represent the mean ± s.e.m. and two-tailed Student's t-tests were used to assess statistical significance).*

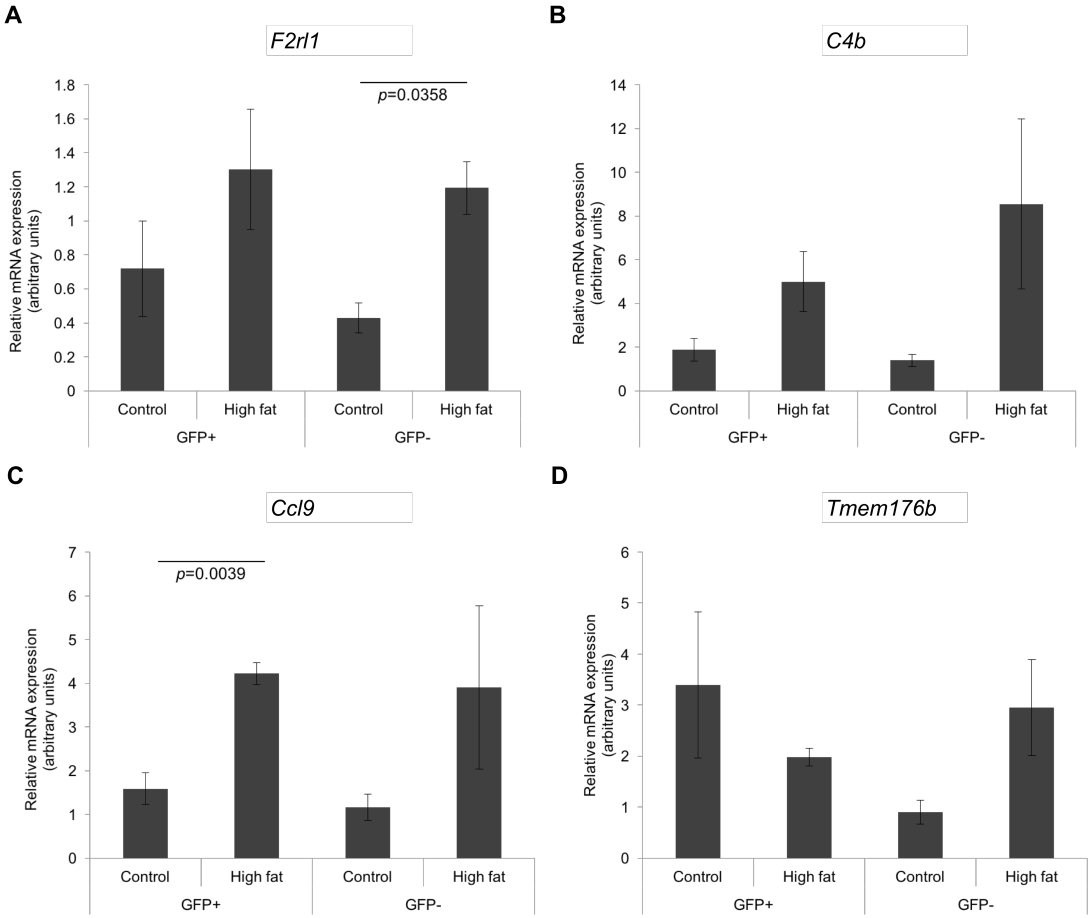


Figure 3.21. qRT-PCR validation of genes upregulated in Lin$^-$;CD31$^-$;CD29$^+$;CD34$^+$ perigonadal GFP$^-$ (Wt1$^-$) cells in the HFD state, as identified by microarray analysis. *The majority of the genes identified by the microarray analysis as being upregulated in the GFP$^-$ (Wt1$^-$) cells in the HFD state, were not validated by qRT-PCR.* ***(A)*** *F2rl1 did show significant upregulation of expression in the GFP$^-$ (Wt1$^-$) cells in the HFD state compared to the CD state.* ***(B-D)*** *C4b, Ccl9 and Tmem176b also appeared to be upregulated in the GFP$^-$ (Wt1$^-$) cells in the HFD state compared to the CD state, although not significantly. Ccl9 was also significantly upregulated in the GFP$^+$ (Wt1$^+$) cells in the HFD state compared to the CD state. All genes appeared in the GO term identified by DAVID: immune system process (Table 3.16). (n=3; data represent the mean ± s.e.m. and two-tailed Student's t-tests were used to assess statistical significance).*

3.7 The effect of a high fat diet on the proportion of Wt1 lineage traced cells using *Wt1-Cre^{ERT2};R26R-mTmG* mice

One of the most interesting results obtained from the HFD study using *Wt1$^{GFP/+}$* knock-in mice, was that there were fewer GFP^{+} (Wt1^{+}) APCs in the SVF of the visceral adipose tissue (with the exception of the pericardial depot) from mice fed a HFD compared to those fed a CD (section 3.6.1). A possible explanation for this result could be that, in the HFD state, a higher proportion of Wt1^{+} APCs differentiate into adipocytes than in the CD state, therefore reducing the percentage of Wt1^{+} APCs present in the SVF of the HFD mice, compared to CD mice. In order to test this hypothesis, the *Wt1-Cre^{ERT2};R26R-mTmG*, lineage tracing mouse line was used. The *Wt1$^{GFP/+}$* knock-in mouse line was not suitable for this experiment because once APCs differentiate into mature adipocytes, they lose *Wt1* expression, and therefore also lose GFP expression. However, the lineage tracing model permits the permanent labelling of any APCs that express *Wt1* at the time of tamoxifen administration, and additionally, any cells that are subsequently derived from them. Prior to Cre mediated loxP recombination, all cells in the *R26R-mTmG* reporter mouse express Tomato and thus fluoresce red. However, upon Cre expression recombination occurs, Tomato is excised, and eGFP is expressed, meaning that any Cre expressing cells fluoresce green, as do their progeny (Muzumdar *et al.*, 2007). Henceforth, if, as hypothesised, a greater percentage of Wt1^{+} APCs differentiate into adipocytes in the HFD state, compared to the CD, a higher percentage of GFP^{+} mature adipocytes should be observed in the former.

Male *Wt1-Cre^{ERT2}* mice were crossed with homozygous female *R26R-mTmG* mice, and immediately after giving birth, the mother was administered with the first dose of tamoxifen (8mg/40g mouse at a concentration of 20mg/ml). By administering the tamoxifen to the mother, the new born pups received it via her milk. Three further doses were given in the same way, over a period of two weeks. At one month old, the pups were started on a HFD, and remained on this until being culled for tissue at approximately 7.5 months old (Figure 3.22 B). Only male mice were included in this study. Unfortunately, the animals that had been allocated for CD feeding had to be

culled, due to their mother dying, therefore at present we do not have an exact age-matched control cohort for this study. However, we had previously performed a comparable study, in which *Wt1-Cre^{ERT2};R26R-mTmG* pups were also administered with four doses of tamoxifen via their mother, they were then fed normal chow, and harvested for tissue at approximately one year old (Figure 3.22 A). Therefore, aside from the fact that these mice were not exactly age matched when they were culled for tissue, they were treated in the same way as the HFD-fed mice. Whilst these mice were obviously not the ideal control, due to the age difference, we currently do not have a closer match, therefore, the control data described below refers to these mice. However, when analysing and interpreting the data this age difference was considered. Mice are currently being bred to perform the age-matched control, however, due to time constraints the data is not ready for this thesis.

3.7.1 The effect of a high fat diet on the proportion of Wt1 lineage traced cells in the SVF

The perigonadal, omental, pericardial, mesenteric and perirenal visceral adipose tissue was harvested from the mice and each sample was split into two. Half was prepared for analysis of the SVF using flow cytometry and the rest was fixed, embedded in paraffin and sectioned for immunohistochemistry analysis. The percentage of GFP$^+$ cells in the SVF was assessed, revealing that mice fed a HFD had a lower percentage of GFP$^+$ SVF cells than those fed normal chow (Figure 3.22 C,D). This was the case for the five visceral depots analysed (perigonadal, omental, pericardial, mesenteric, perirenal). As the mice fed a HFD were not age-matched to those on normal chow, as explained above, the data from the two conditions was not plotted on the same graph. Nevertheless, for all depots analysed, the percentage of GFP$^+$ cells in the SVF from mice fed a HFD was approximately half that of the mice fed normal chow.

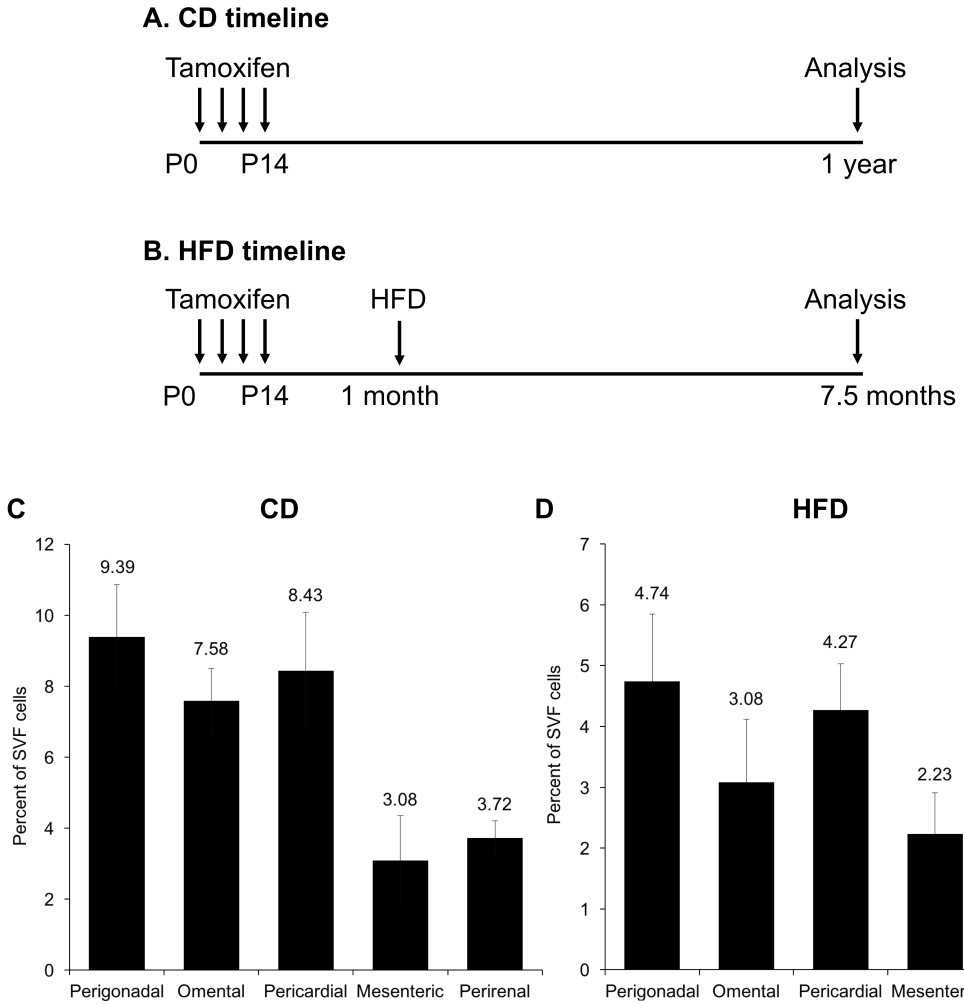
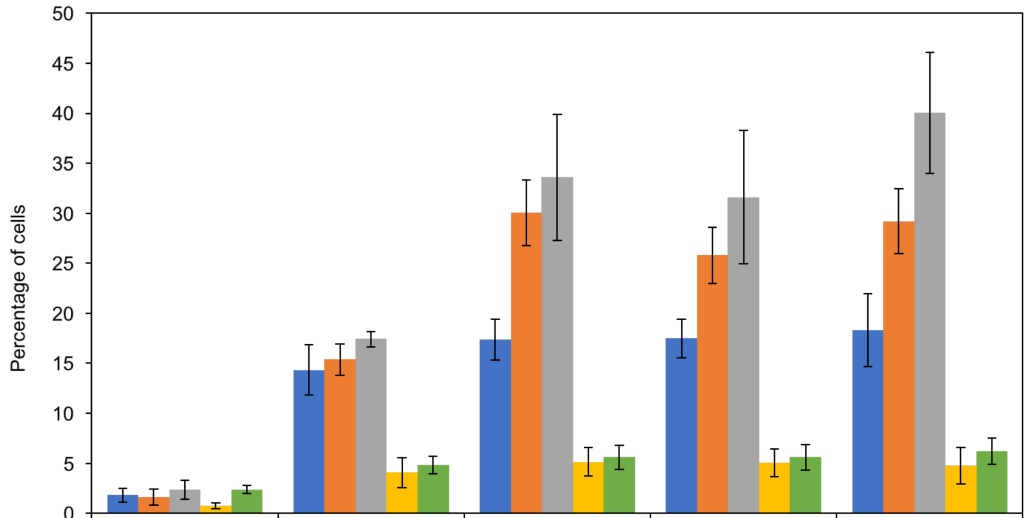


Figure 3.22. The percentage of GFP$^+$ cells in the SVF of male Wt1^{CreERT2};R26R-mTmG mice is lower for the HFD fed mice than for the CD fed mice. *Wt1^{CreERT2};R26R-mTmG mice were administered with four doses of tamoxifen immediately after birth, via their mother's milk.* ***(A)*** *CD mice were fed normal chow and harvested for tissue at approximately 1 year old.* ***(B)*** *HFD mice were fed a HFD and harvested for tissue at approximately 7.5 months old.* ***(C,D)*** *Flow cytometry analysis of the SVF revealed that, for all depots analysed, the percentage of GFP$^+$ cells in the SVF from the HFD mice was approximately half that of the CD mice. (n=3 CD, 4 HFD; data represent the mean ± s.e.m).*

As described for the earlier HFD study (section 3.6), the SVF was stained with the panel of antibodies described previously (Lin, CD31, CD29, CD34, Sca1, CD24), before performing flow cytometry. This allowed the assessment of whether/how the percentage of GFP^+ cells in the various SVF populations differed between the HFD and normal state. Figure 3.23 illustrates the results from this analysis. Again, the data from the HFD and normal chow mice was not plotted on the same graph. However, it is apparent that the percentage of GFP^+ cells in the $Lin^-;CD31^-$ population and all its subpopulations was lower in the SVF from the HFD mice than from those fed normal chow. As the tables of percentages in Figure 3.23 show, for most of the populations the percentage of GFP^+ cells in SVF from the HFD mice was at least half that of the mice fed normal chow. There did not, however, appear to be a much of a difference in the percentage of GFP^+ cells in the $Lin^+;CD31^+$ population between the two states. These results corroborate those obtained from the HFD study using the *Wt1*$^{GFP/+}$ knock-in mice (section 3.6.1). In summary, the percentage of Wt1 lineage traced APCs was lower in the visceral adipose tissue from mice fed a HFD compared to those fed normal chow.

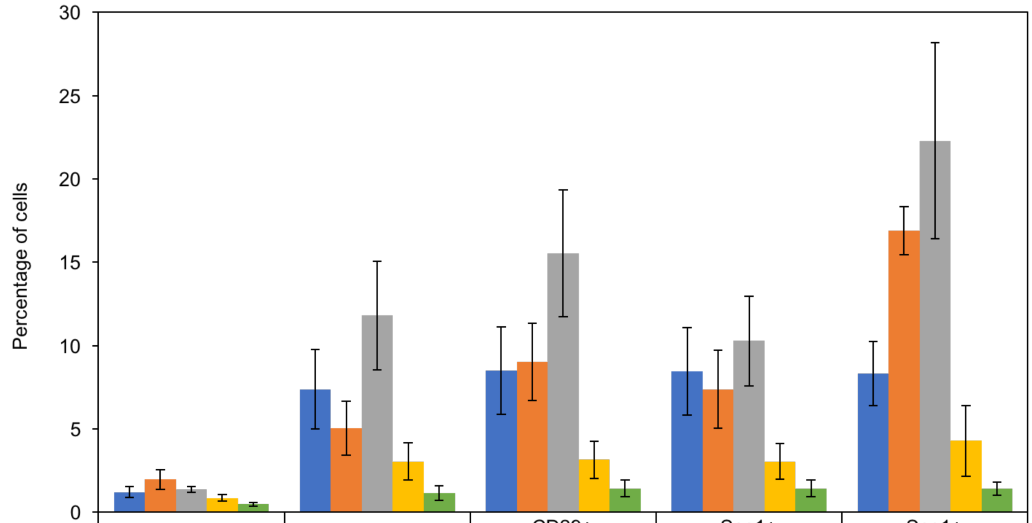
Figure 3.23. (continued on next page)

A **CD**



	Lin+	Lin-	CD29+ CD34+	Sca1+ CD24-	Sca1+ CD24+
Perigonadal	1.81	14.33	17.37	17.5	18.33
Omental	1.61	15.37	30.03	25.8	29.2
Pericardial	2.35	17.43	33.6	31.6	40.03
Mesenteric	0.75	4.07	5.14	5.04	4.74
Perirenal	2.38	4.84	5.6	5.61	6.21

B **HFD**



	Lin+	Lin-	CD29+ CD34+	Sca1+ CD24-	Sca1+ CD24+
Perigonadal	1.21	7.38	8.49	8.45	8.32
Omental	1.96	5.03	9.02	7.38	16.88
Pericardial	1.35	11.81	15.54	10.28	22.28
Mesenteric	0.86	3.05	3.14	3.05	4.28
Perirenal	0.48	1.15	1.43	1.43	1.4

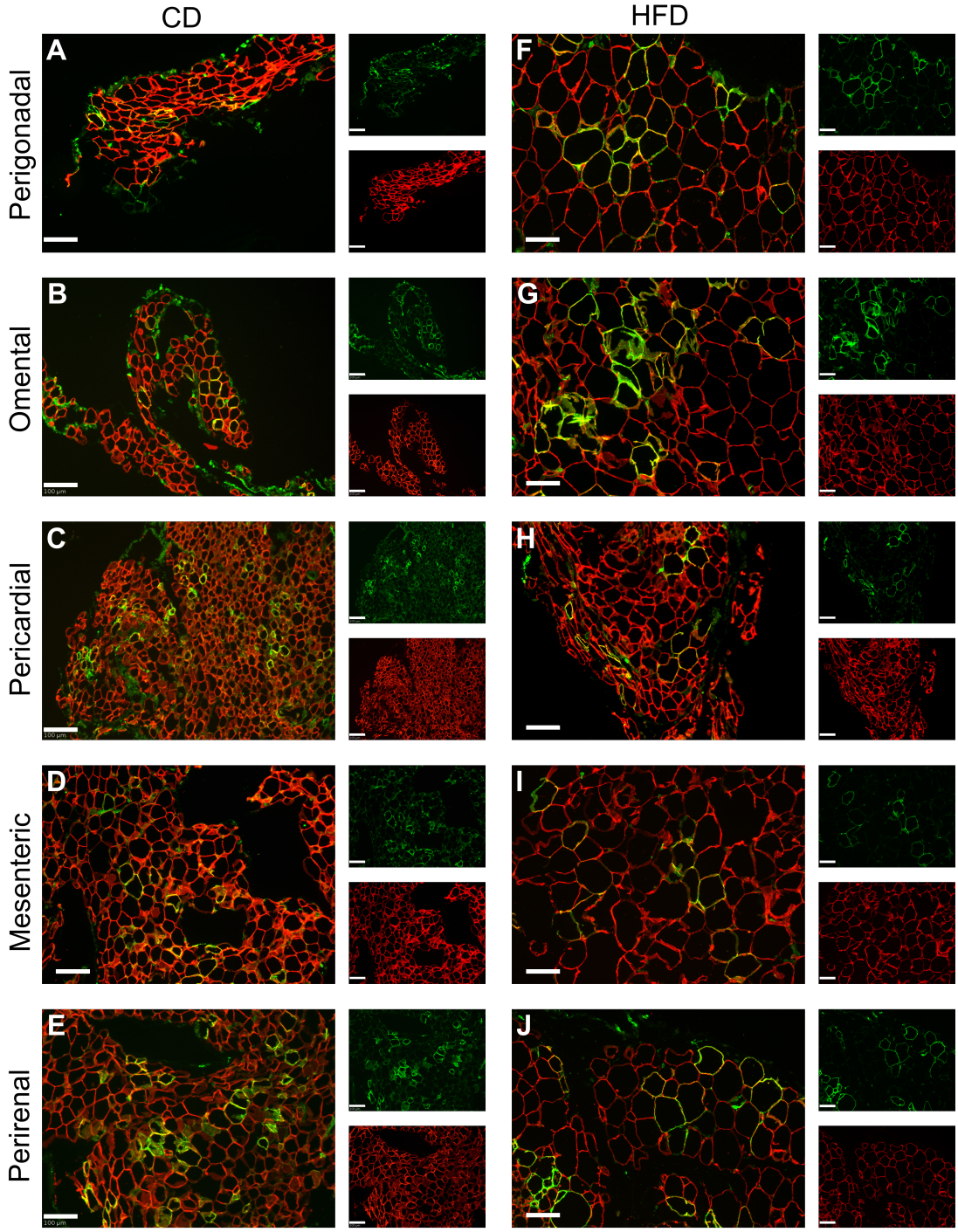
Figure 3.23. A HFD affects the percentage of GFP$^+$ cells in the different populations that make up the SVF of visceral adipose tissue depots from male Wt1^{CreERT2};R26R-mTmG mice. *Wt1^{CreERT2};R26R-mTmG mice were administered with four doses of tamoxifen immediately after birth, via their mother.* ***(A)*** *CD mice were fed normal chow and harvested for tissue at approximately 1 year old.* ***(B)*** *HFD mice were fed a HFD and harvested for tissue at approximately 7.5 months old. The SVF was isolated and stained with a panel of antibodies (Lin, CD31, CD29, CD34, Sca1, CD24), before being analysed using flow cytometry.* ***(A,B)*** *The y axis represents the percentage of cells in each population shown on the x axis that were labelled with GFP. For all depots analysed, the percentage of GFP$^+$ cells in the Lin- population and all its sub-populations was lower for the mice fed a HFD than for those fed a CD. However, for the Lin+ population was no such difference. (Lin+ represents Lin$^+$;CD31$^+$. Lin- represents Lin$^-$;CD31$^-$. CD29$^+$;CD34+ represents Lin$^-$;CD31$^-$;CD29$^+$;CD34$^+$. Sca1$^+$;CD24$^-$ represents Lin$^-$;CD31$^-$;CD29$^+$;CD34$^+$;Sca1$^+$;CD24$^-$. Sca1$^+$;CD24$^+$ represents Lin$^-$;CD31$^-$;CD29$^+$;CD34$^+$;Sca1$^+$;CD24$^+$) (n=3 CD, 4 HFD; data represent the mean ± s.e.m).*

3.7.2 The effect of a high fat diet on the proportion of Wt1 lineage traced mature adipocytes

For reasons explained above, we were particularly interested in understanding whether, using the lineage tracing mice, the percentage of GFP$^+$ mature adipocytes was higher in the HFD mice compared to those fed normal chow. The embedded adipose tissue from the various depots was sectioned and stained with an anti-perilipin antibody to label all the mature adipocytes, and an anti-GFP antibody to label any GFP$^+$ adipocytes. The GFP labelling of the reporter *R26R-mTmG* mice is membranous, which is particularly useful given that the presence of large lipid droplets within the

adipocytes displaces the cytoplasm and thus makes visualising cytoplasmic staining difficult. As illustrated in Figure 3.24, the percentages of GFP^+ adipocytes did not obviously differ between the HFD-fed and normal chow-fed mice for any of the visceral depots analysed. However, as indicated by the size of the error bars on the graphs, for both the HFD and normal chow states, there was substantial variation between the mice, possible reasons as to why this is the case are discussed in 3.8.

Figure 3.24. (continued on next page)



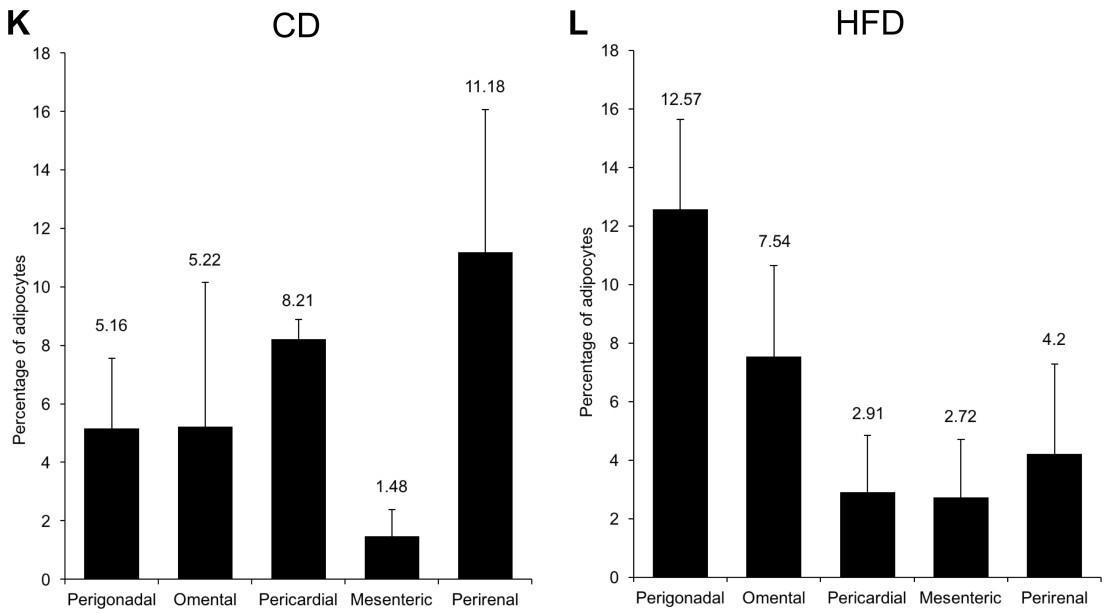


Figure 3.24. Wt1 expressing cells in male Wt1^{CreERT2};R26R-mTmG pups contribute to mature adipocytes in the visceral adipose depots of adult mice, fed either normal or high fat chow. *Wt1^{CreERT2};R26R-mTmG mice were administered with four doses of tamoxifen immediately after birth, via their mother.* ***(A-E)*** *CD mice were fed normal chow and harvested for tissue at approximately 1 year old.* ***(F-J)*** *HFD mice were fed a HFD and harvested for tissue at approximately 7.5 months old. Sections were stained with an anti-GFP antibody (green) and an anti-perilipin antibody (red).* ***(K,L)*** *Quantification of the GFP+ adipocytes in each depot, for the CD* ***(K)*** *and HFD* ***(L)*** *mice. (Scale bar = 100μm). (n=4 HFD, 3 CD; data represent mean ± s.e.m).*

3.8 Discussion

The results described in this chapter have shown that *Wt1* expressing and non-expressing APCs exhibit different behaviours both *in vitro* and *in vivo*, in response to certain conditions. Moreover, the two populations differ at the transcriptomic level, and some of these differences reflect what has been observed in the *in vitro* studies. Initial experiments indicated that the Wt1^{+} cells from the SVF of visceral adipose tissue depots differentiated into adipocytes more readily than the Wt1^{-} cells when cultured *in vitro*. A plausible explanation for this was that the Wt1^{+} population is composed largely of pre-adipocytes (Chau *et al.*, 2014), whilst the Wt1^{-} population contains a mixture of cell types, including all the non-adipogenic cells of the SVF, such as endothelial and haematopoietic. However, despite sorting the SVF cells based on their cell-surface marker profiles using FACS, the same results were obtained. Even when the cells were sorted to acquire only the pre-adipocyte population (Lin^{-};CD31^{-}

;CD29^{+};CD34^{+};Sca1^{+};CD24^{-}), and equal numbers of Wt1^{+} and Wt1^{-} pre-adipocytes plated, the Wt1^{+} cells were consistently more adipogenic than the Wt1^{-}. Therefore, it was concluded that the differences being observed were not a consequence of differences in the composition of the two populations.

This led us to question why this difference in adipogenesis was occurring, and we hoped that in answering this we may understand more about the role of *Wt1* in these cells. We hypothesised that perhaps the two populations were behaving differently, for example one was proliferating more than the other, and/or that the Wt1^{+} APCs were secreting a factor(s) that was required by the Wt1^{-} APCs for them to differentiate, thus implicating paracrine signalling. Preliminary data suggests that both these scenarios may be true. When cultured *in vitro,* murine APCs should be confluent before they will differentiate into adipocytes (Ailhaud *et al.*, 1989; Church, Berry and Rodeheffer, 2014). When observing the cultures, the wells containing Wt1^{-} APCs always appeared to harbour fewer cells than those containing the Wt1^{+} APCs (despite initially plating the same numbers of each). Thus we considered the possibility that either the Wt1^{-} APCs were dying or that they were less proliferative than the Wt1^{+} APCs, therefore resulting in the Wt1^{+} cultures becoming confluent more quickly and thus differentiating more readily.

Apoptosis and proliferation were checked, and whilst no apoptotic cells were present in either culture, it became apparent that the Wt1^{+} cultures contained a higher percentage of proliferating cells than the Wt1^{-} cultures. Furthermore, when the two populations of APCs were cultured together, this difference in proliferation persisted. Hence, this suggested that the variation in proliferation was due to intrinsic differences between the cells. This proliferative difference could certainly explain why the Wt1^{+} cultures appeared to contain more cells than the Wt1^{-}, and thus may also contribute to the contrasting abilities of the cells to differentiate into adipocytes. Despite checking apoptosis by staining with an anti-Caspase 3 antibody, future work should include confirming this result with another method, for example flow cytometry. It is plausible that more cells in the Wt1^{-} cultures were dying, but that in getting rid of the supernatant and washing the cells before staining, the dead cells were removed. Therefore, using

flow cytometry to analyse all cells (including those in the supernatant) would inform as to whether more dead/dying cells were present in the $Wt1^-$ cultures. It would also be informative to check apoptosis at different time points, for example in addition to checking after 3 days, we should also check after 7 days, just before inducing differentiation. Perhaps the $Wt1^-$ cells are more apoptotic, but are not dying until later in the culture. Additionally, it may be interesting to over plate the $Wt1^-$ APCs (for example plate two times more $Wt1^-$ APCs than $Wt1^+$ APCs) and see whether this leads to improved differentiation of the $Wt1^-$ population. If the issue is indeed an inability to reach confluency, this should help to address this problem and thus allow us to understand whether there are other influential factors.

Having demonstrated that $Wt1^+$ APCs were more proliferative than $Wt1^-$, we next wanted to understand whether the expression of *Wt1* was responsible for this proliferative difference. Indeed, several studies have suggested a role for WT1 in proliferation, for example, inhibition of WT1 *in vitro* leads to the reduced proliferation of endothelial cells (Wagner *et al.*, 2008), moreover, WT1 is required for vascular progenitor cell proliferation in heart development (Moore *et al.*, 1999; Hohenstein and Hastie, 2006). Additionally, decreased proliferation of neural progenitor cells has been reported in mice lacking the +KTS isoform of WT1 (Wagner *et al.*, 2005). Conversely, knockdown of *Wt1* using siRNA treatment of kidney organ cultures, results in increased proliferation in regions where nephrons should form (Davies *et al.*, 2004). Hence, WT1 evidently functions in progenitor cell proliferation (and differentiation), although this function may differ between cell and tissue types. Moreover, oncogenic *WT1* expression is evidently tightly linked to cell cycle regulation and proliferation (Hohenstein and Hastie, 2006). However, having used APCs isolated from *CAGG-CreER*^{TM}*;Wt1*$^{loxP/loxP}$ (WER) mice, to delete *Wt1 in vitro,* we showed that there was no significant effect on the percentage of proliferating cells. Therefore suggesting that presence/absence of WT1 expression in the APCs was not the cause of the proliferative difference we previously observed. It is also important to check whether the differentiation of the APCs is affected by the *in vitro* deletion of *Wt1*, given that our initial results showed a clear difference in the ability of the $Wt1^+$ and $Wt1^-$ populations to undergo adipogenesis.

We have also shown that media conditioned by $Wt1^+$ APCs can partially improve the adipogenic differentiation of $Wt1^-$ APCs. This suggests that the $Wt1^+$ APCs do indeed secrete a factor(s) that promotes the differentiation of the $Wt1^-$ APCs. It therefore appears that both potential explanations are at least partially true. However, the results from the conditioned media study are only preliminary. Several additional experiments are required to confirm this result and follow it up further. These include heat inactivating the conditioned media (to denature any secreted proteins that may be responsible for the rescue), and determining whether this abolishes the improved differentiation. If this is the case, future experiments would include performing ELISAs and mass spectrometry to try and understand the nature of the secreted protein(s), potentially using the results from our transcriptomic analysis as a guide.

In addition to examining the behaviours of the $Wt1^+$ and $Wt1^-$ APC populations *in vitro*, transcriptomic analysis was performed using freshly isolated cells. Although the number of genes that differed significantly in their expression was relatively low (261 in total, 121 upregulated in $Wt1^+$ cells and 140 downregulated), analysis using gene ontology tools presented some interesting results. Regarding the genes that exhibited higher expression in the $Wt1^+$ cells compared to the $Wt1^-$ cells, several gene ontology (GO) terms relating to extracellular activity were identified. Therefore, this provides further support for the hypothesis that the $Wt1^+$ APCs secrete a factor(s) that potentially influences the growth and differentiation of the $Wt1^-$ APCs. Moreover, a number of the genes encode secreted proteins, including *Slpi, Dmkn, Tnfrsf11b, Adamts16, Dpp4, Lcn2* and *Sbsn*. The top gene with a LogFC of 2.97 was *Slpi,* which encodes secretory leukocyte protease inhibitor (SLPI). Additionally, *Dpp4* encodes the adipokine: dipeptidyl peptidase-4 (DPP4). It is known that expression of *Dpp4* is highest in differentiated adipocytes, although it is also expressed in precursor cells (Zilleßen *et al.*, 2016). *Lcn2* encodes another adipokine; Lipocalin 2 (LCN2) which functions in glucose and lipid homeostasis and is upregulated in obesity (Yan *et al.*, 2007). These genes are discussed further in chapter 6 (6.2.2), including information about known roles in adipose tissue.

Several genes identified in the microarray as having upregulated expression in the $Wt1^+$ APCs, have previously been described as belonging to a visceral adipose tissue gene set (genes with >3-fold increased expression in visceral compared to subcutaneous adipose tissue) (Cohen *et al.*, 2014). These include *Slpi, Upk3b, Dmkn* and *Cyp2s1*. Hence, this suggests that the $Wt1^+$ APCs exhibit a more visceral-like gene signature than the $Wt1^-$ APCs. Interestingly, although the data are not shown, when we performed the second microarray analysis using the samples from the high fat diet study mice (discussed below), we were also able to compare $Wt1^+$ and $Wt1^-$ APC samples from the mice fed a control diet (so effectively repeating the current study), encouragingly, many of the hits were identified in both studies, including *Slpi, Upk3b, Upk1b* and *Cyp2s1*.

Whilst the genes upregulated in the $Wt1^+$ APCs represented the most interesting category given the results from our *in vitro* studies, several potentially interesting GO terms were also identified for the downregulated genes. These included "angiogenesis", which is required for the development and expansion of fat depots, as well as "cell proliferation" and "cell adhesion". These three terms were all identified when both the complete list of significantly down regulated genes was used for the analysis, and when only those genes that also had a LogFC <-1.5 were used, and therefore represent the top most downregulated genes. Intriguingly, several genes in this category have been implicated in brown adipose tissue biology. For example, *Meox2* has been found to be expressed predominantly in brown, but not white, pre-adipocytes (Timmons *et al.*, 2007). Additionally, *Ednrb* is a positive regulator of *Ucp1* and the deletion of *EDNRB* in human brown pre-adipocytes leads to a significant reduction in UCP1 levels in the mature brown adipocytes, thus indicating that it functions in the regulation of thermogenic activity (Xue *et al.*, 2015). Thus, whilst the $Wt1^+$ cells appear to exhibit higher expression of genes associated with visceral adipose tissue compared to the $Wt1^-$ cells, the opposite is true for several genes associated with brown adipose tissue.

The second part of this chapter focused on results obtained from performing high fat diet (HFD) studies in mice. We were interested in knowing whether differences

between $Wt1^+$ and $Wt1^-$ APC populations would be observed *in vivo*, regarding their behaviour in response to dietary perturbations. Using flow cytometry, we assessed whether/how the percentages of $Wt1^+$ and $Wt1^-$ cells differed in $Wt1^{GFP/+}$ knock-in mice fed a HFD compared to those fed a control diet (CD). The trend across four of the five visceral depots analysed (perigonadal, omental, mesenteric and perirenal) was a reduction in the percentage of GFP^+ ($Wt1^+$) cells in the HFD-fed mice. This result was significant for the omental and perirenal depots, but the perigonadal and mesenteric also showed a reduction. However, there was no difference in the percentage of GFP^+ ($Wt1^+$) cells in the pericardial depot.

We also analysed whether/how the percentages of the different cell populations that comprise the SVF changed in mice fed a HFD. The trend here was an increase in the percentage of $Lin^+;CD31^+$ cells (the haematopoietic/endothelial cell fraction), but a decrease in the $Lin^-;CD31^-$ population and consequently a decrease in the $Lin^-;CD31^-;CD29^+;CD34^+$ APC population, the $Lin^-;CD31^-;CD29^+;CD34^+;Sca1^+;CD24^-$ pre-adipocyte population and the $Lin^-;CD31^-;CD29^+;CD34^+;Sca1^+;CD24^+$ progenitor cell population. Again, whilst this trend was true for most of the depots, the differences were not always significant. It is clear from these results that whilst there is a trend, the individual depots responded differently to the HFD, particularly regarding the pericardial depot. This provides further support for the idea that the different fat depots represent distinct "mini organs" that function quite independently of one another (Cartwright *et al.*, 2010).

Perhaps more interesting than these global differences, are the differences that occurred specifically in the GFP^+ ($Wt1^+$) and GFP^- ($Wt1^-$) fractions of these populations. For example, the increase in $Lin^+;CD31^+$ cells for the omental depot was due only to an increase in the $Lin^+;CD31^+GFP^-$ population and not the $Lin^+;CD31^+GFP^+$ population. Conversely, the decrease in the $Lin^-;CD31^-$ population and its derivatives was due solely to a decrease in the $Lin^-;CD31^-GFP^+$ cells and not the $Lin^-;CD31^-GFP^-$ cells. This result was not as clear-cut for the other depots, with both the GFP^+ and GFP^- cells decreasing for some populations, however the trend was generally the same. Strikingly, no differences were observed for the pericardial depot.

As detailed in chapter 4, we hypothesise that at least a proportion of the APCs and thus adipocytes in the pericardial depot have a different developmental origin from those of the other visceral depots. It is therefore feasible that this could help to explain the contrasting result for the pericardial depot in this HFD study, however this is something that requires further investigation.

In addition to analysing the cells, they were sorted using FACS to be used for microarray analysis. The GFP^+ ($Wt1^+$) and GFP^- ($Wt1^-$) APCs from the perigonadal depot of HFD and CD mice were compared. This allowed a four-way comparison of the transcriptomic profiles; HFD $Wt1^+$, HFD $Wt1^-$, CD $Wt1^+$ and CD $Wt1^-$, thus allowing us to understand not only what changes occurred in response to a HFD, but specifically what changes occurred in the $Wt1^+$ and $Wt1^-$ populations. In total, 451 genes exhibited significantly differential gene expression across the four populations, and the breakdown of these 451 genes is illustrated in Figure 3.16. The genes that were upregulated and downregulated in the cells from the HFD mice (including $Wt1^+$ and $Wt1^-$) populations were interrogated using gene ontology tools. Using both GOrilla and DAVID, several GO terms involving inflammation and immune response were highlighted for the genes upregulated in the cells from the HFD mice. Given that inflammation is a well-known side-effect of obesity (Monteiro and Azevedo, 2010), this result is encouraging. However, whilst the majority of the GO terms identified by DAVID reached significance (FDR q-value <0.05), this was not the case for the GO terms identified by GOrilla. It is likely that this is due to the relatively low amount of input genes that was submitted; 234 genes is a fairly low number to be using for GO analysis. Similarly, when the genes that exhibited downregulated expression in the cells from the HFD mice were analysed using GO tools, only the terms returned by DAVID were significant. Amongst these was “extracellular region”, which, given the results from the previous microarray and the conditioned media experiments is potentially interesting.

The main focus of the analysis and validation was on genes that were upregulated or downregulated specifically in the $Wt1^+$ or $Wt1^-$ populations in response to a HFD. We hoped that this would help us to understand how the different populations responded

to the diet, and therefore inform on the *in vivo* consequences of the heterogeneity within the APC population. Perhaps the most interesting category are the genes that were downregulated in the $Wt1^+$ APCs in the HFD mice. The top hits in this category included *Krt19, Upk3b* and *Msln*, all of which are mesothelial cell markers. As described in the introduction, work from our group has shown that the visceral adipose depots are covered by a WT1 expressing mesothelial layer, and that this layer is a source of APCs (Chau *et al.*, 2014). Therefore, the reduction in expression of several mesothelial cell markers upon HFD feeding caught our attention. It could indicate that the cells are becoming less mesothelial in response to the diet, perhaps meaning that they are differentiating along the adipocyte lineage. The fact that we also observed a decrease in the percentage of $Wt1^+$ APCs in the HFD-fed mice suggests that this may be the case, and is something we followed up using a lineage tracing study, which is discussed later. Similarly, even within the GFP^+ ($Wt1^+$) population, the cells from the HFD-fed mice exhibited significantly lower *Wt1* expression than those from the CD-fed mice. Considering that mature adipocytes do not express *Wt1* (Chau *et al.*, 2014), and thus *Wt1* expression is lost from differentiating APCs, this result provides further support for the hypothesis that the $Wt1^+$ cells are being forced to differentiate into adipocytes in response to the HFD. Generally, the results from the microarray regarding the genes exhibiting downregulated expression in the $Wt1^+$ HFD cells, were well validated by qRT-PCR. Several other significantly downregulated genes, which were not included in Appendix 4 because they did not have a LogFC <-1.5, were also validated. These include *Ptgs1*, *Rspo1, Wnt10b* and *Smo,* and are discussed further in chapter 6 (6.2.3.1).

The genes that were downregulated in the $Wt1^-$ APCs in the HFD mice were also fairly well validated by qRT-PCR, however in many cases, they also exhibited significantly lower expression in the $Wt1^+$ APCs from the HFD mice. Therefore, often the change in expression was not unique to the $Wt1^-$ APCs. Interestingly, when examining the microarray data, many of these genes were shown to be downregulated in the $Wt1^+$ APCs, however this downregulation was not significant, and thus they were not listed in both categories. Nevertheless, when analysed using gene ontology tools, the genes in this category were enriched for GO terms including “extracellular region”, “blood

vessel development", "biological adhesion" and "cell proliferation". "Blood vessel development" is particularly interesting, as it is known that angiogenesis and adipogenesis are closely linked processes. Naturally, an expanding fat depot requires an increased blood supply. However, it is well documented that rapid adipose tissue expansion, as is the case in mice fed a HFD, is not always coupled with a sufficient increase in the vascular network, which ultimately results in hypoxia and thus inflammation (Corvera and Gealekman, 2014). Additionally, differences in cell proliferation could be linked to the adipogenesis in response to a HFD. Furthermore, several genes in this category have known roles/links to adipose tissue biology, which are outlined in Appendix 5 and discussed in chapter 6 (6.2.3.1).

Unfortunately, many of the genes that were upregulated in the APCs from the HFD-fed mice (both in the $Wt1^+$ and $Wt1^-$ populations), were not well validated by qRT-PCR. As described previously, the lack of validation was predominantly due to either the Cp (crossing point) values being too high to be quantitative, or the results from the qRT-PCR not showing any difference in expression between the APCs from the HFD and CD-fed mice. Of the few that were validated for the $Wt1^+$ population, *Cthrc1* was one. In the microarray results this gene did not have a LogFC >1.5 and therefore it is not listed in Appendix 4. However, it was significantly upregulated and has existing links to adipose tissue biology, so was chosen for validation. *Cthrc1* null mice have increased visceral fat when compared to wildtype littermates (Stohn *et al.*, 2015). Moreover, *in vitro* studies have shown that pre-adipocytes from *Cthrc1* null mice display enhanced adipogenesis, and conversely, CTHRC1 inhibits adipocyte differentiation (Stohn *et al.*, 2015). Hence, it appears that CTHRC1 inhibits adipogenesis, therefore it is perhaps surprising that it exhibited increased expression in the $Wt1^+$ cells from the HFD-fed mice. Conversely, CXCL14 deficient mice are resistant to HFD induced obesity and *Plvap* null mice have decreased visceral WAT (Takahashi *et al.*, 2007; Stan *et al.*, 2012). Both these genes exhibited upregulated expression in the $Wt1^+$ APCs from the HFD mice, and in both cases a difference was also shown by qRT-PCR although this was not significant. Evidently, the results present a complicated picture, but what does seem apparent is that many genes known

to function in adipogenesis or with previously reported roles in adipose tissue remodelling, exhibited altered expression in our study.

Regarding the genes that were upregulated in the $Wt1^-$ APCs from the HFD mice, the validation was generally not good, however those that were validated also exhibited upregulation in the $Wt1^+$ APCs. Again, as for the downregulated genes, the microarray data did highlight this, but the difference was not significant for the $Wt1^+$ cells and so they were not listed. The four genes that were validated were listed under the GO term "immune system process" (Table 3.12), therefore their upregulated expression in a HFD setting is perhaps not surprising. Moreover, *Ccl9* has previously been shown to be upregulated in HFD-fed and genetically obese mice (Tourniaire *et al.*, 2013) and *F2rl1* null mice are resistant to weight gain when fed a HFD (Badeanlou *et al.*, 2012).

The final experiments in this chapter addressed whether, in mice fed a HFD, the percentage of visceral adipocytes derived from *Wt1* expressing APCs differed from that of mice fed normal chow. We hoped that knowing this would help us to understand why the percentage of *Wt1* expressing APCs decreased in HFD-fed mice. Using a lineage tracing model revealed that whilst the percentage of GFP^+ (Wt1 lineage traced) APCs decreased in the HFD-fed mice compared to those fed normal chow, there was no clear difference in the percentage of GFP labelled adipocytes between the two. However, as mentioned in section 3.7.2, the error bars on the graphs are large, reflecting a substantial amount of variation between different mice. Some of the mice appeared to have a much higher percentage of GFP^+ adipocytes than others, and this trend was consistent across all the fat pads analysed for each mouse. Considering this, it is possible that this variation is due to the amount of tamoxifen each mouse received. Whilst the mother was given a consistent dose, it was not possible to control how much of her milk each pup drank, and therefore how much tamoxifen they obtained. It is therefore likely that several pups may have received lower doses than is necessary to drive complete CreERT2 activation and thus loxP recombination. This large variation between the animals makes it difficult to draw conclusions from the data, particularly if any difference between the two cohorts is subtle. Nevertheless, thus far it does not appear that the percentage of GFP^+ adipocytes in the visceral adipose tissue from the

HFD mice is higher than that from the control mice. To try and overcome this problem we could administer the tamoxifen to the pregnant mother, whilst the mice are *in utero*, as this seems to deliver a more consistent dose across the litter. Having said this, it is still not a perfect method, and the embryos may not necessarily receive exactly the same amount each. Alternatively, it would be worthwhile increasing the number of mice analysed, to increase the power of the study.

In conclusion, the results described in this chapter have shown that $Wt1^+$ and $Wt1^-$ APCs exhibit different behaviours *in vitro*, with the $Wt1^+$ population having a higher proportion of proliferating cells and being more amenable to adipogenesis. Whilst the difference in proliferative capacities seems to be intrinsic, with the two populations still exhibiting a clear difference when cultured together, preliminary data shows that paracrine signalling may also be involved. Media conditioned by $Wt1^+$ cells partially improves the adipogenic differentiation of the $Wt1^-$ cells, however further work is required to confirm this. Additionally, microarray studies have shown that the two APC populations differ at the transcriptomic level, and these results provide some support for the hypothesis that $Wt1^+$ cells secrete a factor that may alter the behaviour of the $Wt1^-$ cells. Moreover, *in vivo*, for the majority of the visceral WAT depots, the percentage of $Wt1^+$ APCs decreases when mice are fed a HFD. Therefore, it is evident that the heterogeneity that exists within the precursor cell populations influences their behaviour and response to physiologically relevant perturbations.

Chapter 4

Prx1-Cre labelling of adipose tissue

4.1 Introduction

Following on from chapter 3, one of my original aims to further address the role of *Wt1* in adipose tissue biology, was to conditionally delete the gene *in vivo*. As described in chapter 1, *Wt1* null mice die at mid-gestation due to defects in the development of the coronary vasculature (Kreidberg *et al.*, 1993; Moore *et al.*, 1999; Martínez-Estrada *et al.*, 2010). Henceforth, the first challenge was to identify a suitable Cre recombinase mouse line to perform targeted *Wt1* deletion in developing adipose tissue, without harming vital organs. The *Prx1-Cre* line was identified as a possible candidate for reasons described in the introduction (1.3) (Logan *et al.*, 2002). Paired-related homeobox gene-1 (*Prx1*) is expressed in lateral plate mesoderm derivatives and neural crest derived mesenchyme (Cserjesi *et al.*, 1992; Higuchi *et al.*, 2013). Furthermore, it has been shown that Prx1-Cre expressing uncommitted mesenchymal cells contribute to WAT in 4-6 week old mice (Calo *et al.*, 2010). More detail on the expression patterns of *Prx1* and generation of the *Prx1-Cre* line can be found in the introduction (1.3). The first task was to fully assess the suitability of this Cre driver for the targeted deletion of *Wt1* in developing visceral WAT. Therefore, lineage tracing was used to understand which adipose depots could be targeted and thus labelled by Prx1-Cre, and more specifically, whether the adipocyte precursor cells (APCs) were labelled. The subcutaneous WAT depot was also included for completeness of analysis. Several interesting results were obtained that have potential implications for the developmental origins of pericardial and subcutaneous WAT.

In summary, this chapter shows that subcutaneous and pericardial adipocytes and APCs are Prx1-Cre lineage positive. Moreover, heterogeneity within the pericardial APC population appears to have functional consequences *in vitro*.

4.2 Prx1-Cre labelling of subcutaneous white adipose tissue

4.2.1 Prx1-Cre labelling of adult mature subcutaneous adipocytes

To investigate whether subcutaneous adipocytes were Prx1-Cre lineage positive, male *Prx1-Cre* mice were crossed with female double-fluorescent *R26R-mTmG* reporter mice. In the resulting *Prx1-Cre;R26R-mTmG* offspring, prior to Cre-mediated loxP recombination, all cells fluoresced red (Tomato). However, upon recombination, the presence of loxP sites led to the excision of Tomato and thus the expression of eGFP. Therefore, any cells that expressed the *Prx1-Cre* transgene fluoresced green, as did their progeny (Logan *et al.*, 2002; Muzumdar *et al.*, 2007). Moreover, the Tomato and eGFP labelling was membranous. This feature is particularly useful when analysing adipose tissue, because the large lipid droplets within the adipocytes make it difficult to visualise cytoplasmic labelling and distinguish individual cells. The inguinal subcutaneous adipose tissue was harvested from 6 week old male and female *Prx1-Cre;R26R-mTmG* mice, and processed for immunohistochemistry. Sections were stained with an anti-eGFP antibody, as well as an anti-perilipin antibody, to label the mature adipocytes. Figure 4.1 shows that 99.5% (male) and 89.1% (female) of the mature adipocytes in the subcutaneous depot expressed eGFP. Therefore, the majority of the subcutaneous adipocytes were Prx1-Cre lineage positive, meaning that they were either derived from Prx1-Cre expressing precursor cells, or they expressed Prx1-Cre themselves.

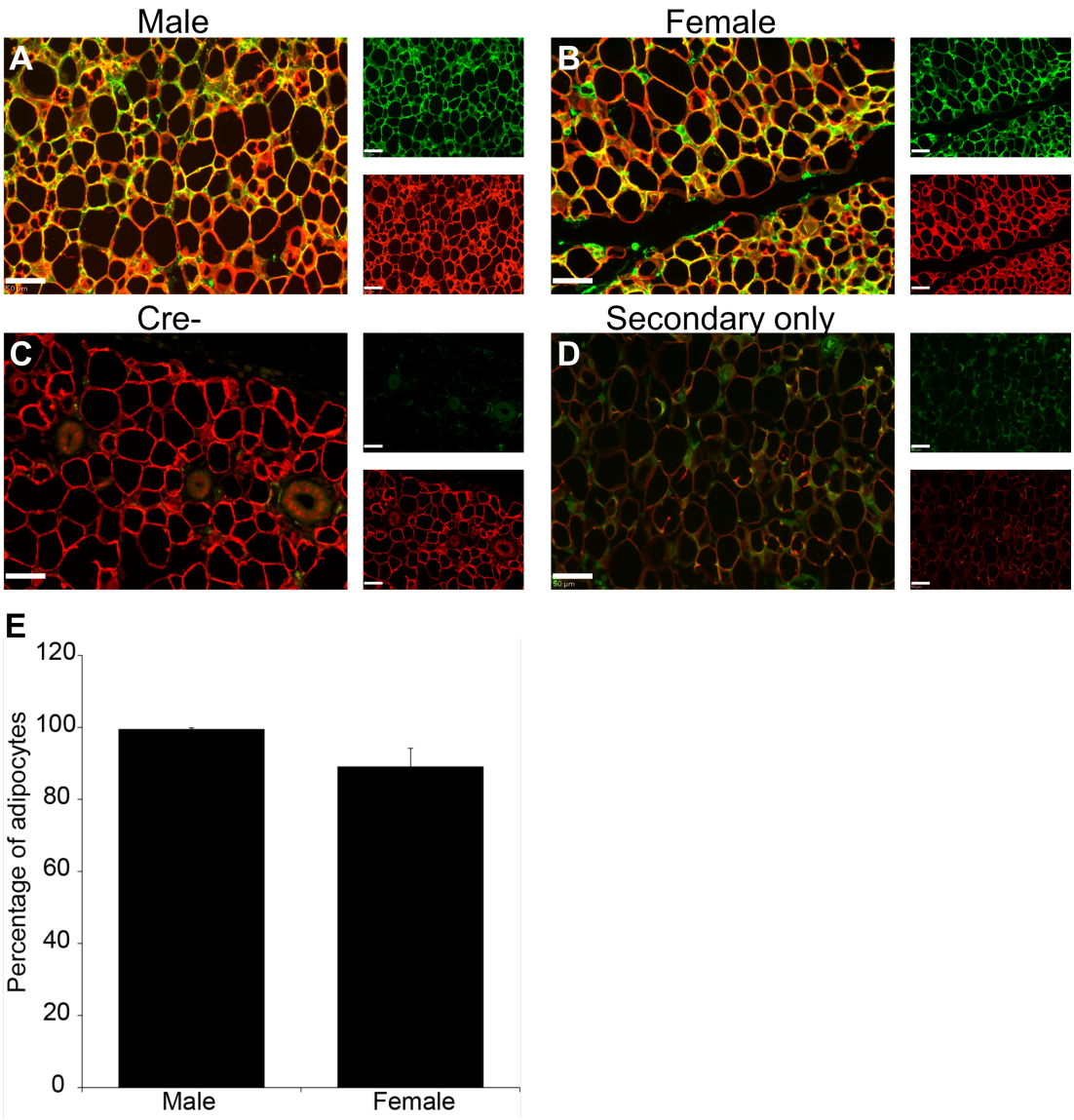
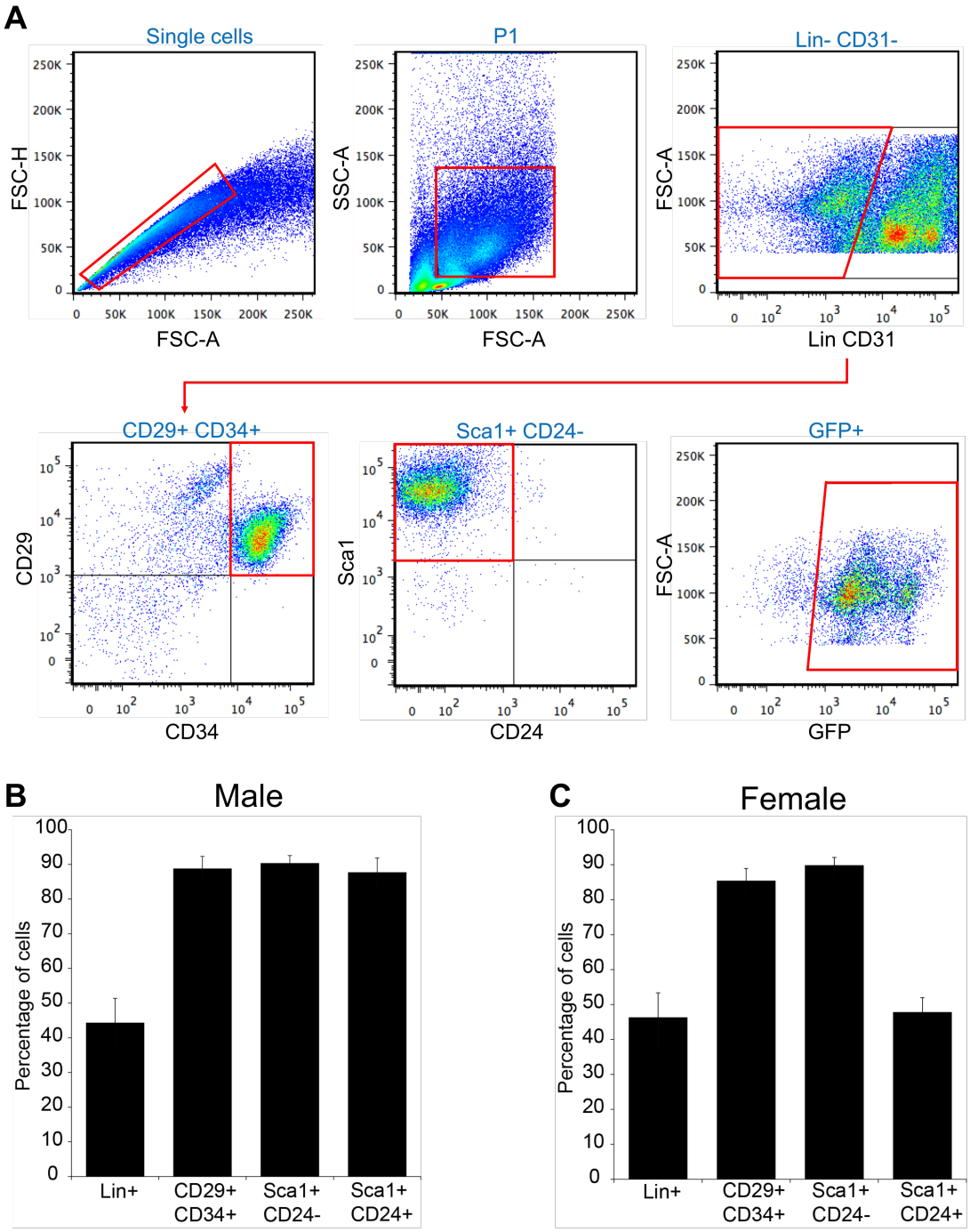


Figure 4.1. Prx1-Cre labels mature adipocytes in the subcutaneous white adipose tissue of 6 week old Prx1-Cre;R26R-mTmG male and female mice. *Subcutaneous adipose tissue was dissected from 6 week old male* ***(A)*** *and female* ***(B)*** *Prx1-Cre;R26R-mTmG mice. Sections were stained with an anti-eGFP antibody (green – upper inset) and an anti-perilipin antibody (red – lower inset). 99.5% (male) and 89.1% (female) of the mature adipocytes expressed eGFP, thus were Prx1-Cre lineage positive* ***(E)****. A section from a Cre negative littermate was included as a control* ***(C)****, and a secondary antibody only control was performed* ***(D)****. (Scale bar = 50μm). (n=4 male, 3 female; a minimum of 100 adipocytes was counted for each sample; data represent mean ± s.e.m).*

4.2.2 Prx1-Cre labelling of cells from the adult subcutaneous SVF

In addition to the mature subcutaneous adipocytes, it was also important to know whether the APCs, present in the SVF of the adipose tissue from *Prx1-Cre;R26R-mTmG* mice, were Prx1-Cre lineage positive. The SVF was isolated from the adipose tissue and stained with the panel of antibodies outlined by Rodeheffer *et al*. (2008), commonly used for labelling adipocyte progenitor cells and pre-adipocytes, as described in the introduction (1.1.2). Multicolour flow cytometry was used to assess whether any eGFP expressing cells were present in the SVF, and if so, which population they belonged to. Representative flow cytometry plots illustrating the gating strategy used are shown in Figure 4.2 (A). Cells from Cre negative littermates were used to establish flow cytometry gates for eGFP, and un-stained cell samples were used to set the gates for the multicolour antibody panel, as outlined in the Appendix 2 and in (Cleal and Chau, 2016). Additionally, for each antibody, a single-stain sample was used to perform compensation (Appendix 3) (Cleal and Chau, 2016). As for the mature adipocytes, the majority of the pre-adipocytes (Lin^-;$CD29^+$;$CD34^+$;$Sca1^+$;$CD24^-$) expressed eGFP and were therefore Prx1-Cre lineage positive (90.3% in male and 89.9% in female) (Figure 4.2 B,C). For the adipocyte progenitor cells (Lin^-;$CD29^+$;$CD34^+$;$Sca1^+$;$CD24^+$), there was a discrepancy between male and female, with 87.7% of the cells expressing eGFP in the males, and 47.8% in the females (Figure 4.2 B,C). Additionally, the composition of the eGFP expressing population was analysed, showing that 40.4% (male) and 36.9% (female) of the eGFP expressing cells were $CD24^-$ pre-adipocytes whilst <5% were $CD24^+$ adipocyte progenitor cells (Figure 4.2 D). As these experiments were being performed, work from another laboratory showed, as we have done here, that both the mature adipocytes and APCs of subcutaneous adipose tissue were Prx1-Cre lineage positive, thus supporting our findings (Sanchez-Gurmaches, Hsiao and Guertin, 2015). In addition to the 6 week old mice, another cohort of male *Prx1-Cre;R26R-mTmG* mice was aged to 1 year. The SVF of the subcutaneous adipose tissue was then isolated from these mice, stained with the same panel of antibodies and analysed using flow cytometry. Figure 4.2 (E) shows that, comparable with the 6 week olds, 91.5% of the $CD24^-$ pre-adipocytes expressed eGFP and thus were Prx1-Cre lineage positive.

Figure 4.2. (continued on next page)



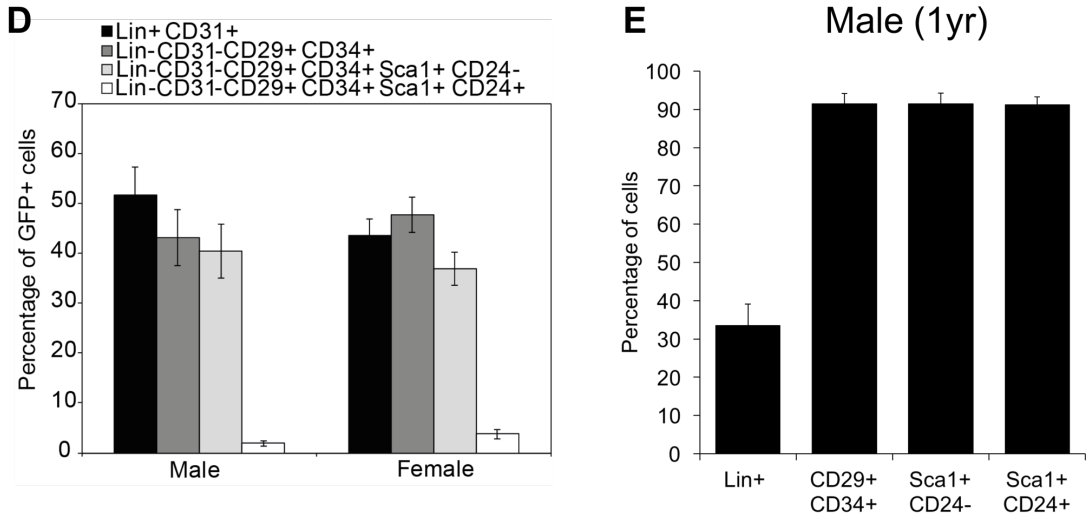


Figure 4.2. Prx1-Cre labels adipocyte precursor cells in the subcutaneous white adipose tissue of 6 week old Prx1-Cre;R26R-mTmG male and female mice. *SVF cells were isolated from the subcutaneous adipose tissue of male and female Prx1-Cre;R26R-mTmG mice and stained with a panel of antibodies (Lin, CD31, CD29, CD34, Sca1, CD24) before being analysed using flow cytometry. Representative flow cytometry plots, outlining the gating prolife used can be seen in* ***(A)****. After gating to remove debris and select for single cells, further gates were applied to identify the eGFP+ Lin-CD31-CD29+CD34+Sca1+CD24- pre-adipocyte cells. Compensation and eGFP- controls were also performed, as well as different gating profiles to investigate different cell populations (not shown). The y axis in* ***(B,C,E)*** *represents the percentage of cells in each population shown on the x axis that were labelled with eGFP. 90.3% (male)* ***(B)*** *and 89.9% (female)* ***(C)*** *of the CD24- pre-adipocytes were labelled with eGFP. 87.7% (male)* ***(B)*** *and 47.8% (female)* ***(C)*** *of the CD24+ adipocyte precursor cells were GFP positive. Additionally, 44.3% (male)* ***(B)*** *and 47.3% (female)* ***(C)*** *of the Lin+ (haematopoietic and endothelial) cells were labelled with eGFP.* ***(D)*** *shows the composition of the eGFP+ cell population; 40.4% (male) and 36.9% (female) of the GFP+ cells were CD24- pre-adipocytes, <5% were CD24+ adipocyte progenitor cells and 51.7% (male) and 43.3% (female) were Lin+CD31+. 91.5% of the CD24- pre-adipocytes and 91.3% of the CD24+ progenitor cells from 1 year old male Prx1-Cre;R26R-mTmG mice were eGFP+* ***(E)****. (Lin+ represents Lin+;CD31+. CD29+;CD34+ represents Lin-;CD31-;CD29+;CD34+. Sca1+;CD24- represents Lin-;CD31-;CD29+;CD34+;Sca1+;CD24-. Sca1+;CD24+ represents Lin-;CD31-;CD29+;CD34+;Sca1+;CD24+). (n=4 per sex minimum; data represent mean ± s.e.m).*

Interestingly, in addition to many of the cells in the $Lin^-;CD31^-$ populations expressing eGFP, 44.3% (male) and 46.3% (female) of the $Lin^+;CD31^+$ population also expressed eGFP (Figure 4.2 B,C). Moreover, 51.7% (male) and 43.4% (female) of the eGFP expressing cells were $Lin^+;CD31^+$ (Figure 4.2 D). The lineage panel that was used to separate the haematopoietic Lin^+ and non-haematopoietic Lin^- cells, consisted of five antibodies against different cell surface markers. Therefore, this panel was broken down to understand which of the six antibodies (including CD31) labelled the eGFP

expressing cells. Six samples of subcutaneous SVF cells were stained with just one antibody from the panel each. Thus, the cells were stained with antibodies against either CD3e, CD11b, CD45R, Ly-6G and Ly-6C, TER-119 or CD31 and then analysed using flow cytometry, as outlined in Appendix 8. 13.7% of the eGFP expressing cells from the SVF were $CD11b^+$ and 33.2% were $CD31^+$. For the rest of the populations, these percentages were <5 (Figure 4.3 A). Therefore, CD11b and CD31 expressing cells accounted for the majority of the eGFP expressing cells within the Lin^+CD31^+ population.

CD11b is commonly used to label macrophages, therefore, this result indicated that at least a proportion of the macrophages present in the subcutaneous adipose SVF were Prx1-Cre lineage positive. To further verify this result, additional subcutaneous SVF cells were stained with an antibody against F4/80; another commonly used macrophage marker. Figure 4.3 (B) is a representative flow cytometry plot from this study, showing that 15.2% of the eGFP expressing cells were $F4/80^+$. This percentage is comparable to that of the cells labelled with CD11b (13.7%), therefore providing additional support for the hypothesis that a proportion of the Prx1-Cre lineage positive cells in the subcutaneous adipose SVF were macrophages. Moreover, we wanted to know what percentage of these CD11b/F4/80 labelled cells expressed eGFP. Figure 4.3 (C) shows that 49.7% of the CD11b and 87.8% of the F4/80 labelled cells expressed eGFP, thus indicating that these cells were Prx1-Cre lineage positive. The discrepancy between the percentage of CD11b and F4/80 labelled cells that expressed eGFP, is likely due to differences in the cell types that express the two markers. Both label macrophages, however, F4/80 is specifically a macrophage marker, whilst CD11b antibodies can also recognise granulocytes, natural killer cells, dendritic cells, and others (Lee, Starkey and Gordon, 1985; Solovjov, Pluskota and Plow, 2005). Thus, the lower percentage of eGFP expressing cells in the CD11b+ population compared to the F4/80+ population may be due to the broader range of cell types that express CD11b.

CD31 is an endothelial cell marker, therefore, the results described above suggested that there were Prx1-Cre lineage positive endothelial cells present in the subcutaneous

adipose tissue. 33.2% of the eGFP expressing cells were $CD31^+$ (Figure 4.3 A). Furthermore, 84.1% of the $CD31^+$ cells were eGFP positive (Figure 4.3 C). This suggested that the majority of the $CD31^+$ (endothelial) cells in the subcutaneous adipose tissue were Prx1-Cre lineage positive. This was investigated further, using an antibody against CD31 to stain a section of subcutaneous adipose tissue from a *Prx1-Cre;R26R-mTmG* mouse. The section was co-stained with an anti-GFP antibody, and Figure 4.3 (D) shows an overlap between the CD31 and eGFP staining, thus supporting the flow cytometry data. Interestingly, *Prx1* is expressed in differentiating endothelial cells within foetal lung mesenchyme and is thought to promote their differentiation and the formation of pulmonary vascular networks (Ihida-Stansbury *et al.*, 2004). Therefore, this is not the first time that *Prx1* has been associated with the endothelial cell lineage.

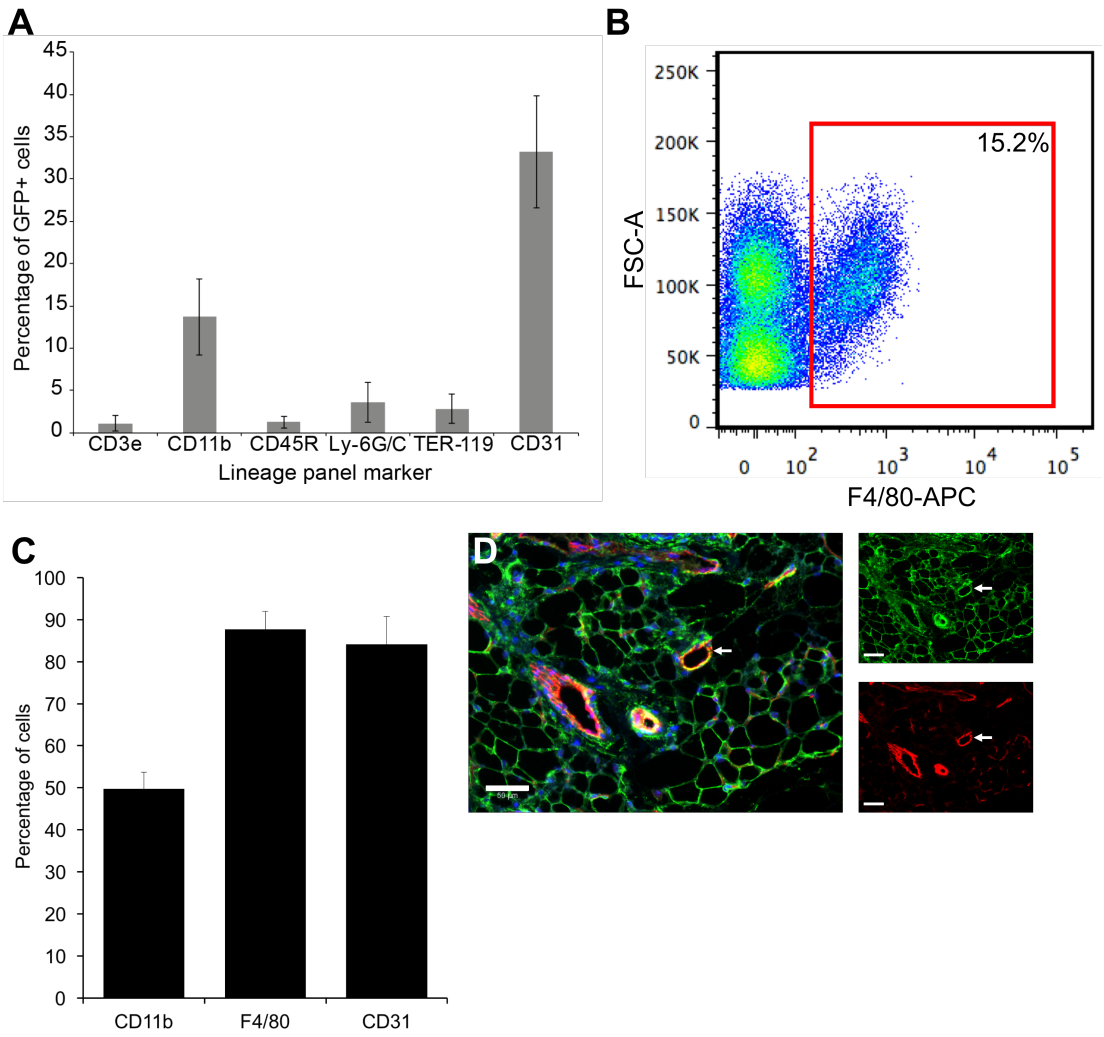


Figure 4.3. GFP positive Lin+CD31+ cells from the subcutaneous SVF of Prx1-Cre;R26R-mTmG mice are predominantly macrophages and endothelial cells*. The lineage panel used to mark haematopoietic cells is comprised of five antibodies,* ***(A)*** *shows how each of these, and CD31, contributed to the eGFP+ cell population from the subcutaneous adipose tissue of Prx1-Cre;R26R-mTmG mice. 13.7% of the eGFP+ cells were CD11b+ and 33.2% were CD31+, with the other markers contributing less than 5%. CD11b is commonly used to label macrophages. The cells were also stained with an antibody against F4/80, another macrophage marker, 15.2% of the eGFP positive cells were labelled with F4/80* ***(B)****. The y axis in* ***(C)*** *represents the percentage of cells in each population shown on the x axis that were labelled with eGFP. 49.7% of the CD11b labelled cells, 87.8% of the F4/80 labelled cells and 84.1% of the CD31 labelled cells were eGFP positive* ***(C)****. CD31 labels endothelial cells,* ***(D)*** *shows a section of subcutaneous adipose tissue from a Prx1-Cre;R26R-mTmG mouse stained with an anti-eGFP antibody (green – upper inset) an anti-CD31 antibody (red – lower inset) and DAPI (blue). Arrows mark vessels where CD31+ eGFP+ cells are present. (Scale bar = 50μm). (n=3 male; data represent mean ± s.e.m).*

4.2.3 Prx1-Cre labelling of embryonic subcutaneous adipose tissue (E18.5)

Subcutaneous adipocytes begin to develop lipid droplets and become visible towards the end of murine gestation. In order to understand whether the subcutaneous adipose tissue is labelled before birth, or whether the labelling we previously observed occurs only in the adult, *Prx1-Cre;R26R-mTmG* E18.5 embryos were harvested and prepared for immunohistochemistry, then stained with an anti-perilipin antibody to highlight the adipose tissue and an anti-eGFP antibody. Figure 4.4 clearly shows that the subcutaneous adipose tissue of the embryos expressed eGFP. Therefore, subcutaneous adipose tissue is Prx1-Cre lineage positive prenatally.

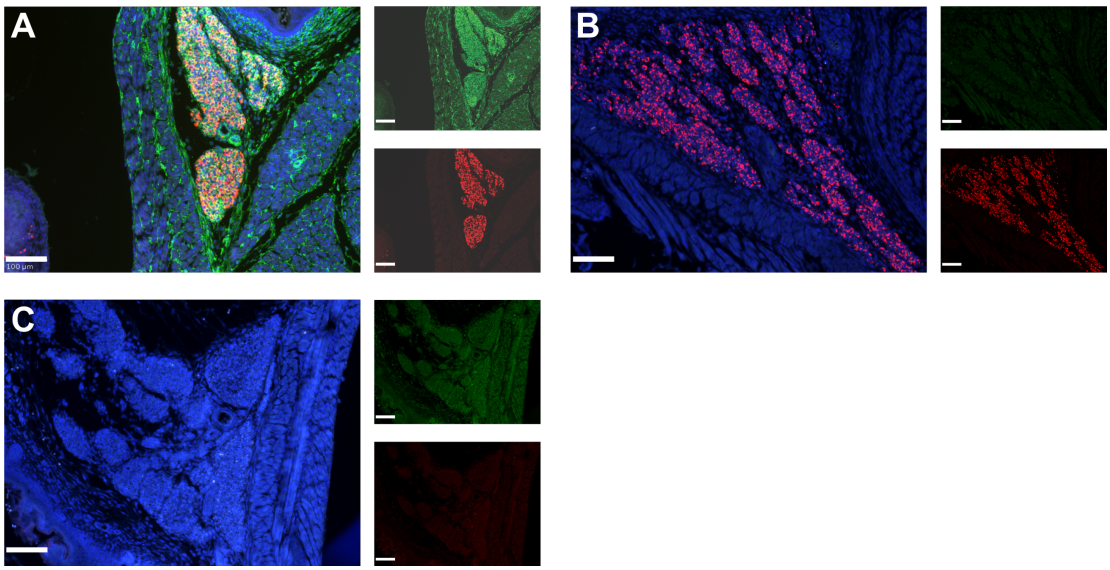


Figure 4.4. Prx1-Cre labels subcutaneous adipose tissue of E18.5 Prx1-Cre;R26R-mTmG mouse embryos. *E18.5 Prx1-Cre;R26R-mTmG embryos were harvested and prepared for immunohistochemistry. Sections were stained with an anti-eGFP antibody (green – upper inset), an anti-perilipin antibody (red – lower inset) and DAPI (blue). The majority of the subcutaneous adipose tissue, as highlighted by the red perilipin staining, was labelled with eGFP* ***(A)****. A section from a Cre negative littermate was included as a control, perilipin staining is still visible, but there is no eGFP* ***(B)****. A secondary antibody only control was also included* ***(C)****. (Scale bar = 100μm) (n=3).*

4.3 Prx1-Cre labelling of visceral white adipose tissue

4.3.1 Prx1-Cre labelling of adult mature visceral adipocytes

Given that the original aim was to use the *Prx1-Cre* mouse model to delete *Wt1* in visceral APCs, the visceral adipose tissue of male and female 6 week old *Prx1-Cre;R26R-mTmG* mice was also analysed. In contrast to the subcutaneous depot, very low percentages of mature adipocytes in the perigonadal, omental and mesenteric depots were labelled with eGFP, meaning that most of the adipocytes were Prx1-Cre lineage negative (Figure 4.5 A-F). Just 0.8% of the perigonadal adipocytes in males expressed eGFP, although this percentage was higher at 8.8% for the females (Figure 4.5 A,B,J). In the mesenteric depot, 4.7% (male) and 4.1% (female) of the adipocytes expressed eGFP (Figure 4.5 B,C,J). In males, 10.5% of the omental adipocytes expressed eGFP and in females this was 9.0% (Figure 4.5 E,F,J). Similar results regarding the perigonadal and mesenteric depots were recently reported by Sanchez-Gurmaches *et al*. (2015). However, labelling of the pericardial visceral depot by Prx1-Cre has not previously been described. Intriguingly we found that much higher percentages of eGFP expressing adipocytes were present in the pericardial adipose tissue compared to the other visceral depots, (57.9% in male, 75.9% in female) (Figure 4.5 G,H,J). Therefore, it appears that in addition to the subcutaneous adipocytes, Prx1-Cre also labels a significant proportion of the visceral pericardial adipocytes.

Figure 4.5. (continued on next page)

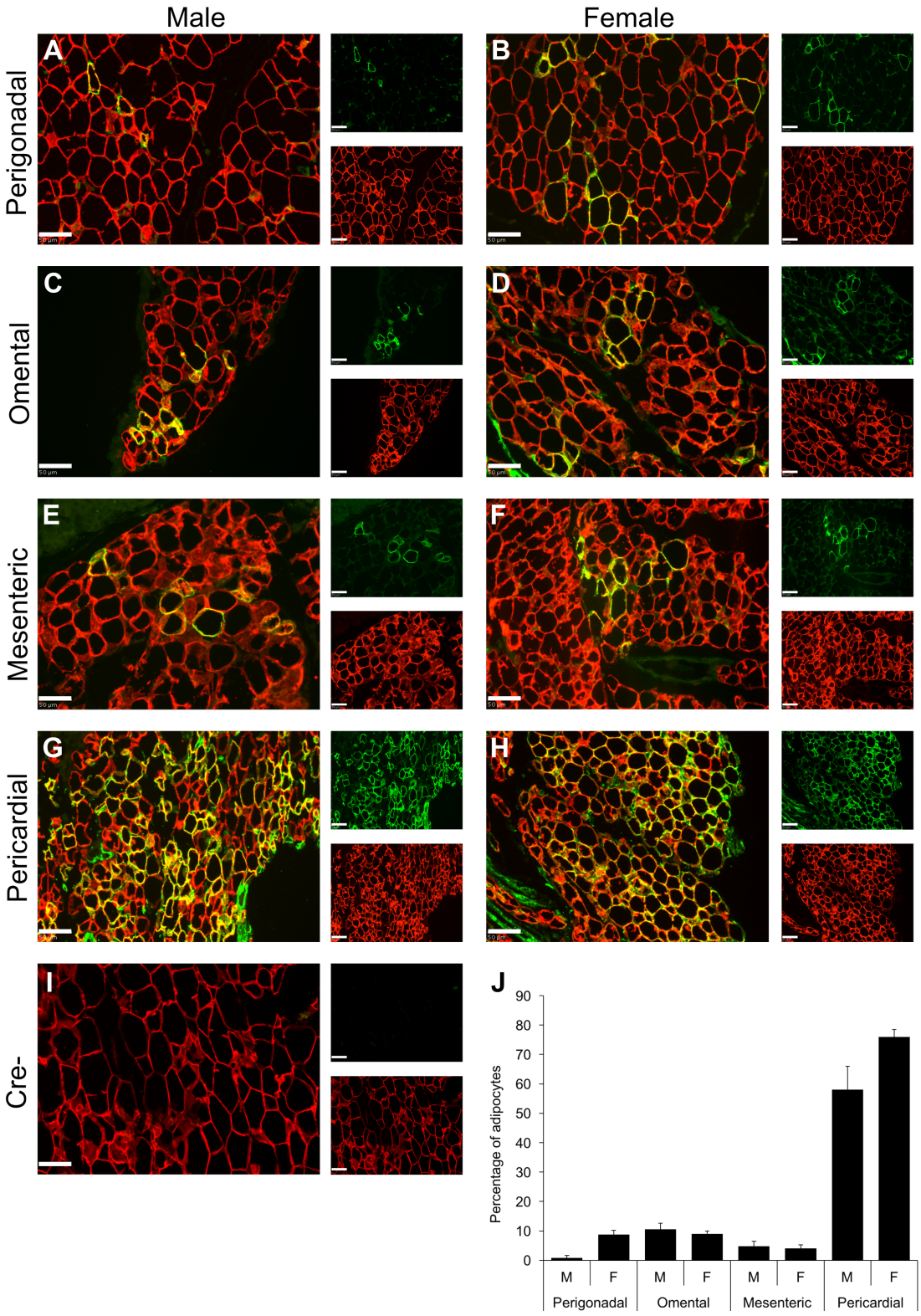


Figure 4.5. Prx1-Cre labels mature adipocytes in pericardial white adipose tissue of 6 week old Prx1-Cre;R26R-mTmG male and female mice, but labels very few adipocytes in other visceral adipose depots. *Perigonadal **(A,B)**, mesenteric **(C,D)**, omental **(E,F)** and pericardial **(G,H)** adipose tissue was dissected from 6 week old male **(A,C,E,G)** and female **(B,D,F,H)** Prx1-Cre;R26R-mTmG mice. Sections were stained with an anti-eGFP antibody (green – upper inset) and an anti-perilipin antibody (red – lower inset). 57.9% (male) and 75.9% (female) of the pericardial adipocytes expressed eGFP, whilst in the other visceral depots, a maximum of 10.5% of the adipocytes were eGFP positive **(J)**. A section of perigonadal fat from a Cre negative littermate was included as a control **(I)**. (Scale bar = 50μm). (n=3 per sex minimum; a minimum of 100 adipocytes was counted for each sample; data represent mean ± s.e.m).*

4.3.2 Prx1-Cre labelling of cells from the adult visceral SVF

As with the subcutaneous depot, it was important to know whether any cells in the SVF of the visceral depots expressed eGFP, and if so, which population they belonged to. The SVF from the various visceral depots was stained with the panel of antibodies described previously, to study the adipocyte progenitor cells and pre-adipocytes. As illustrated in Figure 4.6, the results of this flow cytometry analysis followed the same trend that was observed for the mature adipocytes. Within the perigonadal adipocyte progenitor population ($Lin^-;CD29^+;CD34^+;Sca1^+;CD24^+$), 1.2% (male) and 5.4% (female) of the cells expressed eGFP. Similarly, in the pre-adipocyte population ($Lin^-;CD29^+;CD34^+;Sca1^+;CD24^-$), 0.7% (male) and 5.6% (female) expressed eGFP. In the mesenteric depot, 1.1% (male) and 0.8% (female) of the two cell populations were labelled with eGFP. For the omental depot, 8.7% (male) and 14.8% (female) of the adipocyte progenitor cells, and 9.5% (male) and 10.9% (female) of the pre-adipocytes were labelled with eGFP.

On par with the results obtained for the mature adipocytes, 35.1% (male) and 40.8% (female) of the pericardial pre-adipocytes expressed eGFP. However, only 5.9% (male) and 7.2% (female) of the pericardial adipocyte progenitor cells were labelled with eGFP (Figure 4.6 A,B). This last result may be explained by the findings of Rodeheffer *et al*. (2008), where they show that $CD24^+$ cells make up only 0.08% of the total SVF, whilst ~53% of the SVF is $CD24^-$. Therefore, the actual number of cells in the $CD24^+$ population is very low, meaning that the percentage of eGFP expressing cells within this population can be substantially raised or lowered by the presence/absence of just a few cells. This explanation is better illustrated in Figure 4.2 (A), where the whole flow cytometry gating protocol can be observed. Additionally,

in Figure 4.6 (C,D), the composition of the eGFP expressing populations is illustrated, showing that in the pericardial SVF, only 1.6% of the eGFP expressing SVF cells were $Lin^{-};CD29^{+};CD34^{+};Sca1^{+};CD24^{+}$, again a reflection of how few $CD24^{+}$ cells are present in the SVF. As described for the subcutaneous depot (4.2.2), male *Prx1-Cre;R26R-mTmG* mice were aged to 1 year. The SVF of the pericardial depot was analysed and showed that 37.4% of the $CD24^{-}$ pre-adipocytes expressed eGFP (Figure 4.6 E). Therefore, the 6 week old and 1 year old mice had comparable percentages of Prx1-Cre lineage positive pre-adipocytes.

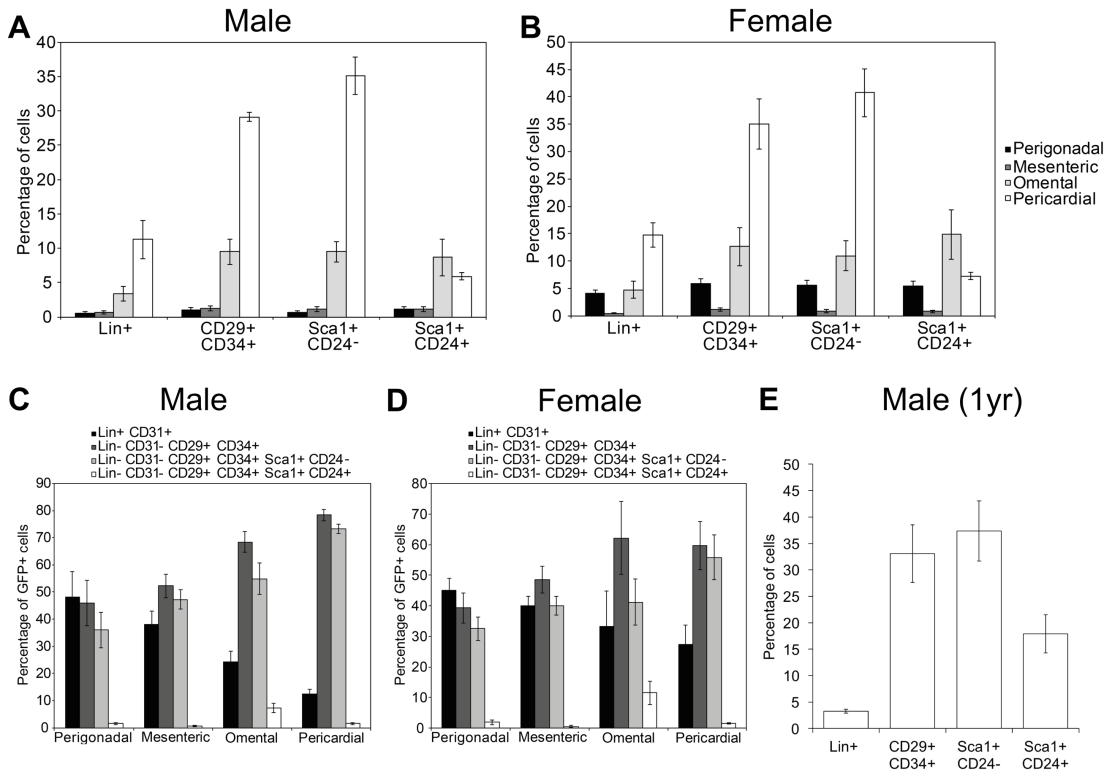


Figure 4.6. Prx1-Cre labels adipocyte precursor cells in the pericardial white adipose tissue of 6-week old Prx1-Cre;R26R-mTmG male and female mice. *SVF cells were isolated from the perigonadal, mesenteric, omental and pericardial visceral white adipose tissue of male and female Prx1-Cre;R26R-mTmG mice and stained with a panel of antibodies (Lin, CD31, CD29, CD34, Sca1, CD24) before being analysed using flow cytometry (as in Figure 4.2). The y axis in* ***(A,B)*** *represents the percentage of cells in each population shown on the x axis that were labelled with eGFP. 35.1% (male) and 40.8% (female) of the pericardial CD24- pre-adipocytes were labelled with eGFP. A maximum of 10.9% of the omental CD24- pre-adipocytes were labelled with eGFP and <5% of the mesenteric and perigonadal CD24- pre-adipocytes were eGFP positive* ***(A,B)****. For all depots, <15% of the CD24+ adipocyte precursor cells were eGFP positive* ***(A,B)****.* ***(C&D)*** *show the composition of the eGFP+ cell populations; i.e. 75% (male) and 60% (female) of the pericardial eGFP+ cells were CD24- pre-adipocytes. 37.4% of the pericardial CD24- pre-adipocytes and 17.9% of the CD24+ progenitor cells from 1 year old male Prx1-Cre;R26R-mTmG mice were eGFP+* ***(E)****. (n=3 per sex minimum, data represent mean ± s.e.m).*

4.4 Lineage tracing using *Prx1-Cre^{ERT2};R26R-mTmG* mice

4.4.1 Induction embryonically and analysis at E18.5

The work described thus far revealed which fat depots can be labelled using the constitutively active *Prx1-Cre* mouse model. However, the caveat of this model is that it is not possible to know when Cre is first expressed, and therefore when the recombination event occurs, meaning that it doesn't inform about origin. For example, it cannot be determined whether Cre is expressed during early development, and is then switched off, meaning that all eGFP expressing cells observed in the adult mice originate from a population of Cre expressing cells present in early embryogenesis. Or alternatively, whether Cre is expressed at various stages of development and/or in the cells of the adult mouse. Whilst knowing the expression pattern of the *Prx1* gene is informative, the expression of the *Prx1-Cre* transgene may not faithfully recapitulate that of the endogenous gene. This has in fact been shown to be the case; Sanchez-Gurmaches *et al*. (2015) described the mRNA expression of *Prx1* in the subcutaneous depot, but were unable to detect *Cre* mRNA in any of the depots (Sanchez-Gurmaches, Hsiao and Guertin, 2015). One option to help overcome this caveat is to use a tamoxifen inducible form of the Cre: *Prx1-Cre^{ERT2}* (Hasson, Del Buono and Logan, 2007). In these transgenic mice, Cre has been fused to a mutated form of the ligand-binding domain of the oestrogen receptor (ERT2), allowing temporal control of activation. Therefore, Cre mediated loxP recombination does not occur until tamoxifen (a ligand for the oestrogen receptor), is administered.

Male *Prx1-Cre^{ERT2}* mice were crossed with female *R26R-mTmG* mice, and the pregnant females were given tamoxifen at various stages of gestation. As *Prx1* is first expressed at around E9-E9.5, the tamoxifen was administered when the embryos were at this stage. Alternatively, tamoxifen was given E11.5, to allow the comparison of embryos dosed at different developmental stages. As subcutaneous adipose tissue begins to form prenatally, the embryos were initially analysed at E18.5, to understand whether any of the subcutaneous fat in these tamoxifen dosed *Prx1-Cre^{ERT2};R26R-mTmG* embryos expressed eGFP. Figure 4.7 illustrates that the embryos given tamoxifen at either E9.5 or E11.5 both exhibited labelling of the subcutaneous adipose

tissue, however more eGFP expressing adipocytes were observed in those dosed at E9.5. This finding indicates that cells present during early embryonic development contribute to the subcutaneous adipose tissue of E18.5 embryos.

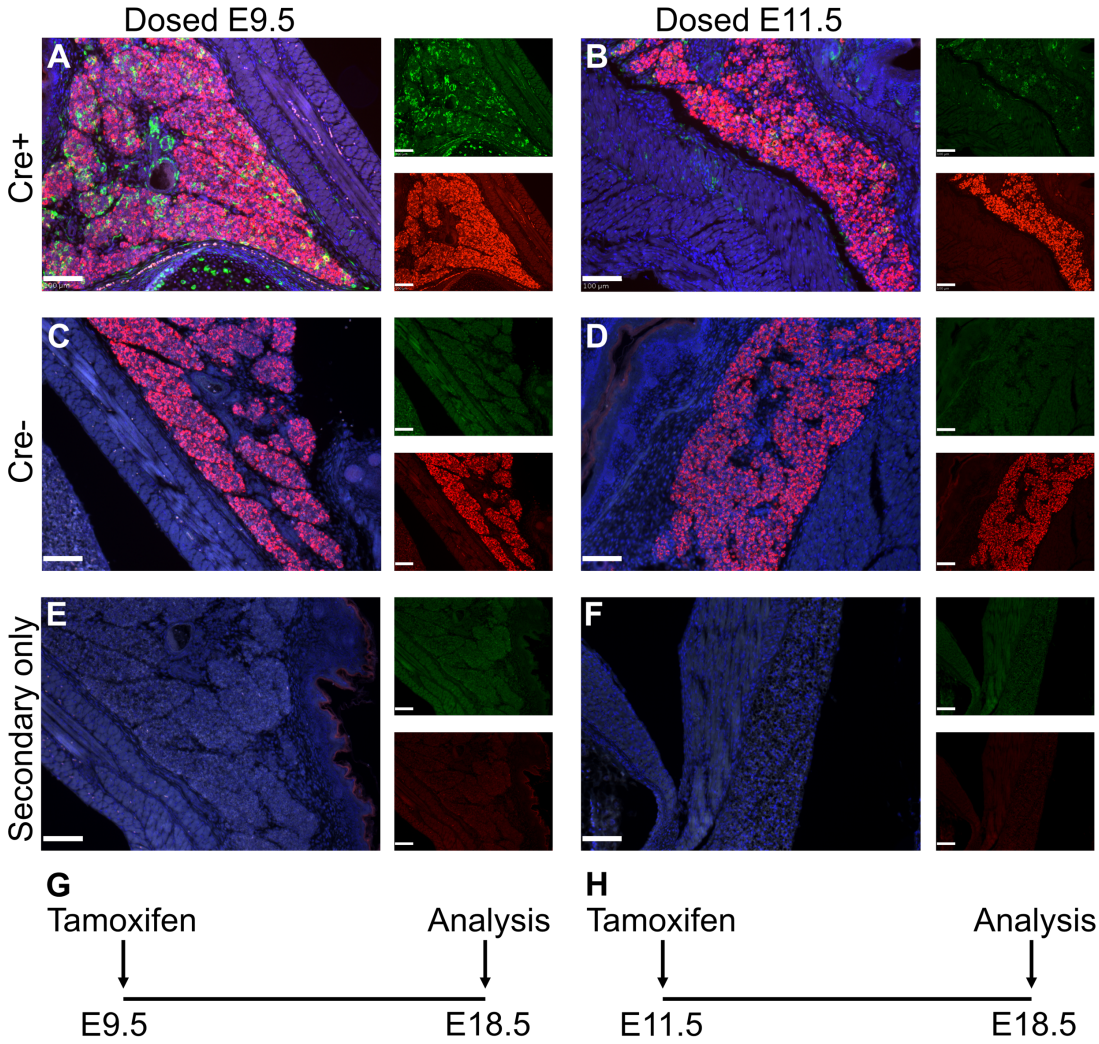


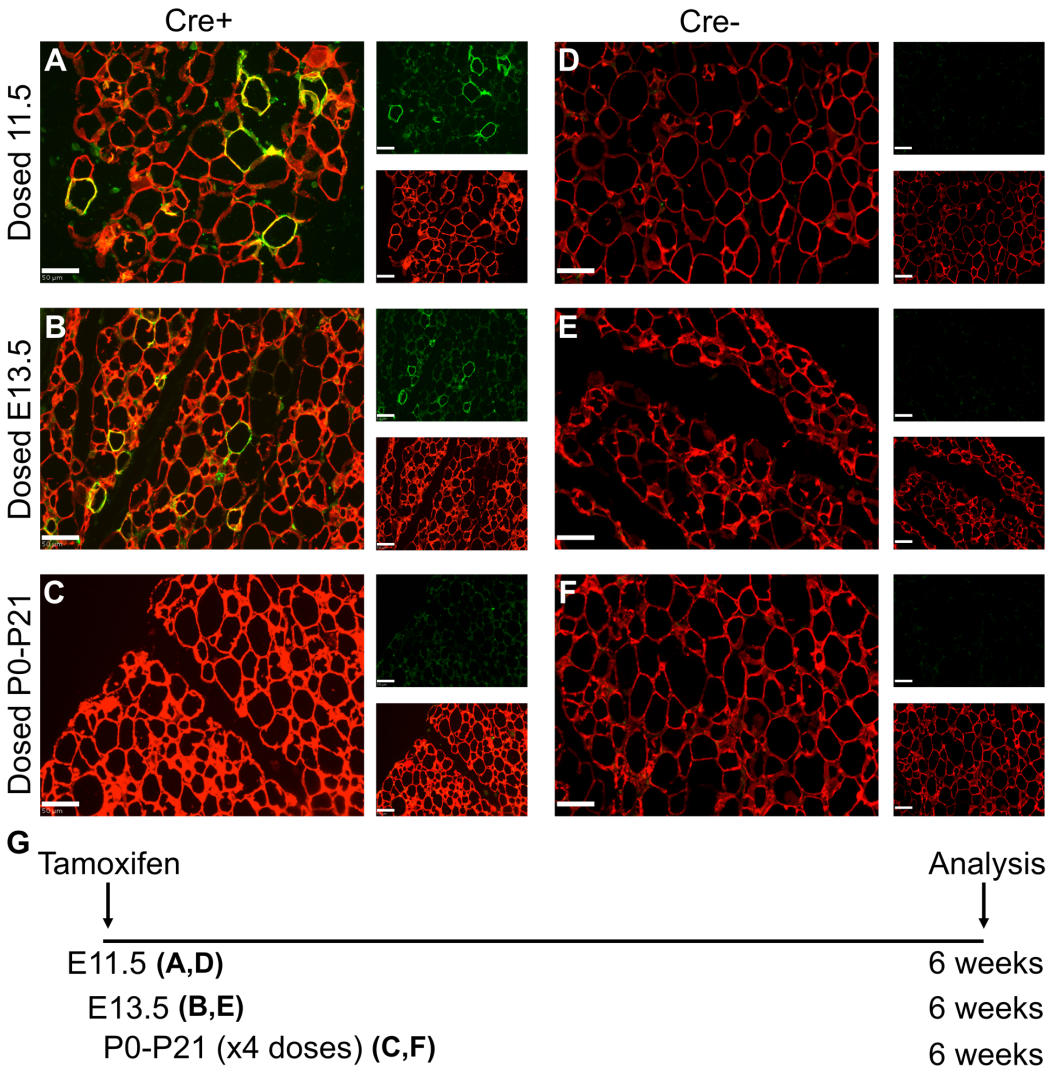
Figure 4.7. Subcutaneous adipose tissue of E18.5 Prx1-Cre^{ERT2};R26R-mTmG mouse embryos induced in vivo at E9.5 has more eGFP labelled cells than that from those induced at E11.5*. E18.5 Prx1-Cre^{ERT2};R26R-mTmG embryos were harvested and prepared for immunohistochemistry. They had been administered with tamoxifen in utero at either E9.5* ***(A,C,E)*** *or E11.5* ***(B,D,F)****. Sections were stained with an anti-eGFP antibody (green – upper inset), an anti-perilipin antibody (red – lower inset) and DAPI (blue). Cre positive embryos, dosed at E9.5* ***(A)*** *had more eGFP staining in the subcutaneous adipose tissue than those dosed at E11.5* ***(B)****. Sections from Cre negative littermates were included as controls* ***(C,D)*** *as well as secondary antibody only controls* ***(E,F)****.* ***G*** *&* ***H*** *illustrate the tamoxifen dosing regimes. (Scale bar = 100μm) (n=3 per dose).*

4.4.2 Induction embryonically/postnatally and analysis at 6 weeks

The next step was to investigate whether any eGFP expressing cells could be observed in 6 week old *Prx1-Cre^{ERT2};R26R-mTmG* tamoxifen dosed mice. Unfortunately, due to issues with breeding, it was not possible to obtain any mice that had been tamoxifen dosed at E9.5. However, 6 week old mice that had been dosed at either E11.5, E13.5, or postnatally were generated. For the E11.5 and E13.5 time-points only one tamoxifen dose was administered to the mother. However, for the postnatal dosing, the mother was dosed 4 times over 2 weeks, and the pups received the tamoxifen through the milk. The dosing regimes are outlined in Figure 4.8 (G). At 6 weeks, the adipose tissue (visceral and subcutaneous) was prepared for immunohistochemistry and flow cytometry, to examine the mature adipocytes and SVF, respectively. In contrast to the constitutively active *Prx1-Cre;R26R-mTmG* mice, very few eGFP expressing adipocytes were observed in the subcutaneous adipose tissue of the mice dosed at E11.5 (7.5%), E13.5 (3.4%) or postnatally (1.2%). (Figure 4.8 A-H). Moreover, analysis of the flow cytometry data from the subcutaneous SVF revealed that only 1.4% of the total SVF cells from the mice dosed at E11.5 expressed eGFP, and this value decreased in those dosed at E13.5 (0.3%) and postnatally (0.16%) (Figure 4.8 I). In this instance, the SVF cells were not analysed using the antibody panel to label adipocyte progenitor cells and pre-adipocytes, as there were so few eGFP expressing cells present in the total SVF. Therefore, this suggests that a very limited number of cells present in the subcutaneous adipose tissue of 6 week old mice are derived from cells present in the embryo at either E11.5, E13.5 or postnatally. To verify that the embryos were receiving the tamoxifen, embryos dosed at E11.5 were harvested at E14.5 and the developing limb buds were checked for the presence of eGFP expressing cells. As described in the introduction (1.3), *Prx1* functions in the skeletal development of the limb and is highly expressed in the developing limb bud from E9.5 (Cserjesi *et al.*, 1992). Moreover, both the *Prx1-Cre* and *Prx1-Cre^{ERT2}* lines can be used to label the limb bud (Logan *et al.*, 2002; Hasson, Del Buono and Logan, 2007). Appendix 9 shows that many eGFP expressing cells were observed in the limb bud, meaning that recombination must have occurred and thus the embryos must have received the tamoxifen.

It is apparent that the earlier the mice were given tamoxifen, the more adipocytes and SVF cells of the 6 week olds were labelled with eGFP. There were significantly more eGFP expressing SVF cells in the mice that were dosed at E11.5, than in those dosed at either E13.5 or postnatally (P0-P21) (Figure 4.8 I). This supports the hypothesis that cells present during early embryogenesis give rise to cells of the adult adipose tissue. In addition to tamoxifen dosing at the developmental stages described, juvenile mice were also dosed. The mice were given four doses of tamoxifen at around 4 weeks of age (2 doses per week for 2 weeks), and analysed using immunohistochemistry and flow cytometry at approximately 7 weeks of age, as illustrated in Figure 4.8 (L). No eGFP expressing adipocytes or SVF cells were observed in the subcutaneous depot from these mice (Figure 4.8 J,K). This indicates that the *Prx1-Cre*^{ERT2} transgene was not expressed in either the SVF cells or adipocytes of the juvenile mice.

Figure 4.8. (continued on next page)



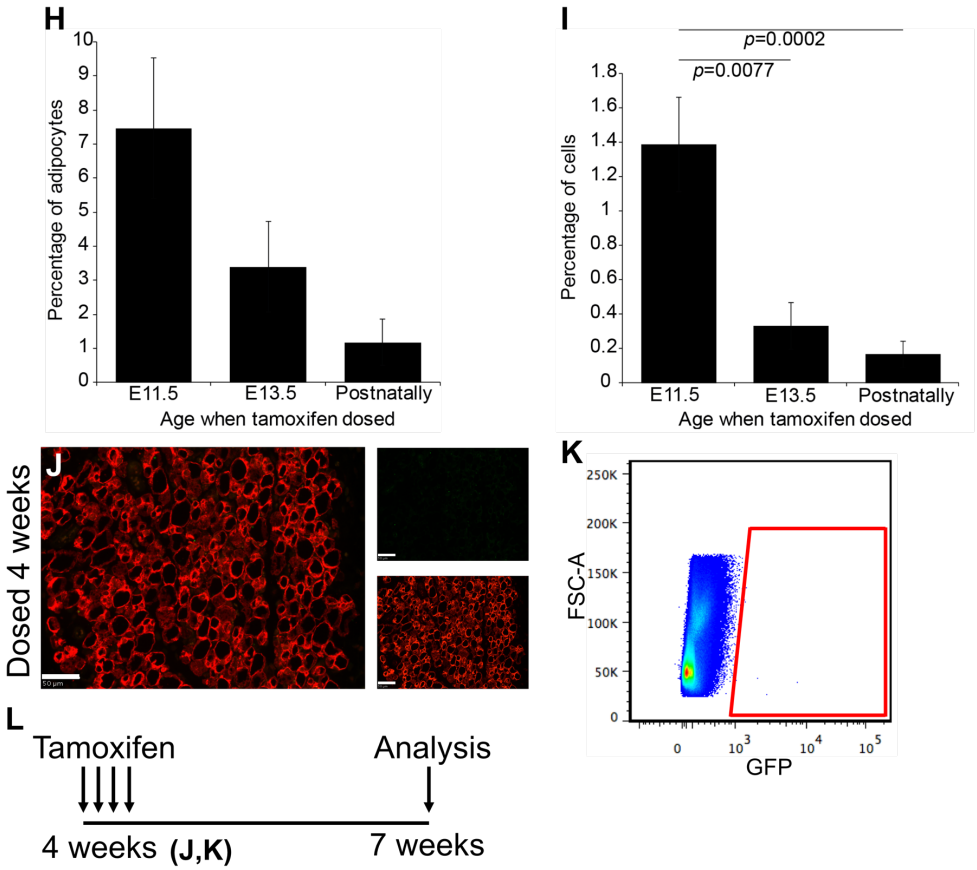
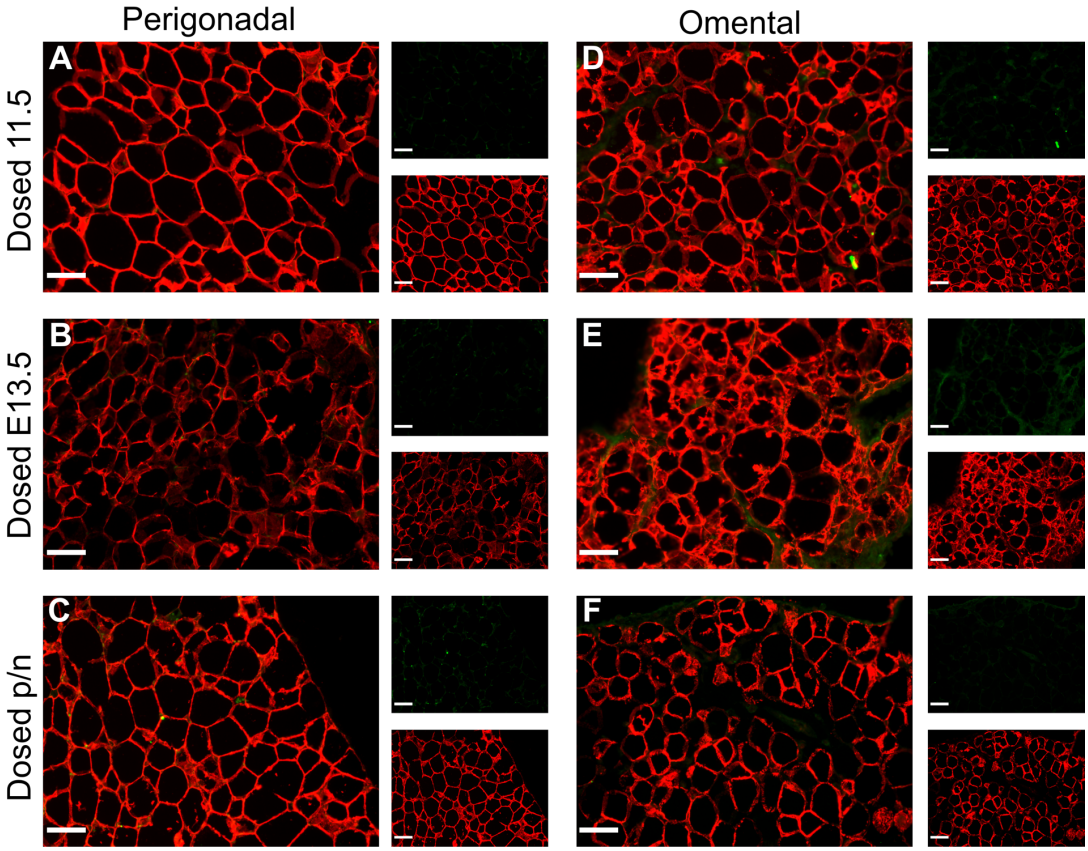


Figure 4.8. Subcutaneous adipose tissue from 6 week old Prx1-Cre^{ERT2};R26R-mTmG mice tamoxifen dosed at either E11.5, E13.5 or postnatally (P0-P21) has low numbers of eGFP labelled cells. Juvenile mice dosed at 4 weeks have no eGFP positive adipocytes. *Subcutaneous adipose tissue from 6 week old Prx1-Cre^{ERT2};R26R-mTmG mice was harvested and prepared for FACS and immunohistochemistry **(A-F)**. The mice had been administered with tamoxifen at either E11.5 (one dose) **(A,D)**, E13.5 (one dose) **(B,E)** or postnatally via the mother's milk (P0-P21, 4 doses across 2 weeks) **(C,F)**. Sections were stained with an anti-eGFP antibody (green – upper inset) and an anti-perilipin antibody (red – lower inset). 7.5% of the adipocytes from the mice given tamoxifen at E11.5 were eGFP positive **(A,H)**, 3.4% of the adipocytes from the mice given tamoxifen at E13.5 were eGFP positive **(B,H)**, and 1.2% of the adipocytes from the mice given tamoxifen postnatally were eGFP positive **(C,H)**. Sections from Cre negative littermates were included as a control **(D,E,F)**. The SVF from the mice was analysed using flow cytometry, showing that 1.4%, 0.3% and 0.16% of the SVF cells from mice dosed at E11.5, E13.5 and postnatally, respectively, were eGFP positive. The percentage of eGFP labelled cells was significantly higher in the mice dosed at E11.5, compared with those dosed at E13.5 and postnatally **(I)**. The dosing regimes for **(A-F)** are shown in **(G)**. Juvenile mice, given 4 doses of tamoxifen over 2 weeks, beginning at 4 weeks of age, had no eGFP positive subcutaneous adipocytes **(J)** or SVF cells **(K)** when analysed at around 7 weeks. The dosing regime for **(J,K)** is shown in **(L).** (Scale bar = 50μm) (n=3 per dosing regime minimum (male and female combined); a minimum of 100 adipocytes was counted for each sample; data represents mean ± s.e.m. and two-tailed Student's t-tests were used to assess statistical significance).*

In addition to the subcutaneous adipose tissue, some of the visceral fat depots from the 6 week old *Prx1-Cre*^{ERT2}*;R26R-mTmG* mice, dosed at various stages of development, were also analysed. As expected, no eGFP expressing adipocytes were observed in either the perigonadal or the omental depots, for any of the dosing times (Figure 4.9 A-F). Moreover, analysis of flow cytometry data from the perigonadal SVF cells revealed no eGFP expressing cells (Figure 4.9 G-L).

Figure 4.9. (continued on next page)



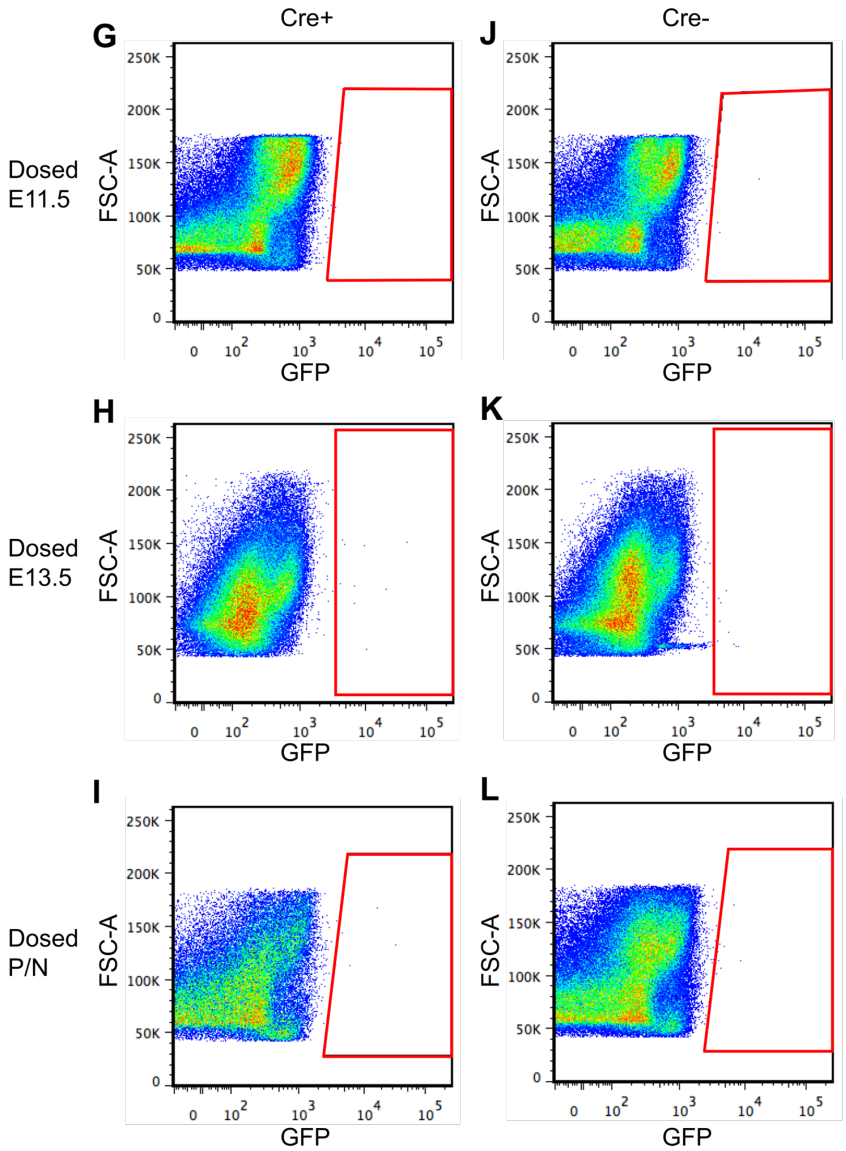


Figure 4.9. Visceral adipose tissue from 6 week old Prx1-Cre^{ERT2};R26R-mTmG mice induced in vivo at either E11.5, E13.5 or postnatally has no eGFP labelled cells. *Visceral adipose tissue from 6 week old Prx1-Cre^{ERT2};R26R-mTmG mice was harvested and prepared for flow cytometry and immunohistochemistry **(A-L)**. The mice had been administered with tamoxifen at either E11.5 **(A,D,G,J)**, E13.5 **(B,E,H,K)** or postnatally via the mother's milk **(C,F,I,L)**. **(A-F)** Sections were stained with an anti-eGFP antibody (green – upper inset) and an anti-perilipin antibody (red – lower inset). There were no eGFP positive adipocytes in either the perigonadal **(A-C)** or omental **(D-F)** depots. **(G-L)** The SVF of the perigonadal depot was analysed using flow cytometry; no eGFP positive cells were present in the SVF of the Cre positive animals **(G-I)**. Cre negative littermates were used as a gating control **(J-L)**. (Scale bar = 50μm) (n=3 per dosing regime minimum (male and female combined); a minimum of 100 adipocytes was counted for each sample)*

4.4.3 Induction *in vitro*

Given the results described above, it was unlikely that SVF cells from the adipose tissue of adult *Prx1-Cre^{ERT2};R26R-mTmG* mice would exhibit Cre^{ERT2} activity. To understand whether this was the case, subcutaneous and pericardial SVF cells were isolated from adult *Prx1-Cre^{ERT2};R26R-mTmG* mice and cultured *in vitro* under standard conditions (5% CO_2 and 95% air (20% oxygen)), with 1 μM 4-OH tamoxifen for one week. The cells were harvested and analysed using flow cytometry to assess whether any expressed eGFP. Representative flow cytometry plots from this study are shown in Figure 4.10. It is clear to see that there were no eGFP expressing cells present in the cultures (cells from Cre negative mice, also cultured and administered with 1 μM 4-OH tamoxifen, were used for gating). Therefore, this suggests that the subcutaneous and pericardial SVF cells from adult *Prx1-Cre^{ERT2};R26R-mTmG* mice do not express Cre, further supporting the hypothesis that Cre is expressed during early development and that adipocytes and progenitors/pre-adipocytes present in the adult mouse are derived from these embryonic cells.

Figure 4.10. (continued on next page)

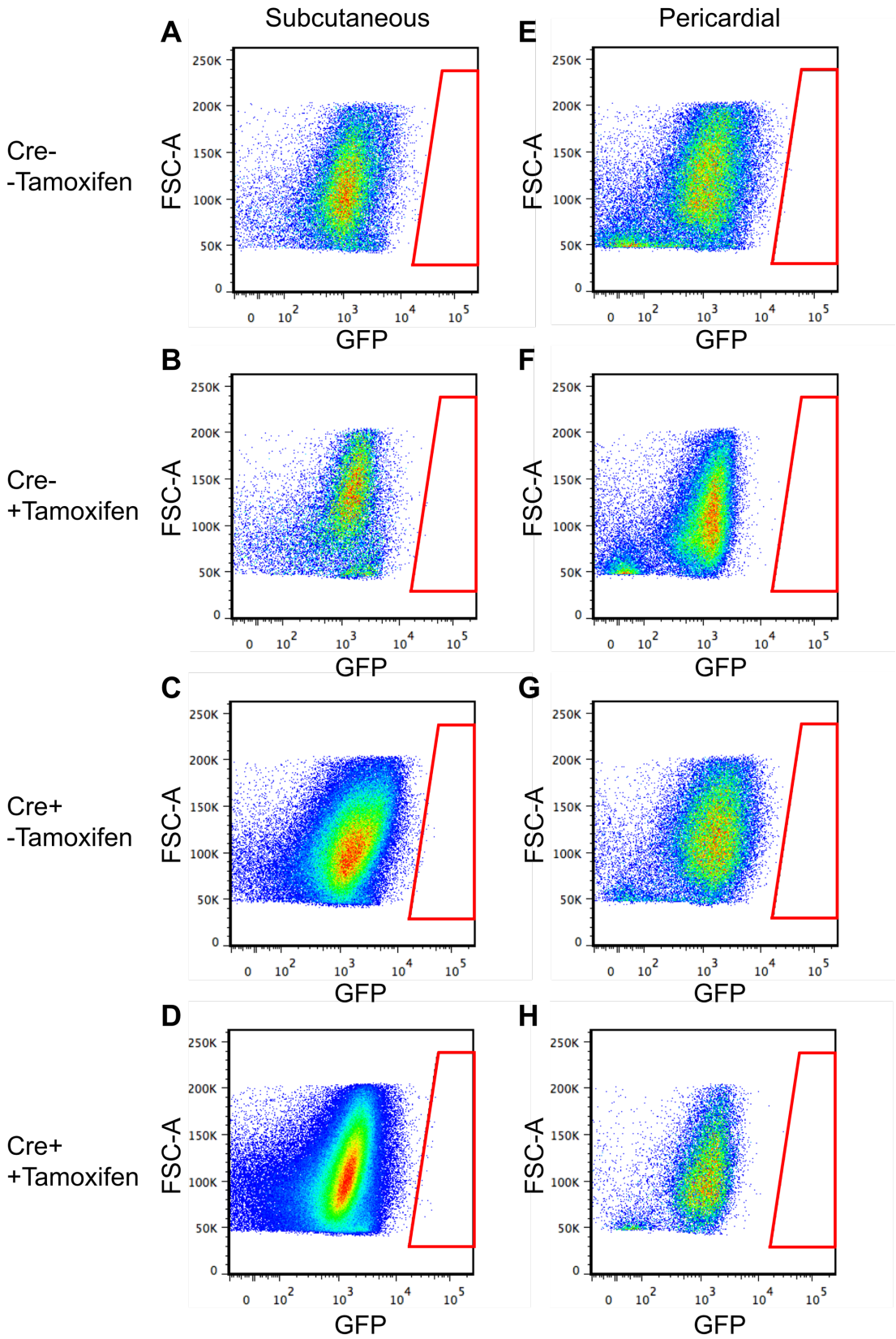


Figure 4.10. SVF cells from subcutaneous and pericardial white adipose tissue of adult Prx1Cre^{ERT2};R26R-mTmG mice do not become eGFP positive when induced in vitro. *The SVF was extracted from the subcutaneous **(A-D)** and pericardial **(E-H)** white adipose tissue of adult Prx1Cre^{ERT2};R26R-mTmG mice and prepared for culture. 1 μM 4-OH tamoxifen was added to the culture medium and the cells were harvested after one week and analysed using flow cytometry. Representative flow cytometry plots are shown. Gating controls included cells from Cre negative littermates **(A,B,E,F)** and Cre positive cells that were not administered with 4-OH tamoxifen **(C,G)**. Cells from Cre positive mice, given 1 μM 4-OH tamoxifen for one week in vitro, did not become eGFP positive, as shown by an absence of cells in the red boxes **(D,H)**. (n=3).*

4.5 *Wt1* expressing and Prx1-Cre lineage positive pericardial pre-adipocyte populations overlap

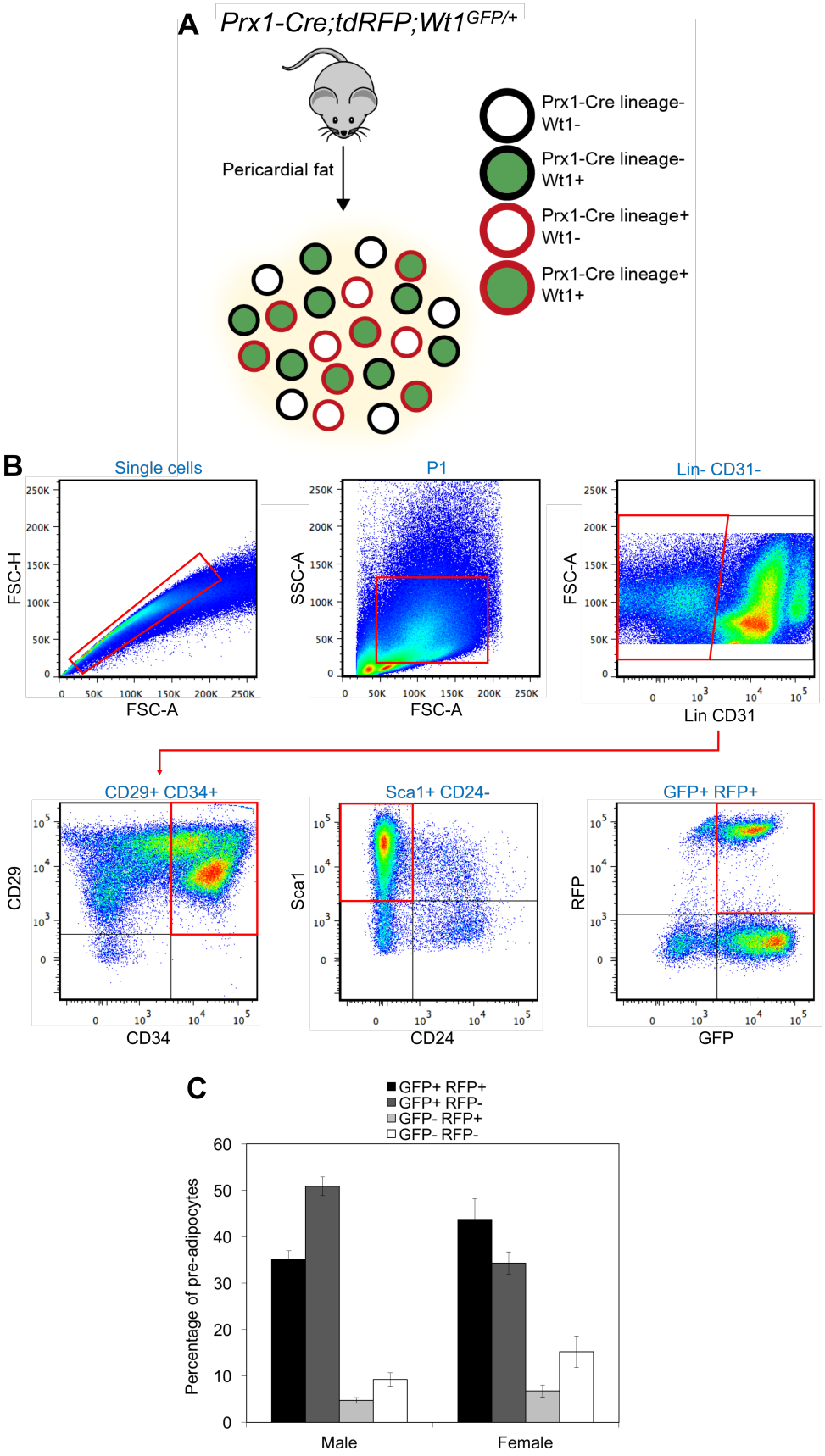
4.5.1 *Wt1* expressing and Prx1-Cre lineage positive pericardial pre-adipocytes

As described previously, work by Chau *et al*. (2014) showed that a proportion of pre-adipocytes and adipocyte progenitor cells in all visceral fat depots express *Wt1*. Moreover, the percentage of *Wt1* expressing cells varies between depots, with the omental and pericardial having the highest amounts (Chau *et al.*, 2014). It has now been shown that a large proportion of pericardial pre-adipocytes are Prx1-Cre lineage positive. We therefore wanted to understand whether the *Wt1* expressing and Prx1-Cre lineage positive populations overlapped, and thus whether additional heterogeneity was being observed.

In order to do this, a new mouse line was generated: *Prx1-Cre;tdRFP;Wt1*$^{GFP/+}$. In these mice, any *Prx1-Cre* expressing cells, and their progeny, express RFP, and thus fluoresce red. Additionally, GFP is knocked-in at the *Wt1* locus, meaning that any *Wt1* expressing cells fluoresce green. Therefore, there is the potential to end up with four cell populations: red only (Prx1-Cre lineage positive only), green only (*Wt1* expressing only), red and green (Prx1-Cre lineage positive and *Wt1* expressing) and no colour (neither Prx1-Cre lineage positive or *Wt1* expressing) (Figure 4.11 A). The SVF was extracted from the pericardial adipose tissue of adult *Prx1-Cre;tdRFP;Wt1*$^{GFP/+}$ mice and prepared for flow cytometry. The cells were stained with the panel of antibodies described previously, in order to investigate the CD24^{-} pre-adipocyte population (an example of the flow cytometry gating profile that was used is outlined in Figure 4.11

B). This analysis showed that pericardial $CD24^-$ pre-adipocytes could be divided into four distinct populations based on their Prx1-Cre lineage and *Wt1* expression status. 35.1% (male) and 43.7% (female) of the pre-adipocytes were labelled with both RFP and GFP, meaning they were Prx1-Cre lineage positive and expressed *Wt1*. 50.8% (male) and 34.3% (female) were labelled with GFP only, therefore expressed *Wt1* but were not Prx1-Cre lineage positive. 4.8% (male) and 6.8% (female) were RFP positive only, so did not express *Wt1* but were Prx1-Cre lineage positive. Finally, 9.3% (male) and 15.2% (female) were neither GFP nor RFP positive, therefore did not express *Wt1* and were not Prx1-Cre lineage positive (Figure 4.11 C). The perigonadal and omental depots were also examined, but as expected given the results obtained using the *Prx1-Cre;R26R-mTmG* mice, <3% of the pre-adipocytes were GFP and RFP positive, due to a lack of Prx1-Cre lineage positive cells (Figure 4.11 D,E).

Figure 4.11. (continued on next page)



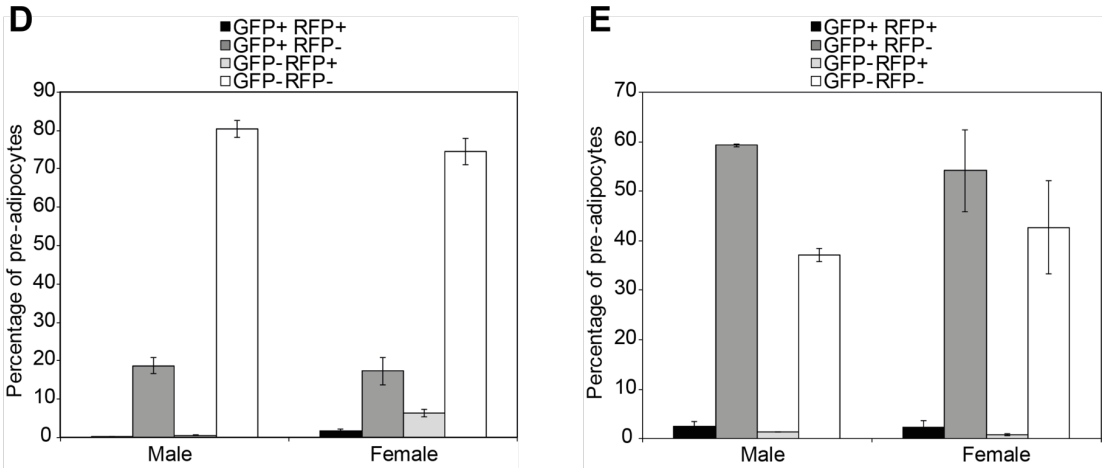


Figure 4.11. A proportion of Wt1 expressing pericardial pre-adipocytes are labelled with Prx1-Cre. *The Prx1-Cre;tdRFP;Wt1$^{GFP/+}$ mouse was generated to understand whether any cells expressed Wt1 and were Prx1-Cre lineage positive. Prx1-Cre lineage positive cells were labelled with RFP, Wt1-expressing cells were labelled with GFP. Therefore it was possible to obtain four populations: double negative, GFP positive only, RFP positive only and double positive* ***(A)****. The pericardial fat was dissected from these mice and prepared for flow cytometry. Representative flow cytometry plots, outlining the gating strategy used, can be seen in* ***(B)****. 35.1% (male) and 43.7% (female) of the pericardial pre-adipocytes were RFP and GFP positive, so Prx1-Cre lineage positive and Wt1-expressing. 50.8% (male) and 34.3% (female) were GFP positive only, <10% were RFP positive only, and the remainder were double negative* ***(C)****. <3% of the perigonadal* ***(D)*** *and omental* ***(E)*** *pre-adipocytes were GFP and RFP positive. (pericardial n=5 per sex, perigonadal and omental n=2 male, 3 female; data represent mean ± s.e.m).*

4.5.2 Comparing behaviour of pericardial pre-adipocyte populations *in vitro*

Having learned that the pericardial pre-adipocyte cell population can be divided into four groups based on their Prx1-Cre lineage and *Wt1* expression status, we wanted to understand whether, when cultured *in vitro*, the different populations of cells behaved differently, to understand whether this heterogeneity had functional consequences. The double positive population (Prx1-Cre lineage positive and *Wt1* expressing) and the single GFP positive population (Prx1-Cre lineage negative, *Wt1* expressing) were studied. These populations were chosen because, firstly, they gave the largest numbers of cells, therefore making the cultures feasible, and secondly, they represent the two most interesting populations, given that they both express *Wt1*. Whilst the GFP positive, RFP negative cells can never have been Prx1-Cre positive, so are certainly a distinct population, the GFP negative, RFP positive cells may have, at some point, been GFP positive, if *Wt1* was previously expressed in these cells.

The pre-adipocytes were isolated, and the different populations separated using FACS. Equal numbers of double positive and GFP positive, RFP negative cells were plated out separately (~10,000 cells/well of a 96 well plate). The cells were cultured for one week in standard media, and a further week with the addition of factors to induce adipocyte differentiation. The cells were then imaged and harvested for RNA extraction, to allow qRT-PCR to be performed. As shown in Figure 4.12, there was a clear difference between the behaviour of the two cell populations *in vitro*. The double positive pre-adipocytes formed many more adipocytes than the GFP positive, RFP negative, despite being cultured under identical conditions. This result was confirmed by qRT-PCR, which revealed that mRNA levels of adipocyte differentiation markers (*Plin*, *AdipoQ* and *Fabp4*), were higher in the double positive cells, compared with the single, GFP positive population (Figure 4.12 C). Therefore, additional heterogeneity within the pericardial pre-adipocyte population has been identified, with a proportion of the cells deriving from a Prx1-Cre expressing lineage. Furthermore, this heterogeneity appears to confer a functional difference in the ability of the cells to differentiate into adipocytes, at least *in vitro*.

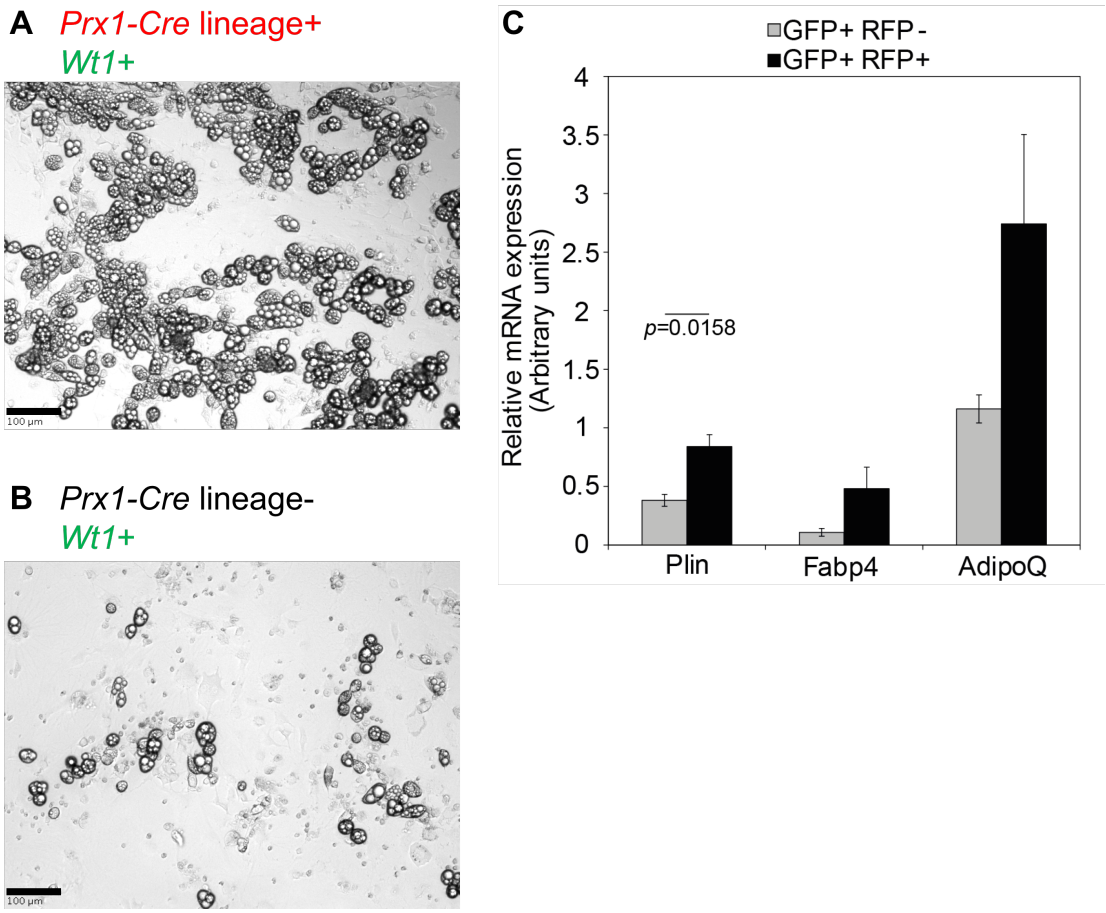


Figure 4.12. Prx1-Cre lineage positive and Prx1-Cre lineage negative Wt1 expressing pericardial pre-adipocytes behave differently in vitro. *Using the Prx1-Cre;tdRFP;Wt1$^{GFP/+}$ mouse, Prx1-Cre lineage positive, Wt1 expressing pericardial pre-adipocytes (RFP+GFP+)* ***(A)****, were separated from Prx1-Cre lineage negative, Wt1 expressing pericardial pre-adipocytes (RFP-GFP+)* ***(B)*** *using FACS. Equal numbers of the cells were plated separately and allowed to grow. Adipogenic differentiation factors were added after one week and the cultures were left for an additional week before imaging (brightfield). Prx1-Cre lineage positive cells* ***(A)*** *differentiate into adipocytes more readily than Prx1-Cre lineage negative* ***(B)****. The cultured cells were harvested and qRT-PCR was performed. The levels of Plin, Fabp4 and AdipoQ mRNA was higher in the double positive cells, confirming what can be observed in the images* ***(C)****. (Scale bar = 100µm) (n=3 minimum; data represent mean ± s.e.m. and two-tailed Student's t-tests were used to assess statistical significance).*

4.5.3 Developmental origins of Prx1-Cre lineage positive cells

A key question that arises from the results described thus far is why can Prx1-Cre be used to lineage trace adipocytes and APCs in the pericardial adipose tissue, but not in other visceral WAT depots? To begin addressing this question, it is first important to know where and when Prx1-Cre driven recombination occurs. Given the results described by Sanchez-Gurmaches *et al*. (2015), regarding the absence of Cre mRNA expression in the adult adipose tissue depots, and the outcome of the *Prx1-Cre^{ERT2};R26R-mTmG* tamoxifen studies performed here (4.4), it seems reasonable to hypothesise that Prx1-Cre is expressed during embryonic development (Sanchez-Gurmaches, Hsiao and Guertin, 2015). This suggests that the recombination event occurs during early embryogenesis, and the Prx1-Cre lineage traced mature adipocytes and APCs in the adult, are derived from these embryonic Cre expressing cells.

To investigate this further, we attempted to use immunohistochemistry to verify the timing and location of Cre expression in the *Prx1-Cre;R26R-mTmG* embryos. However, due to technical difficulties with the anti-Cre antibody, this was not possible. As an alternative to this, E9.5 embryos were sectioned and stained with an anti-eGFP antibody, to detect the expression of the eGFP from the *R26R-mTmG* reporter, at this early developmental stage. As shown in Figure 4.13, eGFP expression was observed in cells of the somatic lateral plate mesoderm (LPM) of the E9.5 *Prx1-Cre;R26R-mTmG* embryos. Therefore, cells of the somatic LPM were Prx1-Cre lineage positive. Importantly, at E9.5 a very limited number of eGFP expressing cells were present in the splanchnic LPM.

As demonstrated by work from our group and detailed in the introduction (1.2.1), at least a proportion of the adipocytes and APCs in the visceral WAT depots are derived from the surrounding mesothelium (Chau *et al.*, 2014). It is known that the visceral mesothelia arise developmentally from the splanchnic LPM (Sheng, 2015). Therefore, given the results illustrated in Figure 4.13, it is not surprising that very low numbers of Prx1-Cre lineage positive adipocytes and APCs were observed in the visceral WAT depots of adult *Prx1-Cre;R26R-mTmG* mice. But what about the pericardial depot? As

defined in the introduction (1.1.1), the heart is encapsulated by the pericardial membrane. Two components of this membrane are largely mesothelial; the epicardium (or visceral pericardium) which is attached to the heart, and the parietal pericardium which is attached to the outer fibrous layer of the pericardial membrane (Figure 1.2 in the introduction) (Rene Rodriguez and Tan, 2017). Figure 4.14 shows a section through the heart of an E14.5 *Prx1-Cre;R26R-mTmG* embryo, stained with an anti-eGFP antibody and an anti-Wt1 antibody (mesothelial cells express WT1). As expected, WT1 expressing cells were observed in the epicardium and pericardium, however eGFP expression was only present in the pericardium and not the epicardium. Therefore, cells of the pericardium were Prx1-Cre lineage positive. It is known that, whilst the visceral mesothelia are derived from the splanchnic LPM, the parietal mesothelia (including the parietal pericardium) are derived from the somatic LPM (Sheng, 2015). Hence, given that cells of the somatic LPM were Prx1-Cre lineage positive (Figure 4.13), it follows that the parietal pericardium was too (Figure 4.14). Thus, we hypothesise that at least a proportion of the adipocytes and APCs of the pericardial visceral WAT depot are derived from the parietal pericardium, and therefore have their origins in the somatic LPM.

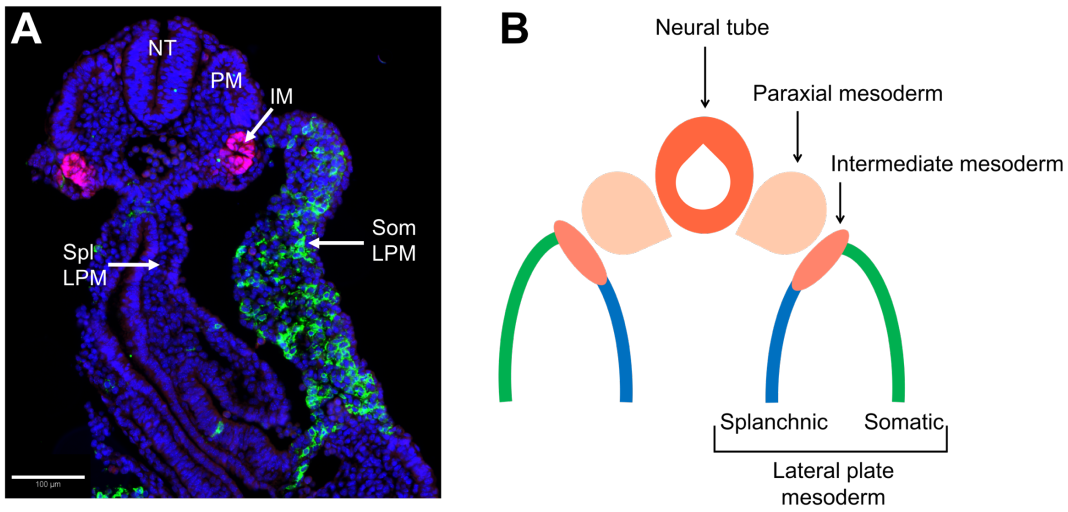


Figure 4.13. Cells of the somatic lateral plate mesoderm (LPM) are Prx1-Cre lineage positive. *E9.5 Prx1-Cre;R26R-mTmG embryos were sectioned and stained with an anti-Pax2 antibody (to label the intermediate mesoderm) (red), an anti-eGFP antibody (green) and DAPI (blue)* ***(A)****. Somatic, but not splanchnic, LPM cells expressed eGFP* ***(A)****. A cartoon illustration of the early embryo is depicted in* ***(B)****, showing the different divisions of the mesoderm. The somatic and splanchnic LPM will form the parietal and visceral mesothelia, respectively. (Scale bar = 100μm) (n=3).*

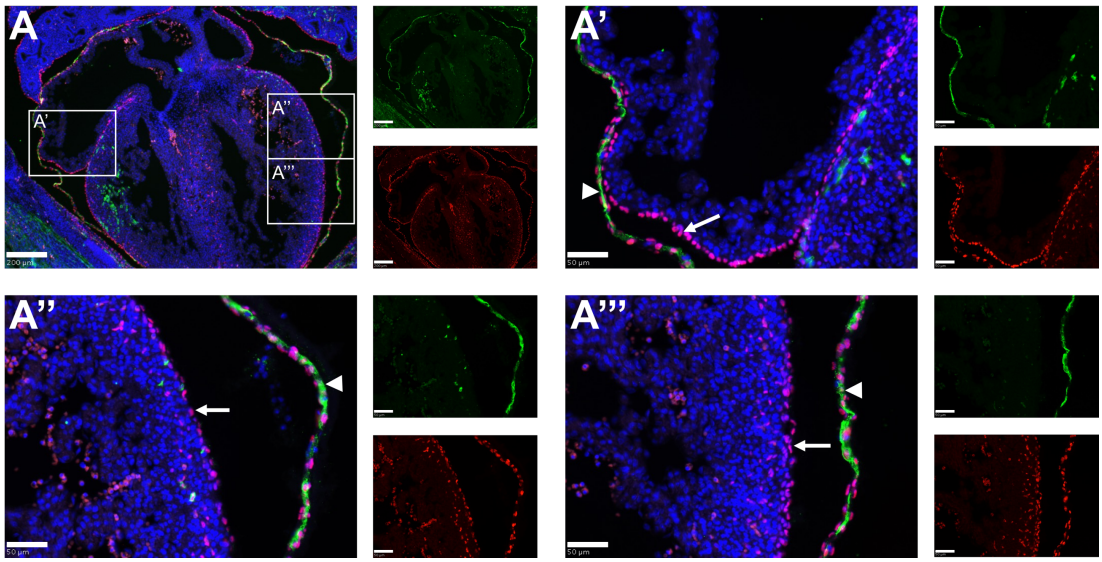


Figure 4.14. The parietal pericardium of the heart is Prx1-Cre lineage positive. *E14.5 Prx1-Cre;R26R-mTmG embryos were sectioned and stained with an anti-Wt1 antibody (to label the mesothelial cells) (red - lower inset), an anti-eGFP antibody (green - upper inset) and DAPI (blue). The epicardium (arrow) expressed WT1 but was not labelled with eGFP, the pericardium (arrow head) expressed WT1 and was labelled with eGFP, so was Prx1-Cre lineage positive.* ***A', A'' and A'''*** *are magnified images of the areas indicated in* ***A****. (Scale bar = 200μm (A), 50 μm (A'-A''')) (n=2).*

4.6 Discussion

The results described in this chapter have shown that the majority of the subcutaneous adipocytes and APCs can be labelled by Prx1-Cre. Additionally, >50% of the pericardial visceral adipocytes and approximately 40% of the pericardial visceral APCs can also be labelled, however this is not the case for the other visceral WAT depots. Whilst this work was being carried out, another group reported corroborating results regarding the labelling of the subcutaneous, perigonadal and mesenteric depots, however the pericardial depot was not described (Sanchez-Gurmaches, Hsiao and Guertin, 2015). Therefore, the findings regarding the pericardial depot described here are novel. Interestingly, there is an overlapping population of pre-adipocytes in the pericardial SVF, that are both Prx1-Cre lineage positive and express *Wt1*. Moreover, these Prx1-Cre lineage positive, *Wt1* expressing pre-adipocytes are better at differentiating into adipocytes *in vitro* than the Prx1-Cre lineage negative, *Wt1* expressing pre-adipocytes, despite plating the same numbers of cells for each population. Thus, this suggests that the pre-adipocytes from different lineages behave differently, at least *in vitro*. As described in chapter 3, murine pre-adipocytes differentiate best when they are confluent (*in vitro*). Therefore, it is important that future work includes the assessment of whether the two cell populations differ in their proliferative capacities, and additionally, whether the GFP+RFP- population is more apoptotic than the GFP+RFP+. These factors could influence how confluent the cells become, and therefore their ability to differentiate into adipocytes. Therefore, further work is required to understand the differences between the two populations of pre-adipocytes. Moreover, it is proposed that the transcriptomic profiles of the two populations will be investigated, in order to further elucidate how the cells differ.

The presence of Prx1-Cre lineage positive cells in the pericardial visceral WAT, but not in other visceral WAT depots, may be a consequence of differing developmental origins. Preliminary data described in this chapter suggests that, at least a proportion of the pericardial adipocytes and APCs are derived from the parietal pericardium, which is one component of the pericardial membrane that surrounds the heart (Iacobellis, 2009). The parietal pericardium, which is largely mesothelial, is derived

from the somatic LPM, and as shown here, both are Prx1-Cre lineage positive (Brauer, 2003). It has previously been assumed that the *Prx1-Cre* transgene is expressed in the somatic LPM, due to the distribution of the cells that are labelled when crossed with a reporter line (Durland *et al.*, 2008). Therefore, this supports the results that have been obtained here. Given the evidence showing that visceral adipocytes and APCs have a mesothelial origin (Chau *et al.*, 2014), it is feasible that the parietal pericardium is one source of pericardial adipose tissue. Conversely, the visceral mesothelium, that encapsulates and gives rise to the other visceral adipose depots, is derived from the splanchnic LPM, which, as has been shown here, is mostly Prx1-Cre lineage negative (Brauer, 2003; Chau *et al.*, 2014). Hence, it follows that the mesenteric, omental and perigonadal depots examined in this study are largely Prx1-Cre lineage negative.

As described in the introduction (1.1.1), two VWAT depots are associated with the heart; the pericardial, and the epicardial. The epicardial depot is much smaller than the pericardial, and directly abuts the heart myocardium (Iacobellis, 2009). It has been shown that the epicardial adipose tissue is derived from the epicardium (the component of the pericardial membrane that is attached to the heart (Figure 1.2)) (Liu *et al.*, 2014; Suffee *et al.*, 2017). As demonstrated by us, the epicardium is not Prx1-Cre lineage positive, therefore it would follow that the epicardial adipose depot is not labelled using the Prx1-Cre line. This is something that requires further investigation. However, these results indicate that the two heart-associated VWAT depots are (at least partially), derived from different origins. Moreover, one question that has not been addressed is where are the Prx1-Cre lineage negative pericardial fat cells coming from? Evidently, the pericardial pre-adipocyte population is heterogeneous, as the experiments with the *Prx1-Cre;tdRFP;Wt1*$^{GFP/+}$ mice have shown, and it now seems likely that some of this heterogeneity occurs as a result of different lineages contributing to the population.

This leaves open the issue concerning the developmental origin of subcutaneous WAT, something that is currently unknown. Considering the results that have been discussed, it seems likely that the subcutaneous WAT is also derived from the somatic LPM. However, as it has not been possible to identify the exact location and timing of Cre

expression in the *Prx1-Cre;R26R-mTmG* embryos, it cannot be determined exactly when and in which cells the recombination event occurs, and therefore from where the mature adipocytes are being derived. The expression of eGFP in the somatic LPM of the E9.5 *Prx1-Cre;R26R-mTmG* embryos indicates that recombination occurred in these cells, however we cannot rule out the possibility that additional recombination events occur later in development or postnatally in other lineages, which may give rise to the mature adipocytes.

It was thought that utilising the tamoxifen inducible, *Prx1-Cre*^{ERT2} line, would help address this problem. By administering tamoxifen at different developmental stages, as well as postnatally (P0-P21), and subsequently analysing the adult adipose tissue, we hoped that it would become clear as to when the recombination event must occur in order to label the mature adipocytes. Whilst this work has been informative, it is not conclusive. It certainly appears that the earlier tamoxifen is administered, the more eGFP positive cells are present in the adult adipose tissue. For example, tamoxifen administration at E11.5 gave rise to more eGFP expressing adipocytes and SVF cells in 6 week old mice, than administration at either E13.5 or postnatally. Furthermore, administration at E9.5 clearly led to more eGFP expressing cells in the developing SWAT depot at E18.5, compared to those dosed at E11.5. Unfortunately, due to limitations with breeding, it has not been possible to analyse the adipose tissue of 6 week old mice, dosed at E9.5. However, this is something that should be carried out in future experiments, and given what has been shown thus far, it is likely that increased labelling would be observed.

Despite observing a trend regarding the timing of tamoxifen administration and the percentage of cells labelled, we cannot conclude from this that there are more Prx1-Cre expressing cells present in the embryo at earlier developmental stages. Whilst this is a possibility, it is also conceivable that the increased labelling is a consequence of more time having elapsed between dosing and analysis. For example, for the embryos dosed at E9.5, it was 9 days before the analysis (E18.5) was performed, whilst for those dosed at E11.5 it was just 7 days. Therefore, the recombined cells had longer to proliferate and differentiate, thus potentially leading to more labelling. Nevertheless,

the results do provide additional support for the hypothesis that mature SWAT (and pericardial VWAT) adipocytes are derived from cells that express Prx1-Cre/Cre^{ERT2} during early embryonic development, and it is likely that these cells are located in the somatic LPM.

It is also important to note that no eGFP expressing adipocytes or SVF cells were observed in ~7 week old mice, when they had been given tamoxifen at ~4 weeks old. Moreover, when the SVF cells were isolated from adult SWAT and pericardial VWAT, and cultured *in vitro* in the presence of 4-OH tamoxifen, no eGFP expressing cells were obtained. These results imply that neither the APCs, or mature adipocytes, of juvenile/adult mice express Prx1-Cre^{ERT2}. Therefore, any eGFP labelling that was observed in these mice was not due to endogenous Prx1-Cre^{ERT2} expression, but lineage tracing. It has been shown that adult SWAT does express *Prx1* mRNA, but, in Prx1-Cre mice, *Cre* mRNA cannot be detected (Sanchez-Gurmaches, Hsiao and Guertin, 2015). Therefore, it is already known that the *Prx1-Cre* transgene does not exactly reflect the endogenous expression of the *Prx1* gene, thus highlighting how important it is to know exactly where and when Cre is expressed.

Despite observing eGFP expression in the adult *Prx1-Cre^{ERT2};R26R-mTmG* mice that had been given tamoxifen embryonically, the percentage of labelled cells was always notably lower than that observed in the adult *Prx1-Cre;mTmG* mice. Even when the mice were dosed at E9.5, the subcutaneous depot at E18.5 clearly harboured fewer eGFP expressing cells than that of the E18.5 *Prx1-Cre;mTmG* embryo. There are several factors that could explain this discrepancy. Firstly, it is possible that the *Prx1-Cre* and *Prx1-Cre^{ERT2}* transgenes differ in their activity. When the *Prx1-Cre^{ERT2}* construct was developed, its activity was compared to that of *Prx1-Cre*. It was shown that, at early embryonic stages, the *Prx1-Cre* transgene exhibits more robust activity than *Prx1-Cre^{ERT2}* (Hasson, Del Buono and Logan, 2007). For example, when tamoxifen was administered at E8.5, labelling was only present in a small number of sparsely distributed LPM cells at E9-9.5, compared to labelling throughout the LPM of the *Prx1-Cre* line. It was not until E10-10.5 that the labelling in the *Prx1-Cre^{ERT2}* line matched that of the *Prx1-Cre* line (Hasson, Del Buono and Logan, 2007). Hence,

considering that the early developmental stages are evidently crucial in our study, it is likely that this incomplete recombination when using the *Prx-Cre*^{ERT2} line could explain the lower levels of labelling observed in these mice. Moreover, it is possible, given that only a single dose of tamoxifen was administered, that insufficient tamoxifen could partially account for the incomplete recombination. Additionally, it cannot be ruled out that the tamoxifen partially inhibits adipogenesis; something that has been demonstrated previously (Liu *et al.*, 2015). If this is indeed the case in our model, then it is possible that recombination is occurring, but the efficiency with which the cells differentiate into adipocytes is lower, leading to fewer labelled adipocytes.

Another intriguing finding is the presence of eGFP expression in a small percentage of cells of the female perigonadal depot, (8.8% of the adipocytes, compared to 0.8% in males). A similar result has also been reported by another group (Sanchez-Gurmaches, Hsiao and Guertin, 2015). This is not the first time that differing results have been obtained from male and female mice, particularly regarding the perigonadal depot. For example, using the *Pax3-Cre* line, 60% of the male, but not female, perigonadal VWAT is labelled, indicating that there is a gender linked discrepancy in lineage distribution (Sanchez-Gurmaches and Guertin, 2014b). The fact that such differences are observed in the adipose tissue that is associated with the gonads adds further support to this hypothesis. As described in the introduction, the male perigonadal (epididymal) VWAT depot is derived from a mesothelial-like epididymal appendage, however the reciprocal tissue in females has not been described (Han *et al.*, 2011). Knowing this would perhaps help to explain why gender differences are observed. Additionally, a substantial difference in the percentage of eGFP expressing cells between males and females was noted for the CD24^{+} adipocyte progenitor population from the subcutaneous depot (87.7% in male and 47.7% in female). As mentioned previously, the CD24^{+} cells make up just 0.08% of the total SVF (compared to the CD24^{-} preadipocytes which make up 53%) (Rodeheffer, Birsoy and Friedman, 2008), and therefore the percentage of eGFP expressing cells in this population increases or decreases considerably when the actual number differs by just a few cells. This is better illustrated in Figure 4.2 (D), which displays the composition of the eGFP expressing population, revealing that just 2.0% (male) and 3.8% (female) of the eGFP

expressing SVF cells were Lin^{-};$CD29^{+}$;$CD34^{+}$;$Sca1^{+}$;$CD24^{+}$. It is therefore possible that this gender difference is a consequence of the composition of the SVF, however it cannot be ruled out that there may also be a biological explanation for this, and this is something that requires further investigation.

In conclusion, the work described in this chapter has shown that both the subcutaneous WAT and pericardial visceral WAT can be labelled using the *Prx1-Cre* mouse line. However, this is not the case for the other visceral WAT depots. Additionally, data from the *Prx1-Cre;R26R-mTmG* and the tamoxifen inducible *Prx1-Cre^{ERT2};R26R-mTmG* mice suggest that cells present in the somatic lateral plate mesoderm during early embryogenesis give rise to the mature adipocytes and APCs of the adult subcutaneous and pericardial WAT, although this requires further investigation. Preliminary work indicates that the parietal pericardium may be one source of pericardial adipose tissue. Moreover, we have observed increased heterogeneity in the pericardial pre-adipocyte population, with a proportion of the cells being derived from the Prx1-Cre lineage, and this heterogeneity appears to influence the ability of the cells to undergo adipogenesis *in vitro*. In addition to the further work proposed already, it would also be interesting to perform high fat diet studies using the *Prx1-Cre;R26R-mTmG* and *Prx1-Cre;tdRFP;Wt1$^{GFP/+}$* mice. Considering that the pre-adipocytes from the different lineages appear to behave differently *in vitro*, it may be that they do so *in vivo*, perhaps in response to external cues, such as diet. For example, using the *Prx1-Cre;R26R-mTmG* mice it would be possible to assess the percentages of Prx1-Cre lineage positive adipocytes and APCs in mice fed a high fat diet and determine whether these differed from those fed a control diet. Therefore, informing on how the cells from the different lineages respond to physiologically relevant perturbations. Additionally, the focus of this work has been on WAT, however, it would also be interesting to assess the contribution of Prx1-Cre lineage cells to BAT and beige adipose tissue; an area that Sanchez-Gurmaches *et al*. (2015) have begun to explore.

Chapter 5

Wt1 deletion in the Prx1-Cre lineage

5.1 Introduction

To understand more about the function of *Wt1* in the development of visceral WAT, one aim of my PhD was to conditionally delete the gene using the *Prx1-Cre* mouse line, for reasons outlined in the introduction (section 1.3.1). However, as has already been mentioned (section 1.4), it became apparent that the $Prx1^{Cre/+};Wt1^{loxP/loxP}$ pups were dying at birth. As described below, we discovered that this premature death was due to aberrant development of the diaphragm, leading to congenital diaphragmatic hernia (CDH).

The diaphragm is composed of several tissue types including muscle, connective tissue, tendon, nerves, blood vessels, lymphatics and mesothelium (Ackerman and Greer, 2007). A number of mouse models have been used to study how defects in the various tissues can lead to CDH (Yuan *et al.*, 2003; Ackerman *et al.*, 2005; You *et al.*, 2005; Jay *et al.*, 2007; Coles and Ackerman, 2013; Domyan *et al.*, 2013; Zhang *et al.*, 2014; Merrell *et al.*, 2015; Carmona *et al.*, 2016). However, despite much work, the etiology of CDH remains incompletely understood. Moreover, as detailed in section 1.4.2, mutations in *WT1* have been seen in patients with CDH (Scott *et al.*, 2005; Holder *et al.*, 2007; Suri *et al.*, 2007; Antonius *et al.*, 2008) and homozygous *Wt1* null mouse embryos develop diaphragmatic hernias (Kreidberg *et al.*, 1993). Hence, it is already recognised that WT1 has a role in diaphragm development, however its exact function remains unknown.

In summary, this chapter shows that deletion of *Wt1* in the Prx1-Cre lineage leads to the formation of diaphragmatic hernias, which we show is due to the defective development of the pleuroperitoneal folds. Additionally, several causative mechanisms are explored.

5.2 $Prx1^{Cre/+};Wt1^{loxP/loxP}$ mice have diaphragmatic hernias

Male $Prx1^{Cre/+};Wt1^{loxP/+}$ mice were crossed with female $Wt1^{loxP/loxP}$ mice and the pups genotyped at approximately two weeks of age, to check for the presence of

Prx1$^{Cre/+}$;*Wt1*$^{loxP/loxP}$ animals in the litter. However, after having had over 40 pups born, none of which were *Prx1*$^{Cre/+}$;*Wt1*$^{loxP/loxP}$, it became apparent that the deletion was probably embryonic lethal. Whilst this result meant that this cross was not going to be useful to investigate the effect of *Wt1* deletion in visceral adipose tissue (specifically pericardial adipose tissue, as discussed in chapter 4), we were interested in understanding why the embryos were dying. To begin this investigation, embryos were collected from pregnant *Wt1*$^{loxP/loxP}$ mothers at various stages of development, beginning at embryonic day 10.5 (E10.5). At all stages analysed (E11.5, E12.5, E14.5, E16.5, E18.5, and E19.5), *Prx1*$^{Cre/+}$;*Wt1*$^{loxP/loxP}$ embryos were present in the litters, and had no obvious phenotype upon initial external examination (Table 5.1 summarises the number of *Prx1*$^{Cre/+}$;*Wt1*$^{loxP/loxP}$ embryos found at each developmental stage). Moreover, when the mothers were allowed to give birth, mutant embryos were present in the litters that were born. The litters were monitored closely and it became apparent that the *Prx1*$^{Cre/+}$;*Wt1*$^{loxP/loxP}$ pups were dying within a few hours of being born. It is common for the mothers to eat any deceased or unwell pups, and as we had not previously been monitoring the mice during and immediately after birth, this may explain why no mutant pups had been found in earlier litters. By understanding when the pups were dying we concluded that it was unlikely that the lethality of this cross had the same cause as that for *Wt1* null mice (defects in coronary vasculature development, causing death at mid-gestation). Additionally, finding that mice carrying the deletion could survive until birth led us to hypothesise that their death may have been the result of an inability to breathe; something which would not be an issue prenatally.

Table 5.1. The number of Prx1$^{Cre/+}$;Wt1$^{loxP/loxP}$ embryos obtained at each developmental stage, compared to the expected number

EMBRYO STAGE	TOTAL # EMBRYOS	# EXPECTED MUTANTS	# ACTUAL MUTANTS
E10.5	27	6.75 (25%)	6 (22%)
E11.5	18	4.5 (25%)	4 (22%)
E12.5	26	6.5 (25%)	6 (23%)
E14.5	9	2.25 (25%)	3 (33%)
E16.5	22	5.5 (25%)	8 (36%)
E18.5	6	1.5 (25%)	1 (17%)
E19.5	25	6.25 (25%)	4 (16%)
P0	24	6 (25%)	4 (16%)

A common consequence of diaphragmatic defects is disrupted breathing (largely due to pulmonary hypoplasia caused by the presence of abdominal organs in the thoracic cavity preventing proper lung formation) (Greer, 2013). It is already known that WT1 functions in diaphragm development, and that *Wt1* null embryos often have holes, or diaphragmatic hernias, in the posterolateral region of the diaphragm (Kreidberg *et al.*, 1993). Therefore, we hypothesised that diaphragm development may have been disrupted in the $Prx1^{Cre/+};Wt1^{loxP/loxP}$ embryos/pups, and thus could explain the lethality. To understand whether this was the case, deceased $Prx1^{Cre/+};Wt1^{loxP/loxP}$ pups and E19.5 $Prx1^{Cre/+};Wt1^{loxP/loxP}$ embryos were dissected. As shown in Figure 5.1, the mutant embryos/pups had large holes in their diaphragms, most commonly in the posterolateral region, often accompanied by herniation of the liver and stomach into the thoracic cavities. Subsequently, younger embryos (E14.5 and E16.5) were examined, either by dissection of the whole embryo, or by fixation, sectioning and H&E staining. Large diaphragmatic holes were observed in the majority of the mutant embryos, and these were often accompanied by the herniation of the liver into the thoracic cavity (Figures 5.2 and 5.3). Therefore, having discovered that the $Prx1^{Cre/+};Wt1^{loxP/loxP}$ genotype was lethal we concluded that this lethality was most likely due to the presence of diaphragmatic hernias due to disrupted diaphragm development.

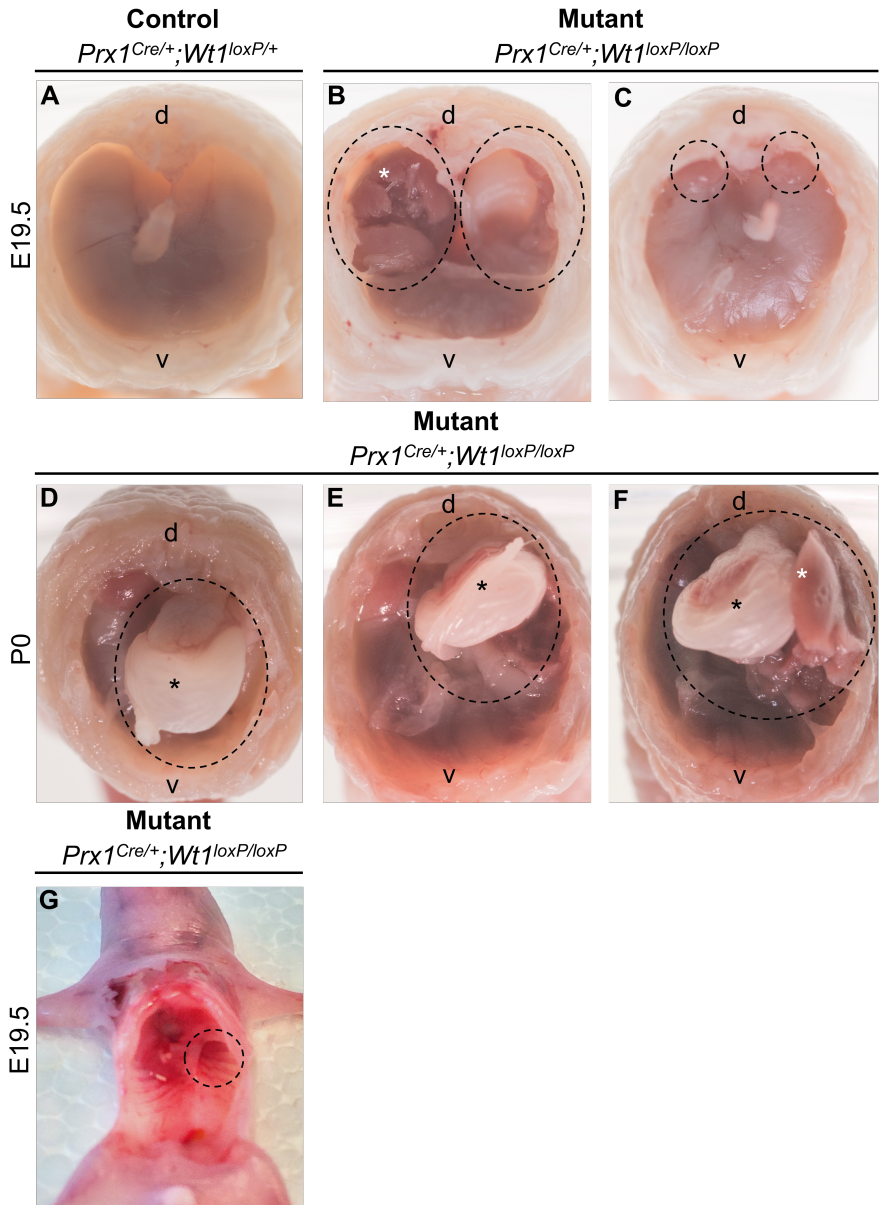


Figure 5.1. E19.5 Prx1$^{Cre/+}$;Wt1$^{loxP/loxP}$ embryos and P0 Prx1$^{Cre/+}$;Wt1$^{loxP/loxP}$ pups have diaphragmatic hernias. *Male Prx1$^{Cre/+}$;Wt1$^{loxP/+}$ mice were crossed with female Wt1$^{loxP/loxP}$ mice and the embryos were collected at either E19.5 or immediately after birth and dissected for imaging. 8/49 pups were Prx1$^{Cre/+}$;Wt1$^{loxP/loxP}$ and all exhibited diaphragmatic hernias.* ***(A-F)*** *Pups were dissected, their heads and contents of the thoracic cavity removed, and the diaphragm imaged from the top.* ***(B,C)*** *Representative images of hernias in the E19.5 Prx1$^{Cre/+}$;Wt1$^{loxP/loxP}$ embryos.* ***(B)*** *had bilateral, dorsally located holes in the diaphragm (circled), with liver herniation into the thoracic cavity (asterisk) and* ***(C)*** *had small bilateral, dorsally located holes (circled). A littermate control is shown for comparison* ***(A).*** ***(D-F)*** *Representative images of hernias in the P0 Prx1$^{Cre/+}$;Wt1$^{loxP/loxP}$ pups, all three had large, left-sided dorsally located holes (circled) with herniation of the stomach (black asterisk) and in one case* ***(F)****, the liver (white asterisk), into the thoracic cavity.* ***(G)*** *An E19.5 Prx1$^{Cre/+}$;Wt1$^{loxP/loxP}$ embryo was dissected, the contents of its peritoneal cavity removed and the diaphragm imaged from below, revealing a left-sided dorsally located hole in the diaphragm (circled). (Abbreviations: d: dorsal, v: ventral).*

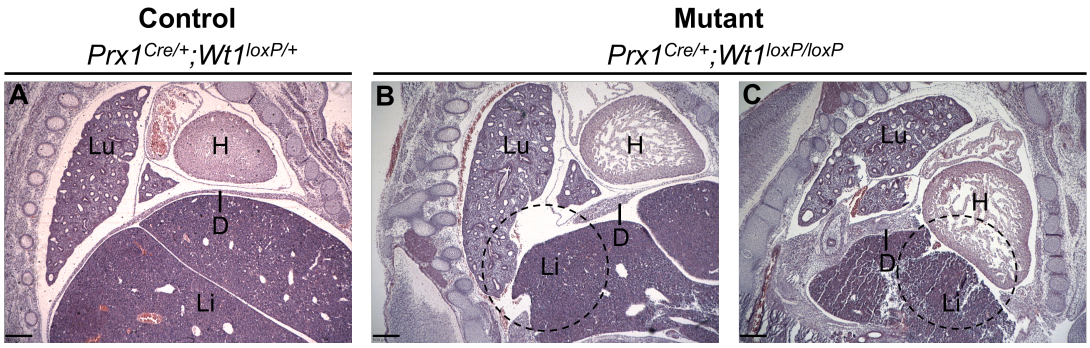


Figure 5.2. E14.5 $Prx1^{Cre/+};Wt1^{loxP/loxP}$ embryos have diaphragmatic hernias. *Male $Prx1^{Cre/+};Wt1^{loxP/+}$ mice were crossed with female $Wt1^{loxP/loxP}$ mice and the embryos were collected at E14.5 and processed for H&E staining. 3/9 embryos were $Prx1^{Cre/+};Wt1^{loxP/loxP}$ and all exhibited diaphragmatic hernias.* ***(B,C)*** *Representative images of the hernias in the $Prx1^{Cre/+};Wt1^{loxP/loxP}$ embryos.* ***(B)*** *had a left sided, dorsally located hole in the diaphragm (circled), with liver herniation into the thoracic cavity and* ***(C)*** *had a left sided, ventrally located hole (circled). A littermate control is shown for comparison* ***(A)****. All embryos were sectioned in the sagittal plane. (Abbreviations: Lu: Lungs, Li: Liver, H: Heart, D: Diaphragm). (Scale bar = 500μm).*

Figure 5.3 (continued on next page)

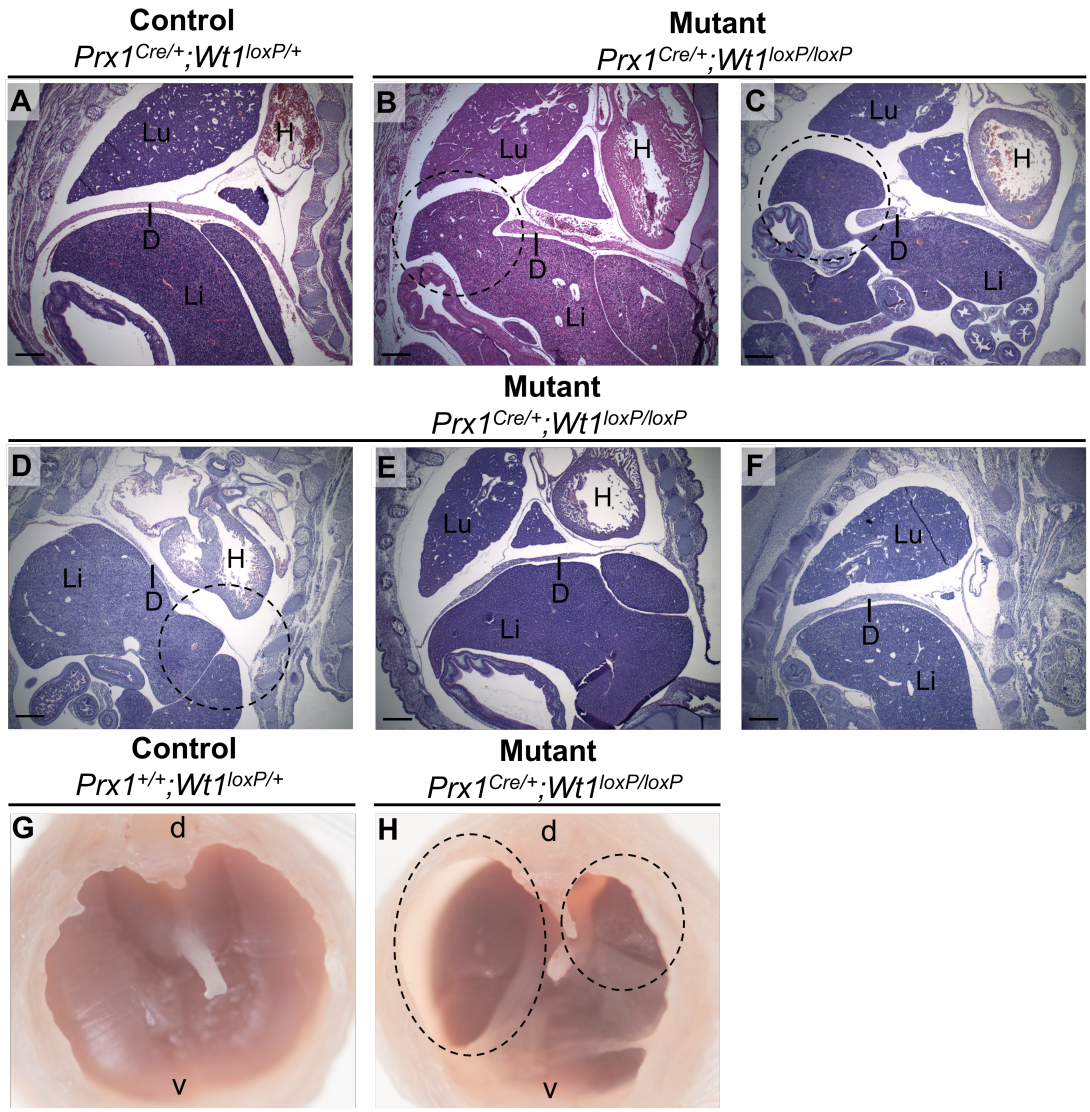


Figure 5.3. E16.5 $Prx1^{Cre/+};Wt1^{loxP/loxP}$ embryos have diaphragmatic hernias. *Male $Prx1^{Cre/+};Wt1^{loxP/+}$ mice were crossed with female $Wt1^{loxP/loxP}$ mice and the embryos were collected at E16.5 and either dissected for imaging or processed for H&E staining. 8/22 embryos were $Prx1^{Cre/+};Wt1^{loxP/loxP}$. **(B,C)** Representative images of large hernias in the $Prx1^{Cre/+};Wt1^{loxP/loxP}$ embryos . **(B)** had bilateral, dorsally located holes in the diaphragm, with liver herniation into the thoracic cavity (circled) and **(C)** had a left sided, dorsally located hole, with liver herniation into the thoracic cavity (circled). **(D)** had no herniation, but the diaphragm was thinned at the left hand side (circled). **(E,F)** No obvious diaphragmatic phenotype was observed in 4 of the $Prx1^{Cre/+};Wt1^{loxP/loxP}$ embryos. A littermate control is shown for comparison **(A)**. All embryos were sectioned in the sagittal plane, with the exception of **(D)** which was sectioned in the coronal plane. **(G,H)** Freshly isolated embryos were dissected, their heads and contents of the thoracic cavity removed, and the diaphragm imaged from the top of the embryo, bilateral dorsal holes were present in the diaphragm of the $Prx1^{Cre/+};Wt1^{loxP/loxP}$ embryo (circled) **(H)**, compared to a littermate control **(G)**. (Abbreviations: Lu: Lungs, Li: Liver, H: Heart, D: Diaphragm, d: dorsal, v: ventral). (Scale bar = 400μm).*

Table 5.1 outlines the number of embryos/pups we obtained at each developmental stage, and of these how many were $Prx1^{Cre/+};Wt1^{loxP/loxP}$. According to Mendel's Laws of Inheritance, 25% of each litter should have been $Prx1^{Cre/+};Wt1^{loxP/loxP}$. As shown in the table, generally the expected number of $Prx1^{Cre/+};Wt1^{loxP/loxP}$ embryos was present. The exception to this was for the later stage embryos (E18.5 and older), where the numbers were slightly lower than expected. Nevertheless, at least a proportion of the mutants did survive until birth. Descriptions of the diaphragmatic phenotypes observed for the $Prx1^{Cre/+};Wt1^{loxP/loxP}$ embryos can be found in Table 5.2. Additionally, the pie chart in Figure 5.4 summarises the diaphragmatic phenotypes of the embryos aged E14.5 and older. The most common diaphragmatic defect present in the $Prx1^{Cre/+};Wt1^{loxP/loxP}$ embryos/pups was a left sided hernia, with 45% of the mutants falling into this category. 20% of the mutant embryos/pups had bilateral hernias, and 10% had holes on the right side only. Another 10% did not have fully formed holes, but did have sections that were very thin in comparison to the wildtype controls. Additionally, with the exception of one mutant (Figure 5.2 C), all the defects observed were located dorsally. Finally, in 20% of the mutants, no diaphragmatic phenotype was observed.

Table 5.2. Phenotype and image information for the $Prx1^{Cre/+};Wt1^{loxP/loxP}$ embryos/pups at all developmental stages.

EMBRYO STAGE	TOTAL # MUTANTS	GENDER/DIAPHRAGM PHENOTYPES	CORRESPONDING FIGURES
E11.5	4	Female. PPFs not formed properly; cells of PHMP and down-growth from body wall not connected on either side.	No image
		Female. PPFs not formed properly; cells of PHMP and down-growth from body wall not connected on either side.	No image
		Female. PPFs not formed properly; cells of PHMP and down-growth from body wall not connected on either side.	No image
		Female. No phenotype information.	No image
E12.5	6	Male. PPF not formed properly; cells of PHMP and down-growth from body wall not connected on left side.	No image
		Female. PPF not formed properly; cells of PHMP and down-growth from body wall not connected on left side.	5.6 (B)
		Male. PPF not formed properly; cells of PHMP and down-growth from body wall not connected on left side.	No image
		Male. No phenotype information.	No image
		Female. No phenotype information	No image
		Female. No phenotype information.	No image
E14.5	3	Hole left side, dorsal, with liver herniation.	5.2 (B)
		Hole left side, ventral, with liver herniation.	5.2 (C)
		Hole in right side dorsal, possible liver herniation.	No image
E16.5	8	Female. Bilateral holes, dorsal, with liver herniation.	5.3 (B)
		Male. Hole left side, dorsal, with liver herniation.	5.3 (C)
		Female. No obvious hole/hernia – possible thinning of diaphragm on left side. NB: Embryo sectioned in the coronal plane.	5.3 (D)
		Male. No obvious hole/hernia. Possible thinning at edges.	5.3 (E)
		Male. No obvious hole/hernia.	5.3 (F)
		Female. Bilateral holes, dorsal, with liver herniation.	5.3 (H)
		Female. No obvious hole/hernia.	No image
		Male. No obvious hole/hernia.	No image
E18.5	1	Bilateral thinning of the diaphragm, dorsal. No obvious hole/herniation.	No image
E19.5	4	Bilateral holes, dorsal, with liver herniation.	5.1 (B)
		Small bilateral holes/thinning of the diaphragm, dorsal.	5.1 (C)
		Hole left side, dorsal.	5.1 (G)
		Hole left side, dorsal.	No image
P0	4	Male. Large hole left side, dorsal, with stomach and liver herniation.	5.1 (D)
		Male. Large hole left side, dorsal, with stomach and liver herniation.	5.1 (E)
		Female. Large hole left side, dorsal, with stomach and liver herniation.	5.1 (F)
		Female. Large hole left side, dorsal, with stomach and liver herniation.	No image

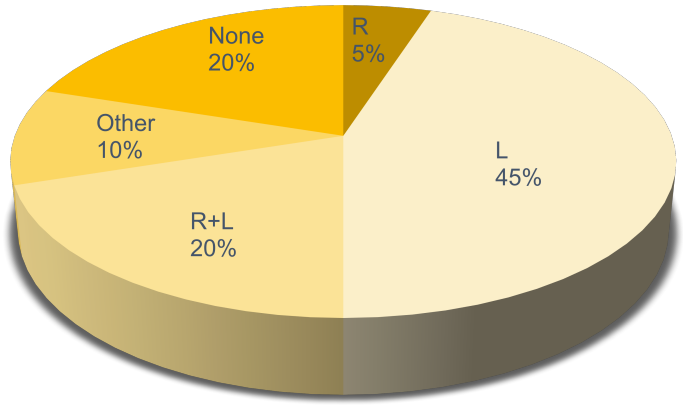


Figure 5.4. The percentage of diaphragmatic hernias in different locations in $Prx1^{Cre/+};Wt1^{loxP/loxP}$ embryos/pups aged E14.5 and older. *The diaphragmatic phenotypes of all $Prx1^{Cre/+};Wt1^{loxP/loxP}$ embryos/pups (E14.5-P0) were examined and the presence/location of the diaphragmatic hernia was recorded. All hernias in R (right), L (left) and R+L (bilateral) categories were dorsal. The two cases in the "other" category include a ventrally located hernia, and a thinning of the diaphragm but no hole. (n=20)*

5.3 PPF development is disrupted in *$Prx1^{Cre/+};Wt1^{loxP/loxP}$* embryos

To better understand the cause of the defects, embryos were analysed at earlier stages of development (E11.5 and E12.5). As described in the introduction (section 1.4), structures present during embryonic development, known as the pleuroperitoneal folds (PPFs), function in, and are necessary for correct diaphragm development. The PPFs are usually formed between E10.5-E12.5, and are mesodermal in origin. They establish the initial separation between the thoracic and peritoneal cavities, and go on to generate the connective tissue of the diaphragm. It is also believed that the cells of the PPFs guide the myogenic cells of the diaphragm into place, although they do not contribute to the muscle tissue themselves (Merrell *et al.*, 2015; Carmona *et al.*, 2016). Hence, diaphragmatic hernias are often caused by the disrupted development of the PPFs. Also described in the introduction (section 1.4), is the posthepatic mesenchymal plate (PHMP), which is a sheet of cells that resides on the surface of the liver, either side of the septum transversum. The cells of the PHMP migrate over the surface of the liver and infiltrate/fuse with the developing PPFs to form a continuous band of cells, separating the body cavities (Iritani, 1984; Carmona *et al.*, 2016). E11.5 and E12.5 *$Prx1^{Cre/+};Wt1^{loxP/loxP}$* embryos were sectioned transversely and stained with H&E. It was evident that this continuous band of cells that should separate the body cavities

had failed to form correctly in the mutant embryos. When compared to control littermates, large gaps were present between the PHMP and the PPFs in the mutants, resulting in a lack of separation of the thoracic and peritoneal cavities (Figures 5.5 and 5.6). The E11.5 embryos illustrated in Figure 5.5 are *Prx1*$^{Cre/+}$;*Wt1*$^{GFP/loxP}$ (mutant) and *Prx1*$^{+/+}$;*Wt1*$^{GFP/loxP}$ (control), and these are described in detail in section 5.5. Essentially, instead of both copies of *Wt1* being flanked by loxP sites, one copy is and the other has GFP knocked in, disrupting function. Therefore, the phenotype was the same as for the *Prx1*$^{Cre/+}$;*Wt1*$^{loxP/loxP}$ embryos.

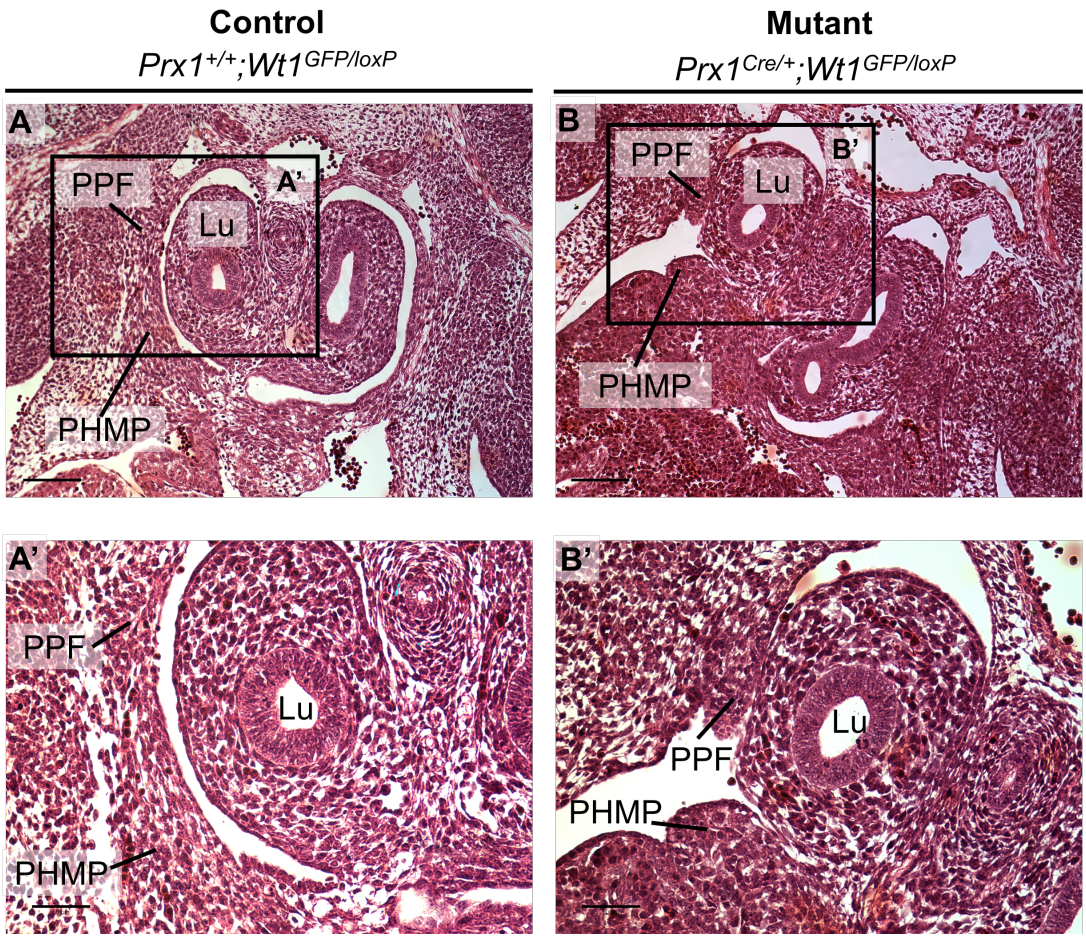


Figure 5.5. E11.5 Prx1$^{Cre/+}$;Wt1$^{GFP/loxP}$ embryos have disrupted PPF formation. *Male Prx1-Cre;Wt1$^{GFP/+}$ mice were crossed with female Wt1$^{loxP/loxP}$ mice and the embryos were collected at E11.5 and processed for H&E staining.* ***(B)*** *A representative image of a Prx1$^{Cre/+}$;Wt1$^{GFP/loxP}$ embryo, illustrating disrupted PPF development, causing the presence of a gap between the PPF and PHMP (star in* ***B*** *and* ***B'****). A littermate control is shown for comparison* ***(A)****. Embryos were sectioned in the transverse plane.* ***A'****, and* ***B'*** *are magnified images of the areas indicated in* ***A*** *and* ***B****. (Abbreviations: Lu: Lungs, PPF: pleuroperitoneal fold, PHMP: posthepatic mesenchymal plate). (Scale bar = 100μm (A,B), 50μm (A',B')).*

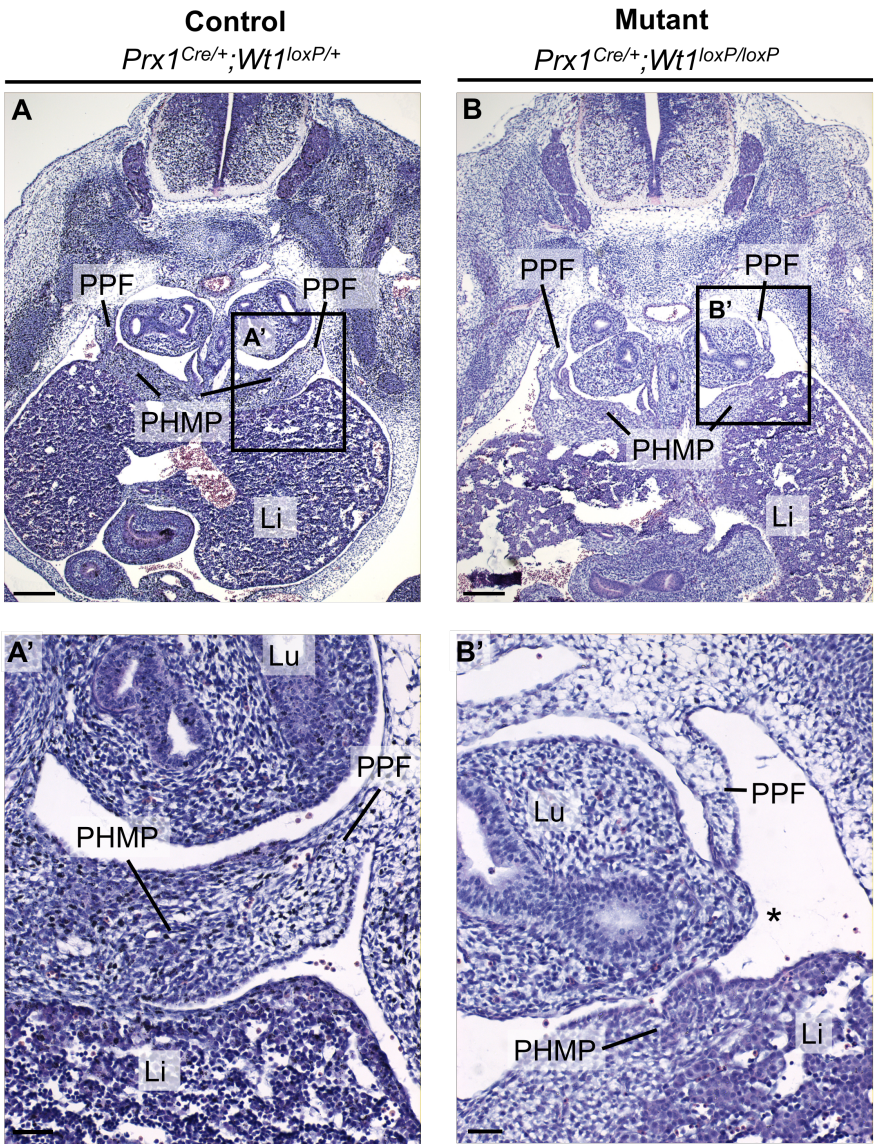


Figure 5.6. E12.5 Prx1$^{Cre/+}$;Wt1$^{loxP/loxP}$ embryos have disrupted PPF formation. *Male Prx1$^{Cre/+}$;Wt1$^{loxP/+}$ mice were crossed with female Wt1$^{loxP/loxP}$ mice and the embryos were collected at E12.5 and processed for H&E staining. 4/18 embryos were Prx1$^{Cre/+}$;Wt1$^{loxP/loxP}$. **(B)** A representative image of a Prx1$^{Cre/+}$;Wt1$^{loxP/loxP}$ embryo, illustrating disrupted PPF development, causing the presence of a gap between the PPF and PHMP (asterisk in **B'**). A littermate control is shown for comparison **(A)**. Embryos were sectioned in the transversel plane. **A'**, and **B'** are magnified images of the areas indicated in **A** and **B**. (Abbreviations: Lu: Lungs, Li: Liver, PPF: pleuroperitoneal fold, PHMP: posthepatic mesenchymal plate). (Scale bar = 200μm (A,B), 50μm (A',B')).*

5.4 Prx1-Cre labelling of the developing diaphragm

An essential first step in elucidating the causative mechanism(s) responsible for the developmental defect was to know exactly which cells were being affected by the conditional deletion of *Wt1*. To begin to understand this, the *Prx1-Cre;R26R-mTmG* lineage tracing model was used. WT1 is expressed in both the PPFs and the PHMP (Carmona *et al.*, 2016), and therefore we wanted to know whether one, or both, of these structures was being affected by *Wt1* deletion in the Prx1-Cre lineage.

Male *Prx1-Cre* mice were crossed with female *R26R-mTmG* mice and the embryos collected at E11.5 and E12.5. Transverse sections were stained with anti-GFP and anti-Wt1 antibodies. As shown in Figure 5.7, WT1 was expressed in the cells of the PHMP and PPFs. However, whilst the cells of the PPFs expressed GFP and were thus Prx1-Cre lineage positive, the cells of the PHMP did not express GFP, and therefore were not derived from the Prx1-Cre lineage. This was particularly evident in the E11.5 embryos (Figure 5.7 A,B). At this embryonic stage, the PPFs and PHMP have just begun to fuse and therefore a boundary can still be observed between the two structures. This boundary was clearly reflected by the distinct domains of GFP expressing cells present in the E11.5 embryos. Figures 5.7 A and B represent consecutive sections (B anterior to A). In A' and A'' the PPFs (GFP+) and PHMP (GFP-) can be seen just abutting one another, whilst in B' and B'', it is clear that they have fused and have begun to form a continuous band of cells. Furthermore, especially evident in B", it appeared that the GFP+ PPF cells were migrating downwards and infiltrating the PHMP. At E12.5 the thoracic and peritoneal cavities are completely separated by the fully formed PPF/PHMP continuum. As shown in Figure 5.7 C, the expression of GFP was still localised to the edges of this continuum at E12.5 (i.e. the component derived from the PPFs), but the two structures had completely fused. Moreover, as indicated by the red arrowhead in Figure 5.7 C'', the mesothelial cells of the developing diaphragm did not express GFP and therefore were not Prx1-Cre lineage positive. As discussed later, WT1 was still expressed in the diaphragmatic mesothelial cells of the $Prx1^{Cre/+};Wt1^{loxP/loxP}$ mutant embryos, therefore corroborating this result. In summary, these results revealed that only the PPFs were Prx1-Cre lineage positive, and not the PHMP. Therefore, the deletion of *Wt1* in the Prx1-Cre

lineage could only have affected the cells of the PPFs, hence these structures became the focus of subsequent investigation.

Figure 5.7 (continued on next page)

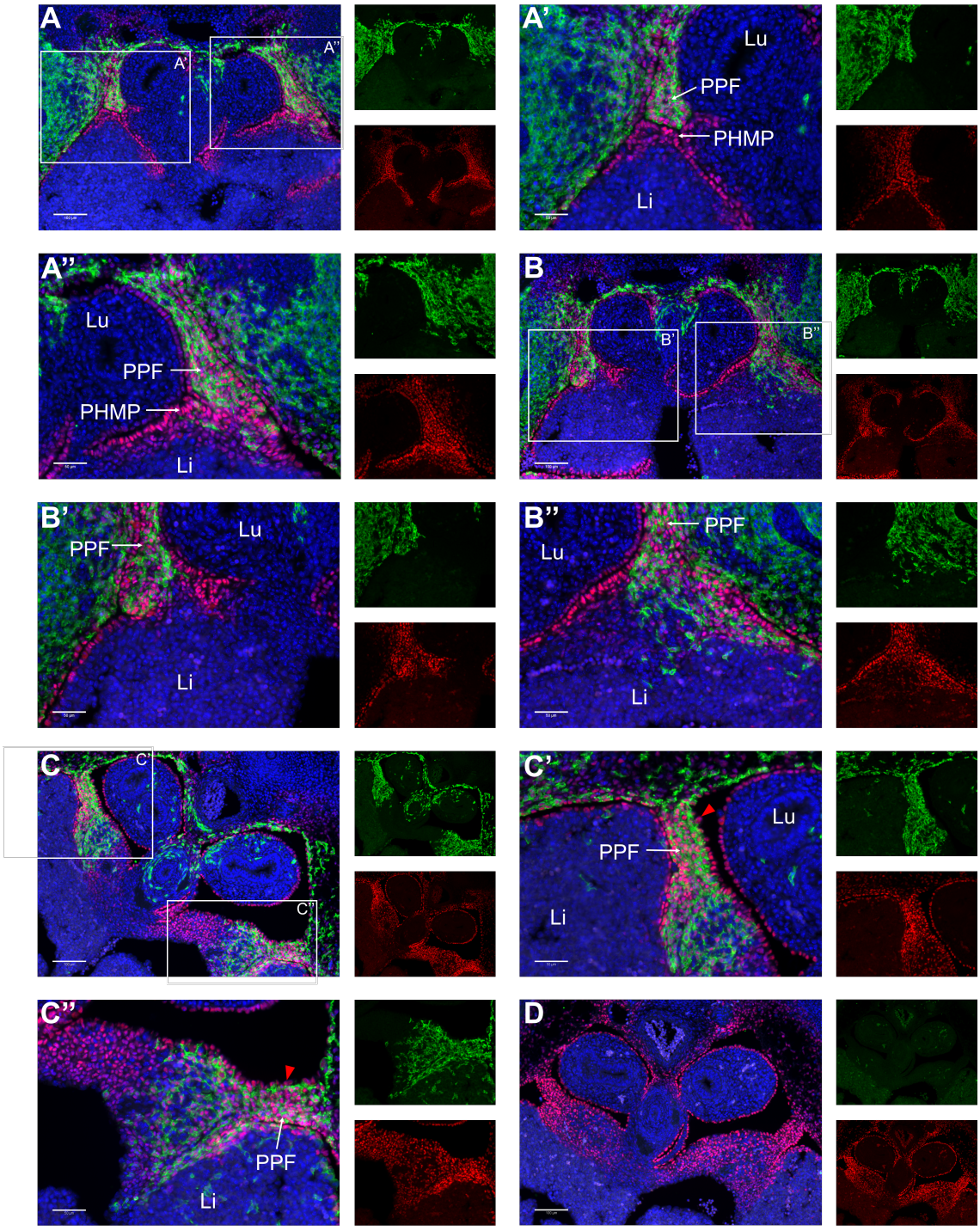


Figure 5.7. The PPFs, but not the PHMP, are Prx1-Cre lineage positive. *Male $Prx1^{Cre/+}$ mice were crossed with female R26R-mTmG mice and the embryos were collected at E11.5* ***(A,B)*** *or E12.5* ***(C)*** *and processed for immunofluorescence. Embryos were sectioned in the transverse plane. Sections were stained with an anti-GFP antibody (green – upper inset), an anti-Wt1 antibody (red – lower inset) and DAPI (blue).* ***A*** *and* ***B*** *are consecutive sections taken from the same embryo (****B*** *anterior to* ***A****). WT1 expression was seen in the PPFs and PHMP of the E11.5 embryos, but GFP expression was only observed in the PPFs. Once fused, the GFP expressing cells appeared to migrate into the PHMP to form a continuum (best illustrated in* ***B''****). The fully developed PPF/PHMP continuum is visible in* ***C****, GFP expressing cells were located at the edges of this continuum. The mesothelial cells of the PPFs did not express GFP (red arrowhead in* ***C'*** *and* ***C''****).* ***A'&A'', B'&B'', C'&C''*** *are magnified images of the areas indicated in* ***A, B*** *and* ***C****. An image of a $Prx1^{+/+}$;R26R-mTmG E12.5 littermate is shown as a control* ***(D)****. (Abbreviations: Lu: Lungs, Li: Liver, PPF: pleuroperitoneal fold, PHMP: posthepatic mesenchymal plate). (Scale bar = 100μm (A,B,C), 50μm (A',A'',B',B'',C',C'')). (n=3).*

5.5 PPF development is disrupted in $Prx1^{Cre/+};Wt1^{GFP/loxP}$ embryos

To aid further investigations, a new mouse model was generated. Male *Prx1-Cre;*$Wt1^{GFP/+}$ mice were crossed with female $Wt1^{loxP/loxP}$ mice. In the resulting litters, approximately one quarter of the embryos were $Prx1^{Cre/+};Wt1^{GFP/loxP}$. Therefore, one copy of *Wt1* was flanked by loxP sites, and the other had GFP knocked-in, replacing exon 1 and disrupting function. Hence, all *Wt1* expressing cells fluoresced green, and upon Cre mediated loxP recombination (driven by the expression of the *Prx1* enhancer element), the second copy of *Wt1* was conditionally deleted. Due to the GFP knock-in, even the cells in which both copies of *Wt1* had been deleted, fluoresced green. Consequently, it was possible to determine exactly where *Wt1* would normally be expressed, but had been deleted, and the resulting phenotype of these structures/cells. Embryos were collected at E11.5, sectioned transversely and stained with an anti-Wt1 antibody and an anti-GFP antibody. As illustrated in Figure 5.8, PPF development was clearly disrupted in the $Prx1^{Cre/+};Wt1^{GFP/loxP}$ embryos, with an obvious gap present between the PPFs and PHMP, which was not the case in the littermate controls. Furthermore, the PPFs of the controls expressed WT1, but this expression was totally lacking in the $Prx1^{Cre/+};Wt1^{GFP/loxP}$ embryos. Additionally, strong GFP expression was observed in the disrupted PPFs of the Prx$1^{Cre/+};Wt1^{GFP/loxP}$ embryos, thus confirming that *Wt1* would normally be expressed in these cells. Intriguingly, the GFP signal in the PPFs of the $Prx1^{Cre/+};Wt1^{GFP/loxP}$ embryos was much stronger than that in the control littermates. We hypothesise that this may be a consequence of the disrupted migration of these PPF cells, causing them to become bunched up, rather than

migrating down towards the PHMP, therefore making the GFP signal seem brighter due to the accumulation of cells in the region. Therefore, as predicted by the lineage tracing studies (section 5.4), *Wt1* deletion was observed in the PPFs of the $Prx1^{Cre/+};Wt1^{GFP/loxP}$ embryos, and this deletion resulted in the defective development of the PPF/PHMP continuum, which we hypothesised was due to disrupted migration of the PPF cells.

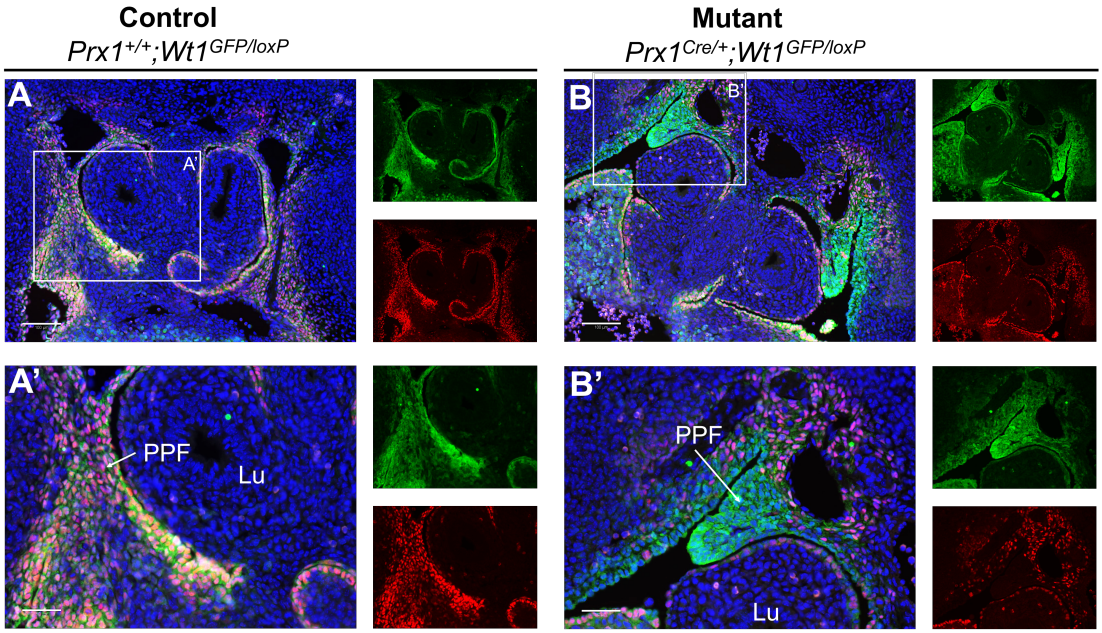


Figure 5.8. Wt1 deletion in the PPFs causes disrupted PPF development in $Prx1^{Cre/+};Wt1^{GFP/loxP}$ embryos. *Male $Prx1^{Cre/+};Wt1^{GFP/+}$ mice were crossed with female $Wt1^{loxP/loxP}$ mice and the embryos were collected at E11.5 and processed for immunofluorescence. Embryos were sectioned in the transverse plane. Sections were stained with an anti-GFP antibody (green – upper inset), an anti-Wt1 antibody (red – lower inset) and DAPI (blue). Representative images of a $Prx1^{Cre/+};Wt1^{GFP/loxP}$ embryo are shown in **(B** and **B')**, the disrupted PPF expressed GFP but not WT1, indicating deletion in this structure. A littermate control is shown for comparison **(A, A')** ($Prx1^{+/+};Wt1^{GFP/loxP}$), WT1 expression was observed in the fully formed PPF. **(A'** and **B')** are magnified images of the areas indicated in **(A** and **B)**. (Abbreviations: Lu: Lungs, PPF: pleuroperitoneal fold. (Scale bar = 100μm (A,B), 50μm (A',B')). (n=3).*

5.6 Muscle fibre orientation is altered in $Prx1^{Cre/+};Wt1^{loxP/loxP}$ embryos

Older embryos were also investigated, to assess both WT1 expression and the muscle architecture of the diaphragm. Sections from E16.5 $Prx1^{Cre/+};Wt1^{loxP/loxP}$ embryos were stained with anti-Wt1 and anti-MF20 antibodies. The anti-MF20 antibody detected the heavy chain of Myosin II and thus labelled the muscle. Interestingly, as shown in

Figure 5.9, whilst the cells at the edge of the diaphragm (the mesothelium), retained their WT1 expression in the mutant (red arrows), there was a loss of WT1 expression/ WT1 expressing cells within the diaphragm itself (white asterisks). Moreover, as previously described, in addition to forming the connective tissue of the diaphragm, the cells of the PPFs guide the myogenic cells of the diaphragm into place (Merrell *et al.*, 2015). Therefore, if the migration of the PPF cells is disrupted, the muscle also does not develop correctly. Moreover, a thickening and mis-orientation of the muscle fibres at the edges of the diaphragm around the hernia, has been described in other models, and this is thought to be the result of an inability to migrate correctly (Clugston *et al.*, 2006). This phenotype was evident in the $Prx1^{Cre/+};Wt1^{loxP/loxP}$ embryos (Figure 5.9). In the control littermates, the muscle fibres lay horizontally, however, in the mutants, where the diaphragm ends, the fibres were arranged vertically (white arrow). Furthermore, the diaphragm appeared to thicken in the region just before the hole. This thickening is perhaps more obvious in the H&E stained images of the E14.5 and E16.5 embryos (Figures 5.2 and 5.3). Crucially, aside from the mis-orientation, the actual muscle fibres themselves were comparable in the control and mutant embryos. Therefore, these results provide support for the hypothesis that a lack of WT1 expression in the mesenchymal cells of the PPFs in $Prx1^{Cre/+};Wt1^{loxP/loxP}$ embryos, results in the disrupted migration of the PPF cells, which, in turn prevents the myogenic cells from migrating correctly, leading to a hole in the diaphragm and incomplete separation of the thoracic and peritoneal cavities.

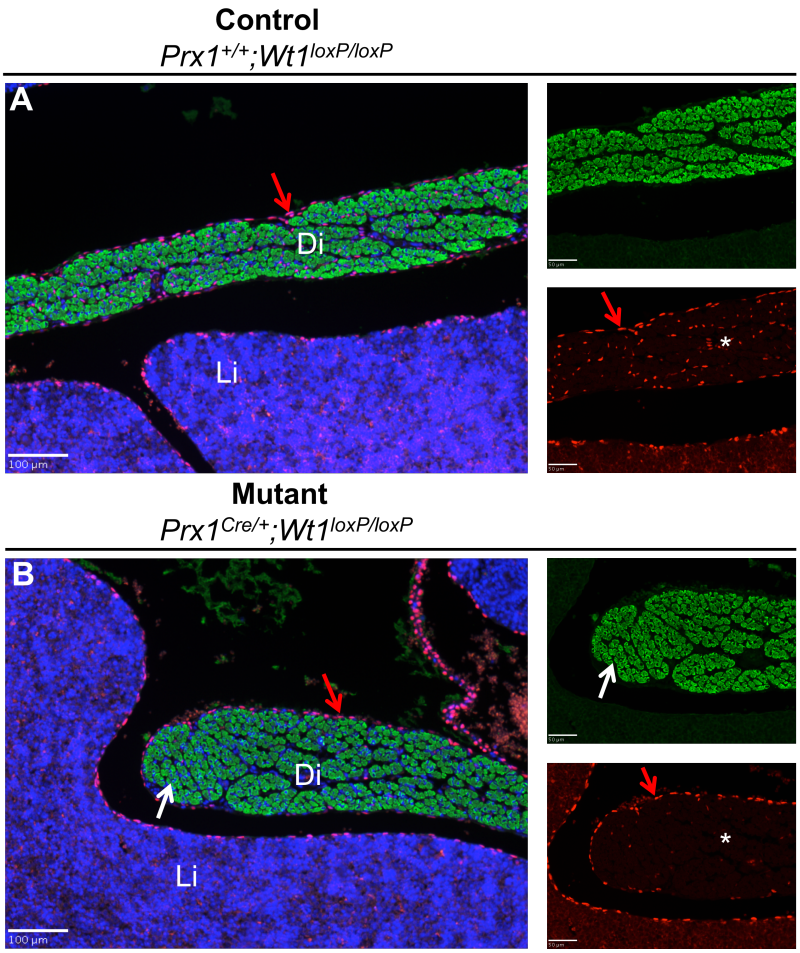


Figure 5.9. E16.5 $Prx1^{Cre/+};Wt1^{loxP/loxP}$ embryos have thickened diaphragms and disrupted muscle fibre orientation. *Male $Prx1^{Cre/+};Wt1^{loxP/+}$ mice were crossed with female $Wt1^{loxP/loxP}$ mice and the embryos were collected at E16.5 and processed for immunofluorescence staining. Embryos were sectioned in the sagittal plane. Sections were stained with an anti-MF20 antibody (green – upper inset), an anti-Wt1 antibody (red - lower inset) and DAPI (blue). A representative image of a $Prx1^{Cre/+};Wt1^{loxP/loxP}$ embryo is shown in **(B)**. The muscle fibres were arranged vertically at the edge of the malformed diaphragm (white arrow) and this region was thickened. WT1 expression was lost in the mesenchymal cells of the diaphragm (white asterisk) but not in the mesothelial cells (red arrow). A littermate control ($Prx1^{+/+};Wt1^{loxP/loxP}$) is shown for comparison **(A)**. (Abbreviations: Li: Liver, Di: Diaphragm). (Scale bar = 100µm). (n=2).*

5.7 Investigating the molecular mechanisms responsible for disrupted diaphragm development

Thus far it has been shown that *Wt1* deletion in the Prx1-Cre lineage results in defective diaphragm development. This deletion specifically affects the cells of the PPFs, and we hypothesise that their migration is disrupted, therefore suggesting that WT1 is required for the correct migration of the PPF cells during diaphragm

development. To further interrogate the molecular mechanisms responsible for this defect, several lines of enquiry were followed.

As described in the introduction (1.2), WT1 is known to be required for EMT during development, particularly in the developing heart. The conditional deletion of *Wt1* in the epicardium results in a reduction in the level of SNAI1 (a mesenchymal cell marker) and an increase in the level of CDH1 (an epithelial cell marker), and the lack of EMT ultimately results in disrupted coronary vasculature formation (Martínez-Estrada *et al.*, 2010). Moreover, it has recently been shown that CDH1 expression is increased in the PHMP cells of E11.5 *G2-Gata4*^{Cre}*;Wt1*$^{loxP/loxP}$ embryos (which subsequently present with diaphragmatic hernias), suggesting that WT1 may also be important for EMT in the developing diaphragm (Carmona *et al.*, 2016). Given this, the expression of CDH1 and VIM (a mesenchymal cell marker) was checked in our *Prx1*$^{Cre/+}$*;Wt1*$^{GFP/loxP}$ embryos. Sections from E11.5 *Prx1*$^{Cre/+}$*;Wt1*$^{GFP/loxP}$ embryos and *Prx1*$^{+/+}$*;Wt1*$^{GFP/loxP}$ littermates were stained with either an anti-Vimentin (VIM) antibody or an anti-E-cadherin (CDH1) antibody. The sections stained with the anti-Vimentin antibody were co-stained with an anti-Wt1 antibody and representative images can be seen in Figure 5.10 (A,B). As expected, the development of the PPFs in the *Prx1*$^{Cre/+}$*;Wt1*$^{GFP/loxP}$ embryos was disrupted, and WT1 expression was clearly lacking. However, no difference in the expression of VIM was observed between the *Prx1*$^{Cre/+}$*;Wt1*$^{GFP/loxP}$ mutants and *Prx1*$^{+/+}$*;Wt1*$^{GFP/loxP}$ controls. The sections stained with the anti-E-cadherin antibody were co-stained with an anti-GFP antibody, so the PPFs were clearly marked (Figure 5.10 C,D). Whilst CDH1 was strongly expressed in the developing lung, no expression was seen in the PPFs of either the *Prx1*$^{Cre/+}$*;Wt1*$^{GFP/loxP}$ mutants or *Prx1*$^{+/+}$*;Wt1*$^{GFP/loxP}$ controls. Therefore, we did not observe upregulated CDH1 expression in the mutant embryos. Together these results indicate that conditional *Wt1* deletion in the PPFs does not result in disrupted EMT, at least at E11.5.

Whilst we hypothesised that the migration of the PPF cells was disrupted, we also considered the possibility that the deletion of *Wt1* was affecting the proliferation of the PPF cells. A lack of proliferation could prevent the PPFs from expanding sufficiently

to meet the PHMP. To check this, sections from E11.5 *Prx1*$^{Cre/+}$;*Wt1*$^{GFP/loxP}$ mutants and *Prx1*$^{+/+}$;*Wt1*$^{GFP/loxP}$ controls were stained with an anti-Ki67 antibody. As shown in Figure 5.11, the sections were co-stained with an anti-GFP antibody to highlight the PPFs. As expected given their early developmental stage, many KI67 positive, and thus proliferating cells, were observed throughout the embryos. However, we did not see an obvious reduction in the number of proliferating cells in the disrupted PPFs of the mutant *Prx1*$^{Cre/+}$;*Wt1*$^{GFP/loxP}$ embryos, thus suggesting that proliferation was not decreased as a result of *Wt1* deletion. A section through the neural tube is included in Figure 5.11 to illustrate that not all cells of the embryo stained positive for KI67, therefore showing that the antibody did stain specifically.

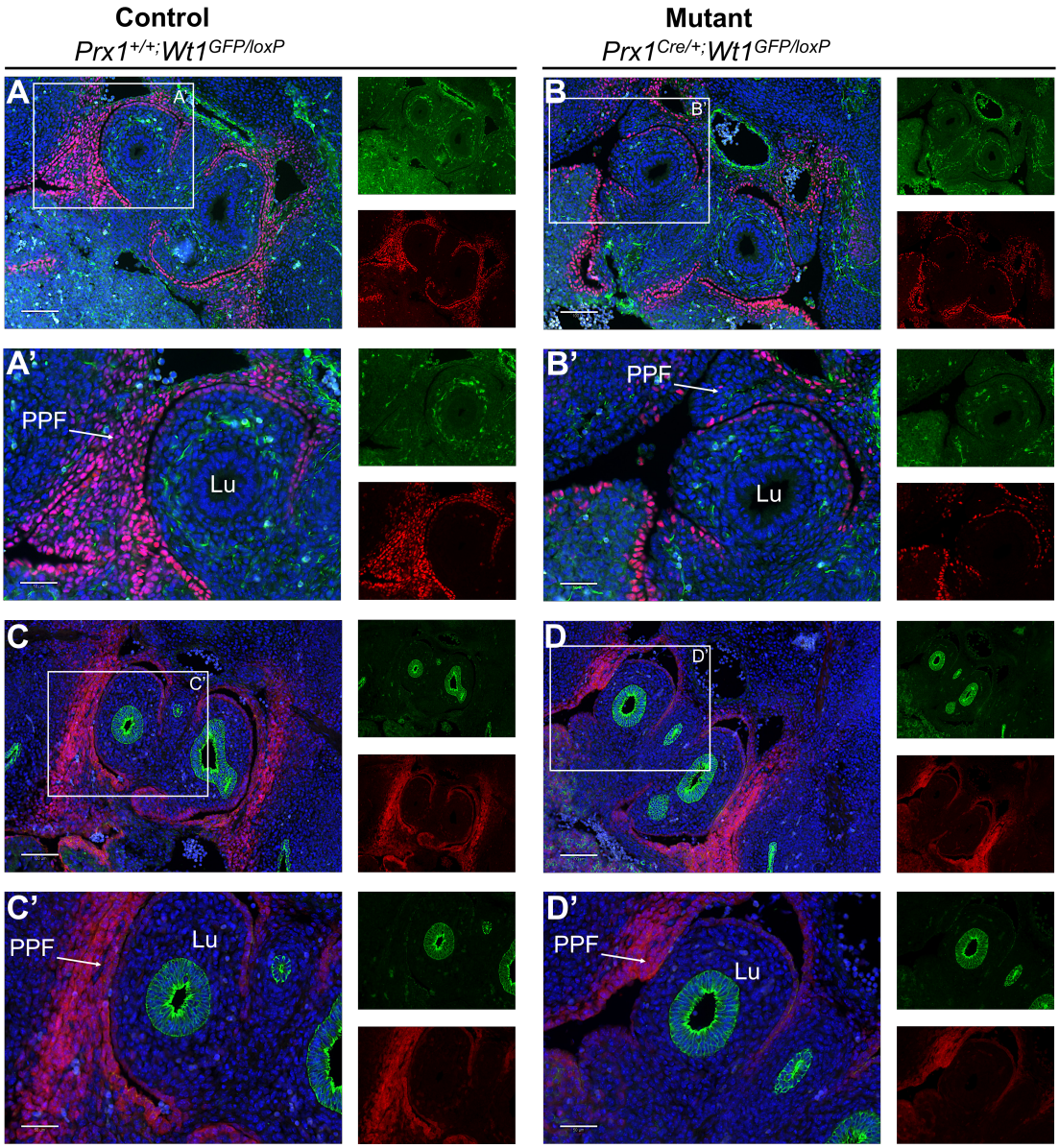


Figure 5.10. Wt1 deletion in the PPFs does not affect VIM or CDH1 expression in Prx1$^{Cre/+}$;Wt1$^{GFP/loxP}$ embryos. *Male Prx1$^{Cre/+}$;Wt1$^{GFP/+}$ mice were crossed with female Wt1$^{loxP/loxP}$ mice and the embryos were collected at E11.5 and processed for immunofluorescence. Embryos were sectioned in the transverse plane.* ***(A,A',B,B')*** *Sections were stained with an anti-Vimentin antibody (green – upper inset), an anti-Wt1 antibody (red – lower inset) and DAPI (blue). Representative images of a Prx1$^{Cre/+}$;Wt1$^{GFP/loxP}$ embryo are shown in* ***(B*** *and* ***B')****, and a littermate control in* ***(A*** *and* ***A')*** *(Prx1$^{+/+}$;Wt1$^{GFP/loxP}$). WT1 expression was lost from the PPFs in the mutant, but no difference in VIM (vimentin) expression was observed.* ***(C,C',D,D')*** *Sections were stained with an anti-E-cadherin antibody (green - upper inset), an anti-GFP antibody (red – lower inset) and DAPI (blue). Representative images of a Prx1$^{Cre/+}$;Wt1$^{GFP/loxP}$ embryo are shown in* ***(D*** *and* ***D')****, and a littermate control in* ***(C*** *and* ***C')*** *(Prx1$^{+/+}$;Wt1$^{GFP/loxP}$). No difference in CDH1 (E-cadherin) expression was observed between the control and mutant.* ***A',B',C',D'*** *are magnified images of the areas indicated in* ***A,B,C,D****. (Abbreviations: Lu: Lungs, PPF: pleuroperitoneal fold). (Scale bar = 100μm (A,B,C,D), 50μm (A',B',C',D')). (n=2).*

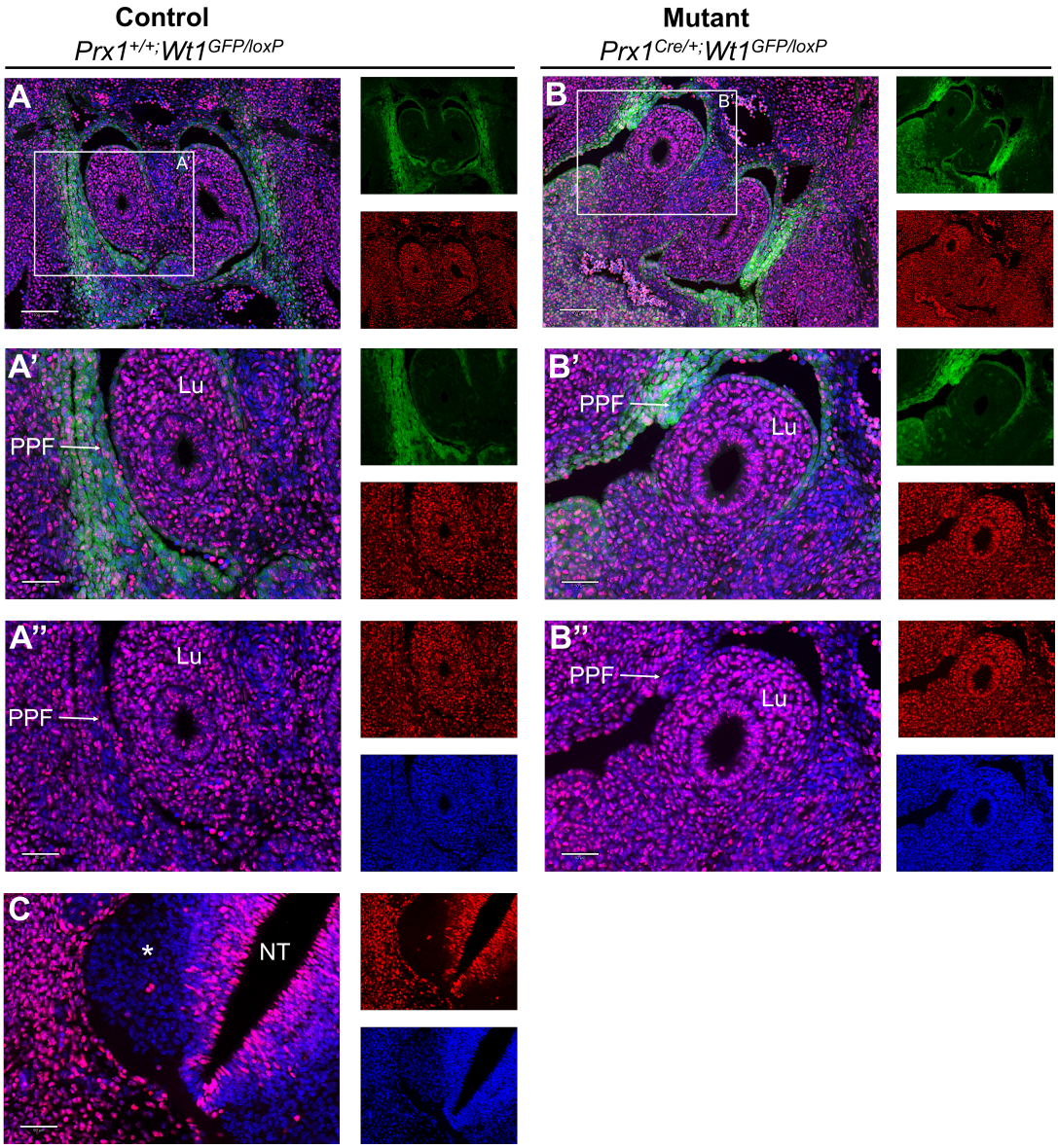


Figure 5.11. Wt1 deletion in the PPFs does not affect proliferation in Prx1$^{Cre/+}$;Wt1$^{GFP/loxP}$ embryos. *Male Prx1$^{Cre/+}$;Wt1$^{GFP/+}$ mice were crossed with female Wt1$^{loxP/loxP}$ mice and the embryos were collected at E11.5 and processed for immunofluorescence. Embryos were sectioned in the transverse plane. Sections were stained with an anti-GFP antibody (green – upper inset), an anti-Ki67 antibody (red – lower inset) and DAPI (blue). Representative images of a Prx1$^{Cre/+}$;Wt1$^{GFP/loxP}$ embryo are shown in **(B,B',B'')**, and a littermate control in **(A,A',A'')** (Prx1$^{+/+}$;Wt1$^{GFP/loxP}$). GFP expression marked the PPFs, and their development was evidently disrupted in the mutant embryos, however there was no obvious difference in the number of proliferating cells in the PPFs of the control and mutant embryos. **(A'' and B'')** show only the KI67 staining (red) and DAPI (blue) so the proliferating cells can be seen more clearly. **(C)** shows a section through the neural tube to illustrate the specificity of the anti-Ki67 antibody. The white asterisk highlights cells that did not stain positive for KI67. (Abbreviations: Lu: Lungs, PPF: pleuroperitoneal fold, NT: neural tube). (Scale bar = 100μm (A,B,), 50μm (A',A'',B',B'',C)). (n=3).*

It is well known that the retinoic acid signalling pathway functions in diaphragm development, indeed one of the most common mouse models of CDH utilises nitrofen to inhibit retinoic acid synthesis and thus causes diaphragmatic hernias (Greer, Babiuk and Thebaud, 2003; Mey *et al.*, 2003). Furthermore, in the epicardium, WT1 transcriptionally activates *Raldh2*, and RALDH2 catalyses the formation of retinoic acid from retinaldehyde (Guadix *et al.*, 2011). Therefore, an obvious explanation for the formation of diaphragmatic hernias in our model is disrupted retinoic acid signalling in the PPFs, as a result of *Wt1* deletion. Hence, RALDH2 expression was checked in E11.5 $Prx1^{Cre/+};Wt1^{GFP/loxP}$ mutants and $Prx1^{+/+};Wt1^{GFP/loxP}$ controls, using an anti-Raldh2 antibody. However, as illustrated in Figure 5.12, we observed an increase in RALDH2 expression in the PPFs of the mutant embryos. Very low expression of RALDH2 was observed in the PPFs of the control littermates, compared to the strong signal seen in the mutants. Given what is known about WT1, RALDH2 and diaphragm development this result was surprising, however it is not the first time that it has been described. Carmona *et al*. (2016), showed a similar result regarding the PPFs when deleting *Wt1* using the $G2\text{-}Gata4^{Cre}$ mouse line (Carmona *et al.*, 2016). The explanation they gave for this increased RALDH2 expression was that the intermediate mesoderm of the renal ridges persists in the PPFs of the $G2\text{-}Gata4^{Cre};Wt1^{loxP/loxP}$ embryos, as evidenced by the *in situ* hybridisation of *Pax2* (a marker of the intermediate mesoderm). As the intermediate mesoderm expresses high levels of RALDH2, this persistence results in an apparent increase in PPF RALDH2 expression (Carmona *et al.*, 2016). To understand whether this was also the case in our mutants, E11.5 $Prx1^{Cre/+};Wt1^{GFP/loxP}$ embryos were stained with an anti-Pax2 antibody. However, as shown in Figure 5.12 (C,D), no PAX2 expression was observed in the PPFs. Therefore, currently we do not know why we see increased RALDH2 expression in the PPFs of the $Prx1^{Cre/+};Wt1^{GFP/loxP}$ embryos, and this is discussed further in 5.8.

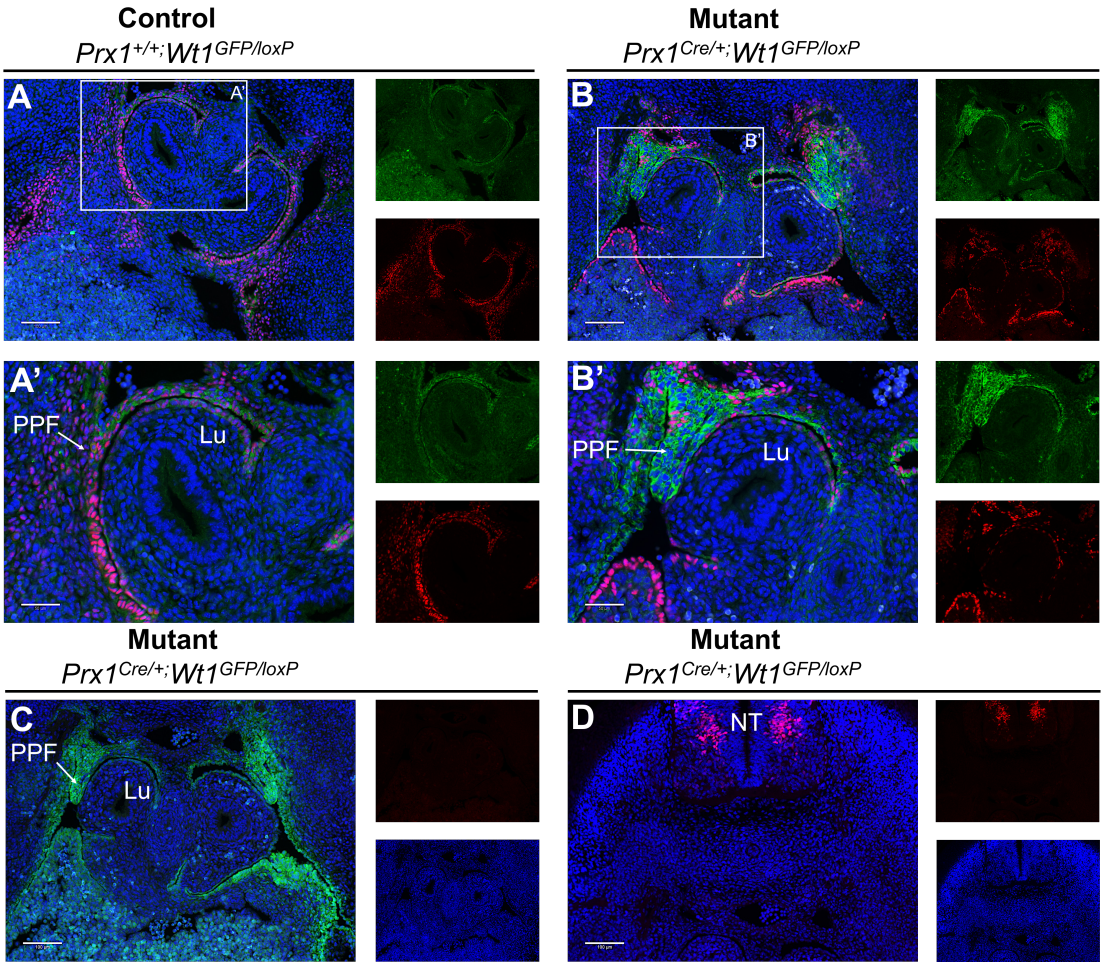


Figure 5.12. The PPFs of Prx1$^{Cre/+}$;Wt1$^{GFP/loxP}$ embryos exhibit increased RALDH2 expression compared to Prx1$^{+/+}$;Wt1$^{GFP/loxP}$ littermate controls. *Male Prx1$^{Cre/+}$;Wt1$^{GFP/+}$ mice were crossed with female Wt1$^{loxP/loxP}$ mice and the embryos were collected at E11.5 and processed for immunofluorescence. Embryos were sectioned in the transverse plane.* ***(A,A',B,B')*** *Sections were stained with an anti-Raldh2 antibody (green – upper inset), an anti-Wt1 antibody (red – lower inset) and DAPI (blue). Representative images of a Prx1$^{Cre/+}$;Wt1$^{GFP/loxP}$ embryo are shown in* ***(B,B')****, and a littermate control in* ***(A,A')*** *(Prx1$^{+/+}$;Wt1$^{GFP/loxP}$). WT1 expression was lost from the PPFs in the mutant* ***(B,B')****, and RALDH2 expression was increased.* ***(C,D)*** *Sections were stained with an anti-Pax2 antibody (red – upper inset), an anti-GFP antibody (green) and DAPI (blue – lower inset). Representative images of a Prx1$^{Cre/+}$;Wt1$^{GFP/loxP}$ embryo are shown in* ***(C,D)****. The lack of PAX2 expression in the PPFs suggests they are not intermediate mesoderm. The neural tube is shown in* ***(D)*** *to illustrate that the anti-Pax2 antibody was working. (Abbreviations: Lu: Lungs, PPF: pleuroperitoneal fold, NT: Neural tube). (Scale bar = 100μm (A,B,C,D), 50μm (A',B')). (n=2).*

As our focus was on disrupted migration of the PPF cells, we also considered the possibility that problems with cell adhesion were occurring in the mutant embryos. β-catenin (CTNNB1) is an important component of adherens junctions and promotes cell adhesion by binding cadherins and thus tethering the cell membrane to the actin cytoskeleton, via α-catenin. A membrane-associated, subcellular pool of stable β-catenin fulfils this role (Bienz, 2005; Nelson, 2008). Therefore, CTNNB1 expression was checked in E11.5 $Prx1^{Cre/+};Wt1^{GFP/loxP}$ mutants and $Prx1^{+/+};Wt1^{GFP/loxP}$ controls. As shown in Figure 5.13, the pattern of CTNNB1 expression in the PPFs was not the same in the mutants and controls. In the controls, expression was observed at the membranes of the PPF cells, however in the mutants this membranous expression was not obvious. However, in other surrounding structures, for example the lung, the expression of CTNNB1 was comparable across the two genotypes. These data are very preliminary, as due to time constraints only one embryo per genotype has been analysed so far. Therefore, significant additional work is required, as discussed further in 5.8.

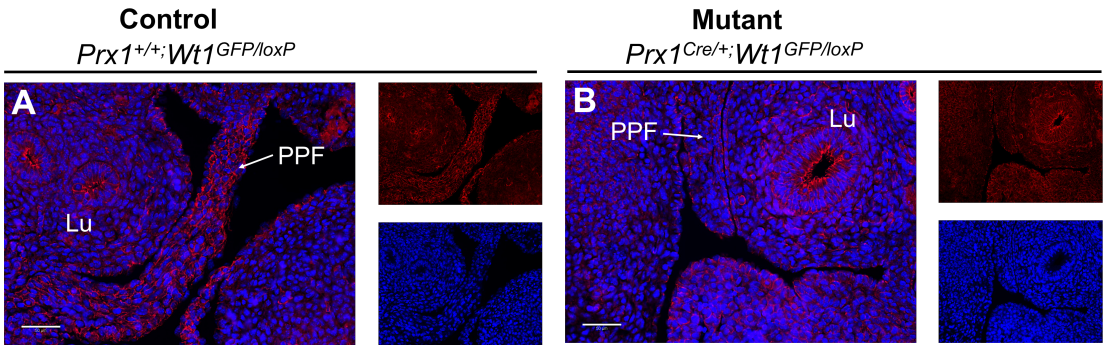


Figure 5.13. The PPFs of $Prx1^{Cre/+};Wt1^{GFP/loxP}$ embryos exhibit decreased β-catenin expression at cell membranes compared to $Prx1^{+/+};Wt1^{GFP/loxP}$ littermate controls. *Male $Prx1^{Cre/+};Wt1^{GFP/+}$ mice were crossed with female $Wt1^{loxP/loxP}$ mice and the embryos were collected at E11.5 and processed for immunofluorescence. Embryos were sectioned in the transverse plane. Sections were stained with an anti-β-catenin antibody (red – upper inset) and DAPI (blue – lower inset). Membranous CTNNB1 (β-catenin) expression was lower in the PPFs of the $Prx1^{Cre/+};Wt1^{GFP/loxP}$ embryos **(B)**, compared to littermate controls ($Prx1^{+/+};Wt1^{GFP/loxP}$) **(A)**. (Abbreviations: Lu: Lungs, PPF: pleuroperitoneal fold). (Scale bar = 50μm). (n=1).*

5.8 Discussion

The results described in this chapter have shown that *Prx1*$^{Cre/+}$;*Wt1*$^{loxP/loxP}$ mice die at birth, and we believe this to be caused by incomplete diaphragm development. Whilst this result meant that this mouse model was not suitable for studying the effects of *Wt1* deletion in adipose tissue, we were interested in knowing what was causing this phenotype. CDH is a relatively common birth defect, however the etiology of it remains poorly characterised, therefore we hoped that this new mouse model of CDH would allow us to increase understanding in this field.

Our initial investigations focused on assessing whether the expected numbers of mutant embryos were surviving until birth, based on Mendel's Laws of Inheritance. At all stages analysed up to and including E16.5, approximately 25% of the embryos were *Prx1*$^{Cre/+}$;*Wt1*$^{loxP/loxP}$, however at later stages (E18.5, E19,5 and P0), the percentage of mutants was slightly below what was expected (~16%). Therefore, it is possible that some of the embryos were dying *in utero*, although the number of embryos analysed makes it difficult to conclude this, and ideally more litters should be assessed. It is feasible that some of the mutants had a more severe phenotype than others, causing them to die at earlier stages, indeed our subsequent studies revealed that the phenotype was quite variable. It is also possible that the embryos suffered from other defects in addition to those observed in the diaphragm, which may have caused premature death of some of the mutants.

Regarding the variability in the diaphragm phenotype, Table 5.2 summarises what was observed in the different embryos, and the chart in Figure 5.4 shows a breakdown of the hernia locations in embryos at stages E14.5 and older. The most common category of CDH are Bochdalek-type hernias, and these are located in the posterolateral region, with 85% of the cases occurring on the left (Pober, Russell and Ackerman, 2010). Indeed, in the *Prx1*$^{Cre/+}$;*Wt1*$^{loxP/loxP}$ embryos, left-sided posterior hernias were the most common type observed. However, just 45% of the embryos presented with this defect, 20% had bilateral posterior hernias and 5% had right sided posterior hernias, both of which are also Bochdalek-type. Intriguingly we also observed one embryo that had a

ventrally (anteriorly) located hernia, and another that exhibited thinning of the diaphragm but no actual hole. Finally, in 20% of the mutants, no diaphragmatic phenotype was observed. Hence, there was significant variability in the phenotype. This phenomenon is not uncommon in mouse models of CDH. When Carmona *et al*. (2016) used the *G2-Gata4*^{Cre} mouse to conditionally delete *Wt1*, 17.4% of the mutant embryos analysed (E13.5 and older) had no diaphragmatic defect, 13% had only a mild defect (thinning of the diaphragm) and 69.6% presented with hernias (one right-sided hernia, and the remainder left sided) (Carmona *et al.*, 2016). Similarly, the conditional deletion of *Gata4* using the *Prx1-Cre* mouse model results in approximately 68% of the embryos presenting with dorsal lateral hernias, and 32% with ventral hernias (Merrell *et al.*, 2015). Why this variability is observed is unknown, however it is also true of human CDH, with several different defects having been described (Ackerman *et al.*, 2012).

Having established that the *Prx1*$^{Cre/+}$*;Wt1*$^{loxP/loxP}$ embryos were suffering from problems with diaphragm development we next wanted to investigate why this was the case and what the mechanisms behind the defects were. We showed that development of the PPF/PHMP continuum, which is essential for the separation of the thoracic and peritoneal cavities, was disrupted, as is often the case in models of CDH. However, elucidating the precise mechanism responsible has been a challenge. The first step involved understanding where exactly the deletion of *Wt1* was occurring. To do so, we attempted to stain embryos of various stages (E9 and older), with an anti-Cre antibody, to know where Cre was being expressed and therefore in which cells recombination was occurring. However, as described in chapter 4, due to technical difficulties with the Cre antibody, we were unable to do so. As an alternative to this, we decided to use the *Prx1-Cre;R26R-mTmG* lineage tracing model to understand which embryonic structures were Prx1-Cre lineage positive. Crucially, this revealed that the PPFs, but not the PHMP, were Prx1-Cre lineage positive, and therefore in our deletion model it was specifically the PPFs that were being affected and not the PHMP (Figure 5.7). This discovery was particularly interesting given that the recent paper by Carmona *et al*. (2016) showed *G2-Gata4*^{Cre}*;Wt1*$^{loxP/loxP}$ embryos with a very similar phenotype to ours, but reported deletion in both the PPFs and PHMP (Carmona *et al.*,

2016). It is thus intriguing that despite the deletion of *Wt1* occurring in different embryonic structures, the phenotypes in later stage embryos are comparable. Moreover, when analysing consecutive sections from the *Prx1*$^{Cre/+}$*;R26R-mTmG* embryos, it appeared as though the Prx1-Cre lineage positive PPF cells were migrating and infiltrating the Prx1-Cre lineage negative PHMP. Interestingly, as described in the introduction (1.4.3), another group used time-lapse videos of an *ex vivo* culture system, to show the collective cell migration of Prx1-Cre lineage positive PPF cells across the surface of the liver (Merrell *et al.*, 2015). Therefore, our result aligns with previous work which shows the importance of PPF cell migration in diaphragm morphogenesis.

In addition to the *Prx1*$^{Cre/+}$*;Wt1*$^{loxP/loxP}$ mutant embryos, another model was developed, which allowed us to conditionally delete *Wt1* in the Prx1-Cre lineage, but also label all cells in which *Wt1* is/would normally be expressed, with GFP (*Prx1*$^{Cre/+}$*;Wt1*$^{GFP/loxP}$). Using this model confirmed that *Wt1* deletion was occurring in the PPFs, and that the morphology and development of the PPFs was disrupted. Interestingly, the PPFs of the *Prx1*$^{Cre/+}$*;Wt1*$^{GFP/loxP}$ mutant embryos, which had an almost "bunched up" appearance, exhibited brighter staining with the anti-GFP antibody (as shown by immunofluorescence) than the PPFs of Prx*1*$^{+/+}$*;Wt1*$^{GFP/loxP}$ littermate controls (Figure 5.8). Whilst we are not entirely sure why this is the case, it is possible that it is caused by an accumulation of GFP expressing cells in this region, due an inability to migrate, whilst in the littermate controls these cells are more spread out as they have migrated to meet the PHMP, therefore causing the fluorescence to be less concentrated in one region.

The results described thus far led us to hypothesise that the deletion of *Wt1* in the PPF cells was resulting in the failure of these cells to migrate, therefore preventing the closure of the thoracic and peritoneal cavities. Further support for this hypothesis came from assessing the diaphragms of later-stage embryos. We observed a thickening of the diaphragm around the region of the hernia in E16.5 embryos, coupled with a disruption to the orientation of the muscle fibres (Figure 5.9). This thickening has been described as a hallmark of CDH, and has been seen in other models (Clugston *et al.*, 2006). It is believed to occur because the muscle precursor cells, which require

guidance by the PPF cells, accumulate in the region of the defective PPF mesenchyme, as they cannot migrate any further (Clugston *et al.*, 2006; Merrell *et al.*, 2015). Therefore, this thickening indicates that the PPF cells have failed to migrate correctly.

Given that WT1 is known to function in EMT through the activation of *Snail1* and repression of *Cdh1* in the epicardium (Martínez-Estrada *et al.*, 2010), and that EMT is evidently important for migration, we investigated the possibility that EMT was disrupted in the mutant embryos. However, no difference in the expression of VIM (a mesenchymal cell marker) and CDH1 (an epithelial cell marker) was observed in the embryos at E11.5. This was perhaps surprising given that deletion of *Wt1* in the PHMP has recently been shown to result in increased CDH1 expression (Carmona *et al.*, 2016). Future work should include assessing the expression of these genes earlier in development (around E10.5), as the PPFs are just starting to form, because it is possible that we are missing the point at which EMT is important for the migration of the cells. Having said this, we chose to look at E11.5 because this is when the increased CDH1 expression was observed in the *G2-Gata4*^{Cre}*;Wt1*$^{loxP/loxP}$ embryos (Carmona *et al.*, 2016), however this does not appear to be the case in our model. Additionally, staining with more markers of epithelial and mesenchymal cells could be of benefit.

A particularly surprising result was that regarding RALDH2 expression in the mutant embryos. It is well known that the retinoic acid signalling pathway is important in diaphragm development, and RALDH2 catalyses the synthesis of retinoic acid (Greer, Babiuk and Thebaud, 2003; Mey *et al.*, 2003). In the epicardium, WT1 directly activates the expression of *Raldh2* (Guadix *et al.*, 2011; von Gise *et al.*, 2011), and in the liver mesothelium of *Wt1* null embryos RALDH2 expression is reduced (Ijpenberg *et al.*, 2007). Hence we hypothesised that *Wt1* deletion would lead to a reduction in RALDH2 expression. However, this was not the case, instead we observed an increase in RALDH2 expression in the PPFs of the mutants, despite clearly showing a loss of WT1 expression. Moreover, using an anti-Pax2 antibody to label the intermediate mesoderm, we showed that this result was not caused by the presence of intermediate mesoderm in the PPFs, as described by Carmona *et al*. (2016). Interestingly, a similar phenotype has been observed in *Wt1* null embryos, whereby increased RALDH2

expression was seen alongside disrupted diaphragm development (Ijpenberg *et al.*, 2007). Currently, we do not know why we observed this increased expression, however it could be contributed to by the bunching up of the PPF cells. As described above, we hypothesise that one reason for the increased GFP fluorescence in the $Prx1^{Cre/+};Wt1^{GFP/loxP}$ embryos was an accumulation of PPF cells due to a lack of migration. It is therefore possible that this apparent increase in RALDH2 expression could be a consequence of this concentrated region of cells. This, of course does not explain why RALDH2 expression was not lost in these cells following *Wt1* deletion, and thus is an area that requires further investigation. It is intriguing to note that exposure to excessive retinoic acid, as well as too little, can lead to developmental defects, including diaphragmatic hernias (L. M. Y. Lee *et al.*, 2012). Therefore, maintaining homeostasis of retinoic acid is essential. Moreover, in zebrafish it has been shown that exogenous retinoic acid results in an increase in the expression of *cyp26a1* (encodes an enzyme that inactivates retinoic acid) but a decrease in the expression of *raldh2*. It was subsequently shown that retinoic acid directly represses the expression of *raldh2* (Dobbs-McAuliffe, Zhao and Linney, 2004). Therefore, feedback mechanisms act to regulate the production and degradation of retinoic acid, therefore maintaining homeostasis. Given that the regulation of retinoic acid signalling is so tightly controlled and that both an increase and decrease in retinoic acid can lead to problems with diaphragmatic development, this is certainly an area that requires additional work.

Given our hypothesis regarding the disrupted migration of the PPF cells, we also considered the possibility that cell adhesion was affected by the deletion of *Wt1*. Although only preliminary, we have shown that the expression of membranous β-catenin (CTNNB1) in the PPF cells differed between the control and mutant embryos. As β-catenin functions at adherens junctions, binding the intracellular domain of transmembrane cadherin proteins, and linking these proteins to the actin cytoskeleton, this differential expression could indicate that cell adhesion is disrupted (Bienz, 2005; Nelson, 2008). On-going work is focused on better understanding this phenotype, both through the analysis of more embryos and by assessing the expression of N-cadherin and its overlap with β-catenin expression. N-cadherin is the transmembrane cadherin

protein to which β-catenin binds in mesenchymal cells and thus functions in cell-cell adhesion and collective cell migration (Nelson, 2008; Shih and Yamada, 2012). Additionally, we intend to study the actin cytoskeleton of the PPF cells to aid our understanding of whether/how cell-cell adhesion and migration are affected.

WT1 expressing mesothelial cells are found on the surface of the developing and mature diaphragm (Shinohara, 1997), and it has been demonstrated that WT1 regulated mesothelial signalling is required for diaphragm formation (Paris, Coles and Ackerman, 2015). Interestingly, in our model of CDH, WT1 was not lost from the diaphragm mesothelium. This was most obvious in the older embryos (Figure 5.9), in which we observed a loss of WT1 expressing mesenchymal cells within the diaphragm itself, but a retention of the WT1 expressing cells at the surface of the diaphragm. Indeed, when we examined the E12.5 *Prx1*$^{Cre/+}$*;R26R-mTmG* lineage tracing embryos (Figure 5.7), it became evident that, whilst the bulk of the PPF cells expressed GFP and were thus Prx1-Cre lineage positive, the cells at the edge of the PPFs were not GFP positive. Hence, the results from the lineage tracing embryos supported our observations regarding the *Prx1*$^{Cre/+}$*;Wt1*$^{loxP/loxP}$ embryos. As described in chapter 4, we have evidence to suggest that Prx1-Cre lineage positive cells are largely derived from the somatic, but not the splanchnic, lateral plate mesoderm. Therefore, given that the visceral mesothelial cells are derived from the splanchnic lateral plate mesoderm (Brauer, 2003), it is perhaps not surprising that we do not get *Wt1* deletion in the mesothelial cells of the diaphragm. Moreover, it is interesting that despite not deleting *Wt1* in the mesothelial cells, or in the cells of the PHMP, but only in the mesenchymal cells of the PPFs, the diaphragmatic phenotype is severe and similar to that described in other models. In particular the *G2-Gata4*^{Cre}*;Wt1*$^{loxP/loxP}$ line described by Carmona *et al*. (2016), where *Wt1* deletion occurred throughout the PPF/PHMP continuum.

In conclusion, the results in this chapter have shown that *Wt1* deletion in the Prx1-Cre lineage results in disrupted diaphragm development, causing diaphragmatic hernias. We have shown that this aberrant development is caused by the defective formation of the pleuroperitoneal folds at approximately E11.5, meaning that the thoracic and peritoneal cavities are not separated from one another. We hypothesise that PPF cell

migration is affected by the deletion of *Wt1*, which in turn leads to a failure of the muscle precursor cells to migrate correctly. We have not yet elucidated the exact mechanism by which the lack of WT1 leads to defective cell migration, however preliminary evidence suggests that PPF cell adhesion may be affected in the mutant mice. Moreover, surprisingly, we observe an increase in the expression of RALDH2 in the PPFs as a consequence of *Wt1* deletion. This result is perhaps counter-intuitive and thus we are looking into it further and considering the possibility that it may also contribute to the diaphragmatic phenotype. The majority of the work performed thus far has concentrated on embryos at E11.5, as this is the point at which the PPFs are forming. However, future work will include looking at the expression of the various proteins at both earlier (~E10.5) and later (~E12.5) stages to understand if differences are present at other developmental time points, that may help us better understand the causative mechanism.

Chapter 6

Discussion

6.1 Introduction

The original aims of this project were to determine the role of *Wt1* in the development of visceral WAT, and to investigate the functional consequences of the heterogeneity that exists within the APC population of visceral WAT, regarding *Wt1* expression. As will have become clear throughout this thesis, the aims of the project changed somewhat over the course of my PhD, as a consequence of certain findings. Therefore, the major areas of investigation have been to study the differences between *Wt1* expressing and non-expressing visceral APCs both at the behavioural and transcriptomic level and to determine the effects of a high fat diet (HFD) on both precursor cell populations. Additionally, for reasons explained in chapter 4, we investigated the labelling of different adipose depots by Prx1-Cre, and have obtained interesting preliminary data regarding the developmental origin of subcutaneous WAT and pericardial visceral WAT. Finally, we have explored the cellular and molecular mechanisms responsible for the development of congenital diaphragmatic hernia caused by the deletion of *Wt1* in the Prx1-Cre lineage.

6.2 Assessing the functional consequences of APC heterogeneity

6.2.1 $Wt1^+$ and $Wt1^-$ APC behaviour *in vitro*

Work from our group previously revealed that populations of APCs are heterogeneous. All visceral WAT depots harbour *Wt1* expressing APCs, but importantly, non-*Wt1* expressing APCs are also present in the SVF (Chau *et al.*, 2014). Moreover, preliminary work suggested that this heterogeneity at the level of the precursor cells may influence the properties of the mature adipocytes (Chau *et al.*, 2014). Therefore, early experiments involved further investigating this heterogeneity and addressing behavioural differences between the two cell populations. We showed that when the *Wt1* expressing ($Wt1^+$) and non-*Wt1* expressing ($Wt1^-$) APCs were cultured separately, the $Wt1^+$ cells were more adipogenic than the $Wt1^-$ cells. This was also the case when a pure population of pre-adipocytes ($Lin^-;CD31^-;CD29^+;CD34^+;Sca1^+;CD24^-$) was split into $Wt1^+$ and $Wt1^-$ populations and cultured. Hence, it appears that the $Wt1^+$ and

$Wt1^-$ APCs do exhibit different behaviours, at least *in vitro*. This result suggests that the differing percentages of $Wt1^+$ and $Wt1^-$ APCs found in different visceral WAT depots could influence the properties and behaviour of the individual depots. This is something that we followed up *in vivo*, by assessing the effects of a HFD on the two cell populations. It is already known that different visceral WAT depots confer differing levels of risk concerning obesity-associated diseases such as cardiovascular disease, with both the omental and pericardial depots being especially implicated (Rosito *et al.*, 2008; Ding *et al.*, 2009). It is also worth noting that these two depots have the highest percentages of $Wt1^+$ APCs (Chau *et al.*, 2014). Therefore, our result showing that the two populations of APCs behave differently could be physiologically relevant, and we have begun to address this *in vivo,* as discussed later.

As to why the two populations of cells displayed differing propensities for adipogenesis when cultured separately, we hypothesised that perhaps it could reflect a difference in confluency. As murine APCs should be confluent before they will differentiate into adipocytes (Ailhaud *et al.*, 1989; Entenmann and Hauner, 1996), differences in apoptosis and/or proliferation could result in contrasting rates of adipogenesis. We were unable to detect any apoptotic cells in either of the cultures, however we showed that the $Wt1^+$ APC population was more proliferative than the $Wt1^-$. Thus, we suggest that this difference in proliferative capacity could contribute to the higher rates of adipogenesis seen in the $Wt1^+$ cultures. Interestingly, the $Wt1^+$ population was also more proliferative even when the $Wt1^+$ and $Wt1^-$ cells were cultured together, suggesting this is an intrinsic property of the cells and not a result of being separated from one another. It would be interesting to perform this experiment *in vivo*, for example to administer $Wt1^{GFP/+}$ knock-in mice with BrdU, and then use flow cytometry to assess the percentage of GFP^+ ($Wt1^+$) and GFP^- ($Wt1^-$) APCs that incorporated BrdU, to understand if the same difference is observed *in vivo*.

We took this investigation further by deleting *Wt1 in vitro* in the APC cultures, to understand whether the expression of WT1 was responsible for this proliferative difference. However, no significant difference in proliferation was observed between cultures in which *Wt1* had/had not been deleted. Additionally, the percentage of KI67

expressing cells in these mixed $Wt1^+$ and $Wt1^-$ cultures was ~6-10%, which is intermediate to the percentage of proliferating $Wt1^+$ cells (~12%) and the percentage of proliferating $Wt1^-$ cells (~4%) as shown in previous cultures. Hence, this percentage of proliferating cells is what would be expected from a mixed population based on our findings. Therefore, whilst *Wt1* appears to be marking a population of APCs that are more proliferative, it does not seem to be responsible for this phenotype. This result was a little surprising given that WT1 is known to play a role in the proliferation of several cell types, as discussed in 6.8.

Another explanation for the differing behaviours of the separately cultured $Wt1^+$ and $Wt1^-$ cells could be that one cell population secretes a factor(s) that influences the other. We considered the idea that $Wt1^-$ APCs required a factor(s) that was secreted by the $Wt1^+$ APCs in order to undergo adipogenesis, and therefore when the two populations were separated, the $Wt1^-$ cells did not differentiate well. A conditioned media assay was used to test this, and when $Wt1^-$ APCs were cultured in media that had been previously conditioned by $Wt1^+$ APCs, an improvement in adipogenesis was observed. Whilst the conditioned media-fed $Wt1^-$ APCs did not differentiate as well as $Wt1^+$ APCs, there was a definite increase in adipogenesis when compared to the $Wt1^-$ APCs not fed with conditioned media. Therefore, we hypothesise that as well as the two populations of cells differing in their proliferative capacity, their growth and differentiation may also be influenced by paracrine signals. Data obtained from microarray studies supports this hypothesis and is further discussed below.

6.2.2 Transcriptomic analysis of $Wt1^+$ and $Wt1^-$ APC populations

Having assessed the behavioural differences of the $Wt1^+$ and $Wt1^-$ APCs *in vitro*, we performed microarray analysis to understand more about the properties of the two populations and how they differ at the transcriptomic level. As discussed in chapter 3 (3.8), the results from this analysis were partially reflective of what we had observed *in vitro*. For those genes that exhibited higher expression in the $Wt1^+$ population, several GO terms linking to extracellular activity were highlighted, thus supporting the secreted factor hypothesis. Furthermore, several of the top genes with higher

expression in the Wt1$^+$ APCs encode secreted proteins. *Slpi* (secretory leukocyte protease inhibitor) was the gene with the highest fold change and encodes an anti-inflammatory protein which has been shown to exert an anti-inflammatory role in adipose tissue (Adapala, Buhman and Ajuwon, 2011). Interestingly, it is known to be more highly expressed in visceral adipose tissue than in subcutaneous and is predominantly expressed in the cells of the SVF as opposed to the mature adipocytes (Adapala, Buhman and Ajuwon, 2011). Furthermore, it has been shown to exert pro-proliferative and anti-apoptotic effects in several cell types (Zhang *et al.*, 2002). Therefore, it may be interesting to follow up this gene, as well as the others that encode secreted proteins, as being potential candidates for factors secreted by Wt1$^+$ cells that influence the growth and differentiation of Wt1$^-$ cells. For example, another highly enriched gene in the Wt1$^+$ population was *Dpp4*, which encodes an adipokine. The knockdown of *Dpp4* leads to a reduction in the expression of proliferation-related genes and thus blocks pre-adipocyte proliferation (Zilleßen *et al.*, 2016), which is intriguing given our results regarding the proliferative difference between the two cell populations. Moreover, several studies have described contrasting phenotypes of *Lcn2*$^{-/-}$ mice, ranging from being lean and insulin sensitive to obese and insulin resistant (Rosen and Spiegelman, 2014). *Lcn2* also encodes an adipokine and exhibited higher expression in the Wt1$^+$ APCs. Furthermore, as discussed in chapter 3 (3.8), many of the genes identified as being more highly expressed in the Wt1$^+$ population have previously been classified as being part of a visceral adipose tissue gene set (Cohen *et al.*, 2014). Therefore, these results have given us an insight into potential secreted protein candidates that we hope to follow up with further conditioned media and ELISA studies.

Regarding the genes that were more highly expressed in the Wt1$^-$ APCs, some interesting GO terms were identified. Intriguingly, "cell proliferation" was amongst these terms, and was identified by both GOrilla and DAVID. This result does not reflect the results from *in vitro* studies which show that the Wt1$^+$ cells are more proliferative. Therefore, further investigation is required, for example we need to look closely at the genes identified in this GO term, and perhaps perform qRT-PCR to validate the results from the microarray regarding the expression of this gene set.

Additionally, “angiogenesis” was also identified by both GOrilla and DAVID. Angiogenesis, as described in chapter 3 (3.8) is an important part of adipose tissue growth and expansion (Corvera and Gealekman, 2014). Thus, this result suggests that perhaps the $Wt1^-$ population plays a role in the formation of blood vessels in adipose tissue.

6.2.3 The effect of a HFD on $Wt1^+$ and $Wt1^-$ APCs

Given the results described regarding the differing behaviours of the $Wt1^+$ and $Wt1^-$ APCs *in vitro*, we wanted to extend this study *in vivo*, and investigate how, when mice were fed a HFD, the two APC populations responded to this physiologically relevant change. Across the five visceral WAT depots analysed (perigonadal, omental, pericardial, mesenteric and perirenal) two trends were noted. Firstly, a reduction in the percentage of $Wt1^+$ cells in the SVF, and secondly a reduction in the percentage of APCs in the SVF, when the mice were fed a HFD. Whilst these trends were true for most of the depots, the differences were not always significant. Moreover, in the pericardial depot, no differences were observed. This last point intrigued us, considering the results described in chapter 4 regarding the origin of the pericardial APCs/adipocytes, and is discussed in 6.3.2. When we looked more closely at the reduction in the percentage of APCs in the other four depots, we found that the contribution of the $Wt1^+$ and $Wt1^-$ cells to this reduction was not equal, and differed between the depots. Most strikingly, in the omental depot, the reduction in APCs was due solely to a reduction in $Wt1^+$ APCs and not to $Wt1^-$ APCs. Therefore, as well as behaving differently *in vitro*, it appears that the two populations of cells exhibit different responses *in vivo* when subjected to obesogenic stimuli. Moreover, these different responses are not uniform across all visceral WAT depots. Thus, the results from this study provide further evidence for the heterogeneity that exists both between and within adipose depots, and importantly that this heterogeneity clearly has an impact on the response to dietary changes.

It would be interesting to perform a comparable experiment, but instead only feed the mice a HFD for a short period before harvesting the adipose tissue for analysis. Jeffery

et al. (2015) showed that there is a burst of APC proliferation in visceral WAT during the first week of HFD feeding, which then declines to normal background rates, and it is only after several weeks that new adipocytes are formed (Jeffery *et al.*, 2015). Thus, using the *Wt1*$^{GFP/+}$ knock-in model we could assess how the Wt1^{+} and Wt1^{-} APCs behave during this proliferative burst period. Given our *in vitro* results, we could speculate that the Wt1^{+} population would be more proliferative than the Wt1^{-}. This initial increase in the rate of proliferation during the first week of HFD feeding was only seen in visceral WAT, not subcutaneous, which is intriguing given that the subcutaneous WAT does not harbour *Wt1* expressing APCs (Jeffery *et al.*, 2015). Considering these results from Jeffery *et al*. (2015), it is interesting that we observe a decrease in the percentage of APCs in the HFD-fed mice. It is possible that this was caused by the length of time the mice were on the diet (17 weeks), meaning that the APCs were well past this proliferative burst phase, and were undergoing increased differentiation.

We considered the possibility that the reason for the decrease in the Wt1^{+} APCs, particularly in the omental depot, was that they were preferentially differentiating into adipocytes in response to the prolonged HFD. To test this hypothesis we used the *Wt1-Cre*^{ERT2}*;R26R-mTmG* lineage tracing model. However, we did not observe an obvious difference in the percentage of *Wt1* lineage positive adipocytes between mice on normal and HFD feeding regimes. If the Wt1^{+} APCs were preferentially differentiating, we would have expected to see a higher percentage of *Wt1* lineage positive adipocytes in the depots from the HFD-fed mice. Nevertheless, this experiment had several caveats, as explained in chapter 3, and therefore is something we intend to repeat and follow up further. Again, it would be interesting to assess the adipose tissue at different time points throughout the duration of the HFD regime, to understand how cells in the *Wt1* lineage contribute at various stages of adipose tissue expansion. Moreover, we could administer tamoxifen at different developmental times, to change the point at which *Wt1* expressing cells are labelled, and subsequently assess their contribution to the various adipose depots under HFD conditions. Chau *et al*. (2014) used *Wt1-Cre*^{ERT2}*;R26R-mTmG* mice to show that when tamoxifen was administered at E14.5, ~77% of the adipocytes in the perigonadal depot were labelled

with eGFP, and thus were *Wt1* lineage positive when the mice were analysed at 1.2 years old (Chau *et al.*, 2014). Evidently this percentage is much higher than that obtained in our study (~5%) when the mice were given tamoxifen postnatally and fed a normal diet for 1 year. Similarly high percentages were obtained by Chau *et al.* (2014) for the other visceral depots. Thus, it appears that cells expressing *Wt1* prenatally make a greater contribution to the mature adipocyte population in adult adipose tissue, than those expressing *Wt1* postnatally. Hence, it would be interesting administer tamoxifen at E14.5 and look at how a HFD affects the percentage of labelled adipocytes in the adult mice.

6.2.3.1 Transcriptomic analysis of $Wt1^+$ and $Wt1^-$ APCs from HFD fed mice

In addition to assessing the effects of a HFD on the percentages of *Wt1* expressing and non-expressing APCs from the $Wt1^{GFP/+}$ knock-in mice, the cells were sorted for transcriptomic analysis. Therefore, allowing us to further investigate the response to the HFD. The results from this are discussed in detail in chapter 3 and so are not comprehensively covered here.

The analysis focused on genes that were specifically up or downregulated in either the $Wt1^+$ APCs or $Wt1^-$ APCs in response to the HFD. The genes that were downregulated in the $Wt1^+$ population formed one of the most interesting categories. They included several genes that are markers of mesothelial cells. Given that the mesothelium is a known source of visceral APCs this result could indicate that these cells are becoming less mesothelial and thus are beginning to differentiate (Chau *et al.*, 2014). In addition to the mesothelial genes, several other interesting hits were identified by the microarray as being downregulated in $Wt1^+$ cells as a result of HFD feeding and these were validated using qRT-PCR. For example, *Ptgs1* has a central role in the regulation of inflammatory processes (Saraswathi *et al.*, 2013), and *Rspo1*, which is a well-known activator of the canonical Wnt signalling pathway, which itself is well documented as having multiple roles in adipose tissue biology (Christodoulides *et al.*, 2009). In this vein, *Wnt10b* has been shown to inhibit the development of white and brown adipose tissue through preventing pre-adipocyte differentiation. Transgenic mice in which

Wnt10b is under the control of the *Fabp4* promoter are resistant to HFD-induced obesity and have a 50% reduction in total body fat (Longo *et al.*, 2004). Additionally, *Smo* encodes a receptor for SHH, and hedgehog signalling has been demonstrated to block adipogenesis (Suh *et al.*, 2006). Therefore, several genes known to inhibit adipogenesis exhibit reduced expression in the $Wt1^+$ APCs in response to a HFD. Interestingly, at least two of these genes are known targets of WT1. *Rspo1* which encodes the secreted activator protein, R-spondin 1, is both a transcriptional and post-transcriptional target of WT1 (Motamedi *et al.*, 2014; Bharathavikru *et al.*, 2017). Additionally, chromatin immunoprecipitation performed using chromatin from embryonic mouse kidneys has shown that *Smo* is also a transcriptional target of WT1 (Hartwig *et al.*, 2010). Therefore, it is possible that the reduction in expression of these genes is a consequence of the decreased *Wt1* expression in the HFD-fed mice.

Several interesting genes were downregulated in the $Wt1^-$ APC population. As described in chapter 3, when the genes in this category were validated by qRT-PCR, many of them also appeared to be downregulated in the $Wt1^+$ cells. Nevertheless, in addition to those that were enriched in GO terms such as "blood vessel development", "cell proliferation" and "biological adhesion", many of them have been described as functioning in adipogenesis. For example *Bmp4*, which has a major role in the regulation of APC commitment and differentiation, as described in the introduction (1.1.6). Additionally, *Arl4d* expression is known to increase during early adipogenesis and subsequently decrease. Moreover, its overexpression in 3T3-L1 cells has been demonstrated to inhibit adipogenesis (Yu *et al.*, 2011). Similarly, SULT1E1 has been shown to block the differentiation of pre-adipocytes, and pre-adipocytes from *Sult1e1* null mice exhibit enhanced differentiation *in vitro* (Wada *et al.*, 2011). Hence, it appears that several genes involved in adipogenesis exhibit altered gene expression as a consequence of HFD feeding. Generally, the genes that were upregulated in response to the HFD were not well validated by qRT-PCR, however a number of those that were, were present in the "immune system process" GO term.

In summary, several genes that encode proteins known to inhibit adipogenesis, were downregulated in the APCs in response to HFD feeding, therefore suggesting that

increased adipogenesis was occurring in these mice. Conversely, several immune response related GO terms were associated with genes exhibiting upregulated expression in the HFD-fed mice. One of the most interesting questions that has arisen from this study is why/how is the expression of *Wt1* altered by diet? And could this give us an insight into the function of *Wt1* in adipose tissue? There is a clear reduction in *Wt1* expression in the APCs from the HFD fed mice, along with a reduction in several *Wt1* associated genes, whether these be other mesothelial cell markers, or direct targets of WT1. It is possible that this is a consequence of the cells starting to differentiate into adipocytes, and thus loosing *Wt1* expression. Alternatively, the loss of *Wt1* expression could be causing the cells to begin differentiating. The fact that the decrease in the percentage of APCs is not uniform across $Wt1^+$ and $Wt1^-$ populations could imply that *Wt1* is indeed influencing the response to the diet. Interestingly, work from our group has shown that when *Wt1* was ubiquitously deleted in two week old mice, one week later there was a reduction in the percentage of *Wt1* expressing cells in the pre-adipocyte population. This result was significant for the perigonadal and omental depots, but the trend was the same in the mesenteric and pericardial (Chau *et al.*, 2014). This result might suggest that WT1 is required to maintain the pre-adipocyte population. Perhaps this is also true in the case of the HFD experiment.

6.3 Prx1-Cre labelling of white adipose tissue

Initially we planned on using the transgenic *Prx1-Cre* mouse line to conditionally delete *Wt1 in vivo*, allowing us to assess the effects of *Wt1* deletion on the development of visceral WAT. To first understand whether this was likely to work, the *Prx1-Cre* line was crossed with the *R26R-mTmG* reporter line. The adult adipose tissue from the offspring was checked for eGFP labelling, both of the mature adipocytes and of the APCs. Any eGFP labelled cells must have been derived from the Prx1-Cre lineage, and therefore would inform as to whether deletion was feasible. The majority of the mature adipocytes and APCs of the subcutaneous WAT were labelled with eGFP, and were therefore Prx1-Cre lineage positive (~90-100%). However, given that we were aiming to delete *Wt1* in the visceral WAT, this was of most interest to us. For most of the visceral WAT depots (perigonadal, mesenteric, omental), the percentage of eGFP

positive adipocytes and precursor cells was very low (<10%). However, in contrast to this, more than 50% of the mature adipocytes, and approximately 40% of the precursor cells in the pericardial depot were labelled with eGFP and were therefore Prx1-Cre lineage positive. Whilst this work was being carried out, another group published similar results regarding the subcutaneous, perigonadal and mesenteric depots, therefore corroborating our findings. However, the labelling of the pericardial depot was not described (Sanchez-Gurmaches, Hsiao and Guertin, 2015).

Considering that work from our group has shown that visceral, but not subcutaneous WAT can be lineage traced using the *Wt1-Cre*^{ERT2} model, and Sanchez-Gurmaches *et al*. (2015) showed that subcutaneous, but not visceral WAT can be labelled using the *Prx1-Cre* model, there is significant evidence to suggest that the two adipose types have different origins (Chau *et al.*, 2014; Sanchez-Gurmaches, Hsiao and Guertin, 2015). Hence, it was a surprise to find that the pericardial depot (visceral), as well as the subcutaneous depot were labelled by Prx1-Cre. Therefore, this is something that we investigated further, as discussed below.

6.3.1 Investigating the origin of subcutaneous white adipose tissue

Whilst the results described thus far demonstrated to us that the *Prx1-Cre* line was not the best choice for the conditional deletion of *Wt1* in the visceral WAT precursor cells (except perhaps for the pericardial depot), the labelling intrigued us and caused us to ask questions about the developmental origins of different adipose tissue types and depots. As work from our group has shown, at least a proportion of the visceral WAT is derived from the lateral plate mesoderm (LPM) (Chau *et al.*, 2014). However, the developmental origin of subcutaneous WAT remains unknown. Therefore, we considered the possibility that by utilising both the constitutive *Prx1-Cre* line and the tamoxifen inducible *Prx1-Cre*^{ERT2} line, we could investigate this. Crucially, we wanted to find out when/where the Cre-driven recombination event was occurring, to allow us to understand where the eGFP labelled cells were arising from. As subcutaneous adipose tissue begins to form *in utero*, we were able to show that, at E18.5, the subcutaneous WAT was largely eGFP positive, therefore meaning that Prx1-Cre was

expressed prenatally either in cells that give rise to subcutaneous adipose tissue, or in the adipose tissue itself.

Whilst the results obtained using the *Prx1-Cre* line were informative, due to its constitutive expression it was not possible to determine when and where recombination was occurring, and importantly whether there were multiple recombination events that contributed to the labelling of the adipose tissue. Work from another group has demonstrated that Cre is not expressed in the subcutaneous WAT from adult *Prx1-Cre* mice, therefore suggesting that recombination occurs during development (Sanchez-Gurmaches, Hsiao and Guertin, 2015). To investigate this further, we utilised the tamoxifen inducible *Prx1-Cre*^{ERT2} line. By administering tamoxifen at various developmental stages, and to juvenile mice, we demonstrated that labelling of adult subcutaneous WAT (adipocytes and precursor cells) could only be achieved when tamoxifen was administered during early embryonic development. Having said this, the labelling that occurred was significantly less than that observed when using the constitutive model. As discussed in chapter 4 (4.6), there are several possible explanations for this discrepancy. However, we have shown that labelling of the subcutaneous WAT does not occur when juvenile mice are given tamoxifen. Moreover, culturing SVF cells from the subcutaneous and pericardial WAT of adult *Prx1-Cre*^{ERT2} mice in the presence of tamoxifen did not lead to the generation of eGFP expressing cells. Thus, these results suggest that Prx1-Cre^{ERT2} is not expressed in juvenile/adult SWAT, which supports the findings from Sanchez-Gurmaches *et al*. (2015), regarding the expression of Cre in the adipose tissue from adult *Prx1-Cre* mice (albeit that one is the constitutive model, and the other tamoxifen inducible). Collectively these results indicate that the labelling observed in the adult adipose tissue is the result of recombination during embryonic development and not postnatally. Future work will include using qRT-PCR to verify that Cre is not expressed in the adult subcutaneous adipose tissue of *Prx1-Cre* mice, and additionally, considering our findings regarding the pericardial adipose tissue, also check Cre expression in this depot.

A second way in which we attempted to elucidate when and where Cre was expressed, and therefore where the eGFP expressing adipose tissue was arising from, was by staining sections from *Prx1-Cre;R26R-mTmG* embryos with an anti-Cre antibody. We speculated that this would help us narrow down both the timing of the recombination event and the location. However, due to technical difficulties this has not yet been possible, but is something we would like to persue in the future. As an alternative to this, we assessed the expression of eGFP in E9.5 *Prx1-Cre;R26R-mTmG* embryos. This revealed that recombination had occurred by this early developmental time point, and that the somatic (but not splanchnic) LPM was largely eGFP positive. Therefore, we suggest that at least a proportion of the adult subcutaneous adipocytes and precursor cells are derived from the somatic LPM. By checking the expression of Cre at other developmental stages and postnatally, using qRT-PCR and an anti-Cre antibody, we hope to be able to verify this result. If Cre expression is only observed during early developmental stages (~E8.5-E10.5), and not later in embryonic development or postnatally, this provides strong evidence to suggest that the eGFP expressing adipocytes and APCs in the adult arise from this pool of embryonic Cre expressing cells (likely in the somatic LPM).

6.3.2 Prx1-Cre labelling of pericardial visceral white adipose tissue

The labelling of the pericardial visceral WAT was suprising, given the lack of labelling in the other visceral depots. We suggest that this can be explained by differences in developmental origin. As work from our group has shown, at least a proportion of the visceral adipocyte population is derived from the mesothelial layer that surrounds each depot (Chau *et al.*, 2014). Whilst the visceral mesothelia are derived from the splanchnic LPM, the parietal mesothelia come from the somatic LPM (Sheng, 2015). As explained above, we observed eGFP expression in the cells of the somatic LPM, but not the splanchnic LPM, of E9.5 *Prx1-Cre;R26R-mTmG* embryos. Therefore, the absense of eGFP positive cells in the perigonadal, mesenteric and omental depots is not surprising. However, we have demonstrated that the parietal pericardium (one component of the pericaridal membrane that encases the heart), is Prx1-Cre lineage positive, as would be expected given that it is derived from the somatic LPM (Brauer,

2003). We therefore hypothesise that at least a proportion of the pericardial adipocytes are derived from the parietal pericardium, therefore explaining why the percentage of eGFP expressing cells is much higher than in other visceral depots. We do not currently know what the origin of the pericardial Prx1-Cre lineage negative adipocytes is, however we speculate that it could be the epicardium (the visceral mesothelial component of the pericardial membrane). If possible, it would be interesting to use an epicardial-specific Cre line to investigate this. It has been shown that epicardial cells give rise to adipocytes of the epicardial adipose depot (the small visceral fat depot located in the atrial-ventricular groove of murine hearts), therefore it is known that the epicardium is a source of visceral adipose tissue during development (Liu *et al.*, 2014).

In addition to showing that a proportion of the pericardial APCs are Prx1-Cre lineage positive, we demonstrated that some of these cells also express *Wt1*. Therefore, we uncovered additional heterogeneity within the pericardial APC population. Moreover, preliminary work shows that this heterogeneity may impact on the adipocytes derived from the precursor cells, at least *in vitro*. When Prx1-Cre lineage positive, *Wt1* expressing pre-adipocytes were cultured seperately from Prx1-Cre lineage negative, *Wt1* expressing pre-adipocytes, the former population were more ameanable to adipogenesis. Considering we hypothesise that the Prx1-Cre lineage positive cells may have a different origin from the Prx1-Cre lineage negative cells, these different behaviours suggest that developmental origin impacts upon the properties and behaviour of the cells. Intriguingly, as shown in chapter 3, when $Wt1^{GFP/+}$ knock-in mice were fed a high fat diet, the pericardial adipose depot was the only visceral depot in which we did not observe a change in the percentage of precursor cells or a change in the percentage of *Wt1* expressing cells. Could this be a consequence of the differing developmental origin resulting in the cells responding differently to external cues? We propose to investigate this further by feeding *Prx1-Cre;tdRFP;*$Wt1^{GFP/+}$ mice a high fat diet and assessing the effect on the different populations of precursor cells in the pericardial adipose tissue.

6.4 *Prx1*$^{Cre/+}$;*Wt1*$^{loxP/loxP}$ mice have diaphragmatic hernias

Having shown that Prx1-Cre labels a proportion of the APCs from the pericardial visceral WAT depot, and that some of these labelled cells also express *Wt1*, we hoped that we would be able to use the *Prx1-Cre* line to conditionally delete *Wt1* and assess the effect this had on the development of the pericardial adipose tissue. However, it became apparent that in fact this cross was lethal, as *Prx1*$^{Cre/+}$;*Wt1*$^{loxP/loxP}$ mice were never present in the litters when the two week old pups were genotyped. Following considerable investigation, we ascertained that this lethality was likely due to the presence of diaphragmatic hernias and thus the disrupted development of the diaphragm. Interestingly, *Prx1*$^{Cre/+}$;*Wt1*$^{loxP/loxP}$ pups with hernias did survive until birth, however clearly struggled with breathing and died soon after being born. Most existing mouse models that have been used to study congenital diaphragmatic hernia (CDH) die during gestation (usually at around E13.5-E14.5), due to additional complications (Kreidberg *et al.*, 1993; Clugston *et al.*, 2006; Paris, Coles and Ackerman, 2015). Hence, this trait makes the *Prx1*$^{Cre/+}$;*Wt1*$^{loxP/loxP}$ model particularly useful for investigating developmental mechanisms in the diaphragm. Despite CDH being a severe and relatively common birth defect, the underlying causal mechanisms remain poorly understood (Greer, 2013). Therefore, we hoped that by utilising the *Prx1*$^{Cre/+}$;*Wt1*$^{loxP/loxP}$ model, we would help advance understanding in this field.

6.4.1 WT1 and the diaphragm

Several mouse models have been used to demonstrate that WT1 functions in diaphragm development (Paris, Coles and Ackerman, 2015; Carmona *et al.*, 2016). Moreover, *Wt1* null mice have diaphragmatic hernias (Kreidberg *et al.*, 1993). Additionally, mutations in *WT1* have been described in patients with CDH (Scott *et al.*, 2005; Holder *et al.*, 2007; Suri *et al.*, 2007; Antonius *et al.*, 2008). Therefore, it is already well known that WT1 is required for the correct development of the diaphragm. However, its exact function remains elusive. For models in which the gene is conditionally deleted, this deletion occurs in specific cell populations. For example, Carmona *et al*. (2016), used the *G2-Gata4*^{Cre} line to delete *Wt1* in the septum

transversum mesenchyme. Thus, combining current knowledge regarding phenotypes resulting from global *Wt1* deletion, with that acquired from models that permit conditional deletion in specific structures (including ours), should lead to an increased understanding of function.

6.4.2 *Wt1* deletion in the PPFs

One of the initial goals of our investigation was to understand which of the tissues/structures required for diaphragm development were affected by the conditional deletion of *Wt1* in the Prx1-Cre lineage. By examining the phenotype of E11.5/E12.5 $Prx1^{Cre/+};Wt1^{loxP/loxP}$ embryos, we found that the pleuroperitoneal fold (PPF)/ post hepatic mesenchymal plate (PHMP) continuum was disrupted. The formation of this continuum is essential for generating the initial separation between the thoracic and peritoneal cavities and ultimately the PPFs generate the connective tissue of the diaphragm (Merrell *et al.*, 2015; Carmona *et al.*, 2016). Subsequently, the lineage tracing model (*Prx1-Cre;R26R-mTmG*) was used to show that only the cells of the PPFs, and not the PHMP were Prx1-Cre lineage positive, and therefore, the deletion of *Wt1* must have been specifically affecting these structures. Furthermore, another model was developed ($Prx1^{Cre/+};Wt1^{GFP/loxP}$) which permitted the deletion of *Wt1* in the Prx1-Cre lineage, but at the same time labelled all cells in which *Wt1* would normally be expressed, with GFP. Utilising this model confirmed the results obtained thus far, showing the disrupted development of the PPFs coupled with an absence of WT1 in these structures. It is therefore interesting that despite the deletion of *Wt1* occurring specifically in the PPFs, the gross diaphragmatic phenotype was comparable to that described by Carmona *et al*. (2016), in which *Wt1* was deleted in the peripheral septum transversum mesenchyme, the PHMP and the PPFs. Moreover, we did not observe a lack of WT1 in the diaphragm mesothelium of the mutant embryos, only in the mesenchymal cells. Thus, our model provides evidence for the importance of the mesenchymal PPF cells in correct diaphragm development. Furthermore, the diaphragmatic phenotype in the $Prx1^{Cre/+};Wt1^{loxP/loxP}$ embryos is not dissimilar to that of *Wt1* null mice, despite only deleting *Wt1* in a limited population of cells (Kreidberg

et al., 1993; Clugston *et al.*, 2006). Hence, this provides additional support for the importance of the PPF cells, and for the expression of *Wt1* in these cells.

6.4.3 Investigating causative mechanisms for disrupted diaphragm development

Having established that *Wt1* deletion was occurring in the cells of the PPFs in our model, the next challenge was to investigate why this deletion resulted in disrupted development of the PPFs and thus ultimately disrupted development of the diaphragm. It is known that, as well as forming the connective tissue of the diaphragm, the PPF cells are respons
ible for guiding the muscle precursor cells into position. Therefore, if PPF cell migration does not occur correctly, the formation of the muscular component of the diaphragm is also affected (Merrell *et al.*, 2015). In E14.5 and E16.5 $Prx1^{Cre/+};Wt1^{loxP/loxP}$ embryos, we noted that the diaphragm was thickened in the region immediately adjacent to the hernia, and that the muscle fibres in this region appeared misaligned. This thickening is commonly observed in models of CDH and is attributed to the disrupted migration of the muscle precursor cells (Clugston *et al.*, 2006). Hence, this caused us to suspect that PPF cell migration was being affected by the deletion of *Wt1* in our model. Moreover, at E11.5, the time point at which the PPF/PHMP continuum is forming, the PPFs looked thickened with a "bunched up" appearance in the mutant embryos.

Given our hypothesis regarding the disrupted migration of the PPF cells in the $Prx1^{Cre/+};Wt1^{loxP/loxP}$ embryos, we explored several potential causative mechanisms. These included looking at EMT, the expression of RALDH2, due to the known involvement of retinoic acid signalling in diaphragm development, and assessing proliferation. Additionally, we are currently investigating whether cell adhesion is perturbed. WT1 is known to both directly and indirectly repress *Cdh1* in epicardial cells. Hence, as CDH1 is a major regulator of EMT, disrupted *Wt1* expression can affect EMT via this route (Martínez-Estrada *et al.*, 2010). For this reason we checked the expression of CDH1 in the PPFs of the $Prx1^{Cre/+};Wt1^{loxP/loxP}$ embryos. However,

we did not observe increased expression when compared to littermate controls. Additionally, we checked the expression of the mesenchymal marker, VIM, but also did not see a difference, suggesting that perhaps EMT is not disrupted. However, it is important that we check the expression of these markers at a slightly earlier development stage (~E10.5) to ensure that we are not missing the point at which a difference is apparent and important.

Conversely, we do see a difference in the expression of RALDH2. However, instead of seeing a decrease in RALDH2 expression in the mutants, as we had expected given that WT1 directly activates the transcription of *Raldh2* in the epicardium (Guadix *et al.*, 2011), and is required for *Raldh2* expression in the liver mesothelium (Ijpenberg *et al.*, 2007), we observed an increase in expression in the PPFs. As explained in detail in 5.8 we do not know why this is the case, and further work regarding this result it required. Given that retinoic acid signalling is well known to be important in diaphragm development it is definitely an area that needs following up (Greer, Babiuk and Thebaud, 2003). It would be interesting to supplement the diet of the pregnant mothers with retinoic acid to ascertain whether this, at least partially, rescues the diaphragmatic phenotype of the pups. Therefore, this would help us to understand whether retinoic acid signalling is disrupted in the mutants and is linked to the phenotype.

Interestingly, we have preliminary data showing a difference in the expression of ß-catenin in the PPFs of the control and mutant embryos at E11.5. ß-catenin has several functions in cellular adhesion and Wnt signalling, including being an important regulator of EMT (Thiery and Sleeman, 2006; von Gise *et al.*, 2011). Intriguingly, one study which showed that EMT is disrupted in the epicardium of *Wt1* knockout embryos, failed to observe a difference in the expression of epicardial E-cadherin, but did show that Wnt/ ß-catenin signalling was altered (von Gise *et al.*, 2011). Moreover, they showed that Wnt/ ß-catenin signalling has an important role in the regulation of epicardial EMT and that WT1 promoted the expression of ß-catenin in the epicardium (von Gise *et al.*, 2011). In fact, a link between *Wt1* and Wnt signalling in diaphragm development has already been established by Paris *et al.* (2015), who propose that ß-

catenin acts downstream of WT1 in the developing diaphragm. Although the focus was on the diaphragm mesothelium, they suggest that a reduction in TWIST1 expression in the non-muscle mesenchymal cells (as a result of disrupted Wnt signalling), leads to a lack of induction of a mesenchymal differentiation programme in these cells (Paris, Coles and Ackerman, 2015). Therefore, it would be worthwhile checking the expression of TWIST1 in our embryos. Alternatively, ß-catenin also acts at adherens junctions, where it is important in the linking transmembrane cadherins to the actin cytoskeleton and thus functions in cell adhesion (Bienz, 2005; Nelson, 2008). Hence, this result requires further investigation to assess whether cell adhesion and/or Wnt/ ß-catenin signalling is disrupted in the mutant embryos. We are currently looking at the expression of N-cadherin and its overlap with ß-catenin in control and mutant embryos, to allow us to further explore the possibility of a cell adhesion phenotype.

6.5 Conclusion

When I embarked on this project, it was intended that the *Prx1-Cre* mouse line would be utilised to investigate the role of *Wt1* in adipose tissue development. Whilst it has not been possible to do so, we have uncovered several interesting findings, both regarding adipose tissue biology and the etiology of CDH. Namely, our results have potential implications for the developmental origins of pericardial visceral WAT and subcutaneous WAT, and have shown increased heterogeneity regarding the pericardial depot. Moreover, we found that the expression of *Wt1* in the mesenchymal PPF cells is essential for the correct development of the diaphragm. Finally, it is evident that the heterogeneity that exists within the visceral APC population, with regards to *Wt1* expression, influences the properties and behaviour of these cells both *in vivo* and *in vitro*. Clearly, as has been discussed throughout, further work is required in all three areas, as several new interesting questions have been raised.

References

Abel, E. D., Peroni, O., Kim, J. K., Kim, Y. B., Boss, O., Hadro, E., Minnemann, T., Shulman, G. I. and Kahn, B. B. (2001) Adipose-selective targeting of the GLUT4 gene impairs insulin action in muscle and liver. *Nature*, 409(6821): 729–33.

Ackerman, K. G. and Greer, J. J. (2007) Development of the diaphragm and genetic mouse models of diaphragmatic defects. *American Journal of Medical Genetics*, 145C: 109–116.

Ackerman, K. G., Herron, B. J., Vargas, S. O., Huang, H., Tevosian, S. G., Kochilas, L., Rao, C., Pober, B. R., Babiuk, R. P., Epstein, J. A., Greer, J. J. and Beier, D. R. (2005) Fog2 is required for normal diaphragm and lung development in mice and humans. *PLoS Genetics*, 1(1): 0058–0065.

Ackerman, K. G., Vargas, S. O., Wilson, J. A., Jennings, R. W., Kozakewich, H. P. W. and Pober, B. R. (2012) Congenital diaphragmatic defects: proposal for a new classification based on observations in 234 patients. *Pediatr Dev Pathol*, 15(4): 265–274.

Adapala, V. J., Buhman, K. K. and Ajuwon, K. M. (2011) Novel anti-inflammatory role of SLPI in adipose tissue and its regulation by high fat diet. *Journal of inflammation*, 8(1): 5.

Ailhaud, G., Dani, C., Amri, E. Z., Djian, P., Vannier, C., Doglio, A., Forest, C., Gaillard, D., Negrel, R. and Grimaldi, P. (1989) Coupling growth arrest and adipocyte differentiation. *Environmental Health Perspectives*, 80(9): 17–23.

Antonius, T., van Bon, B., Eggink, A., van der Burgt, I., Noordam, K. and van Heijst, A. (2008) Denys–Drash syndrome and congenital diaphragmatic hernia: another case with the 1097G>A(Arg366His) mutation. *American Journal of Medical Genetics*, 146A: 496–499.

Armstrong, J. F., Pritchard-Jones, K., Bickmore, W. A., Hastie, N. D. and Bard, J. B. (1993) The expression of the Wilms' tumour gene, WT1, in the developing mammalian embryo. *Mechanisms of development*, 40(1–2): 85–97.

Arner, E., Westermark, P. O., Spalding, K. L., Britton, T., Ryde, M., Frise, J., Bernard, S. and Arner, P. (2010) Adipocyte Turnover : Relevance to Human Adipose Tissue. *Diabetes*, 59: 105–109.

Arner, P., Andersson, D. P., Thörne, A., Wirén, M., Hoffstedt, J., Näslund, E., Thorell, A. and Rydén, M. (2013) Variations in the size of the major omentum are primarily determined by fat cell number. *Journal of Clinical Endocrinology and Metabolism*, 98(5): 897–901.

Asahina, K., Zhou, B., Pu, W. T. and Tsukamoto, H. (2011) Septum transversum-derived mesothelium gives rise to hepatic stellate cells and perivascular mesenchymal cells in developing mouse liver. *Hepatology*, 53(3): 983–995.

Badeanlou, L., Furlan-Freguia, C., Yang, G., Ruf, W. and Samad, F. (2012) Tissue factor-PAR2 signaling promotes diet-induced obesity and adipose inflammation. *Nature medicine*, 17: 1490–1497.

Baer, P. C. (2014) Adipose-derived mesenchymal stromal/stem cells: An update on their phenotype in vivo and in vitro. *World journal of stem cells*, 6(3): 256–65.

Baglioni, S., Francalanci, M., Squecco, R., Lombardi, A., Cantini, G., Angeli, R., Gelmini, S., Guasti, D., Benvenuti, S., Annunziato, F., Bani, D., Liotta, F., Francini, F., Perigli, G., Serio, M. and Luconi, M. (2009) Characterization of human adult stem-cell populations isolated from visceral and subcutaneous adipose tissue. *FASEB journal*, 23(10): 3494–505.

Bell, L. N., Ward, J. L., Degawa-Yamauchi, M., Bovenkerk, J. E., Jones, R., Cacucci, B. M., Gupta, C. E., Sheridan, C., Sheridan, K., Shankar, S. S., Steinberg, H. O., March, K. L. and Considine, R. V. (2006) Adipose tissue production of hepatocyte growth factor contributes to elevated serum HGF in obesity.*American journal of physiology. Endocrinology and metabolism,* 291(4): E843-E848.

Bergman, R. N., Kim, S. P., Catalano, K. J., Hsu, I. R., Chiu, J. D., Kabir, M., Hucking, K. and Ader, M. (2006) Why visceral fat is bad: mechanisms of the metabolic syndrome. *Obesity*, 14 Suppl 1: 16S–19S.

Berry, D. C., Jiang, Y. and Graff, J. M. (2016) Emerging roles of adipose progenitor cells in tissue development , homeostasis , expansion and thermogenesis. *Trends in Endocrinology & Metabolism*, 27(8): 574–585.

Berry, R., Jeffery, E. and Rodeheffer, M. S. (2014) Weighing in on adipocyte precursors. *Cell Metabolism*, 19(1): 8–20.

Berry, R. and Rodeheffer, M. S. (2013) Characterization of the adipocyte cellular lineage in vivo. *Nature cell biology*, 15(3): 302–8.

Bharathavikru, R., Dudnakova, T., Aitken, S., Slight, J., Artibani, M., Hohenstein, P., Tollervey, D. and Hastie, N. (2017) Transcription factor Wilms' tumor 1 regulates developmental RNAs through 3' UTR interaction. *Genes and Development*, 31(4): 347–352.

Bienz, M. (2005) β-Catenin: A pivot between cell adhesion and Wnt signalling. *Current Biology*, 15(2): 64–67.

Billon, N. and Dani, C. (2012) Developmental origins of the adipocyte lineage: new insights from genetics and genomics studies. *Stem Cell Reviews and Reports*, 8(1): 55–66.

Birsoy, K., Berry, R., Wang, T., Ceyhan, O., Tavazoie, S., Friedman, J. M. and Rodeheffer, M. S. (2011) Analysis of gene networks in white adipose tissue

development reveals a role for ETS2 in adipogenesis. *Development*, 138(21): 4709–19.

Blüher, M., Michael, M. D., Peroni, O. D., Ueki, K., Carter, N., Kahn, B. B. and Kahn, C. R. (2002) Adipose tissue selective insulin receptor knockout protects against obesity and obesity-related glucose intolerance. *Developmental Cell*, 3(1): 25–38.

Blüher, M., Patti, M.-E., Gesta, S., Kahn, B. B. and Kahn, C. R. (2004) Intrinsic heterogeneity in adipose tissue of fat-specific insulin receptor knock-out mice is associated with differences in patterns of gene expression. *Journal of Biological Chemistry*, 279(30): 31891–31901.

Boon, M. R., van den Berg, S. A. A., Wang, Y., van den Bossche, J., Karkampouna, S., Bauwens, M., De Saint-Hubert, M., van der Horst, G., Vukicevic, S., de Winther, M. P. J., Havekes, L. M., Jukema, J. W., Tamsma, J. T., van der Pluijm, G., van Dijk, K. W. and Rensen, P. C. N. (2013) BMP7 activates brown adipose tissue and reduces diet-induced obesity only at subthermoneutrality. *PLoS ONE*, 8(9): e74083.

Brauer, P. R. (2003) *Human Embryology: The Ultimate USMLE Step 1 Review*. Philadelphia: Hanley & Belfus Inc.

Call, K., Glaser, T., Ito, C., Buckler, A., Pelletier, J., Haber, D., Rose, E., Kral, A., Yeger, H. and Lewis, W. (1990) Isolation and characterization of a zinc finger polypeptide gene at the human chromosome 11 Wilms' tumor locus. *Cell*, 60(3): 509–520.

Calo, E., Quintero-Estades, J. A., Danielian, P. S., Nedelcu, S., Berman, S. D. and Lees, J. A. (2010) Rb regulates fate choice and lineage commitment in vivo. *Nature*, 466(7310): 1110–1114.

Cano, E., Carmona, R. and Muñoz-Chápuli, R. (2013) Wt1-expressing progenitors contribute to multiple tissues in the developing lung. *American journal of physiology. Lung cellular and molecular physiology*, 305(4): L322-32.

Cantile, M., Procino, A., D'Armiento, M., Cindolo, L. and Cillo, C. (2003) HOX gene network is involved in the transcriptional regulation of in vivo human adipogenesis. *Journal of Cellular Physiology*, 194(2): 225–236.

Carmona, R., Cañete, A., Cano, E., Ariza, L., Rojas, A. and Muñoz-Chápuli, R. (2016) Conditional deletion of WT1 in the septum transversum mesenchyme causes congenital diaphragmatic hernia in mice. *eLife*, 5: 1–17.

Carmona, R., Cano, E., Mattiotti, A., Gaztambide, J. and Muñoz-Chápuli, R. (2013) Cells derived from the coelomic epithelium contribute to multiple gastrointestinal tissues in mouse embryos. *PLoS ONE*, 8(2): e55890.

Cartwright, M. J., Schlauch, K., Lenburg, M. E., Tchkonia, T., Pirtskhalava, T.,

Cartwright, A., Thomou, T. and Kirkland, J. L. (2010) Aging, depot origin, and preadipocyte gene expression. *Journals of Gerontology - Series A Biological Sciences and Medical Sciences*, 65(3): 242–251.

Cernea, M., Tang, W., Guan, H. and Yang, K. (2015) Wisp1 mediates Bmp3-stimulated mesenchymal stem cell proliferation. *Journal of Molecular Endocrinology,* 56(1): 39-46.

Chau, Y.-Y., Bandiera, R., Serrels, A., Martínez-Estrada, O. M., Qing, W., Lee, M., Slight, J., Thornburn, A., Berry, R., McHaffie, S., Stimson, R. H., Walker, B. R., Chapuli, R. M., Schedl, A. and Hastie, N. (2014) Visceral and subcutaneous fat have different origins and evidence supports a mesothelial source. *Nature cell biology*, 16(4): 367–75.

Chau, Y.-Y., Brownstein, D., Mjoseng, H., Lee, W.-C., Buza-Vidas, N., Nerlov, C., Jacobsen, S. E., Perry, P., Berry, R., Thornburn, A., Sexton, D., Morton, N., Hohenstein, P., Freyer, E., Samuel, K., van't Hof, R. and Hastie, N. (2011) Acute multiple organ failure in adult mice deleted for the developmental regulator Wt1. *PLoS genetics*, 7(12): e1002404.

Chau, Y.-Y. and Hastie, N. (2015) Wt1, the mesothelium and the origins and heterogeneity of visceral fat progenitors. *Adipocyte*, 4(3): 217–221.

Chau, Y.-Y. and Hastie, N. D. (2012) The role of Wt1 in regulating mesenchyme in cancer, development, and tissue homeostasis. *Trends in genetics*, 28(10): 515–24.

Christodoulides, C., Lagathu, C., Sethi, J. K. and Vidal-Puig, A. (2009) Adipogenesis and WNT signalling. *Trends in Endocrinology and Metabolism*, 20(1): 16–24.

Church, C. D., Berry, R. and Rodeheffer, M. S. (2014) Isolation and study of adipocyte precursors. in Macdougald, O. A. (ed.) *Methods in Enzymology*. 1st edn. San Diego, USA: Elsevier Inc., 31–46.

Chusyd, D. E., Wang, D., Huffman, D. M. and Nagy, T. R. (2016) Relationships between rodent white adipose fat pads and human white adipose fat depots. *Frontiers in nutrition*, 3(April): 10.

Cinti, S. (2005) The adipose organ. *Prostaglandins Leukotrienes and Essential Fatty Acids*, 73: 9–15.

Cleal, L. and Chau, Y.-Y. (2016) Isolation and fluorescence-activated cell sorting of murine WT1-expressing adipocyte precursor cells. in Hastie, N. (ed.) *The Wilms' Tumor (WT1) Gene: Methods and Protocols*. New York, NY: Springer New York, 81–91.

Cleal, L., Aldea, T., Chau, Y.Y. (2017) Fifty shades of white: understanding heterogeneity in white adipose stem cells. *Adipocyte*, 6(3):205-216.

Clugston, R. D., Klattig, J., Englert, C., Clagett-Dame, M., Martinovic, J., Benachi, A. and Greer, J. J. (2006) Teratogen-induced, dietary and genetic models of congenital diaphragmatic hernia share a common mechanism of pathogenesis. *The American journal of pathology*, 169(5): 1541–9.

Cohen, P., Levy, J. D., Zhang, Y., Frontini, A., Kolodin, D. P., Svensson, K. J., Lo, J. C., Zeng, X., Ye, L., Khandekar, M. J., Wu, J., Gunawardana, S. C., Banks, A. S., Camporez, J. P. G., Jurczak, M. J., Kajimura, S., Piston, D. W., Mathis, D., Cinti, S., *et al.* (2014) Ablation of PRDM16 and beige adipose causes metabolic dysfunction and a subcutaneous to visceral fat switch. *Cell*, 156(1–2): 304–316.

Coles, G. L. and Ackerman, K. G. (2013) Kif7 is required for the patterning and differentiation of the diaphragm in a model of syndromic congenital diaphragmatic hernia. *PNAS*, 110(21): E1898-905.

Corselli, M., Chen, C.-W., Sun, B., Yap, S., Rubin, J. P. and Péault, B. (2012) The tunica adventitia of human arteries and veins as a source of mesenchymal stem cells. *Stem Cells and Development*, 21(8): 1299–1308.

Corvera, S. and Gealekman, O. (2014) Adipose tissue angiogenesis: Impact on obesity and type-2 diabetes. *Biochimica et Biophysica Acta*, 1842(3): 463–472.

Crandall, D. L., Hausman, G. J. and Kral, J. G. (1997) A review of the microcirculation of adipose tissue: anatomic, metabolic, and angiogenic perspectives. *Microcirculation*, 4(2): 211–232.

Crisan, M., Casteilla, L., Lehr, L., Carmona, M., Paoloni-Giacobino, A., Yap, S., Sun, B., Léger, B., Logar, A., Pénicaud, L., Schrauwen, P., Cameron-Smith, D., Russell, A. P., Péault, B. and Giacobino, J.-P. (2008) A reservoir of brown adipocyte progenitors in human skeletal muscle. *Stem cells*, 26(9): 2425–2433.

Crisan, M., Yap, S., Casteilla, L., Chen, C. W., Corselli, M., Park, T. S., Andriolo, G., Sun, B., Zheng, B., Zhang, L., Norotte, C., Teng, P. N., Traas, J., Schugar, R., Deasy, B. M., Badylak, S., Buhring, H. J., Giacobino, J. P., Lazzari, L., *et al.* (2008) A perivascular origin for mesenchymal stem cells in multiple human organs. *Cell Stem Cell*, 3: 301–313.

Cristancho, A. G. and Lazar, M. A. (2011) Forming functional fat: a growing understanding of adipocyte differentiation. *Nature reviews. Molecular cell biology*, 12(11): 722–34.

Crossno, J. T. C., Majka, S. M., Grazia, T., Gill, R. G. and Klemm, D. J. (2006) Rosiglitazone promotes development of a novel adipocyte population from bone marrow–derived circulating progenitor cells. *Journal of Clinical Investigation*, 116(12): 3220–3228.

Cserjesi, P., Lilly, B., Bryson, L., Wang, Y., Sassoon, D. A. and Olson, E. N. (1992) MHox: a mesodermally restricted homeodomain protein that binds an essential site in

the muscle creatine kinase enhancer. *Development*, 115(4): 1087–1101.

Darimont, C., Avanti, O., Blancher, F., Wagniere, S., Mansourian, R., Zbinden, I., Leone-Vautravers, P., Fuerholz, A., Giusti, V. and Macé, K. (2008) Contribution of mesothelial cells in the expression of inflammatory-related factors in omental adipose tissue of obese subjects. *International journal of obesity*, 32(1): 112-120

Davies, J. A., Ladomery, M., Hohenstein, P., Michael, L., Shafe, A., Spraggon, L. and Hastie, N. (2004) Development of an siRNA-based method for repressing specific genes in renal organ culture and its use to show that the Wt1 tumour suppressor is required for nephron differentiation. *Human Molecular Genetics*, 13(2): 235–246.

Davies, R. C., Calvio, C., Bratt, E., Larsson, S. H., Lamond, A. I. and Hastie, N. D. (1998) WT1 interacts with the splicing factor U2AF65 in an isoform-dependent manner and can be incorporated into spliceosomes. *Genes and Development*, 12(20): 3217–3225.

Ding, J., Hsu, F.-C., Harris, T. B., Liu, Y., Kritchevsky, S. B., Szklo, M., Ouyang, P., Espeland, M. A., Lohmann, K. K., Criqui, M. H., Allison, M., Bluemke, Da. A. and Carr, J. J. (2009) The association of pericardial fat with incident coronary heart disease: the Multi-Ethnic Study of Atherosclerosis (MESA) 1–3. *American Journal of Clinical Nutrition*, 90: 499–504.

Dobbs-McAuliffe, B., Zhao, Q. and Linney, E. (2004) Feedback mechanisms regulate retinoic acid production and degradation in the zebrafish embryo. *Mechanisms of Development*, 121(4): 339–350.

Dominici, M., Blanc, K., Mueller, I., Slaper-Cortenbach, I., Marini, F. and Krause, D. (2006) Minimal criteria for defining multipotent mesenchymal stromal cells. The International Society for Cellular Therapy position statement. *Cytotherapy*, 8: 315–317.

Domyan, E. T., Branchfield, K., Gibson, D. A., Naiche, L. A., Lewandowski, M., Tessier-Lavigne, M., Ma, L. and Sun, X. (2013) Roundabout receptors are critical for foregut separation from the body wall. *Developmental Cell*, 24(1): 52–63.

Dong, L., Pietsch, S., Tan, Z., Perner, B., Sierig, R., Kruspe, D., Groth, M., Witzgall, R., Grone, H.-J., Platzer, M. and Englert, C. (2015) Integration of cistromic and transcriptomic analyses identifies Nphs2, Mafb, and Magi2 as Wilms' Tumor 1 target genes in podocyte differentiation and maintenance. *Journal of the American Society of Nephrology*, 26(9): 2118–2128.

Du, B., Cawthorn, W. P., Su, A., Doucette, C. R., Yao, Y., Hemati, N., Kampert, S., McCoin, C., Broome, D. T., Rosen, C. J., Yang, G. and MacDougald, O. A. (2013) The transcription factor paired-related homeobox 1 (Prrx1) inhibits adipogenesis by activating transforming growth factor-β (TGFβ) signaling. *The Journal of biological chemistry*, 288(5): 3036–3047.

Dunning, M. J., Smith, M. L., Ritchie, M. E. and Tavaré, S. (2007) Beadarray: R classes and methods for Illumina bead-based data. *Bioinformatics*, 23(16): 2183–2184.

Durland, J. L., Sferlazzo, M., Logan, M. and Burke, A. C. (2008) Visualizing the lateral somitic frontier in the Prx1Cre transgenic mouse. *Journal of anatomy*, 212(5): 590–602.

Edelstein, A. D., Tsuchida, M. A., Amodaj, N., Pinkard, H., Vale, R. D. and Stuurman, N. (2014) Advanced methods of microscope control using μManager software. *Journal of Biological Methods*, 1(2): 10.

Entenmann, G. and Hauner, H. (1996) Relationship between replication and differentiation in cultured human adipocyte precursor cells. *The American journal of physiology*, 270(4 Pt 1): C1011-6.

Essafi, A., Webb, A., Berry, R. L., Slight, J., Burn, S. F., Velecela, V., Martinez-estrada, O. M., Wiltshire, J. H., Stefan, G. E., Brownstein, D., Davies, J. A., Hastie, N. D. and Hohenstein, P. (2011) A Wt1-controlled chromatin switching mechanism underpins tissue-specific Wnt4 activation and repression. *Developmental Cell*, 21(3): 559–574.

Faust, I. M., Johnson, P. R. and Hirsch, J. (1977a) Adipose tissue regeneration following lipectomy. *Science*, 197(4301): 391–393.

Faust, I. M., Johnson, P. R. and Hirsch, J. (1977b) Surgical removal of adipose tissue alters feeding behavior and the development of obesity in rats. *Science*, 197(4301): 393–396.

Fedorenko, A., Lishko, P. V. and Kirichok, Y. (2012) Mechanism of fatty-acid-dependent UCP1 uncoupling in brown fat mitochondria. *Cell*. Elsevier, 151(2): 400–413.

Feil, S., Valtcheva, N. and Feil, R. (2009) Inducible Cre Mice. in Wurst, W. and Kühn, R. (eds) *Gene Knockout Protocols: Second Edition*. Totowa, NJ: Humana Press, 343–363.

Festa, E., Fretz, J., Berry, R., Schmidt, B., Rodeheffer, M. and Horowitz, M. (2011) Adipocyte lineage cells contribute to the skin stem cell niche to drive hair cycling. *Cell*. Elsevier Inc., 146(5): 761–771.

Friedman, S. L. (2008) Hepatic Stellate Cells : Protean, Multifunctional, and Enigmatic Cells of the Liver. *Physiological Reviews*, 88: 125–172.

Gao, Y., Toska, E., Denmon, D., Roberts, S. G. E. and Medler, K. F. (2014) WT1 regulates the development of the posterior taste field. *Development*, 141(11): 2271–2278.

Gesta, S., Blüher, M., Yamamoto, Y., Norris, A. W., Berndt, J., Kralisch, S.,

Boucher, J., Lewis, C. and Kahn, C. R. (2006) Evidence for a role of developmental genes in the origin of obesity and body fat distribution. *PNAS*, 103(17): 6676–6681.

Gesta, S., Tseng, Y. H. and Kahn, C. R. (2007) Developmental origin of fat: tracking obesity to its source. *Cell*, 131(2): 242–256.

Gimble, J. M., Katz, A. J. and Bunnell, B. A. (2007) Adipose-derived stem cells for regenerative medicine. *Circulation Research*, 100: 1249–1260.

Giralt, M., Cereijo, R. and Villarroya, F. (2016) Adipokines and the endocrine role of adipose tissues. *Handbook of Experimental Pharmacology*, 233: 265–282.

von Gise, A., Zhou, B., Honor, L. B., Ma, Q., Petryk, A. and Pu, W. T. (2011) WT1 regulates epicardial epithelial to mesenchymal transition through β-catenin and retinoic acid signaling pathways. *Developmental biology*, 356(2): 421–31.

Greenwood, M. R. C. and Hirsch, J. (1974) Postnatal development of adipocyte cellularity in the normal rat. *Journal of lipid research*, 15(5): 474–483.

Greer, J. J. (2013) Current concepts on the pathogenesis and etiology of congenital diaphragmatic hernia. *Respiratory Physiology & Neurobiology*, 189(2): 232–240.

Greer, J. J., Babiuk, R. P. and Thebaud, B. (2003) Etiology of congenital diaphragmatic hernia: The retinoid hypothesis. *Pediatric Research*, 53(5): 726–730.

Guadix, J. A., Ruiz-Villalba, A., Lettice, L., Velecela, V., Muñoz-Chápuli, R., Hastie, N. D., Pérez-Pomares, J. M. and Martínez-Estrada, O. M. (2011) Wt1 controls retinoic acid signalling in embryonic epicardium through transcriptional activation of Raldh2. *Development*, 138(6): 1093–1097.

Guimarães-Camboa, N., Cattaneo, P., Sun, Y., Moore-Morris, T., Gu, Y., Dalton, N. D., Rockenstein, E., Masliah, E., Peterson, K. L., Stallcup, W. B., Chen, J. and Evans, S. M. (2017) Pericytes of Multiple Organs Do Not Behave as Mesenchymal Stem Cells In Vivo. *Cell Stem Cell*, 345–359.

Guimarães-Camboa, N. and Evans, S. M. (2017) Are Perivascular Adipocyte Progenitors Mural Cells or Adventitial Fibroblasts? *Cell Stem Cell*, 20(5): 587–589.

Gupta, R. K., Arany, Z., Seale, P., Mepani, R. J., Ye, L., Conroe, H. M., Roby, Y. A., Kulaga, H., Reed, R. R. and Spiegelman, B. M. (2010) Transcriptional control of preadipocyte determination by Zfp423. *Nature*, 464(7288): 619–623.

Gupta, R. K., Mepani, R. J., Kleiner, S., Lo, J. C., Khandekar, M. J., Cohen, P., Frontini, A., Bhowmick, D. C., Ye, L., Cinti, S. and Spiegelman, B. M. (2012) Zfp423 expression identifies committed preadipocytes and localizes to adipose endothelial and perivascular cells. *Cell Metabolism*, 15(2): 230–239.

Gustafson, B., Hammarstedt, A., Hedjazifar, S., Hoffmann, J. M., Svensson, P.

A., Grimsby, J., Rondinone, C. and Smith. U. (2015) BMP4 and BMP antagonists regulate human white and beige adipogenesis. *Diabetes*, 64(5): 1670-1681.

Hammes, A., Guo, J. K., Lutsch, G., Leheste, J. R., Landrock, D., Ziegler, U., Gubler, M. C. and Schedl, A. (2001) Two splice variants of the wilms' tumor 1 gene have distinct functions during sex determination and nephron formation. *Cell*, 106(3): 319–329.

Han, J., Lee, J.-E., Jin, J., Lim, J. S., Oh, N., Kim, K., Chang, S.-I., Shibuya, M., Kim, H. and Koh, G. Y. (2011) The spatiotemporal development of adipose tissue. *Development*, 138(22): 5027–5037.

Den Hartigh, L. J., Wang, S., Goodspeed, L., Ding, Y., Averill, M., Subramanian, S., Wietecha, T., O'Brien, K. D. and Chait, A. (2014) Deletion of serum amyloid A3 improves high fat high sucrose diet-induced adipose tissue inflammation and hyperlipidemia in female mice. *PLoS ONE*, 9(9): 1-13.

Harmancey, R., Senard, J, M., Rouet, P., Pathak, A. and Smih, F. (2007) Adrenomedullin inhibits adipogenesis under transcriptional control of insulin. *Diabetes*, 56(3): 553-563.

Hartwig, S., Ho, J., Pandey, P., Macisaac, K., Taglienti, M., Xiang, M., Alterovitz, G., Ramoni, M., Fraenkel, E. and Kreidberg, J. A. (2010) Genomic characterization of Wilms' tumor suppressor 1 targets in nephron progenitor cells during kidney development. *Development*, 137(7): 1189–1203.

Hasson, P., Del Buono, J. and Logan, M. P. O. (2007) Tbx5 is dispensable for forelimb outgrowth. *Development*, 134(1): 85–92.

Hausman, D. B., DiGirolamo, M., Bartness, T. J., Hausman, G. J. and Martin, R. J. (2001) The biology of white adipocyte proliferation. *Obesity reviews : an official journal of the International Association for the Study of Obesity*, 2(4): 239–254.

Herberg, L., Doppen, W., Major, E. and Gries, F. A. (1974) Dietary-induced hypertrophic-hyperplastic obesity in mice. *Journal of lipid research*, 15: 580–585.

Herzer, U., Crocoll, A., Barton, D., Howells, N. and Englert, C. (1999) The Wilms tumor suppressor gene Wt1 is required for development of the spleen. *Current Biology*, 9(15): 837–841.

Higuchi, M., Kato, T., Chen, M., Yako, H., Yoshida, S., Kanno, N. and Kato, Y. (2013) Temporospatial gene expression of Prx1 and Prx2 is involved in morphogenesis of cranial placode-derived tissues through epithelio-mesenchymal interaction during rat embryogenesis. *Cell and Tissue Research*, 353(1): 27–40.

Hirsch, J. and Han, P. W. (1969) Cellularity of rat adipose tissue: effects of growth, starvation, and obesity. *Journal of lipid research*, 10(1): 77–82.

Hohenstein, P. and Hastie, N. D. (2006) The many facets of the Wilms' tumour gene, WT1. *Human Molecular Genetics*, 15: 196–201.

Holder, A. M., Klaassens, M., Tibboel, D., de Klein, A., Lee, B. and Scott, D. A. (2007) Genetic factors in congenital diaphragmatic hernia. *American journal of human genetics*, 80(5): 825–45.

Hosen, N., Shirakata, T., Nishida, S., Yanagihara, M., Tsuboi, a, Kawakami, M., Oji, Y., Oka, Y., Okabe, M., Tan, B., Sugiyama, H. and Weissman, I. L. (2007) The Wilms' tumor gene WT1-GFP knock-in mouse reveals the dynamic regulation of WT1 expression in normal and leukemic hematopoiesis. *Leukemia*, 21(8): 1783–91.

Hudak, C. S., Gulyaeva, O., Wang, Y., Park, S. min, Lee, L., Kang, C. and Sul, H. S. (2014) Pref-1 marks very early mesenchymal precursors required for adipose tissue development and expansion. *Cell Reports*, 8(3): 678–687.

Hutley, L. J., Newell, F. M., Joyner, J. M., Suchting, S. J., Herington, A. C., Cameron, D. P. and Prins, J. B. (2003) Effects of rosiglitazone and linoleic acid on human preadipocyte differentiation. *European Journal of Clinical Investigation*, 33: 574–581.

Iacobellis, G. (2009) Epicardial and Pericardial Fat: Close, but Very Different. *Obesity*, 17(4): 625–625.

Iacobellis, G. (2015) Local and systemic effects of the multifaceted epicardial adipose tissue depot. *Nature Reviews Endocrinology*, 11(6): 363–371.

Ihida-Stansbury, K., McKean, D. M., Gebb, S. A., Martin, J. F., Stevens, T., Nemenoff, R., Akeson, A., Vaughn, J. and Jones, P. L. (2004) Paired-related homeobox gene Prx1 is required for pulmonary vascular development. *Circulation research*, 94(11): 1507–14.

Ijpenberg, A., Pérez-Pomares, J. M., Guadix, J. A., Carmona, R., Portillo-Sánchez, V., Macías, D., Hohenstein, P., Miles, C. M., Hastie, N. D. and Muñoz-Chápuli, R. (2007) Wt1 and retinoic acid signaling are essential for stellate cell development and liver morphogenesis. *Developmental Biology*, 312(1): 157–170.

Iritani, I. (1984) Experimental study on embryogenesis of congenital diaphragmatic hernia. *Anatomy and Embryology*, 169(2): 133–139.

Jay, P. Y., Bielinska, M., Erlich, J. M., Mannisto, S., Pu, W. T., Heikinheimo, M. and Wilson, D. B. (2007) Impaired mesenchymal cell function in Gata4 mutant mice leads to diaphragmatic hernias and primary lung defects. *Developmental Biology*, 301(2): 602–614.

Jeffery, E., Church, C. D., Holtrup, B., Colman, L. and Rodeheffer, M. S. (2015) Rapid depot-specific activation of adipocyte precursor cells at the onset of obesity. *Nature cell biology*, 17(4): 376–85.

Jeffery, E., Wing, A., Holtrup, B., Sebo, Z., Kaplan, J. L., Saavedra-Peña, R., Church, C. D., Colman, L., Berry, R. and Rodeheffer, M. S. (2016) The adipose tissue microenvironment regulates depot-specific adipogenesis in obesity. *Cell Metabolism*, 24: 1–9.

Jernås, M., Palming, J., Sjöholm, K., Jennische, E., Svensson, P. A., Gabrielsson, B. G., Levin, M., Sjögren, A., Rudemo, M., Lystig, T. C., Carlsson, B., Carlsson, L. M. S. and Lönn, M. (2006) Separation of human adipocytes by size: hypertrophic fat cells display distinct gene expression. *The FASEB journal*, 20(9): 1540–1542.

Jiang, Y., Berry, D. C., Tang, W. and Graff, J. M. (2014) Independent stem cell lineages regulate adipose organogenesis and adipose homeostasis. *Cell Reports*, 9(3): 1007–1022.

Joe, A. W. B., Lin, Y., Even, Y., Vogl, A. W. and Rossi, F. M. V (2009) Depot-specific differences in adipogenic progenitor abundance and proliferative response to high-fat diet. *Stem Cells*, 27(10): 2563–2570.

Joe, A. W. B., Yi, L., Natarajan, A., Grand, F. Le, So, L., Wang, J., Rudnicki, M. A. and Rossi, F. M. V (2010) Muscle injury activates resident fibro / adipogenic progenitors that facilitate myogenesis. *Nature Cell Biology*, 12(2): 153–163.

Johnson, P. R., Zucker, L. M., Cruce, J. A. F. and Hirsch, J. (1971) Cellularity of adipose depots in the genetically obese Zucker rat. *Journal of lipid research*, 12(6): 706–14.

Kann, M., Ettou, S., Jung, Y. L., Lenz, M. O., Taglienti, M. E., Park, P. J., Schermer, B., Benzing, T. and Kreidberg, J. A. (2015) Genome-wide analysis of wilms' tumor 1-controlled gene expression in podocytes reveals key regulatory mechanisms. *Journal of the American Society of Nephrology*, 26(9): 2097–2104.

Karastergiou, K., Smith, S. R., Greenberg, A. S. and Fried, S. K. (2012) Sex differences in human adipose tissues – the biology of pear shape. *Biology of Sex Difference*, 3(1): 13.

Kim, B., Lee, B., Kyung, M., Seung, K., Gong, P., Hyun, N., Hyun, P., Seung, H., Jae, K., No, H., Yang, W., Ae, P. and Park, K. (2016) Gene expression profiles of human subcutaneous and visceral adipose - derived stem cells. *Cell Biochemistry & Function*, 34(8): 563–571.

Kim, S. M., Lun, M., Wang, M., Senyo, S. E., Guillermier, C., Patwari, P. and Steinhauser, M. L. (2014) Loss of white adipose hyperplastic potential is associated with enhanced susceptibility to insulin resistance. *Cell Metabolism*, 20(6): 1049–1058.

King-Underwood, L. and Pritchard-Jones, K. (1998) Wilms' tumor (WT1) gene mutations occur mainly in acute myeloid leukemia and may confer drug resistance. *Blood*, 91(8): 2961–8.

King-Underwood, L., Renshaw, J. and Pritchard-Jones, K. (1996) Mutations in the Wilms' tumor gene WT1 in leukemias. *Blood*, 87(6): 2171–9.

Kispert, A., Vainio, S. and McMahon, A. P. (1998) Wnt-4 is a mesenchymal signal for epithelial transformation of metanephric mesenchyme in the developing kidney. *Development*, 125(21): 4225–4234.

Koh, Y. J., Kang, S., Lee, H. J., Choi, T. S., Lee, H. S., Cho, C. H. and Koh, G. Y. (2007) Bone marrow-derived circulating progenitor cells fail to transdifferentiate into adipocytes in adult adipose tissues in mice. *Journal of Clinical Investigation*, 117(12): 3684–3695.

Kral, J. G. (1976) Surgical reduction of adipose tissue male Sprague-Dawley rat. *American journal of physiology*, 231(4): 1090–1096.

Kreidberg, J. A., Sarioia, H., Loring, J. M., Maeda, Y., Peiietier, J., Housman, D. and Jaenisch, R. (1993) WT-1 Is Required for Early Kidney Development. *Cell*, 74: 679–691.

Krueger, K. C., Costa, M. J., Du, H. and Feldman, B. J. (2014) Characterization of cre recombinase activity for in vivo targeting of adipocyte precursor cells. *Stem Cell Reports*, 3(6): 1147–1158.

Lamers, D., Famulla, S., Wronkowitz, N., Hartwig, S., Lehr, S., Ouwens, D. M., Eckardt, K., Kaufman, J. M., Ryden, M., Müller, S., Hanisch, F. G., Ruige, J., Arner, P., Sell, H. and Eckel, J. (2011) Dipeptidyl peptidase 4 is a novel adipokine potentially linking obesity to the metabolic syndrome. *Diabetes*, 60(7): 1917-1925.

Larsson, S. H., Charlieu, J. P., Miyagawa, K., Engelkamp, D., Rassoulzadegan, M., Ross, A., Cuzin, F., Heyningen, V. van and Hastie, N. D. (1995) Subnuclear localization of WT1 in splicing or transcription factor domains is regulated by alternative splicing. *Cell*, 81(3): 391–401.

Lee, M.-R., Lim, C.-J., Lee, Y.-H., Park, J.-G., Sonn, S. K., Lee, M.-N., Jung, I.-H., Jeong, S.-J., Jeon, S., Lee, M., Oh, K. S., Yang, Y., Kim, J. B., Choi, H.-S., Jeong, W., Jeong, T.-S., Yoon, W. K., Kim, H. C., Choi, J.-H. and Oh, G. T. (2014) The adipokine Retnla modulates cholesterol homeostasis in hyperlipidemic mice. *Nature Communications,* 5: 4410.

Lee, L. M. Y., Leung, C.-Y., Tang, W. W. C., Choi, H.-L., Leung, Y.-C., McCaffery, P. J., Wang, C.-C., Woolf, A. S. and Shum, A. S. W. (2012) A paradoxical teratogenic mechanism for retinoic acid. *Proceedings of the National Academy of Sciences*, 109(34): 13668–13673.

Lee, S., Starkey, P. M. and Gordon, S. (1985) Quantitative analysis of total macrophage content in adult mouse tissues. *Journal of experimental medicine*, 161: 475–489.

Lee, Y.-K. and Cowan, C. A. (2013) White to brite adipocyte transition and back again. *Nature Cell Biology*, 15(6): 568–569.

Lee, Y. H., Petkova, A. P., Konkar, A. A. and Granneman, J. G. (2015) Cellular origins of cold-induced brown adipocytes in adult mice. *FASEB Journal*, 29(1): 286–299.

Lee, Y. H., Petkova, A. P., Mottillo, E. P. and Granneman, J. G. (2012) In vivo identification of bipotential adipocyte progenitors recruited by B3-adrenoceptor activation and high-fat feeding. *Cell Metabolism*, 15(4): 480–491.

Li, Y., Jiang, C., Wang, X., Zhang, Y., Shibahara, S. and Takahashi, K. (2007) Adrenomedullin is a novel adipokine: Adrenomedullin in adipocytes and adipose tissues. *Peptides,* 28(5): 1129-1143.

Linder, K., Arner, P., Flores-Morales, A., Tollet-Egnell, P. and Norstedt, G. (2004) Differentially expressed genes in visceral or subcutaneous adipose tissue of obese men and women. *Journal of lipid research*, 45(1): 148–154.

Little, M. and Wells, C. (1997) A Clinical Overview of WT 1 Gene Mutations. *Human mutation*, 9: 209–225.

Liu, L., Zou, P., Zheng, L., Linarelli, L. E., Amarell, S., Passaro, A., Liu, D. and Cheng, Z. (2015) Tamoxifen reduces fat mass by boosting reactive oxygen species. *Cell death & disease*, 6(1): e1586.

Liu, Q., Huang, X., Oh, J.-H., Lin, R.-Z., Duan, S., Yu, Y., Yang, R., Qiu, J., Melero-Martin, J. M., Pu, W. T. and Zhou, B. (2014) Epicardium-to-fat transition in injured heart. *Cell research*, 24(11): 1367–9.

Loeb, D. M., Evron, E., Patel, C. B., Sharma, P. M., Niranjan, B., Buluwela, L., Weitzman, S. A., Korz, D. and Sukumar, S. (2001) Wilms' Tumor Suppressor Gene (WT1) Is Expressed in Primary Breast Tumors Despite Tumor-specific Promoter Methylation. *Cancer Research*, 61: 921–925.

Logan, M., Martin, J. F., Nagy, A., Lobe, C., Olson, E. N. and Tabin, C. J. (2002) Expression of Cre Recombinase in the developing mouse limb bud driven by a Prxl enhancer. *Genesis*, 33(2): 77–80.

Longo, K. A., Wright, W. S., Kang, S., Gerin, I., Chiang, S. H., Lucas, P. C., Opp, M. R. and MacDougald, O. A. (2004) Wnt10b inhibits development of white and brown adipose tissues. *Journal of Biological Chemistry*, 279(34): 35503–35509.

Lu, M., Cheng, H., Lacy, A. R., Kern, M. J., Argao, E. A., Potter, S. S., Olson, E. N. and Martin, J. F. (1999) Paired-related homeobox genes cooperate in handplate and hindlimb zeugopod morphogenesis. *Developmental Biology*, 205: 145–157.

Luche, H., Weber, O., Rao, T. N. and Blum, C. (2007) Faithful activation of an

extra-bright red fluorescent protein in " knock-in " Cre-reporter mice ideally suited for lineage tracing studies. *European Journal of Immunology*, 37: 43–53.

Macotela, Y., Emanuelli, B., Mori, M. a., Gesta, S., Schulz, T. J., Tseng, Y. H. and Kahn, C. R. (2012) Intrinsic differences in adipocyte precursor cells from different white fat depots. *Diabetes*, 61(7): 1691–1699.

Majka, S. M., Fox, K. E., Psilas, J. C., Helm, K. M., Childs, C. R., Acosta, A. S., Janssen, R. C., Friedman, J. E., Woessner, B. T., Shade, T. R., Varella-Garcia, M. and Klemm, D. J. (2010) De novo generation of white adipocytes from the myeloid lineage via mesenchymal intermediates is age, adipose depot, and gender specific. *Proceedings of the National Academy of Sciences*, 107(33): 14781–14786.

Majka, S. M., Miller, H. L., Sullivan, T., Erickson, P. F., Kong, R., Weiser-Evans, M., Nemenoff, R., Moldovan, R., Morandi, S. A., Davis, J. A. and Klemm, D. J. (2012) Adipose lineage specification of bone marrow-derived myeloid cells. *Adipocyte*, 1(4): 215–229.

Markus, M. A., Heinrich, B., Raitskin, O., Adams, D. J., Mangs, H., Goy, C., Ladomery, M., Sperling, R., Stamm, S. and Morris, B. J. (2006) WT1 interacts with the splicing protein RBM4 and regulates its ability to modulate alternative splicing in vivo. *Experimental Cell Research*, 312(17): 3379–3388.

Martin, J. F., Bradley, A. and Olson, E. N. (1995) The paired-like homeo box gene MHox is required for early events of skeletogenesls in multiple lineages. *Genes & development*, 9: 1237–1249.

Martin, J. F. and Olson, E. N. (2000) Identification of a prx1 limb enhancer. *Genesis*, 26(4): 225–9.

Martínez-Estrada, O. M., Lettice, L. A., Essafi, A., Guadix, J. A., Slight, J., Velecela, V., Hall, E., Reichmann, J., Devenney, P. S., Hosen, N., Hill, R. E., Muñoz-chapuli, R. and Hastie, N. D. (2010) Wt1 is required for cardiovascular progenitor cell formation through transcriptional control of Snail and E-cadherin. *Nature Genetics*, 42(1): 89–93.

Mayer, S., Metzger, R. and Kluth, D. (2011) The embryology of the diaphragm. *Seminars in Pediatric Surgery*, 20(3): 161–169.

McHaffie, S. L., Hastie, N. D. and Chau, Y.-Y. (2016) Effects of CreERT2, 4-OH Tamoxifen, and Gender on CFU-F Assays. *PLoS ONE*, 11(2): 1–12.

Meissburger, B., Perdikari, A., Moest, H., Müller, S., Geiger, M. and Wolfrum, C. (2016) Regulation of adipogenesis by paracrine factors from adipose stromal-vascular fraction - a link to fat depot-specific differences. *Biochimica et Biophysica Acta - Molecular and Cell Biology of Lipids*, 1861(9): 1121–1131.

Menke, A., McInnes, L., Hastie, N. D. and Schedl, A. (1998) The Wilms' tumor

suppressor WT1 : Approaches to gene function. *Kidney International*, 53: 1512–1518.

Merrell, A. J., Ellis, B. J., Fox, Z. D., Lawson, J. A., Weiss, J. A. and Kardon, G. (2015) Muscle connective tissue controls development of the diaphragm and is a source of congenital diaphragmatic hernias. *Nature genetics*. Nature Publishing Group, 47(5): 496–504.

Merrell, A. J. and Kardon, G. (2014) Development of the diaphragm, a skeletal muscle essential for mammalian respiration. *FEBS J*, 280(17): 1–15.

Mey, J., Babiuk, R. P., Clugston, R., Zhang, W. and Greer, J. J. (2003) Retinal dehydrogenase-2 is inhibited by compounds that induce congenital diaphragmatic hernias in rodents. *The American journal of pathology*, 162(2): 673–679.

Miller-Hodges, E. and Hohenstein, P. (2012) WT1 in disease: shifting the epithelial-mesenchymal balance. *The Journal of pathology*, 226(2): 229–40.

Mitchell, J. B., McIntosh, K., Zvonic, S., Garrett, S., Floyd, Z. E., Kloster, A., Di Halvorsen, Y., Storms, R. W., Goh, B., Kilroy, G., Wu, X. and Gimble, J. M. (2006) Immunophenotype of human adipose-derived cells: temporal changes in stromal-associated and stem cell-associated markers. *Stem cells*, 24(2): 376–385.

Monteiro, R. and Azevedo, I. (2010) Chronic inflammation in obesity and the metabolic syndrome. *Mediators of Inflammation*, 2010.

Moore, A. W., McInnes, L., Kreidberg, J., Hastie, N. D. and Schedl, A. (1999) YAC complementation shows a requirement for Wt1 in the development of epicardium, adrenal gland and throughout nephrogenesis. *Development*, 126(9): 1845–57.

Motamedi, F. J., Badro, D. A., Clarkson, M., Rita Lecca, M., Bradford, S. T., Buske, F. A., Saar, K., Hübner, N., Brändli, A. W. and Schedl, A. (2014) WT1 controls antagonistic FGF and BMP-pSMAD pathways in early renal progenitors. *Nature Communications*, 5.

Muise, E. S., Souza, S., Chi, A., Tan, Y., Zhao, X., Liu, F., Dallas-yang, Q., Wu, M., Sarr, T., Zhu, L., Guo, H., Li, Z., Li, W., Hu, W., Jiang, G., Paweletz, C. P., Hendrickson, R. C., Thompson, J. R., Mu, J., Berger, J. P. and Mehmet, H. (2013) Downstream signaling pathways in mouse adipose tissues following acute in vivo administration of fibroblast growth factor 21. *PLoS ONE,* 8(9): 1-17.

Murahovschi, V., Pivovarova, O., Ilkavets, I., Dmitrieva, R. M., Döcke, S., Keyhani-Nejad, F., Gögebakan, Ö., Osterhoff, M., Kemper, M., Hornemann, S., Markova, M., Klöting, N., Stockmann, M., Weickert, M. O., Lamounier-Zepter, V., Neuhaus, P., Konradi, A., Dooley, S. et al. (2015) WISP1 Is a novel adipokine linked to inflammation in obesity. *Diabetes*, 64(3): 856-866.

Muzumdar, M. D., Tasic, B., Miyamichi, K., Li, L. and Luo, L. (2007) A Global Double-Fluorescent Cre Reporter Mouse. *Genesis*, 45(September): 593–605.

Natoli, T. A., McDonald, A., Alberta, J. A., Taglienti, M. E., Housman, D. E. and Kreidberg, J. A. (2002) A mammal-specific exon of WT1 is not required for development or fertility. *Molecular and cellular biology*, 22(12): 4433–8.

Nelson, W. J. (2008) Regulation of cell-cell adhesion by the caderhin-catenin complex. *Biochem Soc Trans*, 36: 149–155.
Ng, C. W., Pozanski, W. J., Borowiecki, M. and Reimer, G. (1971) Differences in Growth in vitro of Adipose Cells from Normal and Obese Patients. *Nature*, 231: 445.

Niksic, M., Slight, J., Sanford, J. R., Caceres, J. F. and Hastie, N. D. (2004) The Wilms' tumour protein (WT1) shuttles between nucleus and cytoplasm and is present in functional polysomes. *Human Molecular Genetics*, 13(4): 463–471.

Oji, Y., Miyoshi, S., Maeda, H., Hayashi, S., Tamaki, H., Nakatsuka, S., Yao, M., Takahashi, E., Nakano, Y., Hirabayashi, H., Shintani, Y., Oka, Y., Tsuboi, A., Hosen, N., Asada, M., Fujioka, T., Murakami, M., Kanato, K., Motomura, M., *et al.* (2002) Overexpression of the wilms' tumor gene wt1 in de novo lung cancers. *International Journal of Cancer*, 100: 297–303.

Oji, Y., Suzuki, T., Nakano, Y., Maruno, M., Nakatsuka, S., Jomgeow, T., Tatsumi, N., Yokota, A., Aoyagi, S., Nakazawa, T., Ito, K., Kanato, K., Nishida, S., Hosen, N., Kawakami, M., Tsuboi, A., Oka, Y., Yoshimine, T. and Sugiyama, H. (2004) Overexpression of the Wilms' tumor gene WT1 in primary astrocytic tumors. *Cancer Science*, 95(10): 822–827.

Oji, Y., Yamamoto, H., Nomura, M., Nakano, Y., Ikeba, A., Nakatsuka, S., Abeno, S., Kiyotoh, E., Jomgeow, T., Sekimoto, M., Nezu, R., Yoshikawa, Y., Inoue, Y., Hosen, N., Kawakami, M., Tsuboi, A., Oka, Y., Ogawa, H., Souda, S., *et al.* (2003) Overexpression of the Wilms' tumor gene WT1 in colorectal adenocarcinoma. *Cancer Science*, 94(8): 712–717.

Paris, N. D., Coles, G. L. and Ackerman, K. G. (2015) Wt1 and β-catenin cooperatively regulate diaphragm development in the mouse. *Developmental Biology*, 407(1): 40–56.

Paulmyer-Lacroix, O., Desbriere, R., Poggi, M., Achard, V., Alessi, M. C., Boudouresque, F., Ouafik, L. H., Vuaroqueaux, V., Labuhn, M., Dutour, A. and Grino, M. (2006) Expression of adrenomedullin in adipose tissue of lean and obese women. *European Journal of Endocrinology*, 155(1): 177-185.

Pelletier, J., Schalling, M., Buckler, A. J., Haber, D. A. and Housman, D. (1991) Expression of the Wilms' tumor gene WT1 in the murine urogenital system. *Genes & Development*, 5: 1345–1356.

Pérez-Pomares, J. M. and Muñoz-Chápuli, R. (2002) Epithelial-mesenchymal

transitions: A mesodermal cell strategy for evolutive innovation in metazoans. *Anatomical Record*, 268(3): 343–351.

Perrini, S., Ficarella, R., Picardi, E., Cignarelli, A., Barbaro, M., Nigro, P., Peschechera, A., Palumbo, O., Carella, M., De Fazio, M., Natalicchio, A., Laviola, L., Pesole, G. and Giorgino, F. (2013) Differences in gene expression and cytokine release profiles highlight the heterogeneity of distinct subsets of adipose tissue-derived stem cells in the subcutaneous and visceral adipose tissue in humans. *PLoS ONE*, 8(3): e57892.

Petrovic, N., Walden, T. B., Shabalina, I. G., Timmons, J. A., Cannon, B. and Nedergaard, J. (2010) Chronic peroxisome proliferator-activated receptor γ (PPARγ) activation of epididymally derived white adipocyte cultures reveals a population of thermogenically competent, UCP1-containing adipocytes molecularly distinct from classic brown adipocytes. *Journal of Biological Chemistry*, 285(10): 7153–7164.

Phipson, B., Lee, S., Majewski, I. J., Alexander, W. S. and Smyth, G. K. (2016) Robust hyperparameter estimation protects against hypervariable genes and improves power to detect differential expression. *Annals of Applied Statistics*, 10(2): 946–963.

Pober, B. R., Russell, M. K. and Ackerman, K. G. (2010) Congenital diaphragmatic hernia overview. in *Pagon RA, Adam MP, Ardinger HH, et al., editors. GeneReviews.* University of Washington: Seattle, 1993–2017.

Que, J., Wilm, B., Hasegawa, H., Wang, F., Bader, D. and Hogan, B. L. M. (2008) Mesothelium contributes to vascular smooth muscle and mesenchyme during lung development. *Proceedings of the National Academy of Sciences*, 105(43): 16626–16630.

Rao, M. K., Pham, J., Imam, J. S., Maclean, J. A., Murali, D., Furuta, Y., Sinha-hikim, A. P. and Wilkinson, M. F. (2006) Tissue-specific RNAi reveals that WT1 expression in nurse cells controls germ cell survival and spermatogenesis. *Genes & development*, 20: 147–152.

Rene Rodriguez, E. and Tan, C. D. (2017) Structure and anatomy of the human pericardium. *Progress in Cardiovascular Diseases*, 59(4): 327–340.

Ritchie, M. E., Phipson, B., Wu, D., Hu, Y., Law, C. W., Shi, W. and Smyth, G. K. (2015) limma powers differential expression analyses for RNA-sequencing and microarray studies. *Nucleic acids research*, 43(7): e47.

Rivera, M. N. and Haber, D. A. (2005) Wilms' tumour: connecting tumorigenesis and organ development in the kidney. *Nature Review Cancer*, 5: 699–712.

Rodbell, M. (1964) Metabolism of isolated fat cells. *The Journal of biological chemistry*, 239(2): 375–380.

Rodeheffer, M. S., Birsoy, K. and Friedman, J. M. (2008) Identification of white

adipocyte progenitor cells in vivo. *Cell*, 135(2): 240–249.

Rosen, E. D. and Spiegelman, B. M. (2014) What we talk about when we talk about fat. *Cell*, 20–44.

Rosenwald, M., Perdikari, A., Rülicke, T. and Wolfrum, C. (2013) Bi-directional interconversion of brite and white adipocytes. *Nature cell biology*. Nature Publishing Group, 15(6): 659–67.

Rosito, G. A., Massaro, J. M., Hoffmann, U., Ruberg, F. L., Mahabadi, A. A., Vasan, R. S., O'Donnell, C. J. and Fox, C. S. (2008) Pericardial fat, visceral abdominal fat, cardiovascular disease risk factors, and vascular calcification in a community-based sample the framingham heart study. *Circulation*, 117(5): 605–613.

Rourke, J. L., Muruganandan, S., Dranse, H. J., McMullen, N. M. and Sinal, C. J. (2014) Gpr1 is an active chemerin receptor influencing glucose homeostasis in obese mice. *Journal of Endocrinology*, 222(2): 201-215

Russell, M. K., Longoni, M., Wells, J., Maalouf, F. I., Tracy, A. A., Loscertales, M., Ackerman, K. G., Pober, B. R., Lage, K., Bult, C. J. and Donahoe, P. K. (2012) Congenital diaphragmatic hernia candidate genes derived from embryonic transcriptomes. *Proceedings of the National Academy of Sciences*, 109(8): 2978–2983.

Rydén, M., Uzunel, M., Hård, J. L., Borgström, E., Mold, J. E., Arner, E., Mejhert, N., Andersson, D. P., Widlund, Y., Hassan, M., Jones, C. V., Spalding, K. L., Svahn, B. M., Ahmadian, A., Frisén, J., Bernard, S., Mattsson, J. and Arner, P. (2015) Transplanted bone marrow-derived cells contribute to human adipogenesis. *Cell Metabolism*, 22(3): 408–417.

Sanchez-Gurmaches, J. and Guertin, D. A. (2014a) Adipocyte lineages: Tracing back the origins of fat. *Biochimica et Biophysica Acta - Molecular Basis of Disease*. Elsevier B.V., 340–351.

Sanchez-Gurmaches, J. and Guertin, D. A. (2014b) Adipocytes arise from multiple lineages that are heterogeneously and dynamically distributed. *Nature communications*, 5: 4099.

Sanchez-Gurmaches, J., Hsiao, W. Y. and Guertin, D. A. (2015) Highly selective in vivo labeling of subcutaneous white adipocyte precursors with Prx1-Cre. *Stem Cell Reports*, 4: 1–10.

Sanchez-Gurmaches, J., Hung, C. M. and Guertin, D. A. (2016) Emerging Complexities in Adipocyte Origins and Identity. *Trends in Cell Biology*, 26(5): 313–326.

Sanchez-Gurmaches, J., Hung, C. M., Sparks, C. A., Tang, Y., Li, H. and Guertin, D. A. (2012) PTEN loss in the Myf5 lineage redistributes body fat and reveals subsets of white adipocytes that arise from Myf5 precursors. *Cell Metabolism*. Elsevier Inc.,

16(3): 348–362.

Saraswathi, V., Ramnanan, C. J., Wilks, A. W., Desouza, C. V., Eller, A. A., Murali, G., Ramalingam, R., Milne, G. L., Coate, K. C. and Edgerton, D. S. (2013) Impact of hematopoietic cyclooxygenase-1 deficiency on obesity-linked adipose tissue inflammation and metabolic disorders in mice. *Metabolism: Clinical and Experimental*, 62(11): 1673–1685.

Scott, D. A., Cooper, M. L., Stankiewicz, P., Patel, A., Potocki, L. and Cheung, S. W. (2005) Congenital diaphragmatic hernia in WAGR syndrome. *American Journal of Medical Genetics*, 134A: 430–433.

Seale, P., Bjork, B., Yang, W., Kajimura, S., Chin, S., Kuang, S., Scimè, A., Devarakonda, S., Conroe, H. M., Erdjument-Bromage, H., Tempst, P., Rudnicki, M. A., Beier, D. R. and Spiegelman, B. M. (2008) PRDM16 controls a brown fat/skeletal muscle switch. *Nature*, 454(7207): 961–967.

Seale, P., Conroe, H. M., Estall, J., Kajimura, S., Frontini, A., Ishibashi, J., Cohen, P., Cinti, S. and Spiegelman, B. M. (2011) Prdm16 determines the thermogenic program of subcutaneous white adipose tissue in mice. *Journal of Clinical Investigation*, 121(1): 96–105.

Sengenès, C., Lolmède, K., Zakaroff-Girard, A., Busse, R. and Bouloumié, A. (2005) Preadipocytes in the human subcutaneous adipose tissue display distinct features from the adult mesenchymal and hematopoietic stem cells. *Journal of Cellular Physiology*, 205(1): 114–122.

Sera, Y., LaRue, A. C., Moussa, O., Mehrotra, M., Duncan, J. D., Williams, C. R., Nishimoto, E., Schulte, B. A., Watson, P. M., Watson, D. K. and Ogawa, M. (2009) Hematopoietic stem cell origin of adipocytes. *Experimental Hematology*, 37(9): 1108–1120.

Sharp, L. Z., Shinoda, K., Ohno, H., Scheel, D. W., Tomoda, E., Ruiz, L., Hu, H., Wang, L., Pavlova, Z., Gilsanz, V. and Kajimura, S. (2012) Human BAT possesses molecular signatures that resemble beige/brite cells. *PLoS ONE*, 7(11).

Sheng, G. (2015) The developmental basis of mesenchymal stem/stromal cells (MSCs). *BMC Developmental Biology*, 15(1): 44.

Sheng, X., Yung, Y. C., Chen, A. and Chun, J. (2015) Lysophosphatidic acid signalling in development. *Development,* 142(8): 1390-1395.

Shih, W. T. and Yamada, S. (2012) N-cadherin as a key regulator of collective cell migration in a 3D environment. *Cell Adhesion & Migration*, 6(6): 513–517.

Shinohara, H. (1997) Distribution of lymphatic stomata on the pleural surface of the thoracic cavity and the surface topography of the pleural mesothelium in the golden hamster. *Anatomical Record*, 249(1): 16–23.

Solovjov, D. A., Pluskota, E. and Plow, E. F. (2005) Distinct roles for the alpha and beta subunits in the functions of integrin alphaMbeta2. *Journal of Biological Chemistry*, 280(2): 1336–1345.

Spalding, K. L., Arner, E., Westermark, P. O., Bernard, S., Buchholz, B. A., Bergmann, O., Blomqvist, L., Hoffstedt, J., Näslund, E., Britton, T., Concha, H., Hassan, M., Rydén, M., Frisén, J. and Arner, P. (2008) Dynamics of fat cell turnover in humans. *Nature*, 453(7196): 783–7.

Stan, R. V, Tse, D., Deharvengt, S. J., Smits, N. C., Xu, Y., Luciano, R., Mcgarry, C. L., Buitendijk, M., Nemani, K. V, Kobayashi, T., Shipman, S. L., Moodie, K. L., Charles, P., Ernst, P. A., Lee, H., Suriawinata, A. A., Schned, A. R., Longnecker, D. S., Fiering, S. N., *et al.* (2012) The diaphragms of fenestrated endothelia – gatekeepers of vascular permeability and blood composition. *Developmental cell*, 23(6): 1203–1218.

Starr, M. E., Hu, Y., Stromberg, A. J., Carmical, J. R., Wood, T. G., Evers, B. M. and Saito, H. (2013) Gene expression profile of mouse white adipose tissue during inflammatory stress: Age-dependent upregulation of major procoagulant factors. *Aging Cell,* 12(2): 194-206.

Stark, K., Vainio, S., Vassileva, G. and McMahon, A. P. (1994) Epithelial transformation of metanephric mesenchyme in the developing kidney regulated by Wnt-4. *Nature*, 372: 679–683.

Stohn, J. P., Wang, Q., Siviski, M. E., Kennedy, K., Jin, Y.-R., Kacer, D., DeMambro, V., Liaw, L., Vary, C. P., Rosen, C. J., Prudovsky, I. and Lindner, V. (2015) Cthrc1 Controls Adipose Tissue Formation, Body Composition, and Physical Activity. *Obesity*, 23: 1633–1642.

Suffee, N., Moore-Morris, T., Farahmand, P., Rücker-Martin, C., Dilanian, G., Fradet, M., Sawaki, D., Derumeaux, G., LePrince, P., Clément, K., Dugail, I., Puceat, M. and Hatem, S. N. (2017) Atrial natriuretic peptide regulates adipose tissue accumulation in adult atria. *Proceedings of the National Academy of Sciences*, 114(5): E771–E80.

Suh, J. M., Gao, X., McKay, J., McKay, R., Salo, Z. and Graff, J. M. (2006) Hedgehog signaling plays a conserved role in inhibiting fat formation. *Cell Metabolism*, 3(1): 25–34.

Suri, M., Kelehan, P., O'Neill, D., Vadeyar, S., Grant, J., Ahmed, S. F., Tolmie, J., McCann, E., Lam, W., Smith, S., FitzPatrick, D., Hastie, N. D. and Reardon, W. (2007) WT1 mutations in meacham syndrome suggest a coelomic mesothelial origin of the cardiac and diaphragmatic malformations. *American Journal of Medical Genetics*, 143A: 2312–2320.

Takahashi, M., Takahashi, Y., Takahashi, K., Zolotaryov, F. N., Hong, K. S., Iida,

K., Okimura, Y., Kaji, H. and Chihara, K. (2007) CXCL14 enhances insulin-dependent glucose uptake in adipocytes and is related to high-fat diet-induced obesity. *Biochemical and Biophysical Research Communications*, 364(4): 1037–1042.

Tang, W., Zeve, D., Suh, J. M., Bosnakovski, D., Kyba, M., Hammer, R. E., Tallquist, M. D. and Graff, J. M. (2008) White fat progenitor cells reside in the adipose vasculature. *Science*, 322(5901): 583–586.

Tchkonia, T., Giorgadze, N., Pirtskhalava, T., Tchoukalova, Y., Karagiannides, I., Forse, R. A., Deponte, M., Stevenson, M., Guo, W., Han, J., Waloga, G., Lash, T. L., Jensen, M. D. and Kirkland, J. L. (2002) Fat depot origin affects adipogenesis in primary cultured and clone human preadipocytes. *American Journal of Physiology Regulatory, Integrative and Comparitive Physiology*, 282: R1286–R1296.

Tchkonia, T., Giorgadze, N., Pirtskhalava, T., Thomou, T., DePonte, M., Koo, A., Forse, R. A., Chinnappan, D., Martin-Ruiz, C., Von Zglinicki, T. and Kirkland, J. L. (2006) Fat depot-specific characteristics are retained in strains derived from single human preadipocytes. *Diabetes*, 55(9): 2571–2578.

Tchkonia, T., Lenburg, M., Thomou, T., Giorgadze, N., Frampton, G., Pirtskhalava, T., Cartwright, A., Cartwright, M., Flanagan, J., Karagiannides, I., Gerry, N., Forse, R. A., Tchoukalova, Y., Jensen, M. D., Pothoulakis, C. and Kirkland, J. L. (2007) Identification of depot-specific human fat cell progenitors through distinct expression profiles and developmental gene patterns. *American journal of physiology. Endocrinology and metabolism*, 292(1): E298-307.

Tchkonia, T., Morbeck, D. E., Von Zglinicki, T., Van Deursen, J., Lustgarten, J., Scrable, H., Khosla, S., Jensen, M. D. and Kirkland, J. L. (2010) Fat tissue, aging, and cellular senescence. *Aging Cell*, 9(5): 667–684.

Tchkonia, T., Tchoukalova, Y. D., Giorgadze, N., Pirtskhalava, T., Karagiannides, I., Forse, R. A., Koo, A., Stevenson, M., Chinnappan, D., Cartwright, A., Jensen, M. D. and Kirkland, J. L. (2005) Abundance of two human preadipocyte subtypes with distinct capacities for replication, adipogenesis, and apoptosis varies among fat depots. *American journal of physiology. Endocrinology and metabolism*, 288(1): E267–E277.

Tchkonia, T., Thomou, T., Zhu, Y., Karagiannides, I., Pothoulakis, C., Jensen, M. D. and Kirkland, J. L. (2013) Mechanisms and metabolic implications of regional differences among fat depots. *Cell Metabolism*, 17(5): 644–656.

Teng, M. S., Wu, S., Hsu, L. A., Chou, H. H. and Ko, Y. L. (2015) Differential associations between CDH13 genotypes, adiponectin levels, and circulating levels of cellular adhesive molecules. *Mediators of Inflammation,* 2015.

Thiery, J. P. and Sleeman, J. P. (2006) Complex networks orchestrate epithelial-mesenchymal transitions. *Nature reviews. Molecular cell biology*, 7(2): 131–42.

Timmons, J. A., Wennmalm, K., Larsson, O., Walden, T. B., Lassmann, T., Petrovic, N., Hamilton, D. L., Gimeno, R. E., Wahlestedt, C., Baar, K., Nedergaard, J. and Cannon, B. (2007) Myogenic gene expression signature establishes that brown and white adipocytes originate from distinct cell lineages. *Proceedings of the National Academy of Sciences of the United States of America*, 104(11): 4401–4406.

Tomiyama, K., Murase, N., Stolz, D. B., Toyokawa, H., O'Donnell, D. R., Smith, D. M., Dudas, J. R., Rubin, J. P. and Marra, K. G. (2008) Characterization of transplanted green fluorescent protein + bone marrow cells into adipose tissue. *Stem Cells*, 26(2): 330–338.

Toska, E. and Roberts, S. G. E. (2014) Mechanisms of transcriptional regulation by WT1 (Wilms' tumour 1). *The Biochemical journal*, 461(1): 15–32.

Tourniaire, F., Romier-Crouzet, B., Lee, J. H., Marcotorchino, J., Gouranton, E., Salles, J., Malezet, C., Astier, J., Darmon, P., Blouin, E., Walrand, S., Ye, J. and Landrier, J. F. (2013) Chemokine Expression in Inflamed Adipose Tissue Is Mainly Mediated by NF-kB. *PLoS ONE*, 8(6): 1–9.

Toyoda, M., Matsubara, Y., Lin, K., Sugimachi, K. and Furue, M. (2009) Characterization and comparison of adipose tissue-derived cells from human subcutaneous and omental adipose tissues. *Cell biochemistry and function*, 27: 440–447.

Traktuev, D. O., Merfeld-Clauss, S., Li, J., Kolonin, M., Arap, W., Pasqualini, R., Johnstone, B. H. and March, K. L. (2008) A population of multipotent CD34-positive adipose stromal cells share pericyte and mesenchymal surface markers, reside in a periendothelial location, and stabilize endothelial networks. *Circulation Research*, 102: 77–85.

Tran, K. V, Gealekman, O., Frontini, A., Zingaretti, M. C., Morroni, M., Giordano, A., Smorlesi, A., Perugini, J., De Matteis, R., Sbarbati, A., Corvera, S. and Cinti, S. (2012) The vascular endothelium of the adipose tissue gives rise to both white and brown fat cells. *Cell Metab*, 15(2): 222–229.

Tuna, M., Chavez-Reyes, A. and Tari, A. M. (2005) HER2/neu increases the expression of Wilms' Tumor 1 (WT1) protein to stimulate S-phase proliferation and inhibit apoptosis in breast cancer cells. *Oncogene*, 24: 1648–1652.

Uezumi, A., Fukada, S., Yamamoto, N., Takeda, S. and Tsuchida, K. (2010) Mesenchymal progenitors distinct from satellite cells contribute to ectopic fat cell formation in skeletal muscle. *Nature Cell Biology*, 12(2): 143–152.

Vishvanath, L., Long, J. Z., Spiegelman, B. M. and Gupta, R. K. (2017) Do Adipocytes Emerge from Mural Progenitors? *Cell Stem Cell*, 20(5): 585–586.

Vishvanath, L., Macpherson, K. A., Hepler, C., Wang, Q. A., Shao, M., Spurgin,

S. B., Wang, M. Y., Kusminski, C. M., Morley, T. S. and Gupta, R. K. (2016) Pdgfrβ+ mural preadipocytes contribute to adipocyte hyperplasia induced by high-fat-diet feeding and prolonged cold exposure in adult mice. *Cell Metabolism*, 23(2): 350–359.

Vohl, M., Sladek, R., Robitaille, J., Gurd, S., Marceau, P., Richard, D., Hudson, T. J. and Sladek, R. O. B. (2004) A survey of genes differentially expressed in subcutaneous and visceral adipose tissue in men. *Obesity research*, 12(8): 1217–1222.

Wada, T., Ihunnah, C. a, Gao, J., Chai, X., Zeng, S., Philips, B. J., Rubin, J. P., Marra, K. G. and Xie, W. (2011) Estrogen sulfotransferase inhibits adipocyte differentiation. *Molecular endocrinology*, 25(9): 1612–1623.

Wagner, K., Wagner, N., Vidal, V. P. I., Schley, G., Wilhelm, D., Schedl, A., Englert, C. and Scholz, H. (2002) The Wilms' tumor gene Wt1 is required for normal development of the retina. *The EMBO Journal*, 21(6): 1398–1405.

Wagner, N., Michiels, J. F., Schedl, A. and Wagner, K.-D. (2008) The Wilms' tumour suppressor WT1 is involved in endothelial cell proliferation and migration: expression in tumour vessels in vivo. *Oncogene*, 27(26): 3662–3672.

Wagner, N., Wagner, K., Hammes, A., Kirschner, K. M., Vidal, V. P., Schedl, A. and Scholz, H. (2005) A splice variant of the Wilms' tumour suppressor Wt1 is required for normal development of the olfactory system. *Development*, 132: 1327–1336.

Wajchenburg, B. L. (2014) Subcutaneous and visceral adipose tissue : their relation to the metabolic syndrome. *Endocrine Reviews*, 21: 697–738.

Walker, C., Rutten, F., Yuan, X., Pass, H., Mew, D. M. and Everitt, J. (1994) Wilms Tumor Suppressor Gene Expression in Rat and Human Mesothelioma. *Cancer Research*, 54: 3101–3107.

Wang, Q. A., Tao, C., Gupta, R. K. and Scherer, P. E. (2013) Tracking adipogenesis during white adipose tissue development, expansion and regeneration. *Nature medicine*, 19(10): 1338–44.

Wang, S. and Yang, X. (2017) Inter-organ regulation of adipose tissue browning. *Cellular and Molecular Life Sciences*, 74: 1765–1776.

Wang, W. and Seale, P. (2016) Control of brown and beige fat development. *Nature Reviews Molecular Cell Biology*, 17(11): 691–702.

Wassermann, F. (2011) The development of adipose tissue. in *Comprehensive Physiology*. John Wiley & Sons, Inc., 87–100.

White, H. M., Acton, A. J., Kamocka, M. M. and Considine, R. V. (2014) Hepatocyte growth factor regulates neovascularization in developing fat pads.

American journal of physiology. Endocrinology and metabolism, 306(2): E189-E196.

WHO (2015) *Fiscal Policies for Diet and Prevention of Noncommunicable Diseases*.

Wilm, B., Ipenberg, A., Hastie, N. D., Burch, J. B. E. and Bader, D. M. (2005) The serosal mesothelium is a major source of smooth muscle cells of the gut vasculature. *Development and disease*, 132(23): 5317–5328.

Wu, J., Boström, P., Sparks, L. M., Ye, L., Choi, J. H., Giang, A. H., Khandekar, M., Virtanen, K. A., Nuutila, P., Schaart, G., Huang, K., Tu, H., Van Marken Lichtenbelt, W. D., Hoeks, J., Enerbäck, S., Schrauwen, P. and Spiegelman, B. M. (2012) Beige adipocytes are a distinct type of thermogenic fat cell in mouse and human. *Cell*, 150(2): 366–376.

Wu, J., Jun, H. and McDermott, J. R. (2015) Formation and activation of thermogenic fat. *Trends in Genetics*, 31(5): 232–238.

Wu, Y., Kim, J. Y., Zhou, S. and Smas, C. M. (2008) Differential screening identifies transcripts with depot-dependent expression in white adipose tissues. *BMC Genomics*, 9: 397.

Xu, X. J., Gauthier, M.-S., Hess, D. T., Apovian, C. M., Cacicedo, J. M., Gokce, N., Farb, M., Valentine, R. J. and Ruderman, N. B. (2012) Insulin sensitive and resistant obesity in humans: AMPK activity, oxidative stress, and depot-specific changes in gene expression in adipose tissue. *Journal of lipid research*, 53(4): 792–801.

Xue, R., Lynes, M. S. M. D., Dreyfuss, J. M., Shamsi, F., Schulz, T. J., Zhang, H., Huang, T. L., Townsend, K. L., Li, Y., Takahashi, H., Weiner, L. S., White, A. P., Lynes, M. S. M. D., Rubin, L. L., Goodyear, L. J., Cypess, A. M. and Tseng, Y. (2015) Clonal analyses and gene profiling identify genetic biomarkers of the thermogenic potential of human brown and white preadipocytes. *Nature medicine*, 21(7): 760–768.

Yamaguchi, Y., Cavallero, S., Patterson, M., Shen, H., Xu, J., Kumar, S. R. and Sucov, H. M. (2015) Adipogenesis and epicardial adipose tissue: a novel fate of the epicardium induced by mesenchymal transformation and PPARγ activation. *Proceedings of the National Academy of Sciences of the United States of America*, 112(7): 2070–5.

Yamamoto, Y., Gesta, S., Lee, K. Y., Tran, T. T., Saadatirad, P. and Kahn, C. R. (2010) Adipose depots possess unique developmental gene signatures. *Obesity (Silver Spring, Md.)*, 18(5): 872–8.

Yan, Q., Yang, Q., Mody, N., Graham, T. E., Hsu, C., Xu, Z., Houstis, N. E., Kahn, B. B. and Rosen, E. D. (2007) The adipokine lipocalin 2 is regulated by obesity and promotes kinsulin resistance. *October*, 56(October): 2533–40.

Yang, L., Han, Y., Suarez Saiz, F., Saurez Saiz, F. and Minden, M. D. (2007) A tumor suppressor and oncogene: the WT1 story. *Leukemia*, 21(5): 868–76.

You, L.-R., Takamoto, N., Yu, C.-T., Tanaka, T., Kodama, T., Demayo, F. J., Tsai, S. Y. and Tsai, M.-J. (2005) Mouse lacking COUP-TFII as an animal model of Bochdalek-type congenital diaphragmatic hernia. *PNAS*, 102(45): 16351–16356.

Yu, J., Ka, S. O., Kwon, K. B., Lee, S. M., Park, J. W. and Park, B. H. (2011) Overexpression of the small GTPase Arl4D suppresses adipogenesis. *International Journal of Molecular Medicine*, 28(5): 793–798.

Yuan, W., Rao, Y., Babiuk, R. P., Greer, J. J., Wu, J. Y. and Ornitz, D. M. (2003) A genetic model for a central (septum transversum) congenital diaphragmatic hernia in mice lacking Slit3. *Proc Natl Acad Sci USA*, 100(9): 5217–5222.

Zhang, B., Xiao, W., Qiu, H., Zhang, F., Moniz, H. A., Jaworski, A., Condac, E., Gutierrez-Sanchez, G., Heiss, C., Clugston, R. D., Azadi, P., Greer, J. J., Bergmann, C., Moremen, K. W., Li, D., Linhardt, R. J., Esko, J. D. and Wang, L. (2014) Heparan sulfate deficiency disrupts developmental angiogenesis and causes congenital diaphragmatic hernia. *Journal of Clinical Investigation*, 124(1): 209–221.

Zhang, D., Simmen, R. C., Michel, F. J., Zhao, G., Vale-Cruz, D. and Simmen, F. A. (2002) Secretory leukocyte protease inhibitor mediates proliferation of human endometrial epithelial cells by positive and negative regulation of growth-associated genes. *Journal of Biological Chemistry*, 277(33): 29999–30009.

Zhang, Z., Liu, X., Morgan, D. A., Kuburas, A., Thedens, D. R., Russo, A. F. and Rahmouni, K. (2011) Neuronal receptor activity-modifying protein 1 promotes energy expenditure in mice. *Diabetes,* 60(4): 1063-1071.

Zheng, B., Cao, B., Li, G. and Huard, J. (2006) Mouse adipose-derived stem cells undergo multilineage differentiation in vitro but primarily osteogenic and chondrogenic differentiation in vivo. *Tissue Engineering*, 12(7): 1891–1901.

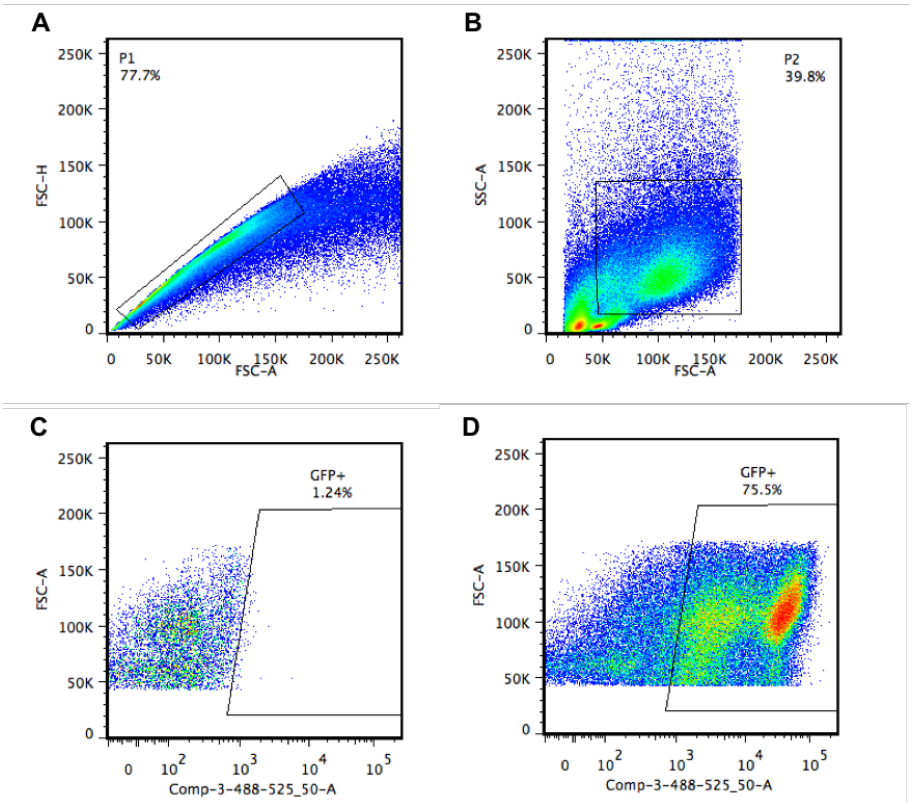
Zhou, B., Ma, Q., Rajagopal, S., Wu, S. M., Domian, I., Rivera-Feliciano, J., Jiang, D., von Gise, A., Ikeda, S., Chien, K. R. and Pu, W. T. (2008) Epicardial progenitors contribute to the cardiomyocyte lineage in the developing heart. *Nature*, 454(7200): 109–13.

Zilleßen, P., Celner, J., Kretschmann, A., Pfeifer, A., Racké, K. and Mayer, P. (2016) Metabolic role of dipeptidyl peptidase 4 (DPP4) in primary human (pre)adipocytes. *Scientific Reports*, 6: 23074.

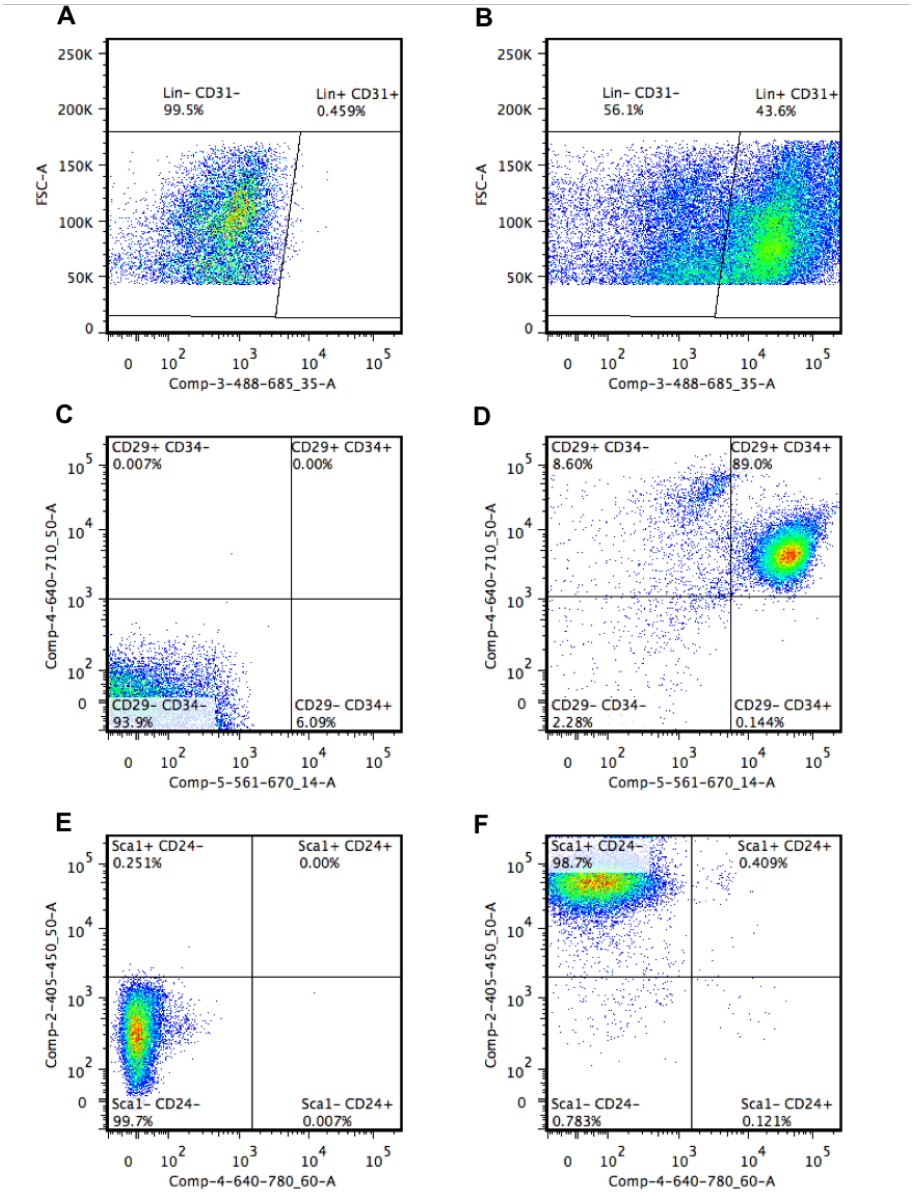
Zuk, P. A., Zhu, M., Ashjian, P., Ugarte, D. A. De, Huang, J. I., Mizuno, H., Alfonso, Z. C., Fraser, J. K., Benhaim, P. and Hedrick, M. H. (2002) Human adipose tissue is a source of multipotent stem cells. *Molecular Biology of the Cell*, 13: 4279–4295.

Appendix

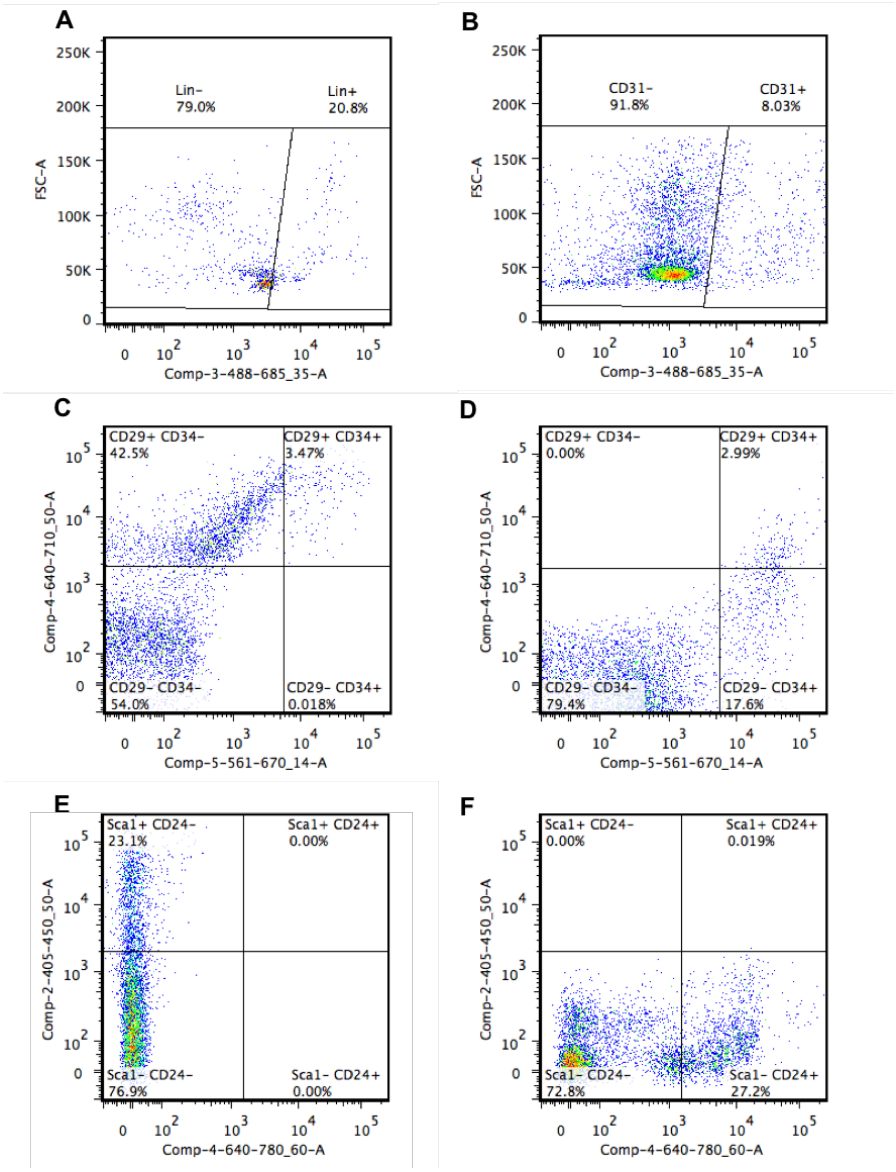
Forward Scatter–Height (FSC-H) values were plotted against Forward Scatter-Area (FSC-A) to exclude doublets and select for singlets (A). The FSC-H and FSC-A values for singlets should be approximately the same, and therefore the cells can be selected by applying a gate around the diagonal (45 degrees, passing through zero), as shown in Figure A. Subsequently, the central population in a Side Scatter-Area (SSC-A) vs. FSC-A plot was selected to remove debris and dead cells (Figure B). When selecting for GFP positive cells (Figure D), a GFP negative control sample was used to establish the gate (Figure C). For example when cells from the *Wt1*$^{GFP/+}$ knock-in mouse were being analysed/sorted, a control sample from a *Wt1*$^{+/+}$ littermate was always included for gating.



When samples were stained with the panel of antibodies to permit sorting of APCs/pre-adipocytes, un-stained controls were always included for gating. Figures A, C and E all represent un-stained cell samples and B, D and F represent stained samples. Figure B shows gating for the lineage panel of antibodies (CD3e, CD11b, CD45R, Ly-6G and Ly-6C, TER-119) and CD31. Gating for CD29 and CD34 is illustrated in Figure D, and Figure F shows the gating for Sca-1 and CD24.



In addition to un-stained controls, single-stained controls were always included to allow compensation to be performed. Compensation is an important process when performing multicolour flow cytometric analysis and sorting. When using multiple stains, it is possible that the emission spectra of two or more fluorochromes may overlap. Therefore, a population of cells that is negative for the antigen of interest appears positive as a consequence of bleed through of the signal from another fluorescent antibody. By staining a sample of cells with just one fluorescent antibody from the panel, the gates can be established in the correct places. Figures A-F show single-stained controls for each antibody on the panel used to analyse/sort APCs/pre-adipocytes: lineage panel (A), CD31 (B), CD29 (C), CD34 (D), Sca-1 (E), CD24 (F).



All genes downregulated in $Wt1^{+}$ Lin^{-};$CD31^{-}$;$CD29^{+}$;$CD34^{+}$ perigonadal SVF cells from mice fed a HFD, with a q-value <0.05 and a LogFC <-1.5. All genes in this table were selected for validation by qRT-PCR.

GENE	LOG FOLD CHANGE	Q VALUE	NAME/BRIEF DESCRIPTION (UNIPROT HTTP://WWW.UNIPROT.ORG AND ENTREZ GENE HTTPS://WWW.NCBI.NLM.NIH.GOV/GENE)	EXISTING LINKS TO ADIPOSE TISSUE FOUND IN THE LITERATURE
Krt19	-2.55	$2.35x10^{-2}$	Keratin 19. Mesothelial cell marker. Intermediate filament protein. Involved in the organisation of myofibers	Visceral adipose tissue depots have a mesothelium and this is a source of adipocyte precursor cells (Chau *et al.*, 2014). Mesothelial cells from human omental adipose tissue taken from obese females, express inflammatory-related factors (Darimont *et al*., 2008).
Upk3b	-2.46	$4.25x10^{-2}$	Uroplakin-3b. Mesothelial cell marker. Component of apical plaques of mammalian urothelium.	Visceral adipose tissue depots have a mesothelium and this is a source of adipocyte precursor cells (Chau *et al.*, 2014). Mesothelial cells from human omental adipose tissue taken from obese females, express inflammatory-related factors (Darimont *et al*., 2008).
Msln	-2.1	$4.24x10^{-2}$	Mesothelin. Mesothelial cell marker. Cell adhesion protein.	Visceral adipose tissue depots have a mesothelium and this is a source of adipocyte precursor cells (Chau *et al.*, 2014). Mesothelial cells from human omental adipose tissue taken from obese females, express inflammatory-related factors (Darimont *et al*., 2008).
Clic3	-1.85	$4.24x10^{-2}$	Chloride intracellular channel protein 3. Inserts into membranes to form chloride ion channels.	
Cldn3	-1.77	$3.86x10^{-2}$	Claudin 3. Integral membrane protein. Component of tight junctions, important for cell-cell adhesion in epithelium.	
Serpina3c	-1.52	$3.53x10^{-2}$	Serine protease inhibitor A3C. Plasma protease inhibitor.	

All genes downregulated in Wt1$^-$ Lin$^-$;CD31$^-$;CD29$^+$;CD34$^+$ perigonadal SVF cells from mice fed a HFD, with a q-value <0.05 and a LogFC <-1.5. Genes in black were selected for validation by qRT-PCR.

GENE	LOG FOLD CHANGE	Q VALUE	NAME/BRIEF DESCRIPTION (UNIPROT HTTP://WWW.UNIPROT.ORG AND ENTREZ GENE HTTPS://WWW.NCBI.NLM.NIH.GOV/GENE)	EXISTING LINKS TO ADIPOSE TISSUE FOUND IN THE LITERATURE
Gnai1	-2.67	9.56×10^{-3}	Guanine nucleotide binding protein (G protein), alpha inhibiting 1. Required for normal cytokinesis during mitosis	
Retnla	-2.54	4.69×10^{-2}	Resistin-like alpha. Probable hormone. Plays a role in pulmonary vascular remodeling.	Adipokine. Expression regulated by food intake. Overexpression decreases cholesterol in mice (Lee *et al*., 2014).
Col4a3	-2.3	1.76×10^{-4}	Collagen alpha-3(IV) chain. Encodes a subunit of type IV collagen; a major structural component of basement membranes.	
Ramp1	-2.13	1.59×10^{-2}	Receptor activity-modifying protein 1. A receptor for calcitonin-gene-related peptide. Main function of calcitonin receptors is to inhibit bone reabsorption and increase calcium excretion by the kidneys.	Regulation energy homeostasis; overexpression in CNS causes reduced body weight and adiposity (Zhang *et al*., 2011).
Slc17a7	-2.05	3.56×10^{-2}	Vesicular glutamate transporter 1. Mediates glutamate uptake into synaptic vesicles at presynaptic nerve terminals of excitatory neural cells.	
Lamc3	-2.04	2.61×10^{-2}	Laminin subunit gamma-3. Major constituent of basement membranes. Involved in many biological processes including cell adhesion, differentiation, migration, and signaling.	
Tubb4a	-2.00	1.34×10^{-2}	Tubulin beta-4A chain. Tubulin is the major constituent of microtubules.	
Nmb	-1.99	4.75×10^{-3}	Neuromedin B. A member of the bombesin-like family of neuropeptides, which negatively regulate eating behavior.	
Scin	-1.94	1.28×10^{-2}	Scinderin. A Ca(2+)-dependent actin-severing and -capping protein. Regulation of exocytosis by influencing microfilament network.	
Sult1e1	-1.92	2.63×10^{-3}	Estrogen sulfotransferase/Sulfotransferase family 1E member 1. Possible role in the regulation of estrogen receptor activity	Inhibits adipocyte differentiation (Wada *et al*., 2011).
Cd82	-1.90	2.49×10^{-2}	CD82 antigen. Membrane glycoprotein that is a member of the transmembrane 4 superfamily	

Slc6a13	-1.9	1.22×10^{-2}	Solute Carrier Family 6 Member 13. GABA transporter.	
Anxa3	-1.87	9.50×10^{-3}	Annexin A3. Regulation of cellular growth. Role in signal transduction pathways. Possible role in anti-coagulation.	
Slc47a1	-1.87	2.51×10^{-2}	Solute Carrier Family 47 Member 1.	
Atp6v0e2	-1.86	5.67×10^{-3}	ATPase H+ Transporting V0 Subunit E2. Enzyme transporter that functions to acidify intracellular compartments in eukaryotic cells.	
Anxa9	-1.85	1.74×10^{-2}	Annexin A9. May act as a low affinity receptor for acetylcholine.	
Vit	-1.85	8.51×10^{-3}	Vitrin. Promotes matrix assembly and cell adhesion.	
Fbxo2	-1.84	4.53×10^{-2}	F-Box Protein 2. F-box proteins constitute one subunit of the ubiquitin protein ligase complex: SCFs (SKP1-cullin-F-box). This functions in phosphorylation-dependent ubiquitination	
Arhgap22	-1.82	3.15×10^{-3}	Rho GTPase Activating Protein 22. Involved in regulating endothelial cell capillary tube formation during angiogenesis.	
St6gal1	-1.82	7.77×10^{-3}	Beta galactoside alpha 2,6 sialyltransferase 1.	
Amph	-1.80	3.95×10^{-3}	Amphiphysin. Associated with the cytoplasmic surface of synaptic vesicles	
Sbsn	-1.79	1.22×10^{-2}	Suprabasin.	
Tcf21	-1.77	4.89×10^{-3}	Transcription factor 21. Involved in epithelial-mesenchymal interactions in kidney and lung morphogenesis that include epithelial differentiation and branching morphogenesis.	Expressed in white pre-adipocytes (not brown). Positively regulates Bmp4 expression (Timmons *et al.*, 2007.
Gpr1	-1.76	3.86×10^{-2}	G-protein coupled receptor 1. Chemerin receptor. Chemerin is an adipokine.	Expressed in the SVF of WAT. Knockout mice on a HFD are more glucose intolerant than wild type (Rourke *et al.*, 2014.
Limch1	-1.76	1.12×10^{-2}	LIM and calponin homology domains-containing protein 1	
Fez1	-1.76	1.45×10^{-2}	Fasciculation And Elongation Protein Zeta 1.	
Prokr1	-1.76	1.46×10^{-3}	Prokineticin Receptor 1.	
Bmp7	-1.74	3.09×10^{-2}	Bone morphogenetic protein 7. Functions in bone, kidney and brown adipose tissue development.	Implicated in “browning” of WAT and activation of BAT (Boon *et al.*, 2015).
Cdh13	-1.72	7.72×10^{-3}	Cadherin 13. Lacks cytoplasmic domain characteristic of other cadherins, so not thought to be a cell-cell adhesion glycoprotein.	GWAS reveal associations between CDH13 gene variants and adiponectin levels (Teng *et al.*, 2013).

Adm	-1.66	$2.48x10^{-2}$	Adrenomedullin. Several functions, including vasodilation, regulation of hormone secretion, promotion of angiogenesis, and antimicrobial activity	Adipokine, expression is increased in adipose tissue in obesity (Li *et al*., 2007). Expressed in SVF cells, not adipocytes (Paulmyer-Lacroix *et al*., 2006). Reduced synthesis *in vitro* accelerates adipocyte differentiation. Insulin inhibits Adm expression (Hamancey *et al*., 2007).
Dpp4	-1.63	$4.94x10^{-2}$	Dipeptidyl Peptidase 4. An intrinsic membrane glycoprotein and a serine exopeptidase that cleaves X-proline dipeptides from the N-terminus of polypeptides	Adipokine. Impairs insulin sensitivity. Expressed at highest levels in differentiated adipocytes, and serum concentrations correlate with adipocyte size. Highest expression in visceral WAT (Lamers *et al*., 2011).
Bmp4	-1.63	$4.47x10^{-2}$	Bone Morphogenetic Protein 4. Major role in bone and cartilage development.	Major role in regulating adipocyte precursor cell commitment and differentiation. Induced and secreted by differentiated adipocytes (Gustafson *et al*., 2015).
Alpl	-1.56	$3.48x10^{-3}$	Alkaline Phosphatase, Liver/Bone/Kidney. Possible role in bone mineralisation.	
Osr2	-1.52	$3.48x10^{-2}$	Odd-Skipped Related Transciption Factor 2.	
Pkp2	-1.51	$2.37x10^{-2}$	Plakophilin 2. Role in linking cadherins to intermediate filaments in the cytoskeleton	
Lpar3	-1.51	$7.08x10^{-3}$	Lysophosphatidic Acid Receptor 3. Cellular receptor for lysophosphatidic acid, involved in calcium mobilisation.	Lysophosphatidic acid is synthesised during white adipocyte differentiation (Sheng *et al*., 2015).
Arl4d	-1.51	$4.29x10^{-2}$	ADP Ribosylation Factor Like GTPase 4D. Possible role in membrane-associated intracellular trafficking.	Expression increases during early adipogenesis, then decreases. Overexpression in 3T3-L1 cells inhibits adipogenesis (Yu *et al*., 2011).

All genes upregulated in $Wt1^{+}$ Lin^{-};$CD31^{-}$;$CD29^{+}$;$CD34^{+}$ perigonadal SVF cells from mice fed a HFD, with a q-value <0.05 and a LogFC >1.5. Genes in black were selected for validation by qRT-PCR.

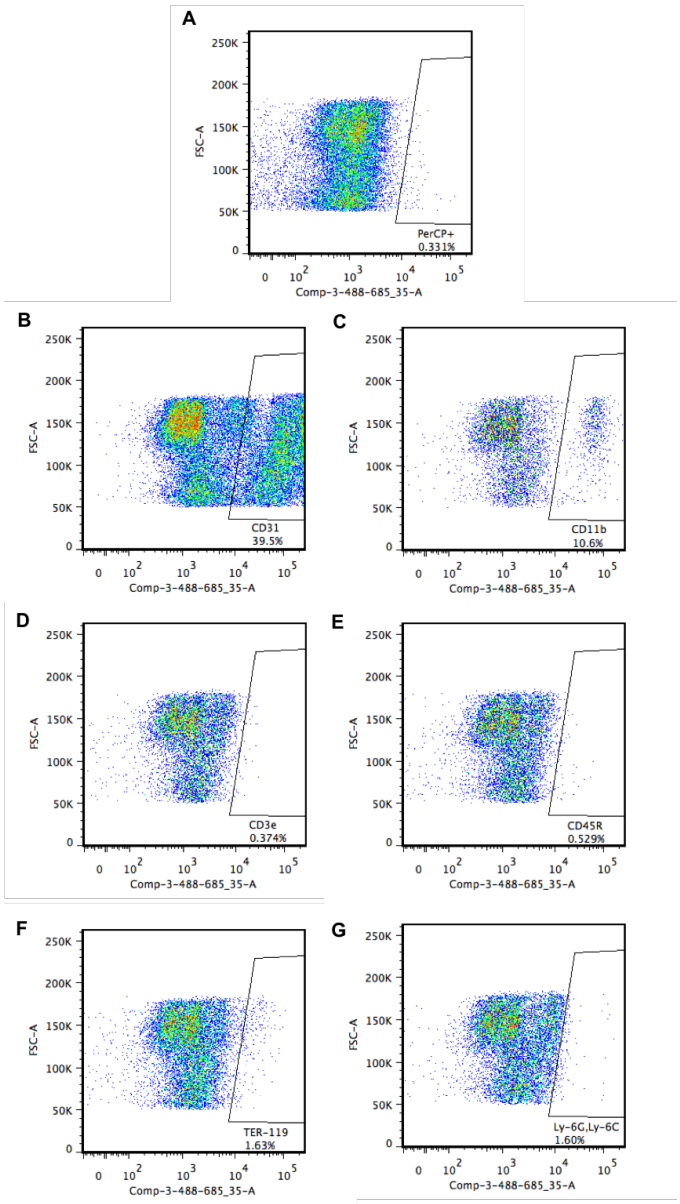
GENE	LOG FOLD CHANGE	Q VALUE	NAME/BRIEF DESCRIPTION (UNIPROT HTTP://WWW.UNIPROT.ORG AND ENTREZ GENE HTTPS://WWW.NCBI.NLM.NIH.GOV/GENE)	EXISTING LINKS TO ADIPOSE TISSUE FOUND IN THE LITERATURE
Enpp6	2.80	$9.08x10^{-3}$	Ectonucleotide pyrophosphatase/phosphodiesterase 6. Member of a family of enzymes with a role in the regulation of extracellular nucleotide metabolism.	
Cxcl14	2.74	$4.76x10^{-3}$	C-X-C motif chemokine 14. Cytokine that belongs to the CXC chemokine family.	Enhances insulin-dependent glucose uptake in adipocytes. Deficient mice are resistant to HFD-induced obesity (Takahashi *et al*., 2007).
Col28a1	2.2	$2.48x10^{-3}$	Collagen, type XXVIII, alpha 1.	
Pqlc1	1.86	$4.64x10^{-2}$	PQ Loop Repeat Containing 1.	
Plvap	1.85	$1.21x10^{-2}$	Plasmalemma Vesicle Associated Protein.	Knockout mice have decreased WAT (Stan *et al*., 2012).
Sox11	1.81	$4.68x10^{-3}$	SRY (sex determining region Y)-box 11. Member of the SOX family of transcription factors, important for regulation of embryonic development.	
Hgf	1.74	$1.40x10^{-2}$	Hepatocyte growth factor. Regulates cell growth, motility and morphogenesis in multiple tissue types.	Secreted by pre-adipocytes, and regulates fat pad vascularization (White *et al*., 2014). HGF in serum is increased in obesity, due to secretion from adipose tissue (Bell *et al*., 2006).
Kcne1l	1.72	$3.19x10^{-2}$	Potassium voltage-gated channel, Isk-related family, member 1-like, pseudogene. A membrane protein that has sequence similarity to the Kcne1 gene product.	Increased expression in FGF21-treated WAT to levels similar to those in BAT (Muise *et al*., 2013).
Il6	1.69	$1.19x10^{-2}$	Interleukin 6. Member of the interleukin family of cytokines. Important in immune response, hematopoiesis, inflammation and the acute phase response.	Recruitment of macrophages to adipose tissue during HFD feeding is prevented when Il6 signaling is blocked (Kraakman *et al*., 2015).
Kcnv2	1.66	$1.37x10^{-2}$	Potassium channel, subfamily V, member 2.	
Tmem51	1.60	$1.33x10^{-2}$	Transmembrane protein 51.	
Specc1	1.58	$3.68x10^{-2}$	Sperm Antigen With Calponin Homology and Coiled-Coil Domains 1. Belongs to the cytopsin-A family.	
Areg	1.51	$2.76x10^{-2}$	Amphiregulin. Member of the epidermal growth factor family. Functions in development of mammary glands, oocytes and bone.	

All genes upregulated in $Wt1^{-}$ Lin^{-};$CD31^{-}$;$CD29^{+}$;$CD34^{+}$ perigonadal SVF cells from mice fed a HFD, with a q-value <0.05 and a LogFC >1.5. Genes in black were selected for validation by qRT-PCR.

GENE	LOG FOLD CHANGE	Q VALUE	NAME/BRIEF DESCRIPTION (UNIPROT HTTP://WWW.UNIPROT.ORG AND ENTREZ GENE HTTPS://WWW.NCBI.NLM.NIH.GOV/GENE)	EXISTING LINKS TO ADIPOSE TISSUE FOUND IN THE LITERATURE
Saa3	3.20	$1.22x10^{-2}$	Serum amyloid A 3. Apolipoprotein of the HDL complex.	Deletion improves HFD-induced adipose tissue inflammation in female mice (Hartigh *et al*., 2014).
Prg4	2.67	$3.15x10^{-3}$	Proteoglycan 4. Lubrication of joints.	
C4b,C4a	2.34	$3.02x10^{-3}$	Complement C4-A/B. Essential for classical complement pathway.	
Csprs	2.14	$3.95x10^{-3}$	Component of Sp100-rs.	Increased expression in epididymal adipose tissue of aged mice (Star *et al*., 2013).
Mpeg1	2.07	$3.61x10^{-2}$	Macrophage-expressed gene 1.	
Wisp1	1.86	$3.14x10^{-2}$	Wnt1 Inducible Signaling Pathway Protein 1. Downstream regulator in Wnt/Frizzled-signaling pathway.	Bmp3/Wisp1 signaling promote mesenchymal cell proliferation and adipogenesis (Cernea *et al*., 2016). Adipokine linked to obesity-associated inflammation (Murahovschi *et al*., 2015).
F2rl1	1.73	$7.90x10^{-3}$	Proteinase-activated receptor 2. Involved in modulation of inflammatory response.	Knockout mice are resistant to HFD-induced weight gain and insulin resistance (Badeanlou *et al*., 2012).
Lrrn2	1.72	$5.91x10^{-3}$	Leucine Rich Repeat Neuronal 2. Has homology with other proteins functioning as cell-adhesion molecules.	
Itih2	1.66	$7.08x10^{-3}$	Inter-alpha-trypsin inhibitor heavy chain H2. Extracellular matrix stabilisation.	
Adcy2	1.62	$3.81x10^{-3}$	Adenylate Cyclase 2. Catalyse formation of cAMP.	
Tmem176b	1.62	$2.61x10^{-2}$	Transmembrane Protein 176B.	
Ccl9	1.57	$4.39x10^{-2}$	C-C motif chemokine 9. Monokine with inflammatory, pyrogenic and chemokinetic properties.	Known to be upregulated in HFD-induced and genetically obese mice (Tourniaire *et al*., 2013).
Prss12	1.57	$1.93x10^{-2}$	Neurotrypsin. Neuronal plasticity.	
Palld	1.56	$1.30x10^{-3}$	Palladin. Cytoskeletal protein involved in organization of actin cytoskeleton. Cell morphology, motility, and adhesion.	

St6galnac2	1.55	1.29×10^{-2}	Alpha-N-acetylgalactosaminide alpha-2,6-sialyltransferase 2. Protein glycosylation.
Fut4	1.54	1.04×10^{-3}	Alpha-(1,3)-fucosyltransferase 4. Protein glycosylation.
H2-DMb1	1.54	5.73×10^{-3}	
Lrfn2	1.51	5.59×10^{-3}	Leucine-rich repeat and fibronectin type-III domain-containing protein 2.
Cd276	1.51	1.48×10^{-3}	CD276 antigen. Modulates T-cell-mediated immune responses.

The biotinylated lineage panel used to sort haematopoietic and non-haematopoietic fractions was composed of five antibodies against various cell surface markers. Additionally, CD31 was used to label endothelial cells, but had the same emission spectra as the streptavidin-conjugated secondary antibody used to detect the lineage panel. Six samples of cells were stained with just one antibody from the panel each (and the streptavidin-conjugated secondary antibody), or the CD31 antibody. Figure A shows a secondary antibody only control, used to establish the gates. Cells stained with CD31 are shown in B, CD11b (C), CD3e (D), CD45R (E), TER-119 (F), Ly-6G/Ly-6C (G).



To verify that *Prx1-Cre^{ERT2};R26R-mTmG* embryos were receiving tamoxifen when dosed *in utero*, the limb buds were checked for the presence of GFP. Embryos that were dosed at E11.5 were harvested at E14.5, and the limb buds section and stained with an anti-GFP antibody. The presence of many GFP expressing cells in the limb buds indicates that recombination did occur and thus the embryos did receive tamoxifen. (Scale bar = 200μm (A), 100 μm (B-D)).

